

***Bacillus subtilis* biofilm formation under  
extreme terrestrial and simulated extraterrestrial conditions**

**Dissertation**

to obtain the Ph. D. degree "*Doctor rerum naturalium*" (Dr. rer. nat.)

at the Faculty of Biology and Psychology

at the Georg-August-University Göttingen, Germany

in frame of the doctoral program

Georg-August University School of Science (GAUSS) - Biology

submitted by

**Felix Matthias Fuchs**

Born in Münchberg on 10<sup>th</sup> November 1988



Göttingen, February 2020



## Thesis Advisory Committee

### **Prof. Dr. Jörg Stülke**

Department of General Microbiology, Institute of Microbiology and Genetics, Georg-August University of Göttingen

### **Prof. Dr. Ralf Möller**

Space Microbiology Research Group, Radiation Biology Department, Institute of Aerospace Medicine, German Aerospace Center Cologne

### **Prof. Dr. Fabian M. Commichau**

Synthetic Biology, Institute of Biotechnology, Brandenburg University of Technology Cottbus - Senftenberg

## Members of the examination board

### First reviewer:

#### **Prof. Dr. Jörg Stülke**

Department of General Microbiology, Institute of Microbiology and Genetics, Georg-August University of Göttingen

### Second reviewer:

#### **Prof. Dr. Ralf Möller**

Space Microbiology Research Group, Radiation Biology Department, Institute of Aerospace Medicine, German Aerospace Center Cologne

### Additional members of the examination board:

#### **Prof. Dr. Stefanie Pöggeler**

Department of General Microbiology, Institute of Microbiology and Genetics, Georg-August University of Göttingen

#### **Prof. Dr. Ivo Feussner**

Department of Plant Biochemistry, Albrecht von Haller Institute, Georg-August University of Göttingen

#### **PD Dr. Michael Hoppert**

Department of General Microbiology, Institute of Microbiology and Genetics, Georg-August University of Göttingen

#### **Dr. Heiko Liesegang**

Department of Genomic and Applied Microbiology, Institute of Microbiology and Genetics, Georg-August University of Göttingen

Date of Disputation:

17<sup>th</sup> April 2020

---



***B. subtilis* biofilms - a matter of the heart**

For biofilm formation,  $1 \times 10^6$  spores of *B. subtilis* NCIB 3610 were inoculated on SSM-medium. Scale bar represents 5 mm.

- It's the little things that make you happy -

“Now my own suspicion is that the Universe is not only queerer than we suppose,  
but queerer than we can suppose.”

-John Burdon Sanderson Haldane (1927)

For my parents

## Acknowledgements

First of all, I would like to express my deep gratitude to Prof. Dr. Ralf Möller for his supervision, friendship and for the unbelievably versatile possibilities that I was offered as a PhD-student at the DLR. All the conferences, workshops, courses, travels and collaborations added up to a unique experience, for which I am grateful. I kindly would like to thank Prof. Dr. Jörg Stülke, who supervised me as external student and introduced me to the University in Göttingen despite the distance to Cologne. I want to thank PD Dr. Michael Hoppert, Prof. Dr. Pöggeler, Dr. Heiko Liesegang and Prof. Dr. Feussner for examining my thesis as well as Prof. Dr. Fabian Commichau, which supervised me during my TAC-Meetings. While being in Göttingen during an internship course, I really enjoyed the collegial atmosphere and the inclusion to the team. Furthermore, I would like to thank PD Dr. Christine Hellweg and Dr. Günter Reitz, who always supported me as department leaders. A special thanks goes to the DLR & Helmholtz Research School SpaceLife, which provided me a SpaceLife scholarship and therewith the possibility to study in the field of space microbiology. Furthermore, I would like to thank PD Dr. Ruth Hemmersbach as my mentor and for her support from the gravitational biology as well as her colleagues Christian Liemersdorf, Yannick Lichterfeld and Timo Frett. From the radiation biology department, I would like to thank Claudia Schmitz & Sebastian Feles for excellent support, Dr. Sebastian Diegeler for being a good friend and comrade, André Parpart & Carina Fink for our discussions, Dr. Petra Rettberg for her support, Thomas Urlings for his informatics expertise, Dr. Corinna Panitz for our discussions as well as Andrea Schröder, who helped me with thousands of plates, incubation and so many other lab-things - thank you all. I really loved and enjoyed working in the space microbiology working group and I want to thank all of you, whether alumni or present, namely Katharina Siems, Erika Muratov, Stella Koch, Dr. Katja Nagler, Dr. Marina Pyc, Marny Hoef-Emden, Nikea Ulrich, Bahar Djouiai, Aram de Haas, Tim Erler, Florian Rosenbaum and Marta Cortesão (+Tiago Monteiro) for the great time we shared all around Europe. I also want to thank Britta Rowehl, Dagmar Koschnitzki, Claudia Hahn, Dr. Karel Marsalek, Bartos Przybyla, Dr. Kai Schenetten and all of my students and interns. I would like to thank the DGE (Deutsche Gesellschaft für Elektronenmikroskopie) for the financial support to work at the Robert Koch Institute (RKI). In this regard, I would like to send out my special thanks to Dr. Michael Laue for the realization of my project, Gudrun Holland & Janett Piesker & Kazimierz Madela for their excellent technical support and our discussion as well as Dr. Christoph Schaudinn for his biofilm expertise. Many thanks to Prof. Dr. Ákos Kovács for his comments and for providing several mutant strains, as well as PD Dr. Madeleine Opitz for the support of several mutants and Samir Giri for the  $\Delta lysA$ -strain. Furthermore, my special thanks go to Dr. Akira Fujimori & Hirokazu Hirakawa for the support at the HIMAC facility in Japan and JAXA for funding the research trip (STARLIFE project, 13J301, insight-REPAIR, 14J410, "Living in Space" grant) as well as Dr. Daisuke Niwa for introducing me to Japan. I would like to thank Prof. Dr. Lieleg and Carolina Falcón Garcia for realizing the biofilm surface topography studies on biofilms. A very special thanks to all those who supported me in bioinformatics and other experiments: Dr. Sevasti Filippidou, Dr. Bentley Shuster, Prof. Dr. Patrick Eichenberger, Prof. Dr. Peter Setlow, Prof. Dr. Yong-Qing Li, Dr. Anne de Jong, Dr. Jan-Wilm Lackmann, Dr. Marcel Fiebrandt and Michael Morrison. For so many other reasons I want to thank Diana and Dr. Jens Boy, all BioRockers, the Betty-Crew, Britta Osterkamp, Prof. Andrew Gibson, Maximilian Wache, David Mahlberg and Constanza & Magnus von Abercron. Also thanks to all those I forgot to mention, so many personalities have helped and supported me – partwise work-related partwise with other extremely useful and motivating things – thank you all! Further, I would like to thank my family, who supported me all my life: Thank you Mama (Andrea), Papa (Andreas), Jonas, Fiona and Madita Fuchs as well as my grandparents - for your love and dedication. Finally, I would like to thank my wife Felicitas for her infinite love and dedication and our daughter Laetitia for motivating me.

- Felix Fuchs, February 2020

## Affidavit

Here I declare that my doctoral thesis entitled

*“Bacillus subtilis* biofilm formation under extreme terrestrial and simulated extraterrestrial conditions”

has been written independently with no other sources and aids than quoted.

Signature

---

Felix Matthias Fuchs

Göttingen, February 2020

## Table of contents

<b>1. Introduction.....</b>	<b>- 1 -</b>
1.1 Preface: Life.....	- 1 -
1.2 Space microbiology .....	- 1 -
1.3 Microbial burden in space.....	- 2 -
1.5 <i>Bacillus subtilis</i> as model organism.....	- 7 -
1.6 Simulation of space conditions .....	- 14 -
1.7 Relevance and Hypotheses .....	- 17 -
<b>2. Material &amp; Methods.....</b>	<b>- 18 -</b>
2.1 Bacterial strains.....	- 18 -
2.2 Sporulation and spore purification.....	- 25 -
2.3 Cultivation of standardized biofilms.....	- 27 -
2.4 Simulation of microgravity (sim- $\mu$ g).....	- 29 -
2.5 Microscopy .....	- 34 -
2.6 Survival experiments .....	- 37 -
2.7 Germination assays .....	- 39 -
2.8 Molecular biology methods.....	- 39 -
2.9 Statistics, data visualization and other software .....	- 47 -
<b>3. Results.....</b>	<b>- 48 -</b>
3.1 Standardized biofilms.....	- 48 -
3.2 Biofilm maturation in absence of spore-formation .....	- 56 -
3.3 Simulation of microgravity .....	- 59 -
3.4 Cross section analysis via scanning electron microscopy (SEM) .....	- 70 -
3.5 Cross sectional comparison via SEM of <i>B. subtilis</i> biofilms grown under 1g and sim- $\mu$ g..	- 74 -
3.6 TEM-imaging of biofilms and individual cells and spores .....	- 86 -
3.7 Transcriptomics of young <i>B. subtilis</i> biofilms under 1g and sim- $\mu$ g.....	- 92 -
3.8 Germination of <i>B. subtilis</i> spores grown under 1g and sim- $\mu$ g.....	- 98 -
3.9 Survival and resistance properties of 1g and sim- $\mu$ g biofilms and spores.....	- 110 -
<b>4. Discussion.....</b>	<b>- 120 -</b>
4.1 Development of standardized biofilms .....	- 120 -
4.2 Microgravity simulation .....	- 121 -
4.3 Biofilm formation under sim- $\mu$ g.....	- 123 -
4.4 Impact of sim- $\mu$ g on spores.....	- 126 -
4.5 Impact of microgravity on survival of biofilms and spores .....	- 128 -
4.6 Transcriptomics and proteomics.....	- 130 -
<b>5. Outlook .....</b>	<b>- 134 -</b>
<b>6. Bibliography .....</b>	<b>- 135 -</b>
<b>7. Appendix .....</b>	<b>- 155 -</b>
7.1 Short history of microbial space research.....	- 155 -
7.2 Abbreviations and units.....	- 159 -
7.3 Material, Devices & Software.....	- 161 -
7.4 Chemicals, antibiotics, marker and primer .....	- 164 -
7.5 Additional results .....	- 167 -
7.6 Curriculum vitae .....	- 168 -
7.7 Publication list .....	- 169 -



## Abstract

Since the *Apollo 16* mission in 1972, *Bacillus subtilis* served as bacterial model organism in space. Due to the ability to form highly resistant endospores and complex biofilms, it was used to investigate the effects of unshielded space radiation as well as the limits of life in space. Within the International Space Station (ISS), fungal and bacterial biofilms already emerged as a burden that could harm the spacecraft due to material corrosion as well as the crew by causing infections. The ISS is a sensitive environment in which biofilm associated clogging or contaminating of life-support systems (water, electricity, cooling or ventilation) could lead to a termination of the mission. So far, little is known about the effects of biofilm formation under the influence of space conditions, such as altered gravity or enhanced radiation levels. Unfortunately, space research is very expensive, time-consuming and experimentally limited. In order to investigate single space conditions without conducting a space experiment, single parameters can be simulated under laboratory conditions.

In frame of this thesis, *B. subtilis* was used as model organism to intensively study biofilm formation and sporulation as well as germination properties of spores grown under simulated microgravity (sim- $\mu$ g). The aim was to elucidate the structure and the biological response of biofilms to sim- $\mu$ g and further spaceflight-relevant conditions to optimize the preparation of flight experiments and to make space travel safer.

*B. subtilis* NCIB 3610 and biofilm-deficient mutants in the same background were exposed to sim- $\mu$ g by using a fast-rotating 2-D clinostat and biofilm formation was compared to terrestrial gravity (1g). First, a method was developed to generate standardized colony biofilms on membrane filters to guarantee reproducible results. Surface structures (topography) of biofilms grown under both conditions did not exhibit structural differences by white-light profilometry, but exhibited changes in the surface hydrophobicity. Whereas REM and TEM images of biofilm cross sections showed differences in cell phenotypes and in the abundance of matrix components. Phenotypic appearance of biofilms as well as growth(rates) were not affected by sim- $\mu$ g, neither in CFU or spore composition. A transcriptome analysis of young biofilms showed that approximately 7 % of the transcripts differed due to the influence of sim- $\mu$ g. Based on proteome analyses 10 (72 h) - 20 % (24 h) differences in the proteome of young and mature *B. subtilis* biofilms were found. In addition, no differences in sporulation rates, but in the germination behavior of spores isolated from biofilms were observed. Spores isolated after sporulation in sim- $\mu$ g, tended to germinate spontaneously in water, which is atypical compared to 1g-cultivated spores. The time-resolved heterogeneity in germination of individual spores was reduced in sim- $\mu$ g spores, which exhibited a uniform germination behavior. In addition, various space parameters were investigated, such as ionizing and heavy ion radiation, which showed no difference in survivability between spores/biofilms formed under both gravitational conditions.

In the frame of this thesis it was shown that the simulation of microgravity changes the *B. subtilis* biofilm formation with respect to its structure but not its resistance to space parameters. In addition, spores produced under sim- $\mu$ g showed a more homogeneous germination behavior than 1g spores and tended to germinate spontaneously.



## 1. Introduction

### 1.1 Preface: Life

Bíos, or in ancient Greek “βίος” is the word for “life” and it stands for the main characteristic of our planet and maybe our solar system. There are philosophical, religious, spiritual and esoteric definitions of life, as well as other approaches (Tsokolov, 2009, Lovelock, 1995). The scientific definition of life is based on a descriptive, evidence-based methodology, composed by mathematical, physical, chemical and biological research. As far as we know, humankind is searching for an answer to the question “What is life” since our early existence (Blumberg, 2003, Benner, 2010, Schrödinger, 1944). According to Nobel Prize Laureate Sir Paul Nurse, who has researched this subject intensively, philosophers and scientists such as Aristoteles, Leeuwenhoek, Humboldt, Mendel, Pasteur, Darwin and Schrödinger, among many other great scientists were interested in this question – yet it still remains not fully answered. Modern, interdisciplinary research defines life as follows: Life on Earth comprises the ability to reproduce itself and follow a pre-determined heredity (Dix, 2002, Crick, 1970, McKay, 1991), interact with the environment (Mittal, 2012), react to stimuli and adapt or improvise (Shakhnovich & Shakhnovich, 2008), form a homeostasis and metabolize which enabled by seclusion (Koshland, 2002), organize and form compartments (Monnard & Walde, 2015). But all these different key aspects apply only to life on Earth, even if they seem universally valid (Cockell, 2016). In our understanding, life is bound to carbon-based chemistry (Tsokolov, 2009, Cockell, 2015), although silicon-based life could also be conceivable (Pace, 2001). We know that life could exist outside our known boundaries, and one of these boundaries already begins with leaving our atmosphere and thus our planet. So far only little is known about how life changes under extraterrestrial or space conditions (Horneck *et al.*, 2010), but life is never static and constantly evolves (Cleland & Chyba, 2002). However, the direction in which life on Earth develops is highly dependent on us, the human being.

But before humankind could find proof of life on other planets or celestial bodies, the development of a computer-based, electricity-driven "life", the artificial intelligence, took place. Interestingly, in computer sciences, BIOS refers to "basic input/output system", which is a slightly ironic yet fitting metaphor for life as we know it.

### 1.2 Space microbiology

Apart from searching answers for the definition and origin of life, the research field of space microbiology emerged, which is revealing fundamental properties of archaea, bacterial and fungal life under (enclosed) space conditions or individual (simulated) space parameters (Horneck *et al.*, 2010). A small history of space research can be found in the appendix in section 7.1. Typical areas of space microbiology are the investigation of physiological and morphological changes under microgravity, the investigation of potential changes in pathogenicity and microbial behavior as well as risk assessment (Castro *et al.*, 2004). In addition to perform dedicated space experiments, collecting samples from space stations to monitor microbial diversity is an important task (Pierson, 2001, Yamaguchi *et al.*, 2014). Starting with the Apollo-, Skylab- and Space Shuttle missions, microbial samples were taken onboard space crafts, brought back to Earth and were isolated and characterized (Castro *et al.*, 2004, Knox *et al.*, 2016, Sobisch *et al.*, 2019). Since the development of modern sequencing methods, microbiome and metagenome studies are able to detect and classify

almost all microorganisms (including non-cultivable and non-living) found on the ISS (Venkateswaran *et al.*, 2014, Lang *et al.*, 2017, Morrison *et al.*, 2019).

Space microbiological studies showed, that microorganisms behave differently when exposed to space conditions such as microgravity, revealing elevated levels of pathogenicity, higher resistance towards antibiotics, differences in growth and changes in biofilm morphology (Leys *et al.*, 2004, Nickerson *et al.*, 2004, Rosenzweig *et al.*, 2014, Kim *et al.*, 2013, Horneck *et al.*, 2010, Barrila *et al.*, 2016, Zea *et al.*, 2017). Today, more than fifty years after the first manned-moon landing in 1969, space microbiology is still in the infancy of discovering and understanding the microbial behavior in space. As long as astronauts are working in closed habitats onboard space stations, they always will be accompanied by microorganisms, which bring new challenges, but also the potential to discover fundamental microbial properties under changed growth conditions. Microorganisms will always be an integral part of space exploration, which needs to be analyzed and understood to support and ensure safety for crew and spacecraft. Apart from monitoring and controlling potential harmful aspects of microorganism in space, benefits such as the use of biotechnology in space are investigated. By using bacteria, fungi or yeasts onboard spacecraft, chemicals, drugs or other substances could be produced – which might be of particular interest for long-term missions, as the transport route between Earth and spacecraft is usually complicated and time-consuming (Fernández, 2019).

### 1.3 Microbial burden in space

Generally, space hardware is assembled under sterile conditions before being packaged for transport. For quality control, hardware is carefully monitored and tested to detect potential microorganisms (Rummel, 2019). Unfortunately, a complete removal of microorganisms is barely achievable, especially due to the sensitivity of electronic hardware components. Once new space hardware is brought to the ISS or attached to it, remaining microbes can spread all over the space station and microbial colonization is about to be started. Especially pristine and uninhabited surfaces offer new environments, which will be immediately claimed by microorganisms (Cockell *et al.*, 2018).

With increased human space activities and long term missions as first conducted on the *Mir*-station and later on the ISS, new microbial problems arose: Spacecraft are assembled in special clean-rooms in order to reduce the number of microorganisms, especially for lander missions. In the past, landers of the *Viking*-Mars-program (1975) were heat sterilized at 111 °C for 40 h, to prevent potential forward contamination of Mars (Soffen & Snyder, 1976). Unfortunately, as mentioned before, modern landers cannot be heat sterilized because they are carrying highly sensitive equipment. Manned missions are always inevitably accompanied by microorganisms, mostly coming from mucous membranes or skin (i.e. *Staphylococcus* sp. and *Corynebacterium* sp.) as well as many other human associated microorganisms (Novikova *et al.*, 2006, Castro *et al.*, 2004). Dominant cultivable bacterial isolates inside of the ISS were spore-forming *Bacillus* sp. and *Paenibacillus* sp., whereas the genus *Aspergillus* sp. (i.e. *Aspergillus niger*) was the predominantly filamentous fungi found (Checinska *et al.*, 2015a). Several fungal strains (i.e. *A. flavus* or *A. fumigatus*) are known to cause material deterioration and have been found on diverse surfaces aboard the ISS (Novikova *et al.*, 2006). Unfortunately, fungal mold is often associated with allergies, immunosuppression and infections and therefore might negatively affect the astronauts' health (Ward *et al.*, 2010, Chaudhary & Marr, 2011, Agarwal, 2009).

The former *Mir*-station functioned as closed artificial habitat, in which astronauts lived and worked in confined spaces for many years. Microorganisms are known for their ability to adapt quickly to

changing environmental conditions and therefore spread all over the space station. Arriving astronauts were reporting about a “strange smell” when breathing the air inside of the *Mir*-station for the first time, a typical sign for fungal and bacterial activity, which was supported by the finding of a diverse fungal flora (Makimura *et al.*, 2001). Due to the increased microbial burden, the *Mir*-station could no longer be operated among other reasons. The astronauts' risk of illness was excessive and this was one of the main reasons why the station was disposed. Today, astronauts aboard the ISS have a dedicated cleaning-schedule that takes up several hours per week. In addition, HEPA-filter systems (HEPA: high efficiency particulate air filter), which accumulate diverse microorganisms, are replaced at regular intervals. However, in some places that are difficult to clean, microorganisms can occur largely undisturbed. This can result in considerable damage to the material (Figure 1). In addition to various metals, microbial corrosion can also damage plastics and other surfaces (Videla & Herrera, 2005, Li *et al.*, 2013a, Little *et al.*, 1992). The most sensitive life support systems are the drinking water system (Thornhill & Kumar, 2018), the ventilation system (Haines *et al.*, 2019, Checinska Sielaff *et al.*, 2016) as well as the heating and electricity supply. Clogging of water leading pipelines or the ventilation system could lead to an emergency forcing to evacuate the ISS.



**Figure 1: Fungal biofilm contamination aboard the ISS**

Filamentous fungi are omnipresent aboard the international space station and can be found on almost every surface. Most commonly found mold originates from the genus *Aspergillus*, which comprises ‘beneficial’ as well as ‘harmful’ species (Checinska 2015). The picture was taken in 2007 of an already removed panel where astronauts used to place their towels during sportive exercises. Credit: NASA (Bell, 2007).

#### **1.4 Biofilms: Composition and structure**

On the ISS as well as on Earth most microorganisms occur in two different ways: Either as free-living planktonic cells or as interface-attached surface congregations, known as biofilms (Stoodley *et al.*, 2002, Costerton *et al.*, 1987). Biofilms can be found everywhere in the natural environment: In deep subsurface and soil (Flemming & Wueertz, 2019), root-associated (Velmourougane *et al.*, 2017), in any kind of water or wetland (Fernandes *et al.*, 2019, Li *et al.*, 2019b, Wagner-Dobler, 2016), in the oral cavity (Arweiler & Netuschil, 2016) as well as in the intestine of higher organisms (Srivastava *et al.*, 2017). Artificial, man-made systems such as drainage systems, water- or oil-pipelines (Lenhart *et al.*, 2014), food-processing industry (Bridier *et al.*, 2015) or spaceships (Perrin *et al.*, 2018) can be colonized by biofilms. Environmental biofilms consist of fungi, archaea, bacteria or combinations thereof (van Wolferen *et al.*, 2018). They can also occur as symbionts with algae or lichen (Ramanan *et al.*, 2016). The first step of biofilm formation is the adhesion or attachment phase of individual cells to a surface or interface (Figure 2).

. Due to the production of adhesins, cells and the developing biofilm can anchor themselves firmly to their substrate (Soto & Hultgren, 1999). In the developmental stage adhered cells begin to spread and colonize the given surface and start to grow. Microorganisms share the ability to perceive rising levels of cells by excreting and detecting various peptides and other signal molecules to adapt their own gene expression to maximize the benefits of the colony and minimize ecological problems such as nutrient limitation (Miller & Bassler, 2001).

In parallel to quorum sensing, many bacteria start to produce and excrete different extracellular polymeric substances (EPS), which offer high mechanical stability and viscoelasticity (Monds & O'Toole, 2009, Grumbein *et al.*, 2014, Costerton *et al.*, 1999). The extracellular matrix formed by EPS is mainly composed of structural proteins (Sun *et al.*, 2005, Fong & Yildiz, 2015) and polysaccharides as well as nucleic acids (DNA and RNA) (Sutherland, 2001). Matrix-embedded cells are protected against many different environmental stresses such as chemicals (e.g. antibiotics, detergents, and acids), shear forces, temperature changes, nutrient depletion and other physical parameter (e.g. UV-radiation, metal ions and extreme pH) (de Carvalho, 2017, Bridier *et al.*, 2011, Vlamakis *et al.*, 2013, Teitzel *et al.*, 2006). The macroscopic topography of biofilms, which can be highly structured, is significantly determined by the EPS. Matured biofilms can be very heterogeneous, due to cells in various stages of development and growth. Immobile, flagellated or dead cells, spores and spore-formers as well as different microbial species are characteristic for environmental biofilms. Over time, the persistence and resistance of biofilms increases and microenvironments within biofilms and around them develop, which can lead to corrosive, pathogenic or symbiotic interactions with their closer environment (Koo *et al.*, 2017a).

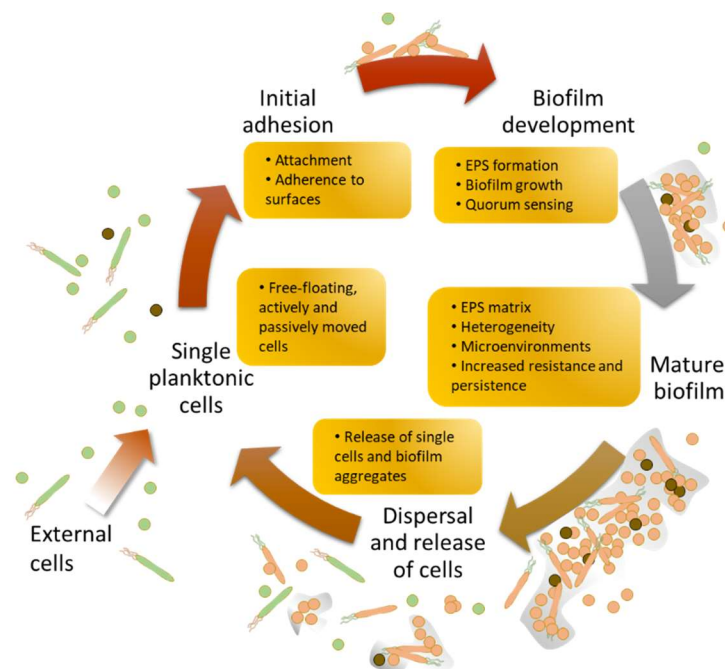


**Figure 2: Stages of biofilms development**

Environmental biofilms are formed in different stages: Planktonic cells or small cell clusters attach and adhere to surfaces or interfaces. With increasing growth, quorum sensing starts and extracellular polymeric substances are excreted, which form a dense matrix to protect individual cells from environmental hazards. During the maturation of biofilms, the EPS/matrix is formed and microenvironments are created with can cause severe problems due to material corrosion or increased pathogenicity. The increased persistence of mature biofilms connects large cell clusters and allows only the dispersal of individual cells and smaller cell-cluster encapsulated in EPS. Scheme was adapted after Koo *et al.*, reviewing potential therapeutic strategies to overcome biofilm resistances with a generalized biofilm life cycle model (Koo *et al.*, 2017b).

Single cells, cell clusters and large fractions of EPS containing microorganisms can be detached from the biofilm and dispersed. Cells which are released lose many protective features from the maternal biofilm and tend to be more susceptible towards all kind of environmental hazards. Therefore, common anti-biofilm strategies often focus the destabilization and dispersal of biofilms to weaken individual cells. On the other hand, dispersal and cell lysis are advantageous for the biofilm to control and regulate nutrient consumption and uptake as well as to maintain the overall biofilm topography and internal structure (Flemming & Wingender, 2010). The global carbon and nitrogen cycles on our planet as well as the processing of almost all biogenic building blocks in water (Decho, 2000, Dang & Lovell, 2015, Li *et al.*, 2019a), soil (Newman & Banfield, 2002) and within all higher multicellular organisms (de Vos, 2015) are driven by biofilm colonization (Flemming *et al.*, 2016). The advantages of biofilms are already applied in wastewater and freshwater treatment (Lewandowski & Boltz, 2011), bioremediation (Singh *et al.*, 2006) and of the production of bulk chemicals (Halan *et al.*, 2012).

### **Biofilm contamination**

Although the metabolic activity of biofilms is lower than observed in planktonic cells, the extreme resistances of biofilms can become a problem for humans and the environment (Blanchette & Wenke, 2018). Therefore, overcoming the intrinsic resistance of multi-species biofilms is one of the greatest modern challenges (Koo *et al.*, 2017a). Biofilms are known to cause severe infections which can be immunocompromising and lead to chronic or incurable diseases (Costerton *et al.*, 2003, Jamal *et al.*, 2018). It is estimated that millions of biofilm-related infections such as nosocomial (Guggenbichler *et al.*, 2011) and implant-associated (Darouiche, 2004, Khatoon *et al.*, 2018) infections are caused every year. Some of these infections are lethal and an even greater number of patients suffer from the consequences of the infections for an extended period of time. This results in a great burden for the affected patients as well as for society, which has to pay for the treatment of the patients. Furthermore, the danger of biofilm-associated infections not only exists for humans, but can also lead to major financial and socio-economic problems if, for example, farm animals (i.e. cattle, poultry) or crops are infected (Earley *et al.*, 2017, Masachis *et al.*, 2016). Due to the enormous use of prophylactic antibiotics in animal breeding and lesser for human-treatments, many biofilm-associated diseases have occurred increasingly. The combination of biofilm formation and single or multiple antibiotic resistances reduces the effectiveness for future use of antibiotics. The genetic transfer of i.e. antibiotic resistances between cells in biofilms is facilitated more frequently in contrast to planktonic phenotypes. Antibiotic and structural resistances in combination with the constant dispersal of biofilms, where single cells or small cell clusters migrate from the maternal biofilm, complicate to counteract bacterial distribution. A single mature biofilm in a hard to clean area within an industrial plant can constantly contaminate products and thus can cause enormous danger for the customer and financial damage for the producer.

### **Biofilms in space**

Biofilm formation often occurs, when the environment is hostile and nutrients are limited. Artificial indoor environments such as spacecraft like the ISS or the former *Mir*-Station can be seen as an example for a hostile environment. In close proximity to astronauts, microbes can be found everywhere on the spaceship depending on the availability of nutrients (Lang *et al.*, 2017). A spacecraft can have many different microclimatic areas, ranging from humid and dry places to cold and hot areas. As nutrient source, a variety of human metabolic products (sweat, urine, saliva, but

also skin particles), food residues and other organic compounds can be accessed by microorganisms (Klintworth *et al.*, 1999). Astronauts spent several hours every week to clean the ISS, but many surfaces are not or only barely cleanable and thus allow biofilms to form. Especially fungal biofilms have been observed frequently (Figure 1), causing corrosive damage to the spacecraft interior due to the creation of chemical microenvironments (Little *et al.*, 1992). This can be extremely dangerous for the crew, especially during long-term missions as seen on the *Mir*, where for the first time microbial corrosion was in space was described (Klintworth *et al.*, 1999, Novikova, 2004). As described above, biofilms can lead to severe inflammatory diseases, but may also cause a discomfort by releasing foul-smelling aerosols. Biofilm growth has to be monitored on the ISS and counteracted to prevent the spacecraft from being uninhabitable for astronauts as happened on the *Mir*-station (Novikova *et al.*, 2006). Compared to Earth, the removal of biofilms and surface attached microorganisms within a spacecraft is complicated. Only a limited amount of detergents and disinfectants are allowed to be used aboard. Unfortunately, many surfaces cannot be cleaned or are unreachable. High contaminated surfaces and items have to be completely removed. Interestingly, both disinfectant- and antibiotic resistant microorganisms have been detected on the ISS (Urbaniak *et al.*, 2018), which might be more difficult to remove when grown to surface-attached biofilms. All liquid-carrying life-support systems such as water (iodine-based water treatment) and air supply (HEPA-filters) constantly need to be maintained or replaced due to biofilm-formation (Checinska *et al.*, 2015b, Blachowicz *et al.*, 2019, Koenig *et al.*, 1995). Clogging by biofilms could lead to reduced performance of these systems or even lead to failure. The consequence would be the abandonment of a mission worth billions and the discontinuation of research on the space station. The influence of microgravity and other space-related growth parameters on biofilm-formation are largely unknown, but in the last decade several studies were conducted aiming to analyze biofilm formation by using space-flights and simulations of microgravity. Some of these studies showed enhanced bacterial growth under the influence of microgravity (Kim *et al.*, 2013, Wang *et al.*, 2016, Mauclair & Egli, 2010, Cheng *et al.*, 2014). Other studies demonstrated, that microgravity did not influence microbial growth (Baker *et al.*, 2004, Rosado *et al.*, 2010) or a decrease in growth when cultured under (simulated) microgravity (Van Mulders *et al.*, 2011, Lam *et al.*, 2002), thus a versatile discussed topic.

Apart from stigmatizing biofilms as burden, controlled biofilms could be used for life support systems such as water purification (Bornemann *et al.*, 2015) or for decomposition processes of organic substances such as feces, plants and food leftovers (Menezes *et al.*, 2015a). Biofilms could be used to compost and detoxify waste, which could be used as fertile soil for future long-term missions. For example, the Eu:CROPIS mission takes advantage of biofilms, which were allowed to settle on a column of porous volcano regolith (Eu:CROPIS: *Euglena* and combined regenerative organic-food production in space). As nutrient source, artificial urine was used to fertilize and irrigate tomatoes within a closed, self-regenerating system on a satellite (Hauslage *et al.*, 2018). Ammonia, which can be primarily found in urine, can be degraded during nitrification to nitrate by use of multi-species biofilms. In addition, the Eu:CROPIS mission uses the unicellular algae *Euglena gracilis* to produce small amounts of molecular oxygen and could potentially be used as fuel or food source (Watanabe *et al.*, 2017) for future missions (Hauslage *et al.*, 2018). Apart from space flight missions, biofilms could be used to perform biomining or bioleaching of metals, biopolymers or carbon sources on celestial bodies or for example on Mars (Byloos *et al.*, 2017, Loudon *et al.*, 2018), thus facilitating terra-forming (Horneck, 2008), which demands a functioning carbon and nitrogen cycle (Menezes *et al.*, 2015b). Modern genetic tools, such as the use of CRISPR/Cas (Ran *et al.*, 2013) and small scale automated bioreactors might help to overcome the need of pharmaceuticals by producing individually tailored drugs by microorganisms (Vogl *et al.*, 2013).



### 1.5 *Bacillus subtilis* as model organism

*Bacillus subtilis* (lat. *bacillum* = rod and *subtilis* = subtle or fine) is a Gram-positive chemoorganoheterotrophic rod-shaped soil bacterium, which is able to form endospores and biofilms under certain conditions. The scientist Christian Ehrenberg described it first in 1835 as *Vibrio subtilis* (lat. *vibrio*, curved) and was renamed by Ferdinand Cohn to *Bacillus subtilis* in 1872. With regards to taxonomy, it belongs to the phylum Firmicutes, class Bacilli, to the order of Bacillales and the family Bacillaceae. Vegetative cells are ubiquitously found in aerobic environments mainly in the upper soil and rhizosphere. *B. subtilis* is known for the symbiosis with plant roots (production of fungicides), but can also be isolated from the air or from gut samples of humans and animals (Hong *et al.*, 2009). Cells grow to a length of 2-8  $\mu\text{m}$  and 0.2-1  $\mu\text{m}$  in thickness. The cell body is flagellated and enables active movement in liquids. The production and excretion of surfactins, which are surface-active lipopeptides, reduces the surface tension of water or semi-solid surfaces and allow the bacterium wetting the surface and actively move over it.

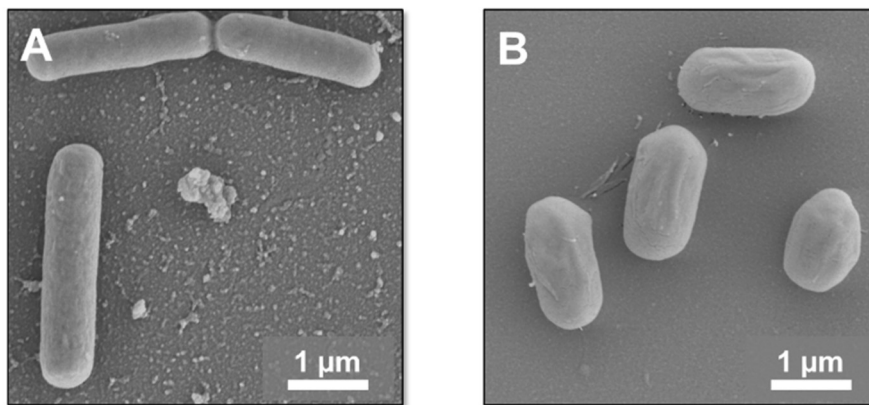


**Figure 3: Vegetative *B. subtilis* cells and spores**

Images represent electron microscopic images of *B. subtilis* 168 in its vegetative cell form (image A) and in its spore form (B). Due to the fixation and preparation method, flagella are not visible in image A. Scale bars represent 1  $\mu\text{m}$ .

Within the 19<sup>th</sup> century, *B. subtilis* emerged in the interest of science, industry and for environmental purposes. It was among the first bacterial strains which were completely sequenced (Kunst *et al.*, 1997) and it is one of the best understood Gram-positive bacterial species. Genetic modification is relatively easy due to the ability of conjugation and the uptake of extracellular DNA as well as the possibility of transduction. According to the organism overview tool of the NCIB genome database, the genome of *B. subtilis* comprises of ~4.13 Mb, resulting in 4087 proteins with a GC-content of ~43.6%. Most *B. subtilis* strains are undemanding, require simple growth media and provide short generation times. Searching for *B. subtilis* related literature, PubMed reveals more than 36.000 entries (PubMed, 2019) and the genetic tool and website SubtiWiki lists all available genetic pathways, their interaction and regulation (Zhu & Stülke, 2018). Besides its modifiability, there are two important properties in particular, the ability to form spores and biofilms, which make *B. subtilis* one of the most popular model organisms in basic research.

In industry *B. subtilis* is used to produce various proteins and enzymes, for example subtilisin, bacitracin, riboflavin (vitamin B2) as well as amylases and proteases (Wang *et al.*, 2015, Rychen *et al.*, 2018, van Dijk & Hecker, 2013, Zweers *et al.*, 2008). Apart from industrial purposes, *B. subtilis* is used

as microbial inoculant in agriculture (Jamily & Toyota, 2019, Bais *et al.*, 2004) and might help to counteract heavy metal pollution via bioremediation (Dobrowolski *et al.*, 2019, Bai *et al.*, 2019). A famous relative of *B. subtilis* which is worth mentioning is *B. natto* which is used to ferment soy beans to Nattō, a traditional Japanese delicacy.

In order to study the effects of simulated space conditions, several strains were used, sharing the same genus (*Bacillus*) and species, but differentiated on their genetic level. Two *B. subtilis* strains among several others were primarily used: (1) The Marburg strain, also known as DSM-10 or mainly mentioned NCIB 3610, which is a wild-type isolate, able to form highly structured biofilms and (2) the *B. subtilis* strain 168, which is a so-called “domesticated” strain that lost most of its ability to form complex, structured biofilms. Interestingly, both strains harbor identical physiological properties apart from the disability of complex biofilm formation in 168. As reference strains for certain sporulation or biofilm deficiencies, mutants of NCIB 3610 are used for several experiments.

### **Biofilm formation of *B. subtilis***

For decades, *B. subtilis* was used in laboratories without recognizing that undomesticated wild type strains harbor the ability to form highly structured biofilms on agar-based media (and in liquid culturing) apart from the flat colony appearance of i.e. *B. subtilis* 168. In 2001 Branda *et al.* described the biofilm formation and the aerial structures of *B. subtilis* as fruiting body formation and related the structures to undomesticated strains (Branda *et al.*, 2001). Under laboratory conditions, in which almost all biofilm studies were conducted, only single-species biofilms were investigated to standardize the experimental design and to confirm the experimental results. Strikingly, individual cells within a biofilm organize themselves embedded in a complex extra polymeric matrix comprised of polysaccharides, proteins and nucleic acids (Branda *et al.*, 2005) to an almost multicellular entity (Aguilar *et al.*, 2007). This becomes visible by the high level of temporal and spatial organization (Branda *et al.*, 2001) of biofilms harboring cells with various cell-differentiation levels (Cairns *et al.*, 2014, Vlamakis *et al.*, 2008). *B. subtilis* biofilms underlay the typical biofilm developmental stages as mentioned before, starting with the initial attachment of cells to an interface, biofilm development and the dispersion, which is negligible for agar-based biofilms. A mature biofilm, grown for three days on a biofilm promoting medium harbors a variety of specialized vegetative cells, producing extra polymeric substances to create a matrix or (exo-)proteases to lyse dead cells (Cairns *et al.*, 2014, Dragoš *et al.*). Pioneering cells, which are still flagellated, might occur in the rim regions (Vlamakis *et al.*, 2008), broadening the diameter of the biofilm (Diethmaier *et al.*, 2011, Guttenplan & Kearns, 2013). The top regions of mature *B. subtilis* biofilms exhibit higher levels of spores and spore-forming cells, which were formerly described as fruiting bodies (Branda *et al.*, 2001). At the interface between air and biofilm the hydrophobic BslA-protein (formerly YuaB) self-assembles to a surface layer which protects the underlying cells from hazardous environmental influences (Hobley *et al.*, 2013, Ostrowski *et al.*, 2011, Kobayashi & Iwano, 2012). The BslA surface layer is one of the most important characteristics of a typical *B. subtilis* biofilm to maintain the osmotic and chemical stability inside the biofilm. Interestingly, the surface-layer is affected by the nutrient medium and differs between individual strains (Werb *et al.*, 2017). BslA-deficient mutants exhibit less-wrinkled phenotypes (loss of surface roughness) and are therefore less resistant to shear forces (Kesel *et al.*, 2016). A representation of a schematic *B. subtilis* cross section is shown in Figure 4, demonstrating the multicellularity and cell differentiation as well as typical architectural characteristics, such as wrinkle formation or the curvy basal biofilm end.

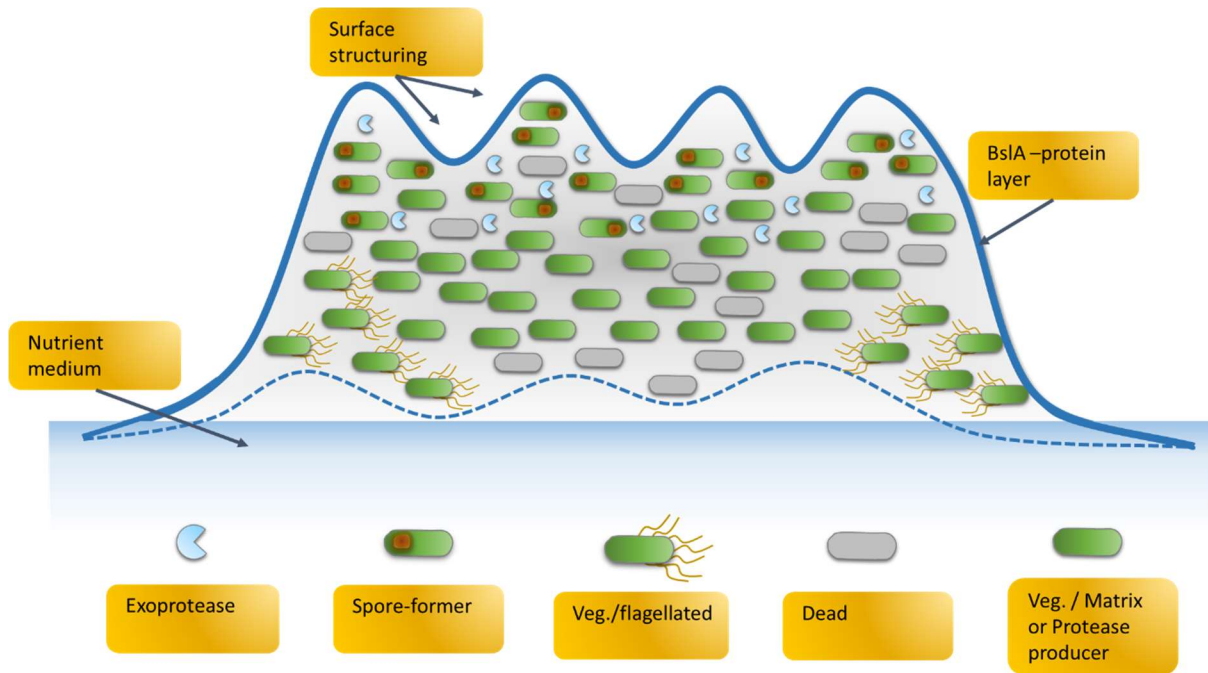


**Figure 4: Schematic cross section of a *B. subtilis* biofilm**

Mature *B. subtilis* biofilms exhibit various characteristic features: The biofilm surface is covered by a BslA protein layer (shown in blue). The basal end towards the substratum or nutrient medium is covered by a mixture of EPS, vegetative (green rods) and dead cells (gray rods). Flagellated rods can be found at the rim regions, where movement enhances the chance of broadening the biofilm diameter. Some of the vegetative cells govern the function as exoprotease producers (blue pie charts), which help to degrade dead cells or actively decay cells which are not of use for the biofilm community. Within the apical regions as well as in regions where more nutrients are depleted, sporulation sets in and spore-forming cells and spores are more prominent. The apical regions are often extremely structured, exhibiting valleys and elevated structures, which are more prominent in the central biofilm region than in the rim regions. To simplify the figure, the interconnecting EPS composed of structural proteins, polysaccharides and nucleic acids is only shown as a grey shadow in the background. Especially the basal regions and the biofilm center as oldest part of a colony biofilm increasingly show EPS-structures. Scheme was adapted after Cairns *et al.*, reviewing regulatory strategies and assembly mechanisms in *B. subtilis* biofilms (Cairns *et al.*, 2014).

### ***B. subtilis* biofilm differentiation and regulation of structural components**

As mentioned before, a population of isogenic *B. subtilis* cells or spores is typically used to form a biofilm under laboratory conditions. After 24 h of incubation a first differentiation of phenotypes becomes visible: Cells lose their ability to move actively while others still exhibit working flagella, other cells produce proteases (bacillopeptidase and subtilisin) (Gonzalez-Pastor, 2011) and excrete them or produce matrix components such as TasA (assembles to amyloid fibers) (Ostrowski *et al.*, 2011) or surfactin which is used as bactericide and fungicide and helps to wet the agar surface (Nakano *et al.*, 1991, Branda *et al.*, 2001). Forming a biofilm on single-cell level is energetically expensive due to the production of many extra-cellular components which in the end provide the building blocks for the matrix and the surface layer. Therefore, the entry of biofilm-formation is regulated over a signal chain that is dependent on sensor kinases which phosphorylate and therewith active different downstream regulatory proteins.

The best studied key regulator is Spo0A (or its phosphorylated version, Spo0A~P), which is the main transcription factor regarding the entry of the biofilm and sporulation stage (Vlamakis *et al.*, 2013, Branda *et al.*, 2001, Hamon & Lazazzera, 2001, Molle *et al.*, 2003). Once activated, two different biofilm-related pathways that are commonly repressed are activated by anti-repressors (for AbbA,

which repressed AbrB and SinI which repressed SinR) (Chai *et al.*, 2008). SinR represses the transcription of typical motility genes such as *hag* (flagellin protein), *lytA* (secretion of major autolysin LytC, needed for flagellar function) and *lytF* (major autolysin, cell separase) (Chai *et al.*, 2010). On the other hand, AbrB enables the transcription of the *epsA-O*-operon (Gerwig *et al.*, 2014, Kearns *et al.*, 2005), which harbors the most important biofilm related genes and activates *tapA-sipW-tasA* operon (TasA, forms amyloid-like fiber structures; TapA, accessory protein for TasA cell attachment) (Branda *et al.*, 2006, Branda *et al.*, 2004, Romero *et al.*, 2010, Romero *et al.*, 2014) and *bslA* (hydrophobic surface layer protein, which is expressed in all biofilm cells at different levels) (Hobley *et al.*, 2013). Therefore, SinR and AbrB are mediated by a double negative feedback loop throughout intermediate levels of SpoA0~P, which if not or barely phosphorylated leads to motile planktonic. On the opposite, very high levels of SpoA0~P slows down matrix production and support the sporulation via the bistability of SinR (and SlrR which is an antagonist of SinR and SlrA that represses SinR) (Kampf *et al.*, 2018, Chai *et al.*, 2008). Solely the inhibition of the flagellar movement triggers the phosphorylation via DegS of DegU → DegU~P, which at intermediate levels promotes biofilm formation (*bslA*, *epsA-O* operon and *tapA-sipW-tasA* operon) similar as SpoA0~P does (Mader *et al.*, 2002, Holscher *et al.*, 2018, Marlow *et al.*, 2014b). Elevated and high levels of DegU~P and in parallel high levels of SpoA0~P inhibit the transcription of the aforementioned genes (Marlow *et al.*, 2014b, Verhamme *et al.*, 2009).

The differentiation of individual cells is directly coupled with their function within the biofilm (Dragoš *et al.*). Apart from the complex genetic regulation of the biofilm, which requires the quorum sensing of environmental and endogenous signals such as surfactin production and excretion, many other external factors have a strong influence on the biofilm phenotype (Veening *et al.*, 2006). Depending on the culture medium, biofilms show differences in their structure (Werb *et al.*, 2017) and therewith resistance and young *B. subtilis* biofilms are far more differentiated than mature or old biofilms, showing low levels of spores and high activity of vegetative cells, which is strongly decreasing with time and the associated nutrient depletion (Fuchs *et al.*, 2017a). Most studies have been performed by using NCIB 3610 that, in contrast to 168 forms highly structured biofilms on biofilm promoting media other than the standard medium LB, on which biofilms are less structured. Other strains such as *B. subtilis* B1 are able to form an extracellular matrix which exceeds the EPS of NCIB 3610 by multiple times (Morikawa *et al.*, 2006, Morikawa *et al.*, 1992) and the wild-type strain PS 216 exhibits more detailed surface structures compared to NCIB 3610 (Durrett *et al.*, 2013b). The phenotype not only depends on the endogenous differences between the species and their complex genetic regulation via double negative feedback loops, which vary on the phosphorylation level of SpoA0 and DegU, but also on the external environmental parameters. *B. subtilis* is therefore able to influence its biofilm formation or its degradation in a self-driven way and always adapts to the given situation (Branda *et al.*, 2004). By degrading certain biofilm regions by producing surfactins as signal molecules or antimicrobial toxins (Skf and Sdp) the biofilm can constantly restructure itself (Lopez & Kolter, 2010).

### ***B. subtilis* germination and outgrowth**

Another key feature of *B. subtilis* as model organism is the ability to form highly resistant endospores (see “Excursion: Sporulation of *B. subtilis*” in the appendix under section 7.1). Spores persist in a status of metabolically inactivity also known as dormancy. Nevertheless, spores are able to sense the environment for nutrients or specific germination triggers (germinants) to detect passively and energy-independent favorable growth conditions to revive into their vegetative form (Setlow *et al.*, 2017). Germination receptors (GRs), located in the inner membrane, are able to bind L-alanine,

L-valine and L-asparagine and activate the cascade of initiating the germination whereas D-amino acids do not show any germinant properties (Setlow, 2014, Atluri *et al.*, 2006). Other germinants can be extreme pressure (100- 350 MPa; GRs and 500-1000 MPa; SpoVA channels) (Reineke *et al.*, 2013), the cationic surfactant dodecylamine (SpoVA channel) (Setlow *et al.*, 2003), sugars such as glucose or fructose (Alzahrani & Moir, 2014), Ca<sup>2+</sup>-DPA or peptidoglycan fragments (Shah *et al.*, 2008) as reviewed by Setlow (Setlow, 2014). Furthermore, spores tend to germinate spontaneously to a small extent (Sturm & Dworkin, 2015). Once germination has started, the process is irreversible and a reentry into the spore-form is energetically not possible without external nutrient uptake and the metabolization thereof (Yi & Setlow, 2010). Right after reaching a threshold of GR- or SpoVA channel activation, monovalent cations such as H<sup>+</sup>, Na<sup>+</sup>, K<sup>+</sup> (and Zn<sup>2+</sup>) are released from the spore core (commitment phase) (Swerdlow *et al.*, 1981). In the next stage (I), Ca<sup>2+</sup>-DPA is released, resulting in a stepwise rehydration of the core (Setlow, 2014). One of the major spore resistance properties, the resistance towards heat is lost upon the release of Ca<sup>2+</sup>-DPA (Luu & Setlow, 2014, Jedrzejewski & Setlow, 2001). Meanwhile, the core expands increasingly with the hydrolysis of the cortex (catalyzed by CwlJ and SleB) and outgrowth to the vegetative state is initiated (stage II) (Li *et al.*, 2013b, Setlow, 2014). In parallel SASP are degraded (ClpP-like protease) and the chromosome regains its full accessibility (Traag *et al.*, 2013).

During the release of Ca<sup>2+</sup>-DPA in stage II of germination, the refractive index of the spore changes, which can be detected by phase contrast microscopy or photo spectrometry (Pandey *et al.*, 2013). Dormant spores appear phase-bright, while germinating spores turn gray to black within several minutes after facing a germinant (Dawes *et al.*, 1969, Sinai *et al.*, 2015).

Once ~80 % of the water content is restored in the core, first cellular functions regain activity and the reentry to the vegetative state transforms the spore into a cell (Setlow, 2014). This process is also known as “ripening”, activating the protein biosynthesis due to the lack of stored proteins within the core under use of the marginal stored endogenous metabolites (mainly ATP by conversion of 3-phosphoglycerate) (Moir, 2006, Sinai *et al.*, 2015, Segev *et al.*, 2013, Singh & Setlow, 1979). Shortly after the consumption of all internal energy sources, exogenous metabolites are needed within the first minutes after germination (Setlow & Kornberg, 1970, Keijser *et al.*, 2007). If germination takes place in absence of nutrients, germination proceeds until all endogenic energy is consumed, but the spore will not result in a viable vegetative phenotype. Depending on the nutrient availability and the intensity of needed DNA-repair, the first full chromosomal copy can be observed 30 min after germination start (Garrick-Silversmith & Torriani, 1973). In the following 30-60 min, the membrane and cell wall are synthesized and the reinforcement allows the former spore to swell (Plomp *et al.*, 2007). Upon swelling, the spore-coat layers and the cortex remains break open ('burst', after ~70-100 min) so that the typical vegetative, rod-shaped phenotype is formed (Pandey *et al.*, 2013, Keijser *et al.*, 2007). Depending on nutrient availability, the first cell division often takes place shortly after the 'burst' and cells are already flagellated and thus motile (Keijser *et al.*, 2007).

### Endospore resistance

Due to their various resistances, spores can survive for long periods and are therefore often used as reference in survival experiments or to verify the effectiveness of autoclaves. Currently an experiment is trying to monitor the viability and germination properties of *B. subtilis* spores over a period of 500 years (Ulrich *et al.*, 2018). Ferdinand Cohn was the first scientist, discovering in 1872 that rod-shaped bacteria (presumably *Bacillus sp.*) can survive boiling – the first indication of a spore-forming species in history (Soule, 1932). Since then, a typical school experiment is a “hay-infusion”, a mixture of water and hay to promote bacterial growth. When boiling all ingredients, spores will

survive and a selection towards *B. subtilis* cells takes place. This experiment is based on the early research of Ferdinand Cohn and helps to educate undergraduates in the field of microbiology.

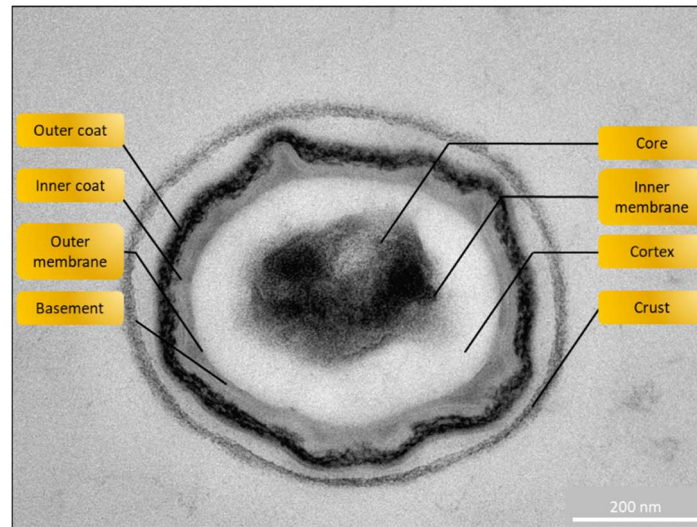


**Figure 5: TEM cross section of a *B. subtilis* spore**

The image demonstrates a *B. subtilis* NCIB 3610 spore grown on MSgg agar for 40 h. The sample was cut along its transverse axis exhibiting concentrically arranged structural characteristics. The center of the spore governs the core, in which the DNA is strongly associated with small acid soluble proteins (SASP). The core is enclosed by the inner membrane. The next surrounding layer comprises the germ cell wall or cortex region that is separated from the spore basement by the outer membrane. The final protein layers are called the inner and outer spore coat, which are significantly involved in resistance to harmful environmental influences. On the spore outside, a crust is formed which in *B. subtilis*, in contrast to other spore formers, is probably a rudiment of a former exosporium. Scale bar represents 200 nm.

Generally, *B. subtilis* spores are able to withstand UV, gamma and heavy-ion irradiation, the aforementioned extreme temperatures (boiling), shear-forces, salinity, acidity and most toxic chemicals such as oxidizing agents or antibiotics (Moeller *et al.*, 2012a, McKenney *et al.*, 2013, Horneck *et al.*, 2010, Nicholson *et al.*, 2000). The resistance is based on several different structural features. Spores are relatively small, ~1-2  $\mu\text{m}$  in length and ~0.5-1  $\mu\text{m}$  in diameter (Carrera *et al.*, 2007). On the outside several concentric protein layers form the crust, followed by the outer and inner spore coat as well as the so-called basement layer (Leggett *et al.*, 2012, McKenney *et al.*, 2010). About 50-80 % of the total proteins within spores belong to more than 70 different coat proteins (McKenney *et al.*, 2013, Driks, 1999), which have a strong influence on withstanding several decontamination procedures (Raguse *et al.*, 2016a, Cortesão *et al.*, 2019, Nagler *et al.*, 2015, Setlow, 2006b, Raguse *et al.*, 2016b). The spore-coat also serves as a chemical barrier (for macromolecules), protecting the outer membrane and the peptidoglycan cortex from lytic enzymes or pH-changing substances (Setlow, 2003, Driks, 1999). The cortex itself is needed to pressurize the spore core to maintain the dehydration which is essential for the dormancy (Popham, 2002). High levels of  $\text{Ca}^{2+}$ -DPA, minerals, the low water content (25-45 %) and the cortex-pressure stabilize the spore core and immobilize all proteins, lipids and the chromosomal and plasmid DNA (Sunde *et al.*, 2009, Kaieda *et al.*, 2013, Loison *et al.*, 2013, Huang *et al.*, 2007).  $\text{Ca}^{2+}$ -DPA furthermore protects the spore from UV and  $\gamma$ -irradiation (Moeller *et al.*, 2014, Nicholson *et al.*, 2000). The chromosome is strongly associated with two major SASP ( $\alpha$  &  $\beta$ ), which protect the DNA by binding from UV- (but not ionizing-) radiation, heat and other harmful conditions (Mohr *et al.*, 1991, Setlow, 2006b, Wang *et al.*, 2006). As Setlow reviewed in 2006, UV-light at 254 nm does not form cyclobutane dimers and 6-4-photoproducts between pyrimidines in the DNA of spores, but leads to a spore specific

5-thymidyl-5,6-dihydrothymine adduct - the spore photoproduct (SP) (Setlow, 2006a, Slieman *et al.*, 2000). SPs lead to less severe lethality than cyclobutane dimers and 6-4-photoproducts can be easily counteracted upon germination by the spore photoproduct-lyase (Spl) or by homologous recombination and excision repair by RecA, a major protein involved in DNA-repair (Slieman *et al.*, 2000, Setlow, 2006b, Vlastic *et al.*, 2014). The water content within the spore core depends on the temperature during sporulation and thus the heat and radiation resistance (among other resistances regarding the spore-coat and cortex) is directly affected (Melly *et al.*, 2002).

### ***Bacillus subtilis* in space research**

Space research is often linked to extreme environmental exposure to cold, radiation, nutrient depleted conditions under the influence of microgravity (Horneck *et al.*, 2010). Apart from tardigrades barely any other animal is capable of surviving these conditions (Jonsson, 2007). Therefore microbes can serve as model systems to investigate the biological effects of exposure to space conditions (Horneck *et al.*, 2012, Moeller *et al.*, 2012b). One of the most prominent space-experienced microorganisms is *B. subtilis*, which was among the first bacteria that have been intentionally sent to space. In a particular experiment in November 1964, dried samples (presumably spores) of *B. subtilis* 168 were carried into the thermosphere by balloon to an altitude of 155 km and were exposed for 233 secs to the conditions prevailing there (Hotchin *et al.*, 1965). Since then, vegetative *B. subtilis* cells and spores were used for many further space studies (Weber & Greenberg, 1985, Horneck, 1993).

The multifactorial resistance due to the ability to form spores is still one of the most important assets mainly the *Bacillus* genus harbors - apart from *Clostridia*, which are more complex to handle (mainly anaerobic) and a potential risk to carry into space (Edwards *et al.*, 2013, Fordtran, 2006). Space experiments are usually protected by several containment levels, but *Clostridia* spores could accidentally be released which pose a potential threat to the crew. Nevertheless, *Clostridia* spores have been found within the *Mir* and the ISS, but in low abundance, compared to the amount of cell/spores typically used for an experiment (Skuratov *et al.*, 2002, Voorhies *et al.*, 2019). The uncomplicated handling of *B. subtilis* regarding their cultivation requirements is a favorable contrast to the already complex space environment. Spores are desiccation resistant so they can easily survive the long storage and waiting times that can occur before a space flight (flight delays) and still remain germinable. In addition, *B. subtilis* spores are immune to cold and show a high resistance to UV- and  $\gamma$ -radiation (Horneck *et al.*, 2010, Horneck *et al.*, 2012). Even without targeted experiments with *B. subtilis*, spores that have survived decontamination according to the planetary protection guidelines can be found on board the ISS (Checinska Sielaff *et al.*, 2019, Venkateswaran *et al.*, 2014).

In parallel to early space research using spores as a model system (1970s-80s), Bill Costerton emerged as one of the most important scientists in the field of intensive biofilm research, who worked considerably on the sensitization of the biofilm-topic (Hoiby, 2017). Previously, bacterial colonies were often regarded as a composition of planktonic cells, and with the increasing understanding of biofilm formation new fields of research were created. Years later, the interest in *B. subtilis* biofilms arose in 2001 when Branda *et al.* published a paper on biofilm formation and thus set a milestone in *Bacillus* research (Branda *et al.*, 2001).

The era of space stations promoted bacterial life in space for longer periods, than shuttle and satellite missions could ever offer before. Bacterial and fungal biofilms were increasingly found on the former *Mir*-station and the ISS, which underlined the importance to understand which processes in biofilm formation differ between microgravity and gravity on Earth (Makimura *et al.*, 2001, Matin

& Lynch, 2005, Checinska Sielaff *et al.*, 2019). In order to answer this question, fungal and bacterial model systems such as *B. subtilis* are used to observe potential fundamental changes. In contrast to several experiments concerning the viability of spores after exposure to space conditions, biofilm formation under the same conditions has so far only been studied to a very limited extent (Loudon *et al.*, 2018, Morrison *et al.*, 2019). However, it is very difficult to cultivate biofilms under 'natural conditions' in a laboratory or on the ISS, therefore monocultures instead of multi species biofilms are used, which have to grow under certain defined conditions. This is the only method to ensure that generated data and knowledge is reliable and reproducible. In consideration of the challenging conditions related to space research, *B. subtilis* offers a non-pathogenic, modifiable platform for spore and biofilm research in space.

## 1.6 Simulation of space conditions

Biological space research is a very complex and difficult task to undertake. It must be planned over a very long period of time with considerable financial commitment (Su *et al.*, 2013). In the past, research was almost exclusively conducted by the several space agencies such as NASA, ESA, Roscosmos or JAXA. From a proposal to an experiment, various bureaucratic hurdles have to be overcome and experiments have to prove themselves against many others in order to be included in the list of possible flight candidates. However, approved experiments cannot be freely designed, but must always be subject to the safety regulations of the respective space agency. For example, two to three safety containment levels are required to safeguard a microbiological experiment so that in case of an emergency the space station is not contaminated. The availability of equipment time such as cooling, heating, the use of centrifuges or the power supply is limited. Especially the crew time (working time of the astronauts) is very expensive, because the astronauts have to be specially trained on the ground for this task or have to learn this on board the space station via instructions. Simple experiments which require little or no human assistance and which can be started and completed externally (com-link) often have a higher success in being admitted. Recently, smaller commercial providers have been offering the opportunity to conduct experiments in space at affordable prices, which were previously strictly controlled by the agencies. However, they are still expensive for small laboratories and are also subject to the usual safety regulations. In order to overcome the limitations of spacecraft-related research, a multitude of different simulation opportunities are available on Earth which are known as ground based facilities (GBFs) (Herranz *et al.*, 2013a, Brungs *et al.*, 2016). Usually the effect of a single space parameter is investigated, to exclude potential side effects and to assure the reliability of the experiment. Therefore, several methods have been developed in the past decades to simulate one or more space conditions such as: space-like vacuum, extremely cold temperatures,  $\gamma$ -, UV- and heavy ion radiation, desiccation, nutrient and water depletion as well as the simulation of microgravity. Simulations offer the possibility to investigate the influence of a certain parameter with a variable number of samples, which in contrast to the space experiment no longer represents a case study. As summarized by Hemmersbach 2016 in a topical issue, ground-based experiments can be easily reproduced and provide reliable data to estimate actual effects of space conditions (Hemmersbach *et al.*, 2016). On the other hand, simulations offer limited capabilities, which - if possible - should be supported by space experiments for the absolute confirmation of the findings (Su *et al.*, 2013). Unfortunately, many experiments cannot be carried out in space, due to the limitations in financing, time, work force, tools and devices. Simulations provide a promising transition between investigating space conditions with the possibilities of GBFs. Acquired simulation-based data of biological experiments is typically used to prepare space missions in order to estimate a potential experimental outcome and



to prevent possible hurdles, such as unexpected results or drawbacks of avoidable errors (Brungs *et al.*, 2016).

### Simulation of microgravity

The omnipresent microgravity in space (ISS:  $\sim 1 \times 10^{-4} / 10^{-6}$  g to  $1 \times 10^{-12}$  g, deep space) is one of the parameters, which is in no relation to the conditions on Earth ( $1g = 9.81 \text{ m/s}^2$ ; within this thesis terrestrial gravity is always abbreviated with “1g” – in literature, sometimes “1xg” can be found which is identical with 1g). Since time immemorial, flora and fauna adapted to gravity on Earth (Anken & Rahmann, 2002) to which all chemical, physical and biological processes have adapted. The changes in the physiology of bacteria under the influence of microgravity have hardly been studied so far, but with increasing research it offers a broader understanding of the adaptation of life on our planet. With regard to biological experiments, several methods were developed to test the influence of microgravity: One of the oldest concepts is the free fall, which can be achieved either within an evacuated free-fall tower or by parabolic flights. Both methods offer up to 9.3 secs (Sondag & Dittus, 2016), respectively  $\sim 20$ -30 sec of free fall (Pletser, 2004), which is suitable for many experiments, but insufficient to investigate cell growth or differentiation. Further suborbital platforms for the simulation of space microgravity are sounding rockets from i.e. the MAXUS (13 min) (Hemmersbach *et al.*, 1998), TEXUS ( $\sim 6$  min) (Corydon *et al.*, 2016) program or re-entry capsules ( $>2$  weeks, i.e. FOTON-missions), which both provide a microgravity quality of  $\sim 10^{-5}$  g, but are rarely available and expensive (Gulimova *et al.*, 2019). For long-term studies to grow bacteria and cell cultures over several generations, different devices and methods have been developed within the GBFs to simulate microgravity on Earth. Von Sachs described 1872 the idea of an omnilateral rotation-based equalization of the gravitational vector to zero-g by rotating plants (0.1, 0.05 and 0.03 revolutions per minute) along a 2-D axis (Newcombe, 1904). In 1904, Newcombe developed the first fully electrically driven clinostat (*lat. klinein*, tilting, tilted and *lat. statós* standing, posed) on the idea of von Sachs device and discussed the evenness of speed with regard to the effects on the given stimulus (Newcombe, 1904). Since then, the 2-D clinostat established as model in science to simulate (micro-) gravitational changes or vector-averaged gravity (Klaus, 2001, Herranz *et al.*, 2013a). The concept is based on the hypothesis, that small objects such as plant seeds, algae or bacteria are not able to perceive the influence of microgravity if they are constantly rotated along an axis (Herranz *et al.*, 2013b). The vector of gravity changes depending on the position of the sample: The closer a sample is located to the rotation axis, the better the microgravity simulation. With decreasing distance to the axis, shear forces occur and the gravitational force increases (van Loon, 2007). Therefore, 2-D clinostats are mainly used for small objects with a small diameter. In addition, the rotation speed strongly affects the outcome of the experiment and should not be too high in order to avoid additional shear forces and not too weak for gravitation to be perceived (van Loon, 2007). Several microgravity studies are conducted in liquid-filled, small diameter pipette clinostats, which allowed clinorotation of eukaryotic cells (and other) (Brungs *et al.*, 2015). In contrast, plant seeds were increasingly used on agar-based nutrient media on clinostats, often while applying minor revolutions per minute (Ishii *et al.*, 1996). Agar offers the advantage that up to 60 rpm and more can be used for the cultivation of bacteria without promoting additional shear forces due to the agar-attachment. Nevertheless, gravity sensing mechanisms and stress-responses could still exceed normal levels if the object of interest (agar-based 2-D clinorotation) is too far away from the axis of rotation or is exposed to additional shear forces (pipette clinostats). Further methods based on the same principle are the rotating wall vessel (RWV), rotating wall bioreactor (RWB), rotary cell culture system (RCCS) and high-aspect rotating vessels (HARVs), which all share the same principle of

rotating mainly liquid samples such as cell cultures along an axis to provide low-shear modeled microgravity (sim- $\mu$ g or LSSMG) (Schwarz *et al.*, 1992, Huang *et al.*, 2018, Brungs *et al.*, 2011). This method was developed by NASA and is used as a ground control or for preliminary experiments for space experiments (Wolf & Schwarz, 1991).

Instead of only one rotation axis, 3-D clinostats or random positioning machines (RPMs) are based on two independently rotating axes, which result in averaging the vector of gravity three dimensionally on the object of interest display (Briegleb, 1992, Klaus, 2001, Hoson *et al.*, 1997, Herranz *et al.*, 2013a). By using the RPM, the movement in the three-dimensional space causes a continuously changing influence of the gravitational vector in the sample, similar to that in the 2-D clinostat (only along the rotation axis), whereby a targeted perception of gravity is prevented (van Loon, 2007). In order to avoid a constant rotation, the speed and direction is randomly generated and nullifies the vector of gravity over time (Wuest *et al.*, 2014). The 2-D and the 3-D clinostat share the same principle of simulating a microenvironment in which the sample is not able to recognize the vector of gravity while being constantly rotated. Furthermore, both simulation devices can be used with agar-based media to facilitate bacterial growth and to minimize potential shear-forces that occur during culturing in rotating liquids (Wuest *et al.*, 2017).

### Simulation of space radiation

Most biological experiments in space were conducted to analyze the effects of microgravity and thus were protected against the harmful space radiation. Latter is composed of mainly protons (hydrogen nuclei) and other charged particles from solar winds (solar cosmic radiation, SCR) as well as cosmic rays (galactic cosmic radiation, GCR). As Horneck reviewed in 2010, GCR is composed of 98 % baryons (85 % protons, 14 %  $\alpha$ -particles and 1 % heavy nuclei) and 2 % electrons also known as HZE particles (high energy charged particles) (Horneck *et al.*, 2010). According to Horneck, cosmic rays with high charges ( $z > 2$ , or greater than helium) cause energies high enough to penetrate space hardware shielding of 1 mm and are therefore biologically harmful, even though they only represent 1 % of the GCR composition (Horneck *et al.*, 2010). Direct effects of radiation mainly rely on the ionization of proteins, nucleic acids or biomolecules or indirect generated by radicals (i.e.: reactive oxygen species, ROS: OH $\cdot$ ; reactive nitrogen species, RNS: NO $\cdot$  or superoxide: O $_2^{\cdot-}$ ), which can cause oxidative stress within cells (Horneck *et al.*, 2006, Hayyan *et al.*, 2016). Direct and indirect radiation effects cause DNA damage, which can mutate the genetic material or damage the cell lethally (Moreno-Villanueva *et al.*, 2017). The effects of radiation and the associated DNA-repair after exposure was already subjected in several space missions (Apollo 16, Spacelab 1, D2), which exposed *B. subtilis* spores to different levels of radiation (Horneck *et al.*, 1994, Facius *et al.*, 1979, Buecker & Horneck, 1975, Horneck *et al.*, 1974). In particular, the DNA-repair of germinating spores after irradiation was intensively studied and provided in-detail knowledge about the molecular mechanisms (Setlow, 2006b, Setlow & Setlow, 1996). So far, most studies have been conducted on the viability and associated DNA repair of spores exposed to either space radiation or defined radiation conditions (Moeller *et al.*, 2014, Zammuto *et al.*, 2018, Nicholson *et al.*, 2012, Wassmann *et al.*, 2012). For that, primary gamma radiation (i.e. X-rays) were used for the simulation of ionizing radiation. However, all studies have been conducted with *B. subtilis* spores grown under terrestrial (1g) gravitational conditions. Experimental-based knowledge regarding the effects on survival of spores grown under simulated microgravity (sim- $\mu$ g) is missing. Although some experiments were carried out in microgravity (Facius *et al.*, 1979, Buecker & Horneck, 1975), germination and DNA-repair was only monitored under 1g conditions. For most radiation-based experiments, X-rays are preferably used to generate ionizing radiation. Many X-ray systems are commercially available, which, depending on the

distance of the emitting cathode, can apply targeted doses to the sample (Moeller *et al.*, 2007b). The dose rate is measured using a dosimeter to calculate the desired dose to be applied. Bacterial samples, such as dried *B. subtilis* spores and biofilms can be irradiated by exposing them in the direct radiation path. The simulation of HZE-particles, which comprise the most dangerous part of GCR can be achieved by accelerating heavy ions using a heavy ion accelerator (Moeller *et al.*, 2008). Depending on the applied ion species, the linear energy transfer (LET, keV/ $\mu\text{m}$ ) rate differs significantly. Therewith the deposited energy and the caused cellular damage increase (Moeller *et al.*, 2008). The effects of heavy ion radiation on *B. subtilis* biofilms have not yet been investigated.

## 1.7 Relevance and Hypotheses

### Relevance

With increasing advances in technology, the commercialization of space travel as well as the intention to colonize Mars or establish permanent space bases, the safety of astronauts or passengers must be guaranteed. With regard to the *Mir*-Station and the ISS, bacterial and fungal biofilm formation showed to cause considerable damage to the spacecraft and even poses a health risk to astronauts. So far only little is known about biofilm formation under space conditions such as the lack of gravity or elevated levels of radiation. A few studies showed that cell growth was influenced or that changes in pathogenicity occurred. Within the framework of this thesis, the Gram-positive bacterium *Bacillus subtilis* was used as model organism to investigate the effects of different simulated space-relevant conditions on its biofilm and spore formation. The aim of this research is to clarify to what extent *Bacillus subtilis* biofilms behave under microgravity, increased radiation or other parameters and whether these observations can also be transferred to other species.

### Hypotheses

- (I) Simulated microgravity affects the architectonical structure and composition of *B. subtilis* biofilms in comparison to biofilms grown under normal gravity conditions (based on the findings of e.g. Kim *et al.*, 2013 and others).
  - To investigate the hypothesis, microscopic techniques, surface analysis methods, as well as physiological and morphological examinations and the investigation of the proteome and transcriptome will be applied.
- (II) Simulated microgravity affects the resistance properties of *B. subtilis* spores and biofilms in comparison to terrestrial gravity conditions (based on the reviews of Senatore *et al.*, 2018, Taylor, 2015 and others).
  - To investigate the hypothesis, spores and biofilms of *B. subtilis* are exposed to nutrient depletion,  $\gamma$ - and heavy ion radiation, vacuum, antibiotics as well as wet and dry heat to evaluate survivability under these conditions.
- (III) Simulated microgravity affects the sporulation and germination behavior of *B. subtilis* in comparison to terrestrial gravity conditions.
  - To investigate the hypothesis, *B. subtilis* cells will be stimulated to sporulation and examined with regard to sporulation efficiency. In addition, spores will be examined with regard to their germination properties.

## 2. Material & Methods

### 2.1 Bacterial strains

In order to investigate the influences of extra-terrestrial conditions on bacterial biofilms, the Gram positive model organism *Bacillus subtilis* offers a variety of useful features. The wild-type strain *B. subtilis* NCIB 3610 (also known as DSM-10, hereinafter NCIB 3610 or *wt*) is able to form highly structured biofilms in contrast to domesticated strains such as *B. subtilis* 168 (Branda *et al.*, 2001, Zeigler *et al.*, 2008, McLoon *et al.*, 2011). Both strains and their close relatives such as wild-type isolates as PS 216 or B1 have the ability to form endospores under nutrient depletion (Morikawa *et al.*, 2006, Durrett *et al.*, 2013b). Spores represent a non-metabolically active, dormant form of life, which strongly preserve and protect their DNA, still able to outgrow under more favorable conditions. Spores can be stored for long periods and remain stable in water. Biofilm experiments in this work were mainly inoculated with dormant spores which allow adjusting the precise number of spore entries. With regard to the elucidation of the biofilm structures under simulated microgravity, various mutants were used (Table 1). These include strains that do not possess individual genes coding for structural elements such as *tasA* or *bslA* or the main operon for biofilm genes, *epsA-O*. All mutant strains were derived from the strain DK1042 (NCIB3610 background) which harbors a deletion of *comI*, that allows easier transformation (Konkol *et al.*, 2013). The strains were obtained from the DSMZ (German Collection of Microorganisms and Cell Cultures GmbH), or friendly supported by Dr. M. Opitz, Prof. D. Dubnau, Prof. Á. Kovács and Prof. J. Stülke as well as M.Sc. S. Giri. Several strains were transformed in frame of this thesis but only one was used for biofilm cultivation experiments. All strains, their genotype, background and origin are listed in the subsequent table (Table 1).

#### Storage of vegetative cells and spores

After arrival, strains were streaked out using the 13-streak method on fresh LB-agar (Luria Bertani) plates containing the respective marker(s) such as antibiotics. Plates were incubated overnight at 37 °C (min. 15 h). Subsequently, a single colony was transferred into a glass tube containing 5 ml LB-broth including the same marker(s) as used before and incubated overnight at 37 °C, shaking at 200 rpm. After incubation, the cell suspension was thoroughly vortexed and 2 ml were pelletized by centrifugation at 20 °C at 3000 × g for 2 min and the supernatant was carefully discarded. After addition of 2 ml 1x PBS-buffer and resuspension, cells were pelletized as described before. The supernatant was carefully removed and 750 µl of 2x LB-broth were added for resuspension. The suspension was used to inoculate 2 ml Nalgene® plastic screw cap tubes containing 750 µl glycerol to prevent ice crystal formation and facilitates thawing of the samples. Screw cap tubes were stored at -80 °C to create a long-term repository. If a strain was needed, a frozen aliquot was thawed on ice and was accessed with a sterile loop to streak out the stored bacteria.

In contrast to storage of vegetative cells, spore solutions can be stored for longer periods at 4 °C. Therefore, purified spores are diluted with sterile ddH<sub>2</sub>O until the desired concentration is reached, mixed with several glass beads (5-10, ø 2 mm) and stored in a screw cap glass tube.

**Table 1: B. subtilis strains used in this study**

<b>Strain</b>	<b>Background</b>	<b>Genotype</b>	<b>Antibiotic resistance [µg/ml]</b>	<b>Reference</b>
<b>168</b>	wild-type	<i>wt</i>	-	(Zeigler <i>et al.</i> , 2008)
<b>NCIB 3610</b>	wild-type	<i>wt</i>	-	(Conn, 1930, Zeigler <i>et al.</i> , 2008)
<b>PS216</b>	wild-type	<i>wt</i>	-	(Durrett <i>et al.</i> , 2013a)
<b>TB34</b>	NCIB 3610	<i>amyE::Phy-gfp(Cm)</i>	cat [5]	(Seccareccia <i>et al.</i> , 2016)
<b>TB35</b>	NCIB 3610	<i>amyE::Phy-mKATE2(Cm)</i>	cat [5]	(Hölscher <i>et al.</i> , 2015)
<b>TB36</b>	NCIB 3610	<i>amyE::Phy-gfp(Cm), Δhag::Km</i>	cat [5], kan [5]	(Richter <i>et al.</i> , 2018)
<b>TB37</b>	NCIB 3610	<i>amyE::Phy-mKATE2(Cm), Δhag::Km</i>	cat [5], kan [5]	(Richter <i>et al.</i> , 2018)
<b>TB159</b>	NCIB 3610	<i>amyE::Phy-gfp(Cm), ΔepsA-O::Tc</i>	cat [5], tet [5]	unpublished
<b>TB160</b>	NCIB 3610	<i>amyE::Phy-mKATE2(Cm), ΔepsA-O::Tc</i>	cat [5], tet [5]	unpublished
<b>N24</b>	NCIB 3610	<i>bslA::cat</i>	cat [5]	(Kobayashi & Iwano, 2012)
<b>B1</b>	wild-type	<i>wt</i>	-	(Morikawa <i>et al.</i> , 2006)
<b>ZK 3660</b>	NCIB 3610	<i>ΔepsA-O::Tet</i>	tet [12,5]	(Branda <i>et al.</i> , 2006)
<b>CA0 17</b>	NCIB 3610	<i>ΔtasA::Kan</i>	kan [50]	(Vlamakis <i>et al.</i> , 2008)
<b>DK1042</b>	NCIB 3610	<i>ΔcomI</i>	-	Konkol 2013
<b>F-030/ ΔsigG</b>	NCIB 3610	<i>ΔcomI, ΔsigG::cat</i>	cat [5]	this study
<b>ΔlysA</b>	NCIB 3610	<i>ΔcomI, ΔlysA::erm</i>	erm [1], lcm [25]	Unpublished, Samir Giri

## Materials & chemicals

Most materials used in this thesis were single-use plastic devices, which were sterile (blister-) packed and are disposed after use. Glass tubes as well as pipette tips, membranes, Eppendorf vessels and other equipment were autoclaved at 121 °C for 40 min and dried at 60 °C afterwards. All other glass devices such as beaker, flasks, Erlenmeyer flasks and petri dishes were heat-sterilized for 4 h at 200 °C. A detailed list of all consumable materials is listed in the appendix as well as a detailed list of all used chemicals including the full name and the manufacturer.

## Media, buffer- and fixation solutions

All culture-media, buffers, stock-solutions, antibiotics and other solutions were prepared with double deionized water (ddH<sub>2</sub>O). Furthermore, all media were autoclaved for 20 min at 121 °C. For most experiments, solidified LB-medium (Luria Bertani, 1.5 % bacto agar) was used to determine the CFU per ml (colony forming units), isolate bacteria, enrich bacteria, grow controls and short-term storage. Other solid media such i.e. MSgg or SSM were solidified with 1.5 % bacto agar. Agar plates were poured in either a laminar flow hood or in a sterile room, which was surface-sterilized using UV-light. Precultures for experiments, sporulation preparations or cryo-stocks were conducted in LB-broth using none or the respective antibiotic, if mutants carrying an antibiotic maker were used. A list of incubation media can be found below, with chemical manufacturers listed in the appendix.

Agar-based media were only used as short term storage and were usually discarded within one day after incubation. In rare cases plates were used for more than one day, for example, for shipment of vegetative cells via courier. Subsequently, a single colony was streaked out on fresh media containing the needed marker to ensure a contamination-free culture.

**LB-broth (Luria Bertani, 1000 ml)**

15 g	Luria-Bertani broth
10 g/l	adjust NaCl to 10 g/l
15 g, optional	Bacto agar
Ad. 1000 ml	ddH <sub>2</sub> O
	Sterilization by autoclaving
Optional:	Addition of antibiotic after cooling to 50-60 °C

**MN-medium (1 l, 10 x)**

136 g	K <sub>2</sub> HPO <sub>4</sub> x 3 H <sub>2</sub> O
60 g	KH <sub>2</sub> PO <sub>4</sub>
10 g	Sodium citrate x 2 H <sub>2</sub> O
Ad. 1000 ml	ddH <sub>2</sub> O
	Sterilization by autoclaving

**MNGE-medium (10 ml)**

1 ml	MN medium (10 x)
400 µl	Glucose (50 %)
50 µl	Sodium-L-Glutamate Monohydrate (40 %)
50 µl	Ferric ammonium citrate (2.2 mg/ml)
100 µl	L-tryptophan (5 mg/ml)
30 µl	MgSO <sub>4</sub> (1 M)
Ad. 10 ml	ddH <sub>2</sub> O, autoclaved

Glucose, K-glutamate, MgSO<sub>4</sub> and Casamino acids (see below) were autoclaved, whereas L-tryptophan and ferric ammonium citrate were sterile filtered

Optional:	
100 µl	Casamino acids (10 %)

**R2A-medium (Reasoner's 2A, 1000 ml)(Reasoner & Geldreich, 1985)**

0.5 g	Yeast extract
0.5 g	Proteose Peptone
0.5 g	Casamino acids (hydrolysate)
0.5 g	D(+)-Glucose
0.5 g	Starch
0.3 g	Na-pyruvate
0.3 g	K <sub>2</sub> HPO <sub>4</sub>
0.05 g	MgSO <sub>4</sub> x 7 H <sub>2</sub> O
15 g, optional	Bacto agar
Adjust to pH 7.2	
Ad. 1000 ml	ddH <sub>2</sub> O
	Sterilization by autoclaving and storage at 4 °C

**MSgg-medium (Minimal Salts Glycerol Glutamate, 1000 ml) Modified after: (Kearns *et al.*, 2005, Branda *et al.*, 2001)**

Option 1: MSgg as solidified medium  
 15 g Bacto Agar  
 825 ml ddH<sub>2</sub>O, stirring, fresh autoclaved ~50-60 °C for MSgg-agar

Option 2: Mmsgg-broth  
 840 ml ddH<sub>2</sub>O, stirring, fresh autoclaved ~50-60 °C for MSgg-broth

Both options: After autoclaving, medium was air-cooled and the following sterile solutions were added while constant stirring at ~50-60 °C:

5 ml K Phosphate buffer (1 M), pH 7 (autoclaved)  
 100 ml MOPS buffer (1 M), pH 7 (sterile filtered)  
 10 ml Glycerol in ddH<sub>2</sub>O, 50 % (autoclaved)  
 0.1 ml Thiamine (Vitamin B1, 20 mM stock, sterile filtered, store at -20 °C)  
 20 ml Glutamate (Sodium-L-Glutamate Monohydrate, sterile filtered), 25 %  
 5 ml L-Tryptophan (10 mg/ml stock, sterile filtered)  
 5 ml L-Phenylalanine (10 mg/ml stock, sterile filtered)  
 8.90 ml L-Alanine (100 mg/ml stock, sterile filtered)  
 2 ml MgCl<sub>2</sub> (1 M stock, autoclaved)  
 1 ml CaCl<sub>2</sub> (0.7 M stock, autoclaved)  
 1 ml MnCl<sub>2</sub> (50 mM stock, autoclaved)  
 1 ml ZnCl<sub>2</sub> (1 mM stock, autoclaved)  
 1 ml FeCl<sub>3</sub> (50 mM, sterile filtered fresh prepared due to short shelf life)  
 Ad. 1000 ml ddH<sub>2</sub>O

Per plate (ø 9 mm) 15-20 ml medium were used. All stock solutions were stored at 4 °C. The medium was protected against direct sunlight.

**NB (Nutrient broth, 1000 ml)**

10 g Peptone  
 10 g Beef extract  
 10 g NaCl  
 15 g, optional Bacto agar  
 Ad. 1000 ml ddH<sub>2</sub>O  
 Sterilization by autoclaving

**SP-medium**

8 g Nutrient broth  
 0.25 g MgSO<sub>4</sub> x 7 H<sub>2</sub>O  
 1 g KCl  
 Ad. 1000 ml ddH<sub>2</sub>O

All ingredients were autoclaved and then following salts were added:

1 ml CaCl<sub>2</sub> (0.5 M)  
 1 ml MnCl<sub>2</sub> (0.01 M)  
 2ml Ferric ammonium citrate (2.2 mg/ml)

**SSM-Medium (Schäffer's Sporulation Medium); adapted and modified after (Schaeffer *et al.*, 1965, Nagler *et al.*, 2015).**

16 g	Nutrient broth (NB)
0.5 g	MgSO <sub>4</sub> · 7H <sub>2</sub> O
2 g	KCl
15 g, optional	Agar
Adjust pH to 7.0	
Ad. 1000 ml	ddH <sub>2</sub> O
	Sterilization by autoclaving

After autoclaving, the medium was air-cooled and the following sterile sporulation salts (solved in ddH<sub>2</sub>O) were added while stirring at ~50-60 °C:

2 ml	Ca(NO <sub>3</sub> ) <sub>4</sub> · 4H <sub>2</sub> O (1 M)
2 ml	MnCl <sub>2</sub> · 4H <sub>2</sub> O (0.01 M)
2 ml	Fe(II)SO <sub>4</sub> · 7H <sub>2</sub> O (1 mM)

**Buffers****Alkylation buffer (Soufi & Macek, 2014)**

550 mM	Iodoacetamide (IAA)
50 mM	Ammonium bicarbonate
Ad.	ddH <sub>2</sub> O, DEPC-treated
	Storage at -20 °C.

Cacodylate Buffer (0.05 M, 500 ml)

Adapted after Bozzola 2007 (Bozzola, 2007).

5.35 g	Cacodylate acid
Adjust to pH 7.4	
Ad. 500 ml	ddH <sub>2</sub> O
	Sterile filtered and stored at 4 °C.

**Expression mix (1 ml)**

500 µl	Yeast extract (5 %)
250 µl	Casamino acids (10 %)
50 µl	L-tryptophan (5 mg/ml)
Ad. 1000 µl	ddH <sub>2</sub> O

Yeast extract, Casamino acids and ddH<sub>2</sub>O were autoclaved whereas L-tryptophan was sterile filtered.

**HEPES buffer (1 M, 500 ml)**

119.15 g	HEPES (acid free)
400 ml	ddH <sub>2</sub> O
5 g	NaOH
Adjust to pH 7.0	
Ad. 500 ml	ddH <sub>2</sub> O
	Sterile filtered using a vacuum pump and stored in the dark at 4 °C.

**K-Phosphate buffer (1 M, 100 ml)**

21.25 g	K <sub>2</sub> HPO <sub>4</sub>
10.62 g	KH <sub>2</sub> PO <sub>4</sub>
Adjust to pH 7	
Ad. 100 ml	ddH <sub>2</sub> O
	Sterilization by autoclaving and storage at room temperature



**LETS buffer (50 ml)**

0.212 g	LiCl (0.1 M, final)
0.186 g	Na <sub>2</sub> EDTA (0.01 M, final)
0.061 g	Tris-HCl, pH 7.4 (0.01 M, final)
0.5 g	SDS (1 %)
Ad. 50 ml	ddH <sub>2</sub> O, DEPC-treated or RNase-free water

For determining the pH of Tris-HCl, a reference vessel is used to adjust the pH, due to a potential contamination of RNases using the pH-meter electrode. Only RNase free vessels were used. Buffer was sterile filtered and stored at 4 °C.

**Loading dye for agarose gels (6x)**

6.6 ml	Glycerol 50 %
25 mg	Bromophenol blue
Ad. 10 ml	ddH <sub>2</sub> O

Storage at 4 °C or at -20 °C (long-term storage)

**MOPS - buffer (1 M)**

104.65 g	MOPS
Adjust to pH 7	
Ad. 500 ml	ddH <sub>2</sub> O

Sterile filtered using a vacuum pump and stored in the dark at 4 °C

**PBS buffer - Phosphate buffered saline 10x (1000 ml)**

80 g	NaCl
2 g	KCl
26.8 g	Na <sub>2</sub> HPO <sub>4</sub> x 7H <sub>2</sub> O
2.4 g	KH <sub>2</sub> PO <sub>4</sub>
Adjust to pH 7.2	
Ad. 100 ml	ddH <sub>2</sub> O

Sterilization by autoclaving and storage at room temperature

**Reduction buffer (Soufi & Macek, 2014)**

1 M	Dithiothreitol (DTT)
20 mM	Ammonium bicarbonate
Ad.	ddH <sub>2</sub> O, DEPC-treated

Storage at -20 °C

**SDS-loading buffer (5x)**

110 mM	Tris-HCl (pH 6.8)
20 %	Glycerol
3.8 %	SDS
8 %	β-mercaptoethanol
Ad. libitum	Bromphenole blue

**TAE buffer - Tris Acetate EDTA buffer for electrophoresis (10x)**

48.5 g	Tris-base
11.4 g	Glacial acetic acid (100 %)
3.7 g	EDTA, disodium salt pH 8.0
Adjust to pH 7.2	
Ad. 1000 ml	ddH <sub>2</sub> O

**TE buffer - Tris EDTA buffer (1x)**

10 ml	1 M Tris-HCl, pH 8.0
2 ml	0.5 M EDTA, pH 8.0
Ad. 1000 ml	ddH <sub>2</sub> O

**TLB buffer – Triton lysis buffer**

150 mM	NaCl
50 mM	Tris-HCl (pH 7.4)
1 %	TritonX-100
1 x	ULTRA tablet Mini® (protease inhibitor, EDTA-free, 1 x tablet per 10 ml TLB-buffer)

**Tris-HCl buffer (1 M, 100 ml)**

12.1 g	Tris base
Adjust to pH 8.0	
Ad. 100 ml	ddH <sub>2</sub> O
	Storage at 4 °C

**Fixative solutions**

In order to prevent the natural decay of biofilms, vegetative cells or spores and to stop all biochemical reactions to preserve the structure, a variety of different fixatives was used. Furthermore, the architecture of biofilms and their cross sections might change during desiccation, which is needed for most electron microscopic imaging procedures. A fixation inactivates the sample and sustains the mechanical properties of complex samples like biofilms. Depending on the sample type and its further use, a suitable fixative was chosen. Samples for electron microscopy often were fixated using the clinic fixative, which produces a minimum of unwanted artefacts. For scanning electron microscopy (SEM), a prior fixation with the clinical fixative was supported by subsequent fixation and staining with osmium tetroxide.

**Clinic fixative (100 ml)**

5 ml	fresh PFA solution (20 %)
10 ml	GA (Glutaraldehyde, 25 %)
5 ml	HEPES-buffer (1 M)
Adjust to pH 7.2	
Ad. 100 ml	ddH <sub>2</sub> O
At a temperature of 4 °C, the shelf life is limited to two months.	

**Osmium tetroxide fixation and staining (50 ml)**

0.5 g	Osmium tetroxide (OsO <sub>4</sub> )
Ad. 50 ml	0.05 M Cacodylate buffer (pH 7.5)
For every use, the osmium-solution was prepared fresh and was used within a closed fume hood.	
Fixation and staining of biofilms took around 1 h (Serra <i>et al.</i> , 2013, Fischer <i>et al.</i> , 2012).	

**Paraformaldehyde 20 % (PFA, 500 ml) – also known as formaldehyde solution**

Paraformaldehyde is polymerized formaldehyde, which dissolves during constant stirring and heating. This process is reversible, especially during longer storage and therefore shelf time is limited.

100 g                      Paraformaldehyde powder  
350 ml                      ddH<sub>2</sub>O

Solution was stirred for 30-60 min at 60-70 °C. Several drops of 10 N NaOH were used to clear the solution and allow cooling until room temperature is reached.

Ad. 500 ml                      ddH<sub>2</sub>O

PFA-solutions were not stored for more than two months at 20 °C. After thawing, the solution was heated for at least 30 min at 60-70 °C before use.

**2.2 Sporulation and spore purification**

*B. subtilis* spores are able to withstand harsh conditions and remain stable for a long time, especially when stored under controlled environmental conditions. This can be used to create spore solutions with a known amount of spores per milliliter or microliter and is needed to create exact conditions for each experiment, while inoculation. Spores can be synchronized by heating them in ddH<sub>2</sub>O at 70 °C for 30 min prior to inoculation to ensure a homogenous germination (Cook & Brown, 1965, Foster & Johnstone, 1990). Two methods were used to produce pure *B. subtilis* spore stocks. Both are based on Schäffer's sporulation medium (SSM) either as solid medium or as broth (Schaeffer *et al.*, 1965). SSM is a full medium containing sporulation supporting salts such as calcium nitrite, iron (II) sulfate and manganese (II) chloride to promote endospore formation. Spore production on solid media was performed after Fuchs *et al.* (Fuchs *et al.* 2017) and spore production in liquid media was performed after the protocol of Nagler *et al.* (Nagler *et al.* 2015).

**Determination of colony forming units (CFU)**

Many experiments and their preparations within this thesis are based on the determination of colony forming units (CFU) also known as titer which represents the bacterial or spore concentration within a solution. CFU is mainly presented in CFU/ml or in CFUheat/ml after a 15 min pasteurizing step at 80 °C. *B. subtilis* spores withstand the effect of wet heat during the pasteurization step and therefore CFUheat/ml can be considered as spores/ml. By subtracting spores/ml from CFU/ml, the number of vegetative cells in a solution can be determined. In order to determine the titer, only liquid samples or samples which can be solved in buffer can be used. The most common example in this work are *B. subtilis* biofilms grown on filter membranes: By dissolving the biofilm in 1 ml PBS-buffer using a sterile loop, transferring it into a 2 ml tube and disrupting it using a vortex and glass beads, a valid solution for CFU-counts was generated. For serial dilutions 96-well plates were used. Each well was filled with 270 µl sterile 1x PBS-buffer using a multi-channel pipette. By adding 30 µl of a sample of interest in i.e. (lane 1, row A, Figure 6) - without mixing, a 1:10 or 1x10<sup>-1</sup> dilution was created. Due to potential bacteria or spores at the pipette tip, mixing of the sample dilution was done in the second step, where the well is thoroughly mixed using a new pipette tip. Using the same tip, 30 µl of the 1x10<sup>-1</sup> dilution were transferred into the next 270 µl PBS-buffer-filled well (lane 1, row B), without mixing, resulting in a 1:100 or 1x10<sup>-2</sup> dilution. In the following, the remaining wells were processed the same way as described for the first two wells. These dilution steps can be facilitated by using a multi-channel pipette. Ultimately a single 96-well plate can fit up to 12 samples with 1:10 dilution steps ranging from 1x10<sup>-1</sup> down to 1x10<sup>-8</sup>.

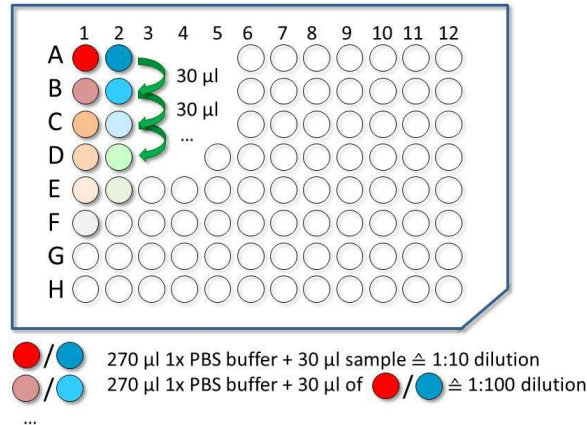


**Figure 6: Dilution series in a 96 well plate for CFU determination.**

Each well is filled with 270 µl PBS-buffer. The first row (A) is mixed with 30 µl of the analyzed sample to create a 1:10 dilution (or  $1:10^{-1}$ , shown in red for sample 1 [A1] or blue, sample 2 [A2]). Afterwards 30 µl of the  $10^{-1}$ -dilution are transferred into the next row of the respective lane to create a 1:100 dilution ( $1:10^{-2}$ , light red [B1] and light blue [B2]). This procedure is repeated until a dilution of  $10^{-8}$  has been created (H1 for sample 1 and H2 for sample 2). Afterwards dilutions can be plated on LB-agar plates in order to determine the CFU per dilution step to calculate the CFU/ml.

All dilutions were pipetted using either 50 µl per dilution on a quarter of an LB-agar plate (2 plates for eight dilutions), or 25 µl on an eighth of an LB-agar plate. The agar is inoculated starting with  $1 \times 10^{-8}$  dilution,  $1 \times 10^{-7}$  and so on, up to  $1 \times 10^{-1}$  and afterwards spread using a sterile loop in the same order. The typical inscription of the individual sections is given in increments of  $1 \times 10^{-1}$  to  $1 \times 10^{-8}$ . Inoculated plates were dried with a closed lid for 15 min and incubated overnight at 37 °C. CFUs of each section were counted as long as they did not exceed 150 per quarter or 100 in an eighth. Resulting CFU and CFU<sub>heat</sub> numbers were conveyed into an excel chart to calculate the amount of CFU/ CFU<sub>heat</sub> per milliliter. Depending on the used volume, 25 or 50 µl, the calculation to determine CFU/ml count was adjusted after counting colonies. Each CFU-count per dilution was multiplied with the respective dilution factor (i.e.  $1 \times 10^{-2}$  was multiplied by 100). All results were added and divided by the number of countable sections and multiplied with a factor (x20 for 50 µl sections and x40 for 25 µl sections) to upscale the amount of used sample to determine the CFU/ml.

$$\frac{\sum_{k=1}^n x_k d_k}{n} f = CFU/ml$$

$d$  = dilution factor of the respective section

$f$  = volume plating factor, x20 for 50 µl or x40 for 25 µl plated

$k$  = index

$n$  = number of countable sections

$x$  = CFU of the respective section

Each experiment was carried out at least in three biological replicates. The repetition of the CFU count is considered a technical replica and was therefore only used for experiments that could not be repeated. CFUs resulting of biological replicates were combined by calculating the mean and the standard deviation. By using technical replicates, the overall error using the CFU-determination method ranges between 5-15 %. In comparison to culture-independent, titer-determination assays such as flow cytometry or cell-counting chambers, the CFU-based approach selects only cells and

spores which are able form colonies. Both other methods often result in false/positive cell counts, whereas the CFU plate-counting method is only applicable for dividing cells, which might result in false/negative results i.e. after an irradiation experiment, where cells or spores might be able to survive, but not divide.

### 2.3 Cultivation of standardized biofilms

Aim of this thesis is the investigation of *B. subtilis* biofilms grown under extreme and simulated space conditions. The most important requirement is a defined growth setup, which allows the reproducible comparison within an experimental series and among different experiments. In the frame of this thesis, a method using membrane filters for growth was developed and published (Fuchs *et al.*, 2017a). Due to the importance of this method, which was used for almost all experimental approaches, the most important steps in growing biofilms on a membrane filter will be briefly explained. Some of the important key results are shown in the results section.

#### Membrane filters

Membrane filter were used to separate the biofilm from the growth medium, mainly MSgg-agar. Hydrophilized PTFE filters (polytetrafluoroethylene, known as Teflon®) with a pore size of 0.4 µm enable the diffusion of water and nutrients towards the growing biofilm. The most used filter in this study is the Millicell Cell Culture Insert filter (Merck Millipore®, PICM03050) with a usable diameter of 25 mm (approx. 4.2 cm<sup>2</sup> surface area). This filter is different in contrast to many other filters, because of the polystyrene frame which is permanently attached to the filter. This allows the addition of buffers such as PBS to a grown biofilm colony to dissolve it and to retrieve a known volume containing the biofilm. Especially for CFU and spore determination, the volume is important for the calculation. Furthermore, the frame enabled the overall handling using sterile forceps. By placing the filter in a sterile petri dish, spores were pipetted on for drying. Moving the inoculated filter onto the growth medium allowed precise handling. After a biofilm is formed, the filter was harvested, dried, and placed on new medium or prepared for fixation. Depending on the experiment, the filter was used in many different ways and allowed highly reproducible results (Fuchs *et al.*, 2017a).

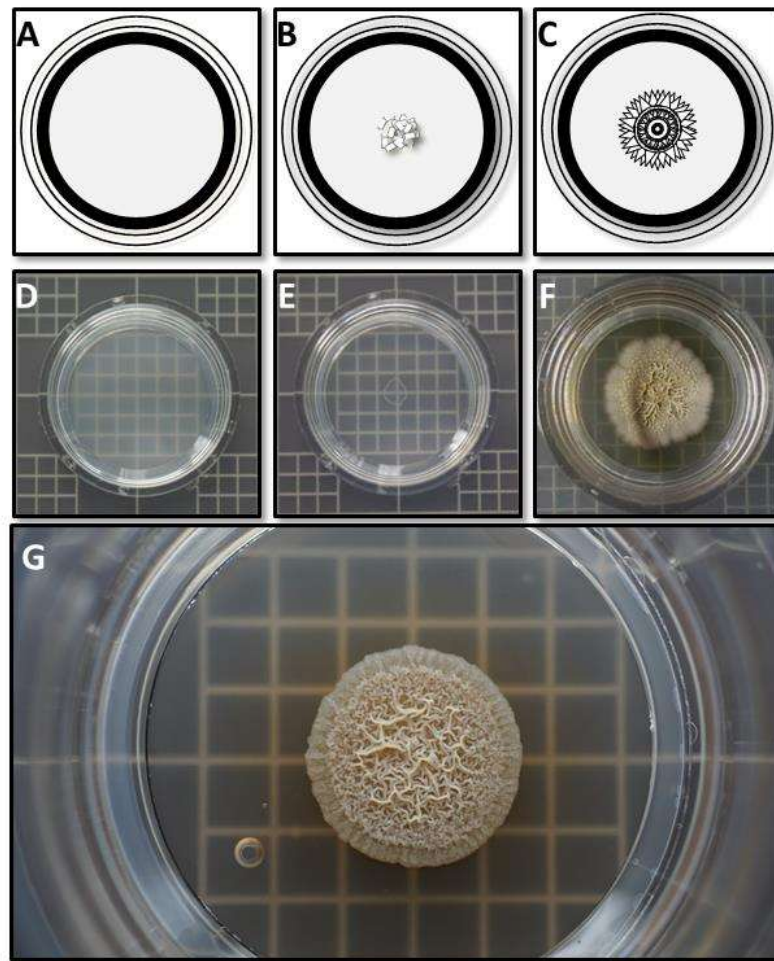


**Figure 7: Steps of growing a defined *B. subtilis* biofilm**

Images **A-C** demonstrate a schematic overview of the inoculation and growing process of defined biofilms, while **D-G** represent images under laboratory conditions. A membrane filter is shown in **A** and **D**, which is placed in the center of a grid petri-dish filled with MSgg medium. For inoculation (not shown), the filter is separately inoculated with  $1 \times 10^6$  *B. subtilis* spores and air dried. For starting the experiment, the membrane is transferred using sterile forceps onto an agar plate (**B** and **E**). After the incubation of 72 h at 37 °C biofilms can be harvested or used for further analyses. Adapted and modified after Fuchs *et al.* 2017. For scale: Sides of three small squares corresponds to one centimeter.

### Membrane handling

All following inoculation steps were performed in a laminar flow hood to prevent potential contaminations. First, membrane filters were carefully unpacked of their blister packaging and transferred using sterile forceps into a sterile petri dish. Spore stock solutions of the desired concentration were used as an inoculum. Therefore, 10  $\mu$ l harboring  $1 \times 10^6$  or  $1 \times 10^7$  heat synchronized spores ( $\sim 1 \times 10^8$  and  $1 \times 10^9$  spores/ml) were carefully placed in the center of a membrane, without touching the membrane with the pipette tip. After 10 min (minimum) to 2 h (maximum) of air-drying at room temperature, the membrane filter was placed in the center of culture-media plates using sterile forceps. Standard-sized plates should not exceed 30 ml of solidified medium. Otherwise petri dishes with higher side walls should be used for inoculation to allow air exchange and prevent pressurizing the membrane. During the placement, the membrane becomes transparent. This enabled the positioning of the dried spores directly in the center of a grid plate (or germ count dish). 2-D clinostat experiments for the simulation of microgravity required the growing

biofilm exactly in the middle of the rotation axis. After incubation, the membrane is carefully removed from the medium using heat-sterilized forceps and placed into a sterile petri dish. For harvesting, 1 ml of 1x PBS-buffer is pipetted into the membrane filter. A sterile one-way loop is used to carefully dissolve the biofilm, beginning on the edges towards to center. The biofilm should easily detach and remains generally intact, as long there is not too much mechanical stress. By shearing the biofilm into smaller fragments using the loop, biofilm fragments can be pipetted into a sterile 2 ml Eppendorf tube containing several glass beads ( $\varnothing$  2 mm). Prior to ultra-sonication at 20 % amplitude for 10 min at 25 °C, samples are thoroughly vortexed for 1 min to assure homogenization.

## 2.4 Simulation of microgravity (sim- $\mu$ g)

### Fast-rotating 2-D Clinostat

Clinostats are used to investigate the influence of simulated microgravity, by equalizing the vector of gravity along a (fast-) rotating (horizontal) axis to zero (Klaus, 2001, Herranz *et al.*, 2013a). The term Clinostat is composed of the Greek words *klínein*, (tilting, tilted) and *statós* (standing, posed). While experimenting, one axis of the clinostat runs perpendicular to the direction of gravity in two dimensions (2-D; x, y), whereas two rotation axes are used in random positioning machines (RPMs), which result in a three dimensional (3-D; x,y,z) simulation display (Briegleb, 1992, Klaus, 2001, Hoson *et al.*, 1997, Herranz *et al.*, 2013a).

**Table 2: Technical specifications of a fast rotating 2-D clinostat**

Information is adapted according to the manufacturer's user manual and factory modification.

<b>Dimensions [cm]</b>	Working position: 24 x 40 x 30 (h/w/d)* Loading position: 45 x 25 x 30 (h/w/d)* Power supply: 10 x 20 x 30 (h/w/d)*
<b>Incubation limits (clinostat)</b>	Temperature: 15- 37 °C Rel. humidity: best < 40%
<b>Rotation axis</b>	0° - parallel to ground 90° - perpendicular to ground clockwise and counter clockwise
<b>Rotation speed</b>	Range: 0.5 - 90 rpm Most used setup: 60 rpm
<b>Samples</b>	9-11 petri dishes ( $\varnothing$ 90 - 120 mm)

\*h = height, w= width, d= depth

The 2-D clinostats used in this thesis are small sized and can be used in almost all common incubators or at room temperature. The frame of the clinostat incorporates four adjustable feet, which can be rotated to alter their horizontal position. Before loading samples, the feet were adjusted regarding the final run-position of the clinostat. A small integrated spirit level can be used to verify the correctness of the horizontal positioning of the frame. The body of the clinostat consists of a small electric driven motor, which is able to rotate a disc-shaped stage, on which samples can be mounted using long screws. Loading of the clinostat is done vertically; Petri dishes were stacked up to eleven plates on top of each other, secured with a plastic disc and fastened with four butterfly-screws. To prevent loosening of the screws, Parafilm® was wrapped around the screws. After loading and securing samples, the inclination handle was used to tilt the body by 90°. A clamp handle was used to

fixate the angle and to calibrate the angle while balancing the body using a small external spirit-level. The final rotation axis has to be exactly 90° (horizontal) to the body and be perfectly aligned in parallel to the ground. In the next step, the clinostat was connected to the power supply unit (PSU) which allows controlling the direction of rotation and the rotation speed. For the experiments in this work only one setup was used: clockwise rotation at 60 rpm.

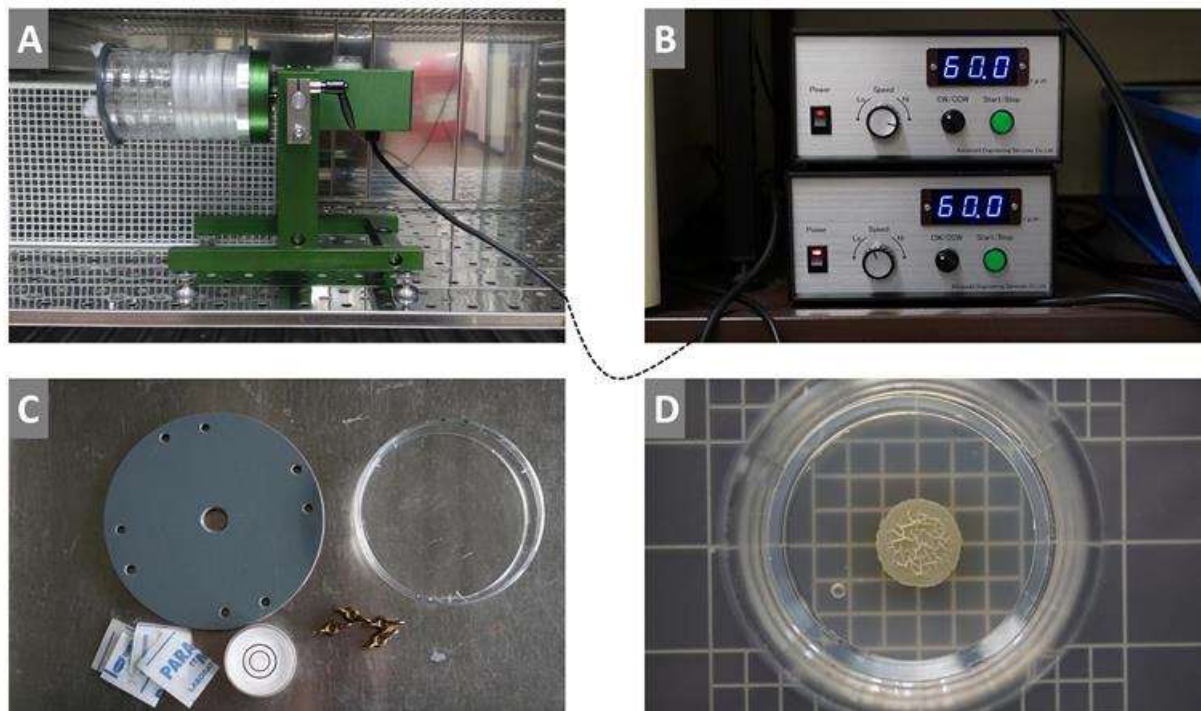


**Figure 8: 2-D Clinostat setup**

Example setup of a fast-rotating 2-D clinostat carrying four sample plates and four placeholder plates (empty plates) using a standard incubator at 37 °C (A). In B, two power supply units (PSU) outside of the incubator are shown of which one is connected to a clinostat. Both PSUs are set to 60 rpm, while rotating in clockwise direction. Standard materials such as butterfly screws, a small portable spirit level, Parafilm®-leaves, a placeholder petri dish and the cover plate are represented in image C. In order to grow biofilms exactly in the center of the rotation axis, grid-petri dishes (one small square equals 0.33 mm) containing the growth media of interest (here MSgg-agar) are used (D). *B. subtilis* spores or washed vegetative cells can be inoculated on a membrane filter, placed on nutrient-agar and incubated within the clinostat to simulate microgravity while growing a biofilm.

### Calculation of remaining g-force

Centrifugal force ( $F$ )

$$\frac{F}{g} = \frac{1 v^2}{g r}$$

Rotational speed ( $\omega$ ) (revolutions per minute)

$$v = 2 \pi r \frac{\omega}{60} = \frac{\pi}{30} r \omega$$



Integration of  $\omega$  to calculate  $F$

$$\frac{F}{g} = \frac{\left(\frac{\pi}{30}\right)^2 r^2}{r} \frac{\omega^2}{9.81} = 1.12 \cdot 10^{-3} r \omega^2$$

$\omega$  = angular velocity [ $\text{m/s}^2$ ], set as rotational speed

$g$  = gravity [ $9.81 \text{ m/s}^2$ , or  $1 \times g$ ]

$r$  = radius [m]

$v$  = rotational velocity [ $\text{m/s}^2$ ]

$F$  = acceleration due to centrifugation [ $\text{m/s}^2$ ]

**Table 3: Example for a calculation of remaining g-forces using a 2-D clinostat**

A typical diameter of a *B. subtilis* colony after 72 h is assumed with  $d=4 \text{ mm}$  ( $r=0.002 \text{ m}$ ) and the rotation speed is given as 60 rpm. The calculation can be combined in one complex formula or can be expressed in several steps for a better understanding. The remaining g-forces [ $\text{m/s}^2$ ] are shown in the last column.

$r$ [m]	rpm	rpm/s [ $\text{s}^{-1}$ ]	$T=1/\text{rpm}$ $\text{s}^{-1}$ [ $\text{s}^{-1}$ ]	$\omega=2*\pi/T$ [1/s]	$F=\omega^2*r$ [ $\text{m/s}^2$ ]	$g=F/g$ [ $\text{m/s}^2$ ]
0.002	60,0	1,000	1,0	6,28	0,07896	0,008049

### Standardized biofilms under sim- $\mu\text{g}$

Standardized biofilms have been successfully grown under regular gravity conditions (1g) by attaching an inoculated membrane filter to the solid nutrient medium (e.g. MSgg-agar). Inoculated petri-dishes are turned upside-down and incubation takes place in a standard incubator at 37 °C. For simulating microgravity (sim- $\mu\text{g}$ ) by using a fast rotating 2-D clinostat, a standardized cultivation method for biofilms was not established in literature. Only a few studies have been performed with agar-based incubation systems using 2-D clinostats. Comparable studies mainly used rotating wall vessels (RWV) with different setups or pipette clinostats for liquid culturing. RWVs are based on the same physical background as 2-D clinostat, but no standardized method to grow *B. subtilis* biofilms or biofilms in general was described. The membrane filter system has proven to be a reliable method for 1g biofilm cultivation and has been specifically developed for sim- $\mu\text{g}$  cultivation. As shown before, the dried spore-ring influences the overall biofilm dimensions. For sim- $\mu\text{g}$  experiments, in which biofilms rotate along one axis, biofilms have to be placed in the exact center of the rotation axis and must have a circular spore inoculum. Grid plates were used to determine the exact center of the agar plate. Membrane filters were placed and aligned in the center of an agar plate by using sterile forceps. The plates were sealed with Parafilm® during incubation so that the convection caused by the rotation could be compared with 1g reference controls, which were also sealed.

First experiments aimed to compare general biofilm development of *B. subtilis* between 1g and sim- $\mu\text{g}$  conditions. The simulation of microgravity by using 2-D clinostats is only one of several methods used to cultivate bacteria under sim- $\mu\text{g}$ . Aim of the simulations is to mimic weightlessness as perceived under space conditions with regards to the limited possibilities on Earth. However, there are experimental steps in which the simulation or rotation along an axis cannot be maintained, i.e. the first phase of the experiment, the inoculation of spores. For 1g as well as sim- $\mu\text{g}$ , spores were pipetted onto membrane filters and air-dried. After transferring membrane-bound spores to the nutrient medium, the hydrophilized filter is wetted and germination is about to begin and thus the experiment itself started. Therefore, after transferring the filter to an agar plate, the plate was sealed as quickly as possible and mounted in a clinostat. As observed in previous experiments (Fuchs *et al.*,

2017a), germination occurs within minutes in MSgg-medium. During early germination and biofilm development, the simulation of microgravity was maintained until the end of incubation. For biofilm analysis after sim- $\mu$ g incubation, subsequent downstream processes needed to be performed quickly to archive pristine results. For DNA, RNA and protein extraction, biofilms were washed in ice-cold PBS immediately after sim- $\mu$ g incubation and frozen in liquid nitrogen. Structural biofilm analyses i.e. for SEM or TEM required immediate fixation. Other experimental approaches like CFU/spore determination were also conducted as fast as possible after incubation.

**Table 4: Influence of the radius while using a 2-D clinostat**

Several radii ranging from 2.5-15 mm of biofilms are compared regarding the influence of the  $g$ -force while being incubated using a fast rotating 2-D clinostat at 60 rpm.

$r$ [mm]	Remaining $g$ [ $m/s^2$ ]
2,5	0,0101
5	0,0201
7,5	0,0302
10	0,0402
12,5	0,0503
15	0,0604

### Random positioning machine (RPM)

Random positioning machines as well as 2-D clinostats are used as ground based devices to simulate microgravity by averaging the gravitational pull over time to zero. In contrast to 2-D clinostats, which rotate samples of interest only on one axis, RPMs rotate on two perpendicular axis and are therefore also known as 3-D clinostats (Hoson *et al.*, 1997, Klaus, 2001). Samples were mounted within a frame, which is positioned within a second frame attached to the base of the RPM. Both frames are operated randomly and independent from each other using an automated algorithm called “random walk” (Wuest *et al.*, 2014). Biological samples require a strict alignment in the gravitational field over a longer time in order to be able to adapt to the gravitational conditions. Due to the permanent rotation of the samples and the associated withdrawal of the gravitational perception, it is assumed that a state similar to weightlessness in the sample can be simulated (Borst & van Loon, 2008). This is the case for both, 2-D and 3-D clinorotation modes, whereas the RPM simulation allows a three-dimensional  $g$ -vector averaging.

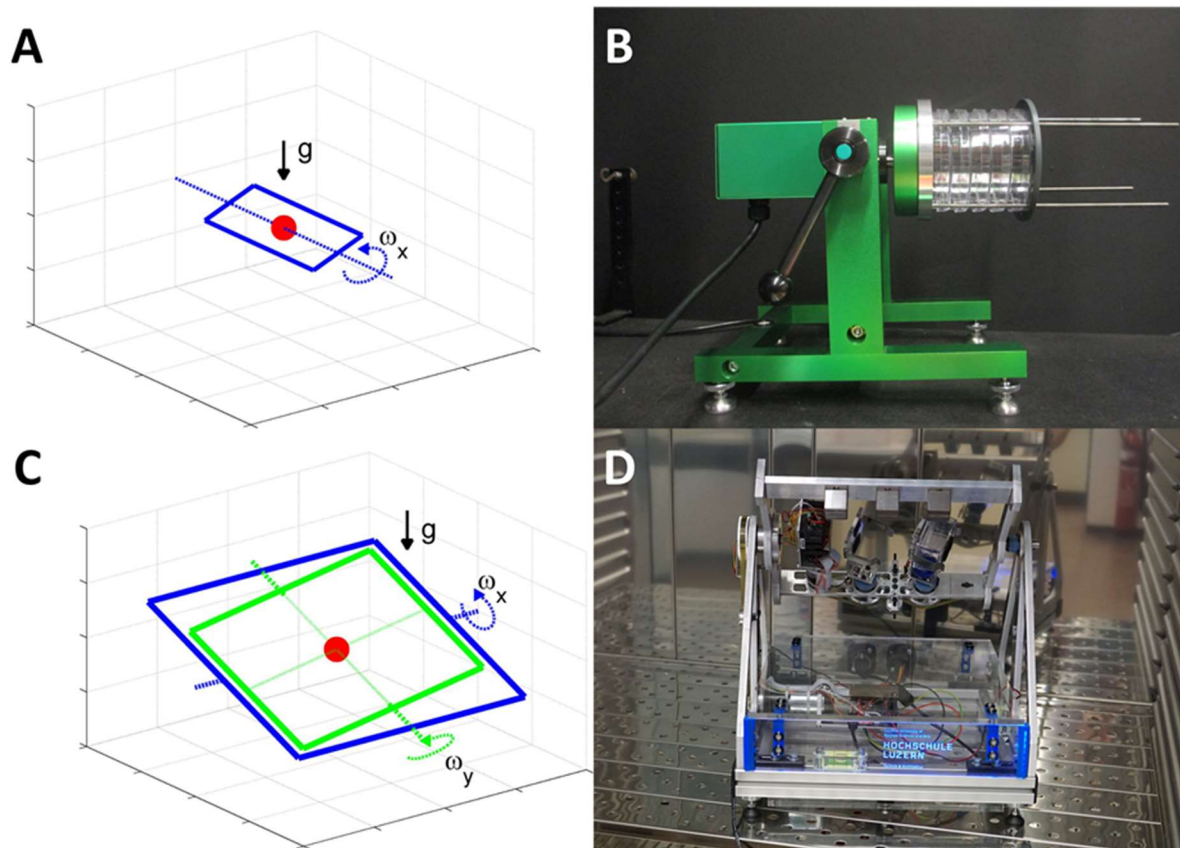


**Figure 9: Comparison of the principle of action of 2-D clinostat and RPM**

Images **A** and **C** represent the schematic working principle during the simulation of microgravity using a clinostat (**B**) and a RPM (**D**). The rotating axis for the clinostat (blue dotted line, **A**) and two axes of the RPM (blue and green dotted lines, **C**) and the resulting angular velocity ( $\omega^{\rightarrow}$ ) are shown for a single sample (red dot) within the three-dimensional space. Figures **A** and **C** are taken and adapted from Wüest *et al.* 2017.

Most experiments concerning the simulation of microgravity within this thesis were generated using a fast rotating 2-D clinostat. To compare the clinostat data, an RPM was used as the second device to simulate microgravity along two axes. The RPM was kindly provided by Dr. Simon Wüest (Lucerne University of Applied Sciences and Arts, School of Engineering and Architecture, CC Aerospace Biomedical Science and Technology, Space Biology Group, Switzerland). Dr. Wüest and colleagues developed the RPM and described the technical and biological features in detail (Wüest *et al.*, 2017, Wüest *et al.*, 2014). In order to develop a solid-culture medium based RPM-assay, a new incubation method was established to generate standardized biofilm growth on membranes on RPMs. Standard ibidi®-dishes were filled with 700  $\mu$ l liquefied nutrient media such as MSgg-agar (microwaved for 20 s, for 1 mm agar thickness) or with 1.2 ml media to cover the whole bottom of the ibidi®-dish. In the latter case, a spore-inoculated ( $1 \times 10^6$  or  $1 \times 10^7$  spores) membrane was placed on the dried agar. Using the 1 mm thick medium, harbored the advantage of a flat medium distribution, but most used membranes did not fit and had to be cut under sterile conditions. After inoculation by pipetting spores directly on the medium or using a membrane, the dish was closed with its original lid. The lid was covered on one side with Velcro tape, so that it was attached to a designated counterpart on the rotating inner frame of the RPM. The RPM itself did not heat the sample to the desired incubation temperature. Therefore, the RPM was setup within a standard incubator without CO<sub>2</sub>-fumigation or artificial humidity. A computer was connected to the RPM via an USB cable (outside of the incubator) and the software developed by Simon Wüest and colleagues, RPM 4.0, was used to start and control the experiment. First the RPM was balancing its frame into a loading position, then the angular

rotation velocity was set to 60 deg/s and the “random walk” algorithm was started. After incubation membranes were harvested under standardized conditions.

## 2.5 Microscopy

### Phase contrast microscopy

Two different microscopes were used for phase contrast microscopy and bright-field microscopy: A Zeiss Axio Imager M2 fluorescence microscope and an Olympus CX43 microscope. Both microscopes have a digital camera (CCD, CMOS) for image acquisition and software to save and edit images and videos. Most images of cells and spores were acquired using an oil-immersion 100x objective (100x/1.3 NA oil) of the respective manufacturer. For overview images of samples of interest 40x (40x/0.95) objectives were used. Vegetative *B. subtilis* cells appeared phase-black using phase contrast, whereas during germination the high refractive index of *B. subtilis* endospores changed the contrast during phase contrast microscopy from contour-only shape to a phase bright appearance with darker edges. This was particularly of use to control the sporulation of a culture or to verify the purity of spore solutions. During germination *B. subtilis* releases intrinsic Ca<sup>2+</sup>-dipicolinic acid (Ca<sup>2+</sup>-DPA, 5- 10 % of dry weight (Slieman & Nicholson, 2001)), which reduces the refraction index visibly and the spore turns phase gray and phase black within minutes (Pandey *et al.*, 2013). For microscopy, 8 µl of a sample of interest were pipetted on a glass slide and covered with a poly-L-lysine treated cover slip which was carefully dried in a lint-free paper towel. To prevent cell and spore movements, the cover slip was thoroughly pressed on the on the sample. Depending on the objective immersion oil was added on top of the cover slip i.e. for 100x magnification, 2 µl of immersive oil were applied.

### Differential interference contrast (DIC) microscopy

For DIC-microscopy of biofilm growth in real time, mainly an inverted Nikon Eclipse TE2000-E, equipped with a color photomultiplier tube and an inverted laser scanning microscope (LSM, Zeiss 780), which both had a heatable stage and incubation chamber were used. Both microscopes were used during a lab visit at the Robert Koch Institute in Berlin. DIC-microscopy enhanced the contrast of a sample and makes it appear three-dimensional. This technique was used to investigate the process of biofilm growth starting with an inoculum of spores ranging to a fully grown, mature biofilm over time. Therefore, several regions of the biofilm were investigated: the oldest region of the biofilm – the spore inoculum crater-like site (due to the coffee-stain effect, spores are spread in a ring if pipetted and dried), an intermediate region and the outer edges (youngest region). Most examinations were performed using a 20 x DIC II objective (CFI Planfluor 20x/0,50 DIC II). Samples of 1x10<sup>5</sup> or 1x10<sup>6</sup> spores were dried on a grid ibidi® µ-dish for 30 min. In parallel, MSgg medium (1.5 % agar), LB- medium (1.5 % agar) or agarose (1.5 %) as control was liquefied using a microwave. By pipetting 700 µl of the respective medium into the inner part of an ibidi® µ-dish, a 1 mm thick agar layer was formed (Fuchs *et al.*, 2017b). After drying at 37 °C, an agar piece of ~ 1x1 cm was cut off using a sterile scalpel and carefully placed on the dried spores to start the incubation. The spores were examined for 30 min to investigate the germination properties and longer observation times (>20 h) were used to investigate early biofilm formation.

### Scanning electron microscopy (SEM)

Scanning electron microscopy offers high-resolution imaging with a depth of field that ranges from micrometer scale down to nanometer scale. In order to visualize the structure of *B. subtilis* biofilms, SEM is a valuable tool to investigate typical biofilm-related architectural properties such as the surface or cross sections of different regions. Therefore, a defined biofilm setup similar as described in section 2.3 was developed to prepare highly-reproducible, standardized biofilms for SEM. A detailed description of the cultivation and the growth of biofilms for SEM was published in frame of this thesis under the title: “Directed freeze-fracturing of *Bacillus subtilis* biofilms for conventional scanning electron microscopy” (Fuchs *et al.*, 2018). Growth, fixation, sample preparation and microscopy were performed at the RKI in Berlin. Microscopy of *B. subtilis* biofilms was done with a field-emission SEM (Gemini 1530, Carl Zeiss Microscopy) at 3 kV and a working distance around 5 mm using an in-lens detector and an Everhard-Thornley secondary electron detector (mixed signals, 50:50). The following section describes the sample preparation for scanning electron microscopy in more detail.

### Sample preparation for SEM

In contrast to most other biofilm growing experiments, biofilms for SEM were grown on HTTP-membranes (polycarbonate, without polystyrene case,  $\varnothing$  47 mm, 0.4  $\mu$ m pore size, hydrophilized) instead of PTFE-membranes. For the inoculum,  $1 \times 10^6$  spores of the respective *B. subtilis* strain were pipetted into the center of an autoclaved membrane and air-dried for at least 15 min. Sterile forceps were used to place the membrane on MSgg-media (1.5 % agar, grid petri dish), aligning the spore-inoculum with the grid of the petri dish. Plates were sealed with Parafilm® and incubated at 37 °C for 40 h. Afterwards, membranes were carefully transferred on the surface of osmium tetroxide fixative (1 % osmium tetroxide in 0.05 M cacodylate buffer) and incubated for 1 h in the dark at room temperature (Fischer *et al.*, 2012, Serra *et al.*, 2013). The filters were not immersed into the fixative to prevent mechanical disruption of biofilms. After incubation residual osmium tetroxide was removed by washing the biofilms three times with 0.05 M cacodylate buffer. Dehydration was achieved by exposing the fixed biofilms on the membrane in an ascending ethanol series starting with 30 and increasing to 50 %, 70 %, 90 %, and 96 % for 15 min each. To finalize dehydration, samples were incubated for 20 min in 100 % ethanol in which the biofilm separated from the filter. For ultrastructural analysis, regional samples were extracted from the biofilm using a scalpel. Samples were either freeze-fractured or directly dried by critical point drying (CPD), which was performed with an automated CPD device (CPD 300, Leica Microsystems) according to the protocol described by Fuchs *et al.* (Fuchs *et al.*, 2018). Dried samples were carefully attached to SEM-stubs in the wished position using modelling dough (LEIT C PLAST, Plano) and sputter-coated (5 nm, Au/Pd, Sputtercoater E5100, Polaron/Quorum Technologies). After CPD and coating, samples were stored under low pressure until they were analyzed using a field-emission scanning electron microscope (see section 0).

### Transmission electron microscopy (TEM)

Transmission electron microscopy (TEM) was mainly performed at the RKI in Berlin. In contrast to SEM, TEM offers in detail information about the inner cell structure and composition. For TEM, samples of interest were embedded in acrylate resin and cut in ultra-thin sections of less than 100 nm. Sections were transmitted by electrons to generate images depending on the contrast of certain sample regions. In addition to the experiments carried out at the RKI, specific samples investigating

the influence of simulated microgravity on spores were acquired from Prof. Dr. Adam Driks according to the protocol of Waller *et al.* (Waller *et al.*, 2004).

### Sample preparation for TEM

Cultivation of *B. subtilis* biofilms for TEM corresponds to the growth protocol for SEM preparation. Biofilms were grown on HTTP membranes for 40 h at 37 °C on MSgg-agar (1.5 %). After incubation, inoculated membranes were carefully transferred into a sterile petri dish and incubated in clinic fixative (1 % PFA, 2.5 % GA, 0.05 M Hepes buffer) at room temperature overnight. Biofilms were stabilized in low-melting point agarose and post-fixed in osmium (1 %) for 1 h (Laue, 2010). Prior blocking contrasting in 2 % uranyl acetate (ddH<sub>2</sub>O), samples were washed with ddH<sub>2</sub>O. Samples were dehydrated within an ascending ethanol series as described for the SEM-preparation and embedded by using an acrylate resin (LR White, polymerization at 60 °C) (Rismondo *et al.*, 2015). Thin-sectioning (~60 nm) was performed using a Leica UC7 ultramicrotome (diamond knife). Sections were counterstained with 2% uranyl acetate, a lead citrate (Reynolds, 1963), and examined using a transmission electron microscope (Tecnai 12 Spirit; FEI) at 120 kV. Images were recorded with a CCD camera, at a resolution of 1376 by 1024 pixels (Megaview III; Olympus SIS, Germany).

### Surface topography

#### Profilometry

White-light profilometry is a useful tool to investigate the surface topography and roughness of small objects such as bacterial biofilms (Larimer *et al.*, 2016). All profilometry experiments were carried out in 2016 at the laboratories at the Institute of Medical Engineering and Department of Mechanical Engineering at the Technical University Munich (TUM). *B. subtilis* biofilms were grown on cell culture membranes for up to 3 d at 37°C using a 2-D clinostat for sim-µg and 1×g controls. A NanoFocus µsurf profilometer with 20x magnification (Zeiss objective) and a working distance of 3.1 mm was used to capture images (512x512 pixel) with a lateral resolution of 1.56 µm and 5 nm vertical resolution. For each biofilm the profilometer was individually adjusted. The measured height parameters were the maximum peak height ( $S_p$ ), the maximum depth (or pit height,  $S_v$ ) and the maximum height ( $S_z = S_p + S_v$ ) of the surface as well as the resulting roughness (root-mean-square height,  $S_q$ ) and the developed interfacial area ratio ( $S_{dr}$ ) as a hybrid parameter (Werb *et al.*, 2017). The roughness parameter  $S_q$  represents the standard deviation of the height distribution of the biofilm ( $s_q = \sqrt{\frac{1}{A} \iint_A z^2(x,y) dx dy}$ ), respectively the root mean squared average of the height deviations from the calculated center of the defined area. The developed interfacial ratio is calculated in percentage as surface texture development compared to a planar surface  $S_{dr} = \frac{1}{A} \left[ \iint_A \left( \sqrt{1 + \left( \frac{dz(x,y)}{dx} \right)^2 + \left( \frac{dz(x,y)}{dy} \right)^2} - 1 \right) dx dy \right]$  according to the ISO 25178 standard. All data was controlled for normality (Shapiro-Wilk) and tested for significance via one-way ANOVA (group comparisons) using the R-scripts from the department of mechanical engineering (Werb *et al.*, 2017).

#### Surface hydrophobicity analysis

Mature *B. subtilis* are covered with a protein layer mainly composed of BslA, which protects the biofilm from harmful environmental influences (Cairns *et al.*, 2014). The protein layer itself is highly hydrophobic and differs according to growth conditions, age or tested region of the biofilm surface. Hydrophobicity and the wetting abilities of *B. subtilis* biofilms, grown under different gravity regimes, were investigated by contact angle measurements as described by Werb *et al.* 2017 (Werb *et al.*,

2017). Biofilms were grown under the wished conditions using a membrane filter. After the incubation, biofilms which were still on the membrane filter on top of the medium were cut (using a scalpel) from the polystyrene frame together with the agar. Fragments (~1.5 x 1.5 cm) were carefully placed on a glass slide. To visualize and measure the effect of the surface hydrophobicity, 10 µl ddH<sub>2</sub>O were pipetted onto the biofilms region of interest. The inoculated fragment was photographed by a horizontally placed camera system in order to capture a side view of the biofilm. Images were analyzed using the ImageJ plugin DropSnake according to the developers instructions (Stalder *et al.*, 2006).

## 2.6 Survival experiments

For testing *B. subtilis* biofilms and spores regarding their ability to withstand stressful conditions, as they might occur under extra-terrestrial circumstances, survival assays were used to verify the survivability. Survival assays allow comparison between different growing conditions such as changed gravity regimes, nutrient limitation and incubation temperatures. In addition, bacterial strains can be compared with each other, which differ in their wild-type phenotype or by mutations. Survival assays were conducted via chemical inactivation by applying H<sub>2</sub>O<sub>2</sub>, ethanol or other chemicals or physically via thermal treatments (dry heat/ wet heat), radiation (UV, X-ray, galactic cosmic radiation - GCR), vacuum, desiccation or nutrient limitation. After treatment, biofilms, cells and spores were prepared for CFU determination, which represents the fraction of surviving cells or spores, that are still able to germinate, grow and divide properly. In general, survival was expressed in absolute CFUs ( $N_x$  - at time point  $x$ ) in comparison to the time point *zero* or the starting inoculum ( $N_0$ ) or as survival ratio:

$$\text{survival ratio} = N_x / N_0$$

The survival or the survival ratio is often represented in a logarithmic scale. Depending on the sample type and condition, which might be subject to biological fluctuations and the treatment itself, more samples than the minimum amount of samples ( $n \geq 3$ ) is needed. Especially irradiated specimens needed more control samples. In the following, all survival assays used in the frame of this thesis are listed.

### Radiation experiments

#### X-ray survival and resistance experiments

To test the effects of ionizing radiation, X-ray radiation was used on dried biofilms and spore solutions. Each experiment was carried out in triplicates, whereas the control samples were treated as the irradiated samples. The closed X-ray system (Gulmay RS225) was used to expose the samples at 200 kV, 15 mA at room temperature. Prior to irradiation, the dose rate was measured with a UNIDOS<sup>webline</sup> dosimeter in combination with a Farmer chamber (ionizing chamber, TM30013). Based on the measured dose rate, the irradiation times for the desired doses were calculated. Samples were placed in ~15 cm distance to the water-cooled anode (X-ray tube, THX 225/G, 0.8 mm beryllium window) without using a filter. Spores were treated in 0.2 ml Eppendorf vessels containing a spore solution with a known concentration (ranging from  $1 \times 10^6$ - $1 \times 10^8$  spores) solved in 100 µl ddH<sub>2</sub>O (Moeller *et al.*, 2014). Membranes harboring *B. subtilis* biofilms were transferred into a sterile petri dish after incubation, dried for 30 min and treated with X-ray radiation. After irradiation, cells and spores were harvested to determine the CFU of the surviving fraction.

### Simulation of galactic cosmic radiation (GCR)

All experiments concerning high doses of heavy ion irradiation on *B. subtilis* biofilms and spores were carried out at the Department of Basic Medical Sciences for Radiation Damages at the National Institutes for Quantum and Radiological Science and Technology (NIRS) in Chiba, Japan. Most experiments were carried out between the 3<sup>rd</sup> and 15<sup>th</sup> of July in 2017. Incubation of biofilms using 2-D clinostats and reference controls was accomplished at the DLR in Cologne. Therefore, biofilms were grown using the standardized growth protocol (starting inoculum of  $1 \times 10^6$  spores per membrane) under 1g and sim- $\mu$ g conditions. After incubation, membranes carrying biofilms were carefully transferred into sterile petri dishes and air-dried at room temperature for 15 h. Biofilms were removed from the surrounding polystyrene frame by using a sterile scalpel. Subsequently, the 1x1 cm membrane fragments were carefully transferred with sterile forceps into a sterile 0.5 ml Eppendorf tube and prepared for shipping. Spores were pipetted into 0.2 ml Eppendorf tubes, each tube containing 100  $\mu$ l ddH<sub>2</sub>O and  $1 \times 10^8$  spores. Biofilms and spores (each individual sample: n=3) were prepared one week ahead of the irradiation experiments and send via express delivery to Japan without being X-rayed by customs. Transport controls as well as laboratory controls were used as references and strictly kept at room temperature. Samples were irradiated at the NIRS, using the HIMAC facility (Heavy Ion Medical Accelerator in Chiba). For this, accelerated Argon ions (500 MeV/n, LET 90 keV/ $\mu$ m) and accelerated Helium ions (150 MeV/n, LET 2.2 keV/ $\mu$ m) were independently applied in doses of 0, 100, 500, 1000 and 1500 Gy. Following the irradiation process, samples were allowed to cool down for 3 days at room temperature and then shipped back to the DLR in Cologne for analysis.

### Wet heat and dry heat survival

For investigating the wet heat resistance of spores, a total volume of 100  $\mu$ l ddH<sub>2</sub>O harboring  $1 \times 10^7$  spores per sample in a standard 2 ml Eppendorf tube was exposed to 90 °C for the desired time (Melly & Setlow, 2001, Melly *et al.*, 2002). Selected time points were 2.5, 5, 7.5 and 10 min as well as a t<sub>0</sub>-control (n $\geq$ 3 per sample/ condition). Subsequently, samples were serially diluted and plated on LB-agar to verify the survivability. For measurement of dry heat resistance properties of spores, aliquots of 50  $\mu$ l ddH<sub>2</sub>O containing  $1 \times 10^7$  spores were air-dried in 2 ml Eppendorf tubes until the solvent is evaporated. Dried samples were heated to 120 °C for 0, 10, 20, 40 and 60 min (Setlow & Setlow, 1995). After treatment, samples were resuspended in 100  $\mu$ l ddH<sub>2</sub>O, serially diluted and plated for CFU determination of the survival fraction.

### Survival in vacuum – low pressure and desiccation assay

In order to verify the survival properties of *B. subtilis* biofilms under low pressure, biofilms were grown under standardized conditions on MSgg + 10 mM L-alanine and R2A (see paragraph 2.3). After incubation, filter membranes harboring biofilms were removed from the medium and air-dried under sterile conditions for one hour. By using sterile forceps, membranes harboring biofilms were carefully transferred into heat sterilized glass petri dishes. To avoid influencing the quality of the applied vacuum because of remaining water within the samples, the biofilms were air-dried under sterile conditions for 24 h. After drying, all glass petri dishes were placed in a vacuum device (assembled by André Parpart at the DLR ground based facilities in Cologne) and incubated for 7 days under low pressure corresponding similar to pressure conditions prevailing in low Earth orbit (at  $\sim 5.7 \times 10^{-7}$  mbar). Subsequently, samples were solved in ddH<sub>2</sub>O (spores) or in 1x PBS and diluted for CFU determination.



## 2.7 Germination assays

For investigating the germination properties of *B. subtilis* spores, a modified germination assay after Nagler *et al.* 2015 was used (Fuchs *et al.*, 2017a, Nagler *et al.*, 2015). During germination, Ca<sup>2+</sup>-dipicolinic acid (Ca<sup>2+</sup>-DPA) is released from the spore into the surrounding medium, which results in a reduction of the refractive index and therefore in a decrease of the optical density at 600 nm. Spores were harvested from SSM-plates or isolated from mature biofilms, which were grown under different gravity regimes or other growth conditions. For this, spores were purified by washing several times in sterile water and microscopically controlled until samples reached a purity of >99 % dormant, phase-bright spores. The titer of spores was determined by plating a serial dilution of the sample of interest and followed CFU-counting. As inoculum, 4x10<sup>7</sup> spores were used (40 µl of 1x10<sup>9</sup> spores/ml stock) per single experimental condition (n= >5). Spores were heated to 70 °C for 30 min to synchronize germination. In the meanwhile, 200 µl of the respective nutrient media (i.e. MSgg or LB), buffers (i.e. PBS, Tris-HCl) germination solutions (i.e. 10 mM L-alanine) or water (negative control, n= > 5 for all substances) were warmed up in a 96-well plate to the desired germination temperature. After spore synchronization and pre-heating the germination medium, each well was inoculated with 40 µl spore suspension (final volume of 240 µl per well, OD<sub>600</sub> of ~0.5) using a multi-channel pipette. Subsequently, the well-plate was immediately transferred into a plate reader (ELx808, BioTek) and the germination kinetics at OD<sub>600</sub> were measured every 2 min for the first hour of incubation, followed by measurements for every 5 min until 4 hours of incubation. For the analysis of data, the mean OD<sub>600</sub> of the control (n≥5) was subtracted from the respective sample measurement. Each time-resolved, corrected measurement was divided separately by the initial OD<sub>600</sub> at the start of the kinetic series to achieve a relative value which represents the OD<sub>600</sub> reduction and therewith the germination efficiency. Maximum germination was reached when the optical density is reduced by 60 % (Chen *et al.*, 2014, Luu *et al.*, 2015).

## 2.8 Molecular biology methods

### Agarose gel electrophoresis

For separation of nucleic acids such as DNA and RNA, a gel consisting of agarose, a polysaccharide, which is able to form a fine-pored polymer matrix when dissolved in TAE-buffer, was used. The pore size of the gel determines the speed and resolution of nucleic acid separation. After warming buffer and agarose, the gel was allowed to cool down while stirring and a gel stain i.e. ethidium bromide was directly pipetted into the cooling gel. Prior to use, a freshly prepared gel was allowed to cool for 20 min and optionally stored overnight in TAE-buffer at 4 °C. Depending on the size of the gel and the amount of samples, different castings with different comb-sizes were used. After solidification and ethidium-bromide staining, the gel was submerged in TAE-buffer within an electrophoresis chamber. The comb was removed and the sample pockets were orientated to the cathode, whereas the bottom of the gel was orientated towards the anode. By applying an electrical field to the electrophoresis chamber, negatively charged nucleic acids move through the gel matrix to the anode. Depending on the voltage (i.e. 90 V) and ampere (2 A, default) used during the runtime (i.e. 40 min) and the final agarose concentration of the gel, smaller fragments migrate faster through the matrix than larger nucleic acids. For comparing fragment lengths, every gel was loaded with a commercially available DNA ladder, harboring fragments of known size and concentration. Depending on the experiment, different ladders were used (Table 5): Before transferring the DNA ladder (2 µl) into the upper left pocket, it was mixed with 1 µl loading buffer and 2 µl TAE-buffer. In the following pockets, premixes of 2 µl loading dye, 2 µl TAE-buffer and 4 µl sample of interest were pipetted. The last two

pockets within one line were usually used for a negative and positive control, with and without a known fragment. In order to visualize the potential run distance of DNA and RNA while running the gel, the bromophenol loading dye is a good indicator. Depending on the research question and the wanted resolution of the separation, the gel can be observed after the loading dye ran for ca. 75 % through the gel. For final analysis, the gel was transferred into a gel documentation chamber. The intercalation between ethidium bromide and nucleic acids can be visualized by emitted fluorescence when exposed to UV-light.

#### Agarose gel (1 %, 100 ml)

1 g	Agarose
Ad. 100 ml	1 x TAE-buffer
3 µl	Ethidium bromide solution (1 %)

Agarose and TAE-buffer were warmed up carefully using a microwave until the agarose was completely dissociated, without boiling the gel. Afterwards, a magnetic stir bar was added, for further mixing and the gel was cooled down for 3 min. In order to stain the gel, 3 µl ethidium bromide solution (1 %) were added directly into the liquid gel, stirred for 30 sec and then transferred into the casting to polymerize.

**Table 5: List of DNA ladders for agarose gel electrophoresis**

DNA ladders were used to compare the approximate size of nucleic acid fragments with a set of fragments with known size.

<b>Name*</b>	<b>Range [kb]</b>	<b>Agarose [%]</b>	<b>Main targets</b>
50 bp	0.05 - 1	2.5	PCR
100 bp	0.1 - 1	1.5	PCR, RNA
100 bp Plus	0.1 - 3	1.5	PCR, RNA
1 kb	0.25 - 10	1	gDNA
1 kb Plus	0.075 - 20	1	gDNA
2-log	0.1 - 10	1 - 1.5	Irradiated DNA

\*Commercial name of all DNA ladders: New England Biolabs, Ipswich, USA

#### Transformation of *B. subtilis*

The wild-type strain *B. subtilis* NCIB 3610 is barely transformable. Instead, a mutant with the NCIB 3610 background, DK1042, which carries a deletion in *comI* (plasmid-encoded), was used as a transformable recipient (Konkol *et al.*, 2013). The transformation protocol was slightly modified after Commichau *et al.* 2015 (Commichau *et al.*, 2015). In order to prepare suitable growing conditions, a fresh overnight pre-culture of DK1042 was used to inoculate 10 ml MNGE-medium (including casamino acids) to an OD<sub>600</sub> of 0.1. Incubation took place at 37 °C under constant agitation at min. 200 rpm until an OD<sub>600</sub> of >1.2 was reached. The culture was diluted with 10 ml pre-warmed MNGE-medium without casamino acids and incubated at 37 °C for one hour to simulate starvation and forcing the strain to be more competent. At this point, competent cells were pelleted and resuspended in 1.5 ml of supernatant, to reduce the volume and mixed 1:1 with sterile 50 % glycerin in order to store 300 µl aliquots at - 80 °C. Fresh aliquots were immediately mixed with 1 µg, 3 µg and 5 µg of the PCR-product of interest or control and incubated in Eppendorf tubes for 30 min at 37 °C prior to addition of 100 µl of expression mix. Cells were incubated for one hour at 200 rpm at 37 °C and plated on SP-medium (1.5 % agar) using the antibiotic corresponding to the transformed PCR-product.

### Polymerase chain reaction (PCR)

For amplifying or ligating DNA-fragments of choice, PCRs (polymerase chain reactions) are a valuable tool. As a template, genomic DNA of *B. subtilis* NCIB 3610 was isolated according to the manufacturer's instructions, via a peqGOLD Bacterial DNA Kit (lysozyme incubation increased to 60 min). Phusion High Fidelity (PHF) Polymerase was used for amplification of gene products. This polymerase harbors a proofreading function, has an elongation speed of 2-4 kb/min (at 72 °C, depending on the length of the fragment) and has a good performance for G/C rich DNA-fragments. Master mixes composed of ddH<sub>2</sub>O, polymerase buffer (HF-buffer), dNTPs (nucleoside triphosphates), primers and High Fidelity Polymerase were prepared on ice (Table 6).

**Table 6: Master mix for standard PCRs**

Concentrations of ingredients used for a single 100 µl PCR sample. For higher sample amounts, ingredients were combined to a single master mix without the template DNA. Due to possible incorrect pipetting calibration, an extra volume of 5-10 % was added for larger batches.

<b>Final concentration</b>	<b>Reagent</b>
0.4 mM	dNTPs
0.4 µM	Primer Fw*
0.4 µM	Primer Rev*
1 x	PHF-Buffer
1 u	PHF-Polymerase
15-250 ng	Template DNA
Ad. 100 µl	ddH <sub>2</sub> O

*\*Primers are resuspended in nuclease-free water to a stock concentration of 100 µM and working solutions of 20 µM.*

The initial denaturation step was performed for usually 1-2 min, followed by 30-35 cycles of repeated denaturation, annealing and elongation steps. The annealing temperature was calculated based on the melting temperature ( $T_m$ ) of used primers and was usually supported by the primer manufacturer. The elongation time depends on the polymerase speed and on the fragment length. After the amplification cycles, a final elongation was performed for 10 min prior to cooling the samples down to 4 °C. A list of used primers is given in the appendix.

**Table 7: Standard amplification PCR-program and LFH-specific PCR-program**

<b>Standard PCR-program</b>			
<b>Step</b>	<b>Time</b>	<b>Temperature [°C]</b>	<b>Cycles</b>
Initial denaturation	1 min	98	1
Denaturation	15 s	98	
Annealing	30 s	$T_m^*$	30-35
Elongation	15-30 s/kb <sup>†</sup>	72	
Final elongation	5-8 min	72	1
Storage	∞	4	1

**LFH-PCR**

Step	Time	Temperature [°C]	Cycles
Initial denaturation	1 min	98	1
Denaturation	15 s	98	
Annealing	30 s	52	10
Elongation	15- 30 s/kb <sup>†</sup>	72	
Addition of LFH primer			
Denaturation	15 s	98	
Annealing	30 s	T <sub>m</sub> *	21
Elongation	4 min + 5 s/cycle	72	
Final Elongation	10 min	72	1
Storage	∞	4	1

\* Annealing temperature: Calculated primer melting temperature

† Elongation time: Adjustment after fragment length

In contrast to standard PCRs, a PCR can also be used to ligate fragments of interest. This is of particular interest, if DNA-sequences for a long-flanking homology (LFH) approach shall be created (Nikawa & Kawabata, 1998, Commichau *et al.*, 2015). The technique allows substituting the gen of interest with an antibiotic cassette as marker. For this, an antibiotic cassette is designed via PCR with homologues sequences to the outer upstream and downstream boundaries of the gen of interest. Technically, three PCRs are needed: cassette modification and amplification, gen-of-interest upstream region modification and gen-of-interest upstream region modification. As templates, gDNA of *B. subtilis* NCIB 3610 and isolated DNA of an antibiotic cassette were used. Amplified fragments were ligated using an LFH-ligation PCR Table 7. After ligation, upstream-flanking and downstream-flanking primers were pipetted to the samples, which were still in the thermocycler to start the finalization of the modified LFH-antibiotic cassette. Resulting amplified DNA-fragments or modified LFH-cassettes were stored at 4 °C for short term storage or at -20 °C for long-time storage.

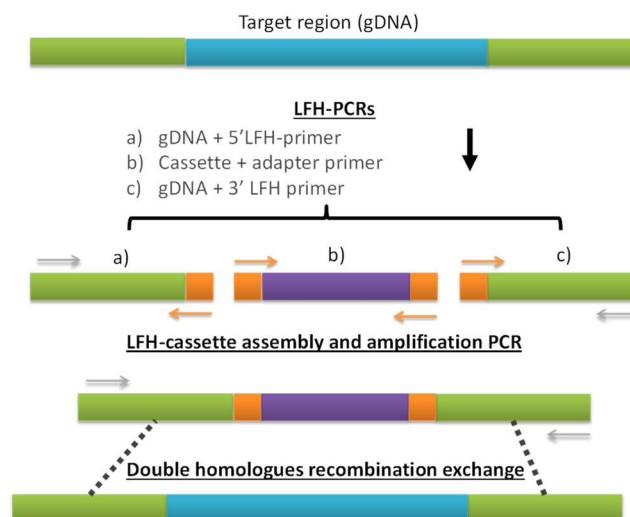


**Figure 10: Schematic overview of the long-flanking homology technique**

The long flanking homology technique is used to specifically delete a target gen or nucleotide sequence (blue sequence) from the gDNA (green) and replace it with an antibiotic cassette whose ends are provided with adapters (orange). In addition, the gDNA is equipped with adapters corresponding to the cassette to be

inserted so that it can be assembled and amplified via PCR. The modified cassette with overlapping gDNA ends is replaced by double homologous recombination with the gDNA *in vivo*. By screening on a nutrient medium containing antibiotics corresponding to the inserted antibiotic cassette, modified mutants can be successfully detected. Modified after (Nikawa & Kawabata, 1998, Commichau *et al.*, 2015).

For quality control, length of amplified DNA-products was confirmed via agarose gel electrophoresis. If fragments and controls were meeting the expectations, a PCR-cleanup was performed using a QIAquick PCR Purification Kit according to the manufacturer. For elution, sterile 50 °C warm ddH<sub>2</sub>O was used and purified DNA samples were stored at -20 °C. After PCR-cleanup, gDNA or LFH-cassettes were directly used for further PCRs or transformation of competent cells.

### **Transcriptomics of biofilms (RNAseq)**

To investigate the influence of simulated microgravity on young biofilms by transcriptome analysis, a time-resolved experiment series was performed. Per biological replica  $1 \times 10^8$  *B. subtilis* NCIB 3610 spores were used as inoculum on hydrophilic PTFE-membranes. After 10 min drying under sterile conditions, membranes were immediately placed on MSgg-medium (supplemented with 10 mM L-alanine, solidified with 1.5 % agar), wrapped with Parafilm® and placed in a fast-rotating 2-D clinostat or stored upside down as reference for 4 h, 8 h and 16 h in at 37 °C. Subsequently, cells were harvested using 1 ml ice-cold PBS-buffer, mechanically solved using sterile loops and pooled by combining three biological replicates in one sample. Pooled samples were treated on ice and centrifuged at 4 °C, at 14000 rpm for 1 min. Before freezing the pellets in liquid nitrogen, the remaining supernatant was discarded. Frozen bacterial pellets were stored at -80 °C.

### **Modified hot phenol RNA isolation using the RNeasy Kit**

RNA extractions tend to be very sensitive towards any minor nucleotide contamination, therefore only RNase free materials such as tips, reaction vessels, buffers and DEPC-water were used. Before starting the RNA-isolation the following solutions was heated to 75 °C: LETS-buffer (1.6 ml/reaction), acid-phenol (1.2 ml/reaction) and acid-phenol-chloroform (1.6 ml/reaction). In addition, a 15 ml falcon tube including 1 ml acid washed beads (~ø 106 µm) and 1.2 ml acid-phenol and a 15 ml falcon tube containing 1.6 ml acid-phenol-chloroform were prepared per reaction. Additionally, two 2 ml vessels containing each 700 µl isopropanol were prepared. All materials such as pipettes and racks were UV-irradiated for 20 min and treated with RNaseZap™. Two different methods to lyse cells or spores were used: Disrupting spores/veg. cells using a FastPrep™ and using a modified hot phenol assay. Both methods resulted in an aqueous phase containing RNA, which is needed to proceed with the RNeasy Kit.

### **Spore/veg. cell pellet - preparation for RNA isolation**

Spores resist mechanical shear forces and therefore need a special treatment using a FastPrep™ to disrupt the spore coat. Frozen spore pellets were resuspended in 500 µl LETS-buffer (4 °C) and transferred to Lysing Matrix B tubes containing 900 µl aqua-phenol (ice-cold). The disruption was carried out by four treatments each for 45 secs at 6 m/s (cool) and finally centrifuged for 10 min at  $8000 \times g$  at 4 °C. The supernatant was transferred into a tube containing 500 µl chloroform, was inverted carefully for several times and centrifuged at  $8000 \times g$  for 10 min at 4 °C. After the resulting phase separation, RNA was present in the upper aquatic phase.

**Vegetative cells: Pellet – hot phenol RNA isolation**

Frozen pellets (-80 °C) were resuspended in 1.6 ml 75 °C hot LETS-buffer and transferred into a 15 ml falcon tube containing acid-washed beads and 75 °C hot acid-phenol. After vortexing each tube for 3 min, 1.2 ml chloroform were added, vortexed for 30 secs and centrifuged at 3200 × g for 15 min at 4 °C. Within the resulting phase separation, RNA remained in the upper aquatic phase.

**RNA isolation and purification (modified) using the RNeasy Kit**

Depending on the method used to isolate RNA from either the FastPrep™-assay (~300 µl sample volume), or the hot phenol method (1.6 ml sample volume), both resulted in an aqueous phase containing RNA. The RNA-containing aqueous phase was carefully transferred with a pipette without touching the interphase. For a), the aqueous phase was transferred into an Eppendorf tube containing 1:1 acid phenol chloroform (75 °C). For b), the aqueous phase was transferred into a 15 ml falcon tube containing 1.6 ml acid phenol chloroform (75°C). Afterwards samples were vortexed for 3 min and centrifuged at 3200 × g for 10 min at 4 °C. The liquid phase was carefully removed and pipetted into an Eppendorf tube containing 0.7 ml isopropanol. Prior to a 10 min incubation time at room temperature, all samples were gently mixed. For pelletizing potential RNA, all samples were centrifuged at max speed for 25 min at 4 °C and the supernatant was removed afterwards. For washing the pellet, 1 ml of 4 °C cold 75 % ethanol was used and subsequently removed after centrifugation at max speed for 5 min at 4 °C. In order to remove remaining ethanol, samples were air-dried for 3 min until no liquid was visible. Elution of RNA was achieved by adding 40 µl of DNase-free water and carefully pipetting up and down for three times. At this point, eluted RNA was stored at -80 °C or immediately processed further to apply the DNase treatment of the RNeasy Kit. For DNA removal, 10 µl RDD buffer and 2.5 µl DNase were added and incubated for at least 25 min at 37 °C. After incubation, 350 µl RLT-buffer and 250 µl ethanol absolute (100 %) were added, mixed and transferred into an RNeasy spin column, which is centrifuged for 15 secs at 8000 × g. The flow-through was discarded. In order to perform a second, on column digestion- DNase treatment step, 350 µl RW1-buffer were added, centrifuged for 15 secs at 8000 × g and a premix of 70 µl RDD buffer and 10 µl DNase were pipetted into the column, which is incubated for 25 min. Subsequently, 350 µl RW1-buffer were added and centrifuged at 8000 × g for 15 secs, whereas the flow-through was discarded and 500 µl RPE-buffer were added. All columns were centrifuged at 8000 × g for 15 secs and for washed with another 500 µl RPF-buffer were applied per column. For removing remaining buffer and drying, each column was centrifuged for 2 min at 8000 × g and transferred into a fresh tube, centrifuged for 1 min at 8000 × g and finally transferred into a 1.5 ml DNase-free collection tube. Elution was performed twice, with 25 µl RNase-free water per run and centrifuging at 8000 × g for 1 min. Following the elution, an agarose-gel (2 %) was used to ensure, that genomic DNA was not contaminating the RNA eluate and to control whether the RNA is degraded. After RNA isolation, the concentration was measured with a Qubit™ or a NanoDrop using 1.5 µl of the eluate. The adsorption ratio at 260 nm/280 nm should be at ~2.0, which corresponds to pure RNA and the adsorption ratio at 260 nm/230 nm should be at ~2.0 - 2.2. Depending on the concentration, the RNA was diluted to 150-300 ng/µl and if several samples were analyzed at the same time, the concentration was adjusted to similar quantities. Following the concentration adjustment, a BioAnalyser assay was run by using the Agilent 6000 Nano Kit for prokaryotes according to the manufacturer, in order to determine the RNA integrity, purity, and the total amount of RNA for calculating the inoculum for the rRNA-depletion kit. Spore RNA shows an additional peak between the characteristic 16S- and 23S-rRNA peaks, which negatively influences the RIN-number (RNA integrity number) calculation. For non-spore samples the best possible RIN number is 10.0, whereas possible samples can be processed

with RINs better than 8.0. For spore samples, an investigation of the histogram is helpful to manually control the sharpness of the rRNA and the spore peak as well as the flat baseline. Therefore, samples with RINs of  $\geq 6.0$  were considered for rRNA-depletion. The “Ribo-Zero® rRNA Removal Kit” (illumina®) was used, following the manufacturer’s manual to reduce the amount of interfering rRNA within all samples. In addition, a fluorometric quantification using a Qubit™ was used to verify successful rRNA depletion. Library preparation was achieved by using the “NEBNext® Multiplex Oligos for Illumina® (Dual Index Primers Set 1)” - kit according to the manufacturer’s instructions. Subsequent sequencing was performed using the illumina® Nextseq® platform with a mid-output at 2x 75 bp, 150 cycles (V2). Acquired RNAseq-data was uploaded into the Google Drive cloud (Google LLC) for multi-purpose access. Due to limited bioinformatic resources at the DLR, sequence data was analyzed in cooperation with Dr. Bentley Shuster (NYU, USA), Dr. Anne de Jong (University of Groningen, NL) and Dr. Michael Dwayne Morrison (Lawrence Livermore National Laboratories, USA).

## Proteomics

### Bradford assay – determination of protein concentration

The Bradford assay is a simple colorimetric method to determine the protein concentration of a sample of unknown protein concentration. A ready-to-use kit (Coomassie Protein Assay Kit, Thermo Scientific, 5 x) was used to perform the protein assay according to the manufacturers manual.

### Stable isotope labelling with amino acids in cell culture (SILAC)

A common technique for the comparison of the proteome of two sets of samples is the stable isotope labelling with amino acids in [cell] culture, hereinafter referred as SILAC. The overall aim was to compare quantitatively the abundance of proteins of biofilms grown under 1g and sim- $\mu$ g conditions. Most biofilm assays in this thesis were performed using a standardized minimal medium based on the receipt of Branda et al. 2001, which supplements of *B. subtilis* NCIB 3610 with L-glutamate as N-source as well as L-tryptophan and L-phenylalanine (Branda *et al.*, 2001). SILAC requires the incorporation of stable isotopes of amino acids into the proteins of the respective sample. L-lysine- $^{13}\text{C}_6$ ,  $^{15}\text{N}_2$  hydro-chloride was used as “heavy” amino acid in this study because after protein extraction, isolated proteins need to be digested with proteases. LysC was used as protease which cleaves at the C-terminal region in proteins after the incorporated heavy L-lysine (Soufi & Macek, 2014). Therefore, only peptides were formed after digestion, which carry at most only one isotope-labelled amino acid. This property facilitates the subsequent mass spectrometry analysis of all peptides. The wild-type variant of *B. subtilis* NCIB 3610 is L-lysine prototroph. Therefore, a  $\Delta$ lysA (coding for diaminopimelate decarboxylase) strain in the background of NCIB 3610 was used for SILAC. The deletion forces the mutant to be auxotrophic for L-lysine, whereby the isotopically labelled L-lysine from the medium is incorporated into newly synthesized proteins (Soufi *et al.*, 2010).

The experimental setup for SILAC comprises two different growth conditions: 1g controls were pre-incubated in MSgg-broth containing 0.025 % heavy L-lysine and were allowed to form biofilms on solidified MSgg medium containing 0.025 % of the labeled amino acid. Samples for simulated microgravity were pre-incubated in 0.025 % “light”/ unmodified L-lysine (MSgg-broth) and were grown under sim- $\mu$ g conditions on MSgg-agar with unlabeled L-lysine (0.025 %) using a fast rotating 2-D clinostat. For the pre-inoculations  $1 \times 10^7$  spores of *B. subtilis* NCIB 3610  $\Delta$ lysA were used as inoculum for each 5 ml MSgg broth harboring the respective labeled or unlabeled amino acid and the antibiotic marker (erm, lcm). After reaching a final OD<sub>600</sub> of  $\sim 0.4$ , 5 ml of the culture was collected via

centrifugation for 2 min at 6000 rpm. Pellets were washed in 1 ml sterile PBS and resuspended in 1 ml PBS. Biofilm formation was carried out using the standardized membrane filter system. For each inoculated filter membrane 10  $\mu$ l of washed cells were used. Filters were air-dried for 5-10 min under sterile conditions and placed on MSgg-agar containing the respective amino acid: heavy L-lysine for the reference control (1g) and normal L-lysine for simulated microgravity samples (sim- $\mu$ g). Samples were incubated at 37 °C for 3 days. After incubation, filters were transferred into sterile petri dishes using heat sterilized forceps. 1 ml of sterile ddH<sub>2</sub>O was added into each filter and a sterile loop was used to loosen the biofilm. Dissolved biofilms were transferred into a sterile 2 ml Eppendorf tube, pelleted and washed in ddH<sub>2</sub>O at 4 °C at 14000 rpm for each 5 min. Pellets were immediately frozen in liquid nitrogen after discarding the supernatant and stored at -80 °C.

For the total protein lysis, pelletized biofilms were resuspended in 500  $\mu$ l of cold (4 °C) TLB-buffer, containing a protease inhibitor, and were incubated on ice for 2 min. Each lysate was transferred into a pre-cooled (4 °C) lysing matrix B tube (MP biomedical) and mixed via vortexing for 7 sec. Lysing matrix tubes were placed in a FastPrep device and treated with 6 m/s for 45 secs for 4 cycles. Between every crushing step, the lysate was allowed to cool down on ice for 3 min. After cell disruption, all samples were centrifuged for 10 min at 14000 rpm at 4 °C. The protein containing supernatant (~250-300  $\mu$ l) was collected in fresh protease-free 1.5 ml Eppendorf tubes. Proteins were either frozen in liquid nitrogen for storage at -20 °C or prepared for SDS-denaturation. In order to denature the lysate 5x SDS buffer was added to a final concentration of 1x (i.e. 60  $\mu$ l 5x SDS-buffer to 300  $\mu$ l lysate). Samples were mixed via vortexing and boiled for 20 min at 99 °C and then cooled down at room temperature. Because SILAC requires samples with equal protein concentration, the protein concentration was determined immediately after denaturation via the Bradford assay or samples were stored at -20 °C.

50  $\mu$ g of heavy and light protein samples were mixed and reduced in 50 mM TEAB buffer (Sigma) by adding TCEP (Tris(2-carboxyethyl)phosphine, Merck) with a final concentration of 5.7 mM. After incubation at 60 °C for 45 min, 0.5 mM Iodacetamididoacetamide (Merck) were added to a final concentration of 0.5 mM and incubated for 20 min at 22 °C. Proteins were digested by incubation with trypsin over night for 18 h at room temperature. Resulting peptides were loaded on STAGE-tips filled with 30  $\mu$ g of Luna C18-Material (Phenomex), which was washed and equilibrated beforehand with acetonitrile and water, respectively (both ChemSolv). Desalting was performed by washing twice with 0.1% acetic acid and centrifugation (9000 rpm, 1 min). To elute peptides from the STAGE-tips, 30  $\mu$ l Acetonitrile acetonitrile containing 0.1% acetic acid were added and pressed through the tip using pressurized nitrogen (3 bar). Eluates were collected in glass vials with micro inserts (ChemSolv). Acetonitrile was removed by adding 20  $\mu$ l 0.1% acetic acid and vacuum centrifugation to a final volume of 10  $\mu$ l.

Eluted peptides were measured on a nanoHPLC-MS setup. An UltiMate 3000 nanoLC (Dionex) was coupled to a QExactive classic mass spectrometer using a NanoSpray Flex source (both Thermo Scientific). Sample aliquots of 2  $\mu$ g were loaded and desalted onto an Acclaim PepMap 100 precolumn (2 cm x 100  $\mu$ m, 5  $\mu$ m particle size, 100 Å pore size) for 6 min at 5  $\mu$ l/min flow before switching onto a PepMap RSLC column (25 cm x 75  $\mu$ m, 2  $\mu$ m particle size, 100 Å pore size). Peptides were separated using the following gradient running H<sub>2</sub>O + 0.1 % acetic acid (eluent A) against 95 % acetonitrile + 0.1 % acetic acid (eluent B) with a flow of 200 nl/min: 2 % to 35 % in 165 min, to 50 % B in 15 min, to 90 % B in 15 min, keeping at 90 % for 15 min, equilibration at 2 % B for 20 min. Each sample was injected twice. The QExactive was run in Top15 DDA mode with a dynamic exclusion of 60 s. MS1 spectra were acquired with a resolution of 70,000, whereas MS2 spectra were acquired in 17,500 x resolution.



## 2.9 Statistics, data visualization and other software

In general, raw data such as CFU counts, OD<sub>600</sub> values or transcriptomic data were saved and processed in Microsoft Excel. Furthermore, Excel was used to calculate mean values and standard deviations or standard errors. Profilometry data was analyzed using “R”-scripts, which were provided by Prof. Dr. Oliver Lieleg and Carolina Falcón García. All other graphs and plots were created using the statistical software SigmaPlot 13.0. Significance tests and statistics were also performed using SigmaPlot. SubtiWiki, a data-base harboring all genetic information about *B. subtilis* was used as library for in-detail information regarding single genes, regulatory networks, physiology and literature research (Zhu & Stülke, 2018). For microscopy, the following software bundles were used: Zen blue and Zen black for Zeiss devices, cellSens for Olympus microscopes, µsoft for the profilometer, Nikon Imaging NIS-Elements, AR for Nikon devices and OSIS Scandium (SEM) and OSIS iTEM (TEM) for electron microscopy devices. For image manipulation and creating figures, ImageJ Fiji (Schindelin *et al.*, 2012) and Microsoft PowerPoint were used. References were sorted and organized with EndNote X7 and EndNote X9. All used software, including not mentioned programs are listed in a separate chart in the appendix.

## 3. Results

### 3.1 Standardized biofilms

#### ***B. subtilis* biofilm formation**

Wild-type *B. subtilis* strains such as NCIB 3610, offer the possibility to investigate a native way of biofilm formation other than the so-called domesticated strains like *B. subtilis* 168 or 168 derivatives (McLoon *et al.*, 2011). Generally, biofilm growth mainly takes place at interfaces between solid, liquid or gas phases and is strongly dependent on the growth conditions. In nature and under laboratory conditions, several types of biofilms can exist for instance at the interface between solid media and air, or liquid media and air or between liquid media and solid materials (i.e. biofilms on the bottom of a culture flask). There is only one exception: biofilms can also be formed as submerged pellicles, the only way of persistence, where settlement does not take place at an interface. Biofilm growth, structure and properties are strongly dependent on water availability. In natural environments, *B. subtilis* biofilms are often associated with plant roots, a habitat, which is frequently subject to changes in water availability (Allard-Massicotte *et al.*, 2016, Beauregard *et al.*, 2013). For the cultivation of biofilms under laboratory conditions, only three cultivation options are applicable: shaking or standing incubation in liquid media or the incubation on solid medium. All three incubation options offer advantages and disadvantages, depending on the research question. Liquid incubation allows defined growth conditions, good aeration and nutrient availability and can be used to produce large amounts of biomass within a short time. Incubation on solid media produces less biomass, requires more manual handling and decelerates the growth in contrast to liquid media. Bacteria, grown on (semi-) solid media, form highly structured biofilms, which are of particular interest in terms of architectural and structural analyses (van Gestel *et al.*, 2014). One of the major analyzed growth parameters in this thesis comprises the simulation of microgravity by using fast rotating 2-D clinostats and RPMs. The simulation is based on the rotation of samples among one axis (clinostat) or two axes (RPM) to zero the gravitational pull over time. For liquid incubation, a rotating pipette clinostat can be used, which offers only a very limited volume of less than 1 ml. This technique allows only a limited range of flexibility and is not suitable for the investigation of complex biofilm structures. Biofilm incubation on agar based (solid) media offers more possibilities to measure and determine the impact of simulated gravity on a structural and architectural level.

#### **Defining a reproducible inoculation procedure**

*B. subtilis* cultivation was usually conducted by using a washed liquid pre-culture and plating out a few microliters on solid LB-media. Incubation was usually at 37 °C for 15 h and colony growth was macroscopically visible. Depending on the definition of biofilm growth, the resulting colonies on solid media can already be classified as biofilms. Highly structured biofilms are usually formed under extreme stressful or harmful growth conditions. In 2001, Branda *et al.* introduced a specific minimal medium for promoting the biofilm formation of *B. subtilis* NCIB 3610 (Branda *et al.*, 2001). In contrast to standard incubation media with variable amounts of nutrients and trace elements, minimal media are particularly suited to culture biofilms under predefined conditions. Limited nutrient availability is known to promote the formation of biofilms.

The inoculation of fresh pre-cultures is a classical approach in which cells are grown to their late exponential phase in order to transfer them on fresh media to start the experiment. As mentioned before, this was usually done after a defined incubation time, i.e. after 15 h hours or after determining the OD<sub>600</sub>. After washing the cells in PBS-buffer, the cell pellet was usually resuspended in more PBS

until a wished concentration was reached. To determine the amount of cells within the buffer, cells were serially diluted and plated or counted in a cell counting chamber for microscopy. Neither of the two methods allows determining the amount of initial founder cells with the needed accuracy, especially when low amounts of cells ( $\leq 1 \times 10^6$ ) were required for starting an experiment. Founder cells represent the inoculum which is used at the beginning of a defined and standardized experiment. Furthermore, the volume of the inoculum for biofilms should not exceed more than 20  $\mu\text{l}$  (rather 10  $\mu\text{l}$ ), to allow the colony biofilm to grow from the smallest spot possible. This helps to enable various experiments, such as diameter or growth determination and is important for the simulation of microgravity which requires small radii to achieve the desired sim- $\mu\text{g}$  accuracy. For achieving a reliable and reproducible amount of founder cells for each experiment, spores of a known concentration were used as inoculum. Spores of all used strains were grown on SSM-agar or in liquid SSM without additional D-glucose at 30 °C for five days (solid incubation) or three days (liquid incubation). Washing in sterile water guaranteed removal of vegetative cells and debris. Verification of spore quality was performed by phase contrast microscopy. By determining the titer of a spore solution, spores were adjusted to different working solutions of e.g.  $1 \times 10^9/\text{ml}$  for  $1 \times 10^7$  spores in 10  $\mu\text{l}$ . As mentioned before, the inoculum of almost all conducted experiments comprised 10  $\mu\text{l}$ . To guarantee best germination, spores were synchronized for 30 min at 70 °C (Setlow, 2013) and cooled down to room or incubation temperature.

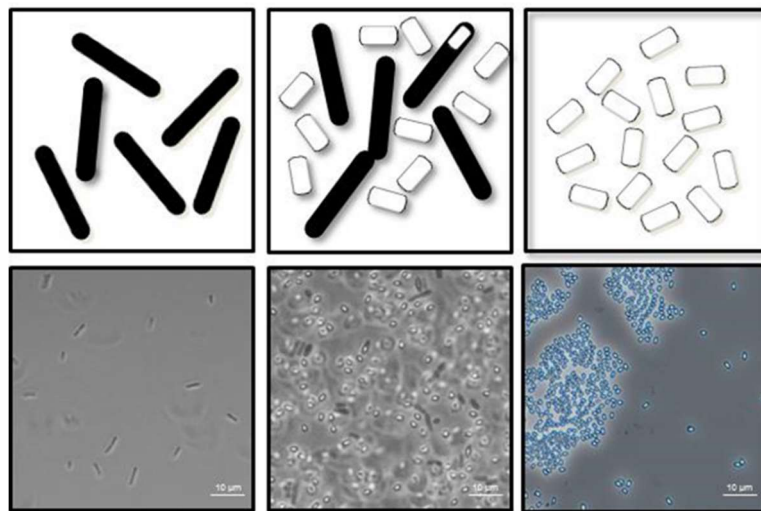


**Figure 11: Visualization of *B. subtilis* spore production and purification**

*B. subtilis* is a rod-shaped bacterium, which does not form spores during short incubation times ( $\sim 15\text{h}$ , 37 °C, LB-broth) such as in liquid overnight cultures **(A)**. Given a fresh overnight culture, 100  $\mu\text{l}$  of washed vegetative cells can be used to inoculate solid (5 days 30 °C) or liquid sporulation media (SSM, 48-72 h at 37°C). After inoculation and harvesting by collecting grown cultures in sterile ddH<sub>2</sub>O, a mixture of cells (partwise including spores), spores and cell debris is collected **(B)**. By applying several washing steps and discarding the supernatant, only spores remain in solution **(C)**. The spore concentration can be adjusted by diluting or concentrating the spore stock to a working solution of known spore content by titer determination. Purified spores are microscopically checked and confirmed whether the concentration of dormant (phase-bright) spores is higher than 99 %. Prior to use spores as inoculum for biofilm experiments, spore solutions were stored at 4 °C. Scale bar represents 10  $\mu\text{m}$ . Modified after (Fuchs *et al.*, 2017a).

### Influence of the germination and incubation temperature

In addition to heat synchronization of spores at 70 °C, the incubation temperature during germination (Figure 12) influenced the germination efficiency. As shown in Fuchs *et al.*, the number of spores not germinated remains high at low temperatures (Fuchs *et al.*, 2017a). In order to investigate the

germination of spores at 4 °C, MSgg medium supplemented with 10 mM L-alanine was used instead of water as storage medium. Despite the presence of the germinant, no germination was observed. At 15 °C, which is on the verge of the favorable growth temperature of *B. subtilis* (van de Vossen *et al.*, 1999), spores germinated up to 50 %, although there was no growth observable. Best germination rates were achieved within the optimal growth temperature (16-46 °C) (Warth, 1978), leaving only 10- 15 % of spores dormant at 22, 30, 37 and 45 °C after 1 h of incubation. At 55 °C, which is within the tolerated temperature spectrum of *B. subtilis*, 80 % of spores germinated, indicating that best germination is related to the favored growth temperature. This effect proved to be a time-dependent kinetic, which can be only observed after short incubation times. After more than 4 hours, no dormant spores could be observed at any temperature other than 4 °C.

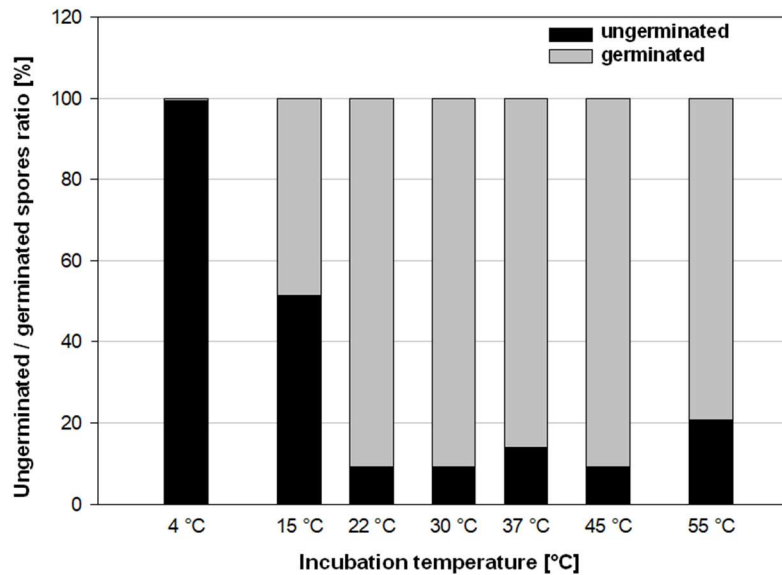


**Figure 12: Influence of temperature during *B. subtilis* spore germination**

In order to use *B. subtilis* spores for standardized biofilm growth or germination experiments, different incubation temperatures were tested to predict optimal spore germination. For each temperature  $1 \times 10^4$  spores (previously stored at 4 °C), were transferred into pre-warmed MSgg-medium (supplemented with 10 mM-L-alanine) of the respective temperature and incubated for one hour under constant agitation (100 rpm). Following the incubation, pasteurization was performed for 10 min at 80 °C to distinguish between germinated and non-germinated spores. CFU and spores were determined by serial dilutions. Spores have not been heat synchronized prior to the experiment. After 4 h of incubation, no dormant spores were observable in samples other than 4 °C. Sample size:  $n \geq 3$  (technical replicates = 2), error bars not shown: 4 °C: 0 %, 15 °C: 8 %, 22, 30, 37, 45 °C: 3-4 %, 55 °C: 5 %. Modified after (Fuchs *et al.*, 2017a).

### Biofilm medium and initiation of biofilm development

Based on the germination data and the standard incubation recommendations from literature, all biofilm experiments were performed with heat-synchronized spores at either 30 °C or 37 °C to ensure the best possible homologous germination. As medium for standardized experiments, MSgg according to the original recipe of Branda *et al.* was used (Branda *et al.*, 2001). Additionally, the medium was supplemented with 10 mM L-alanine as non-growth influencing germinant. MSgg, as minimal growth medium, limited available nutrients and forced vegetative cells to synthesize all needed molecules except for L-tryptophan, L-phenylalanine and thiamine. Growth under these stressful conditions promoted biofilm formation. Mature biofilms strongly attached to agar and could not be removed without destruction. This was problematic for the determination of CFU and the number of spores. To counteract this problem, hydrophilized PTFE-filter membranes encased in a polystyrene ring

(membrane filter) were used to avoid the problem of agar-attachment (see Materials and Methods). Spores were synchronized and 10  $\mu\text{l}$  of a desired spore concentration were pipetted onto the center of a membrane filter. The spore distribution strongly affects the biofilm shape and structure (Figure 13). Ideally and for best comparison of biofilms, the spore suspension was pipetted so that a circular-shaped droplet was formed (Figure 13, A). Due to the coffee-ring effect (Deegan *et al.*, 1997) and therewith convection forces, spores accumulate at the edges of the original droplet and form a spore ring. In the inner circle of the spore ring, spores are uniformly and less dense distributed (Figure 13, B). The shape of the spore distribution strongly influenced biofilm growth.

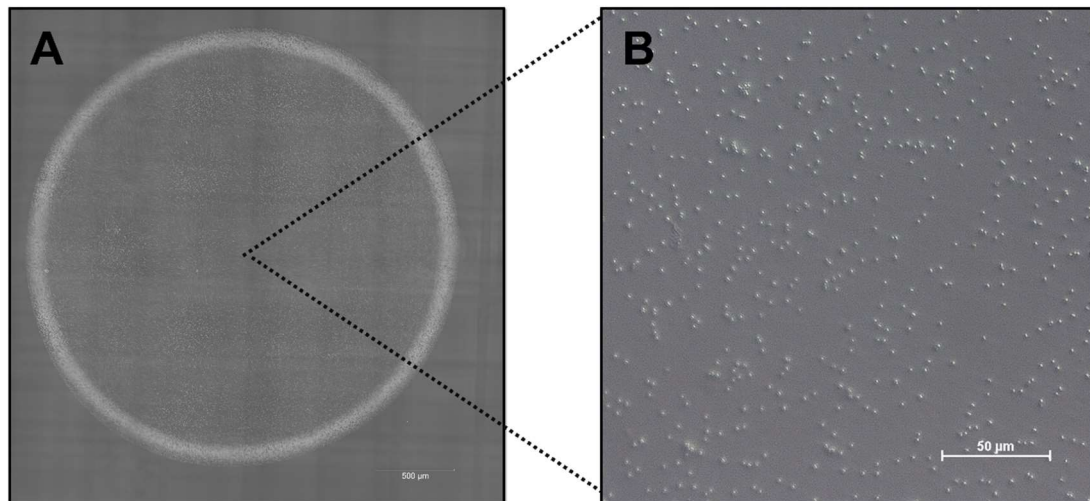


**Figure 13: Spore distribution after drying**

For the inoculation of standardized biofilms, spores were used as inoculum. Spores are stored in known concentrations in water at 4 °C and are pipetted onto PTFE-membranes for air-drying before incubation. Image A represents a typical spore distribution of 10  $\mu\text{l}$  harboring  $\sim 1 \times 10^6$  *B. subtilis* spores after 10 min drying. Due to the drying effects, spores accumulate at the edges of the original droplet (enlarged in Figure 16 A). The inner center of the spore droplet comprises an almost Gaussian spore distribution among the whole area (B). During germination and outgrowth, spores and their descendants are facing less competition regarding nutrient availability and space. This growth advantage allows a faster individual development in the center of the inoculation drop, but becomes negligible over time. Scale bars represent 500  $\mu\text{m}$  (left image) and 50  $\mu\text{m}$  (magnification, right image).

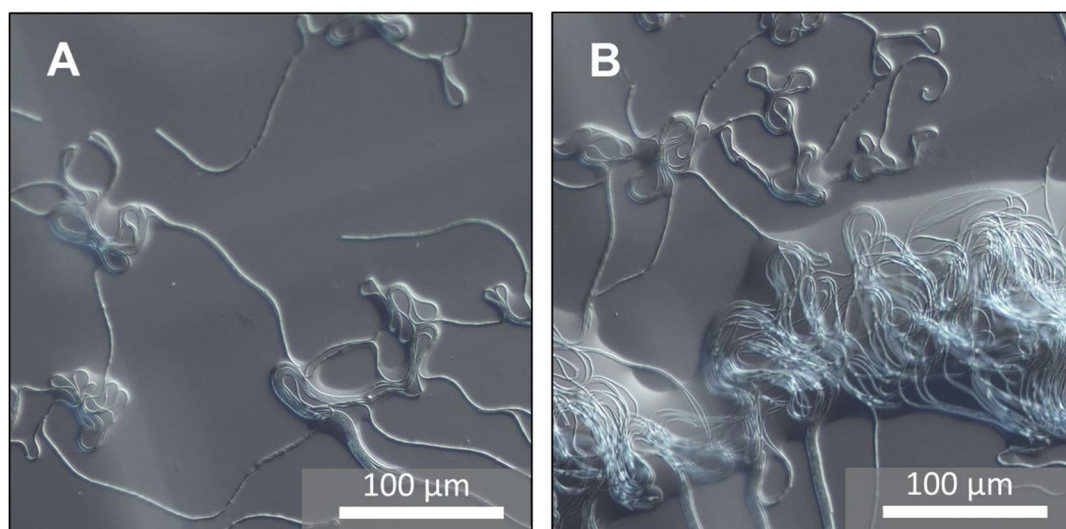


**Figure 14: Surface wetting via surfactin production of young individual *B. subtilis* cells**

Individual *B. subtilis* 168 spores were dried under sterile conditions and were scattered over LB-agar (1 mm thickness) and incubated at 37 °C for 6 h. Vegetative cells are interconnected within long chains surrounded by a

thin film of water (**A** and **B**), which can accumulate on the surface of the medium through the production of surfactin. Surfactin is a lipopeptide which lowers the surface tension of water and enables an improved movement of *B. subtilis* on agar-based media. A higher cell density leads to increased surfactin levels and thus to a larger accumulation of water (**B**). Single cells as well as cells associated in chains are able to move actively within this water to propagate and colonize in more distant regions. Scale bar represents 100  $\mu\text{m}$ .

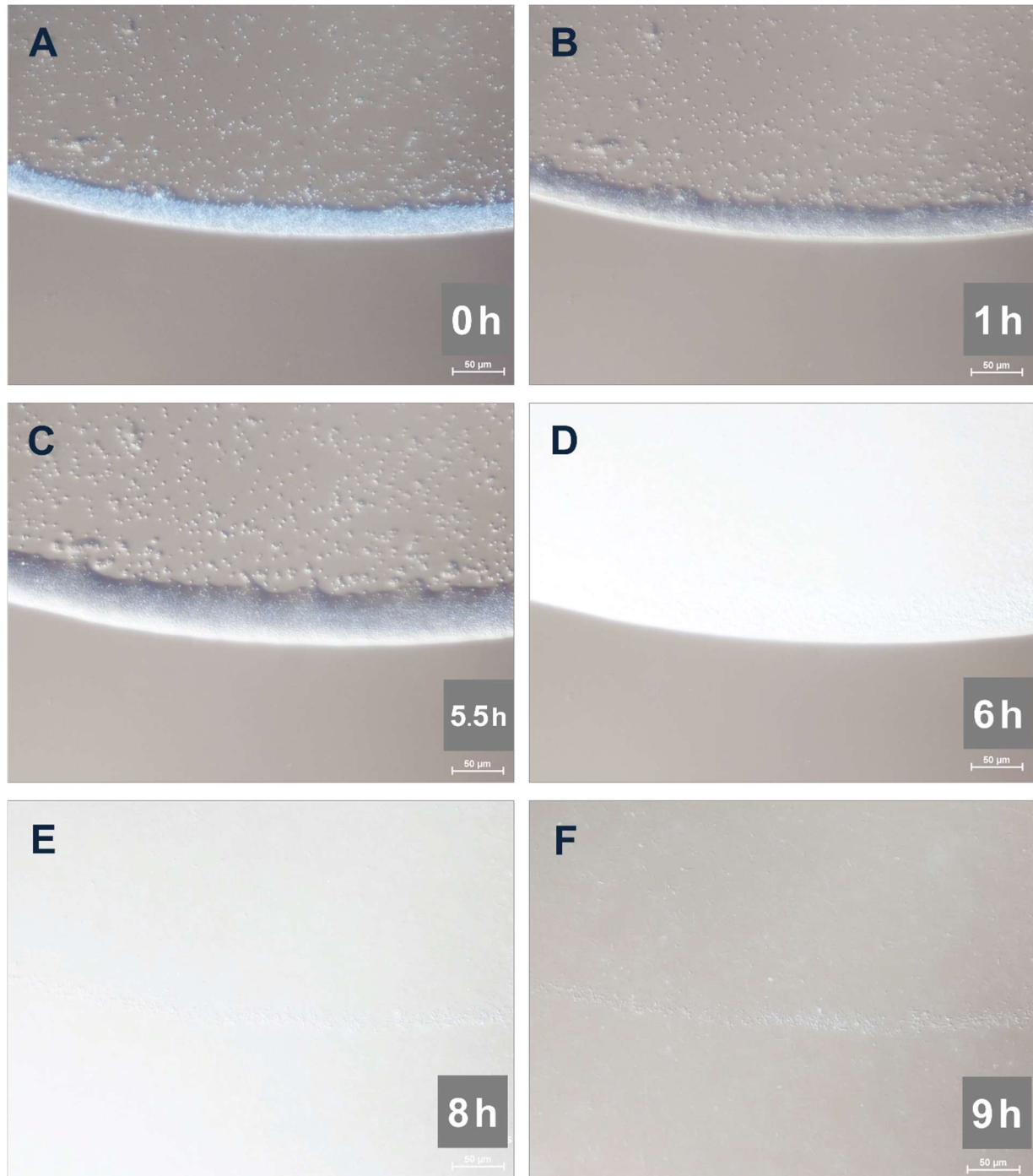


**Figure 15: Initial *B. subtilis* biofilm growth - from spores to biofilm**

MSgg-agar (1 mm thickness, supplemented with 10 mM L-alanine) was inoculated with 10  $\mu\text{l}$  ddH<sub>2</sub>O containing  $1 \times 10^6$  *B. subtilis* NCIB 3610 spores. Incubation took place in a breeding chamber on the microscope stage at 37 °C. All images shown in this figure are sequences from two time lapse series (0-5 h: **A+B** and 5-10 h: **C-F**) of the same biofilm. In **A** spores are shown immediately after inoculation. Due to the coffee-ring effect during pipetting and drying on agar, a ring with a high density of spores is created. Only a small part of the ring-like structure could be observed with the 20 x objective (DIC). After 1h (**B**) and 5.5 h (**C**) spores begin to germinate and the outgrowth

process starts. The shadows in both images represent an aqueous solution, which is created by surfactins excreted from vegetative cells. Vegetative cells use this water (D) for active movement on top of the agar surface to propagate. After around 6 h (D), the inner area of the former spore ring is covered with motile cells and water. The high refractivity makes cells and water appear bright under the preset microscopy conditions (D, E) and will only decline when the largest movements are attenuated and cells start to multiply (F). After 20 h (Figure 16) no more movement is observable within the former spore ring. Scale bar represents 50  $\mu\text{m}$ .

### Biofilm development and differentiation

After 5 to 6 hours, first chains of vegetative cells were clearly visible in the center (Figure 15: A, B and (Figure 15: B, C, shadows on the inside of the spore ring). In addition, cells secreted surfactin, a surface active lipopeptide, which reduces the surface tension of water and thus accumulates nutrient-rich water at the filter surface (Cooper et al., 1981). Depending on the cell density and with increasing population, the center of the former spore ring was filled with a nutrient solution in which the vegetative cells actively moved (Figure 15, D). The outer spore ring germinated less fast compared to spores in the center. Due to the high spore concentration, the spore ring limited the expansion of swimming vegetative cells from the center. Within the spore ring, a pool of actively moving vegetative cells was formed, which spread concentrically over the membrane filter with increasing germination of the outer spore ring (Figure 15, E). Former spore structures, which arose by drying (coffee-ring effect) were overcome after 7 to 8 hours. Remaining spores (Figure 15, F) were delayed in germination due to the high number of spores per area.

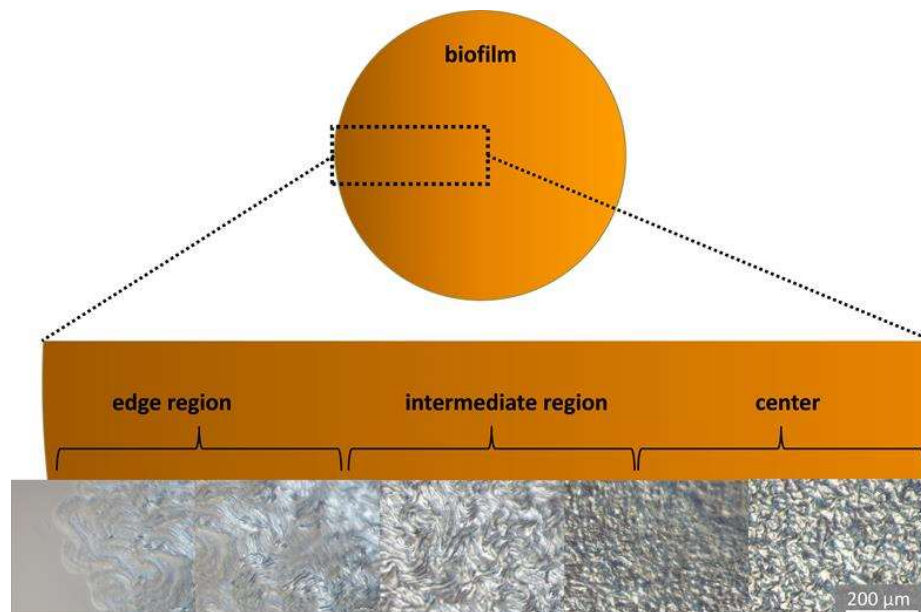


**Figure 16: Differentiation between growth regions in young colony biofilms.**

The figure is composed of a schematic overview of a young *B. subtilis* NCIB 3610 biofilm, magnifying regions along the colony radius of a symmetrically grown colony. Microscopic images show representative regions according to the schematic overview. The biofilm was inoculated with  $1 \times 10^6$  spores on MSgg-agar (1 mm thickness, supplemented with 10 mM L-alanine) and incubated for 20 h at 37 °C within a heated microscope stage, enclosed in an ibidi® dish. From left to the right: The outer propagating areas are composed *B. subtilis* cells, which form chain-like structures in a mono layer, which move with up to 200  $\mu\text{m}$  away from the biofilm center. In 200 - 400  $\mu\text{m}$ , the bacteria-chains stack themselves into loose wave-like structures (edge region). Closer to the center, these structures are getting denser and compressed (intermediate region). Within the biofilm center, the oldest part of the biofilm, aerial structures have been formed. The pressure of the surrounding cells and the incubation time allowed growing in height. While other regions are growing and moving, the center is characterized by its immobility. Scale bar represents 200  $\mu\text{m}$ .

With increasing incubation time, the aqueous solution on the filter surface caused by surfactins was progressively displaced by the sedimentation of cells and their associated growth. At this time point, a cell lawn became macroscopically visible as a flat white colony. The colony started growing in height and ended the two-dimensional colony structure. A clear separation of different colony zones concentrically aligned around the center became visible: The oldest biofilm region, the center, was strongly compressed by the surrounding cells and a 3-D surface structure was slowly emerging. In the peripheral regions, expanding growth zones were observed, which moved in slow wave-like movements over the filter (visible by time-lapse live cell imaging). However, the initial speed of expansion was significantly slower as it has been in the beginning of the breakthrough of the former pore ring. Cells in the outer regions were aligned in chains which slowly expanded due to the growth of individual cells and the pressure of the inner biofilm. After 20 h, biofilm growth in the outer areas progressed more slowly over time and cell movement in the center completely stopped. On the biofilm surface, chains of cells became visible which occurred extensively at the edge and formed fine-meshed aerial structures towards the center (Figure 16).

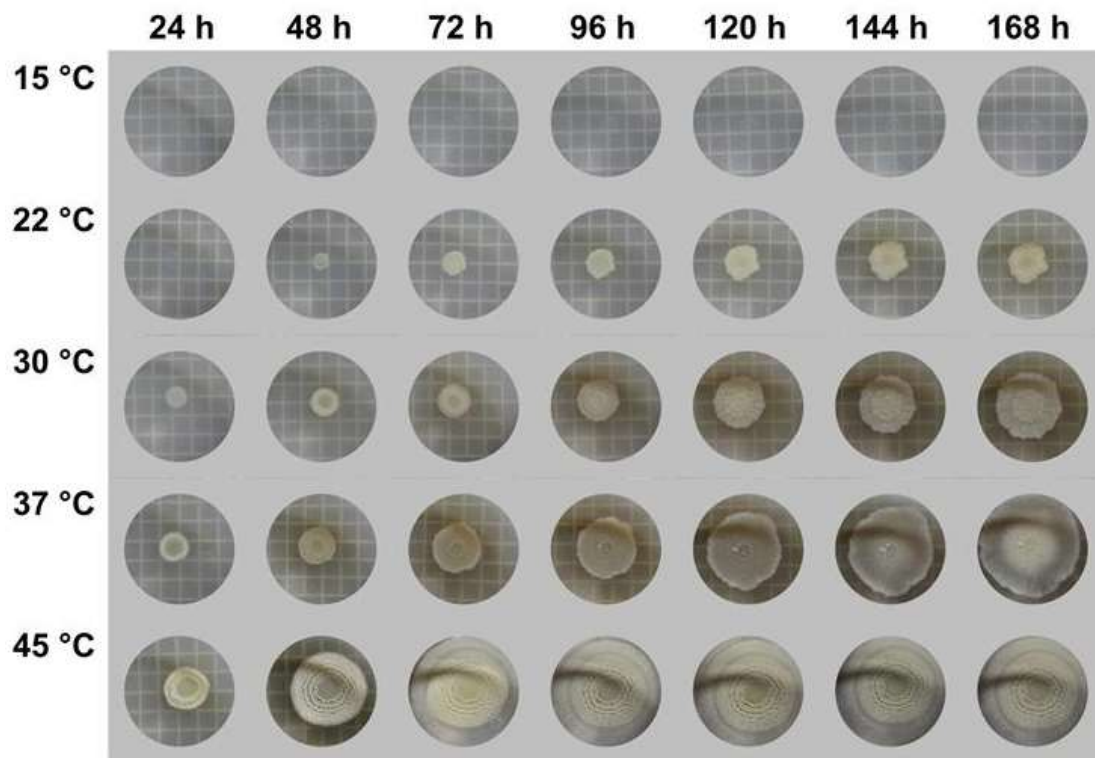


**Figure 17: *B. subtilis* biofilm growth at different incubation temperatures**

The presented compilation shows *B. subtilis* biofilms grown at different temperatures ranging from 15 to 45 °C during one week. For each experiment  $1 \times 10^6$  spores were used to inoculate a membrane filter, which was placed on MSgg-media (solidified with 1.5 % agar and supplemented with 10mM L-alanine). For image acquisition, plates were taken from their respective incubator for a maximum of five minutes. The images of a temperature show the same biofilm over the course of a week. The experiment was carried out in triplicates and data such as biofilm diameter and CFU/spore composition is shown in Figure 18. For scaling: one side of a square (grid-plate) represents 3.3 mm, the length of three consecutive squares corresponds to 1 cm. Figure is taken from (Fuchs *et al.*, 2017a).

Growth and structure of biofilms are closely related to the incubation conditions. Depending on the used media, incubation length, temperature and other factors such as Parafilm®-wrapping of agar plates, the macroscopic appearance of biofilms is influenced. For creating standardized biofilms, several incubation temperatures were investigated on their effects on biofilm growth by using the membrane



filter method (Figure 17). For this experiment  $1 \times 10^6$  NCIB 3610 spores were inoculated on membrane filters and incubated on MSgg supplemented with 10 mM L-alanine for various times at different temperatures. At 15 °C, spores germinated as shown before (Figure 12), but no biofilm formation within one week was observable. Only the spore ring, which was created by drying the spores during inoculation, was visible. At 22 °C colony growth took place after 48 h of incubation. All other incubation temperatures (30, 37, 45 °C) resulted in visible colony biofilms after 24 h.

The solid medium on which biofilms were grown at temperatures above 30 °C changed its color from almost transparent to a diffuse brown after 96 h for 30 °C, 72 h for 37 °C and 48 h for biofilms grown at 45 °C. This effect is generally caused by not-yet specified metabolites created during biofilm growth and expansion. These metabolites were able to move through the filter membrane by diffusion. After removing the filter and therewith the biofilm from the medium, the color change of the solid medium appeared. After removal of biofilms, agar plates were test-wise re-incubated for 24 h, but nor growth or color change of the agar was observed.

### Impact of temperature on CFU/spore formation and biofilm diameter

An increase in temperature strongly affected the growth rate and the biofilm diameter (Figure 18, B). Colonies grown at 45 °C reached a final diameter of  $\sim 2.5$  cm, due to the limitations given by filter dimensions. Surface morphology of biofilms varied between almost no structures at 22 °C, to concentrically wrinkled structures at 30, 37 and 45 °C. Depending on the initial spore distribution while drying on the filter (i.e. Figure 17, 37 °C), the final biofilm proportions were directly influenced. Therefore, a circular spore ring distribution is needed in order to produce standardized biofilms or a spore monolayer distribution on a defined surface area (Raguse *et al.*, 2016c).

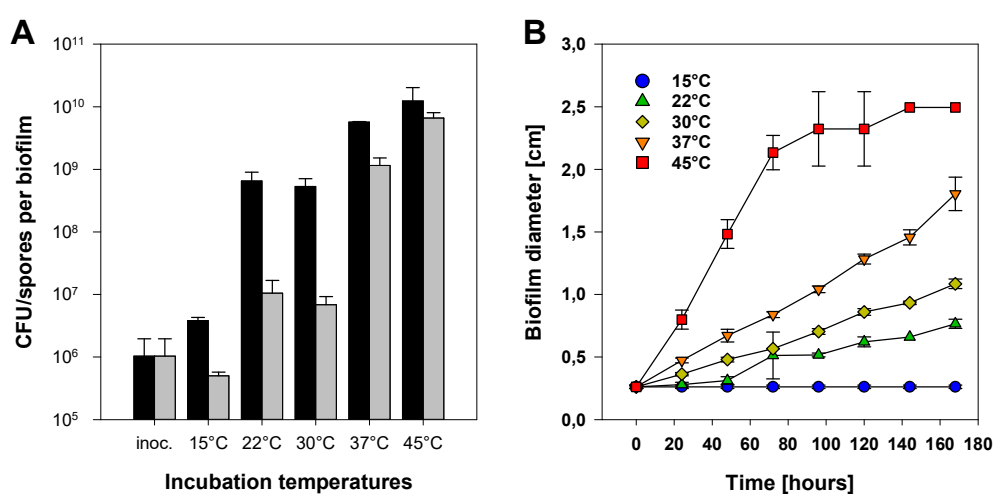


**Figure 18: Influence of temperature on biofilm diameter and CFU/spore composition**

Graph A represents the influence of temperature on the CFU and spore composition of *B. subtilis* biofilms grown for one week. Sets of biofilms (N = 3, per temperature) including these from Figure 17, were inoculated with  $1 \times 10^6$  spores on membrane filters and incubation took place on MSgg-agar plates (supplemented with 10 mM L-alanine). After 7 days of incubation, biofilms were harvested and number of CFU and spores were determined. Black bars represent the overall CFU per biofilm, whereas grey bars only represent the fraction of spores per biofilm (logarithmic scale). In B, the overall biofilm diameter is shown as a function of time and temperature. Error bars represent the standard deviation of the respective sample set, but should not be over interpreted for biofilms grown at 45 °C. Due to the physical limitations of the filter, biofilm diameter was limited to 2.5 cm. Biofilms at 15 °C showed no visible growth (compare: Figure 17), given values represent the dimensions of the dried spore droplet during inoculation. Graphs were taken modified after (Fuchs *et al.*, 2017a).

In Figure 18 (A) the relation of spores and CFUs in biofilms grown at 15-45 °C after one week of incubation on MSgg medium is shown. Given results are related to macroscopic biofilm images presented Figure 17 and their respective diameter is shown in Figure 18 B. Cell growth at 15 °C was limited and did not exceed  $4 \times 10^6$  CFU and  $8 \times 10^5$  spores per biofilm. Higher incubation temperatures resulted in a raise of three (22, 30, 37 °C) or four (45 °C) orders of magnitude compared to the spore inoculum. Biofilms grown at 22 and 30 °C increased by two orders of magnitude in their spore composition and temperatures of 37 and 45 °C led to  $1 \times 10^9$  and  $8 \times 10^9$  spores per biofilm. The differences in biofilm composition at 22 and at 30 °C were identical in contrast to their biofilm diameter. After 7 days of incubation, biofilms showed a mean difference of 4 mm (B; 30 °C:  $1.1 \pm 0.05$  cm, 37 °C:  $1.65 \pm 0.15$  cm). All biofilms increased their diameter linearly over the time course of one week correlated with their CFU and spore composition. After 24 h at 15 and 30 °C, biofilms exhibited almost identical diameter ( $0.25 \pm 0.05$  cm), but became different in size during the following incubation time. The fastest growth rate of biofilms was observed at incubation at 45 °C, reaching the maximum biofilm diameter ( $\sim 2.5$  cm, due to the filter limitation) within 3-4 days of incubation.

### 3.2 Biofilm maturation in absence of spore-formation

Vegetative cells in *B. subtilis* biofilms form spores during longer incubation periods, which leads to an increase in overall resistance towards environmental changes and hazards. Dormant spores do not compete for nutrients with other cells and can migrate or survive until better growing conditions arise. In order to compare biofilms with and without the ability to form spores, the sporulation-deficient mutant,  $\Delta sigG$  (NCIB 3610 background) and the wild-type NCIB 3610 were used. *SigG* codes for the RNA polymerase sporulation (late forespore-specific) sigma factor SigG (Michna *et al.*, 2016, Zhu & Stülke, 2018). In the  $\Delta sigG$ -mutant, spore formation can be initiated by the mother cell, but the forespore formation cannot be completed and spore formation is prevented. In contrast to the standardized biofilm inoculation method, biofilms were incubated with PBS-washed cells of an overnight pre-culture. Membrane filters were inoculated with 10  $\mu$ l cell suspension ( $0.3 OD_{600}$ ,  $\sim 1-4 \times 10^6$  cells), air-dried and incubated under standardized conditions on MSgg-agar at 37 °C. Figure 19 represents the CFU (A) and spore (B) composition of biofilms of both strains after 24 h, 3 d and 7 d as well as examples of biofilm phenotypes (C). Grey bars demonstrate the CFU and spores of the wild-type, whereas the CFU of the  $\Delta sigG$  is given in blue. Both, CFU and spores are displayed on the ordinate as absolute numbers per individual biofilm.

After 24 h of incubation, both strains exhibited  $\sim 9 \times 10^6 - 2 \times 10^7$  CFU, showing no significant differences between both strains (A). Wild-type spore-formation was not observed after 24 h (B). CFU of 72 h-old biofilms ranged between  $\sim 9 \times 10^8$  (wt) and  $\sim 0.5 \times 10^9$  ( $\Delta sigG$ ). After one week of incubation, the wild-type exhibited significantly more CFU ( $\sim 9.4 \times 10^8$ ) compared to the spore-deficient mutant ( $\sim 2.7 \times 10^8$ ,  $P=0.0012$ , two-way ANOVA,  $P<0.05$ ). As expected, biofilms of  $\Delta sigG$  exhibited no spore formation at any time point. Disrupted biofilms of the deficient mutant were analyzed via phase contrast microscopy (not shown) and neither sporulating cells nor spores were observed. On the contrary, biofilms of the wild-type consisted of  $\sim 3 \times 10^7$  spores after 3 d and  $\sim 3.5 \times 10^8$  spores after one week (B). Phenotypes of both strains did not exhibit differences in biofilm size, structure or color after 24 and 72 h. After 24 h of incubation, the diameters of biofilms of both strains reached  $\sim 0.5-0.6$  cm and  $\sim 0.6-0.7$  cm after 72 h. In addition, the MSgg-medium of both strains turned from a milky-white/transparent tone to a light brown after 72 hours. Interestingly, 7 d-old topographically elevated regions of biofilms of the wild-type were significantly brighter in color compared to biofilms of the sporulation-deficient mutant.

In summary, this experiment demonstrated that *B. subtilis* biofilms capable of forming spores have a long-term survival advantage over non-spore formers. This is reflected in the increased number of CFUs and the associated resistance of the spore fraction contained therein.

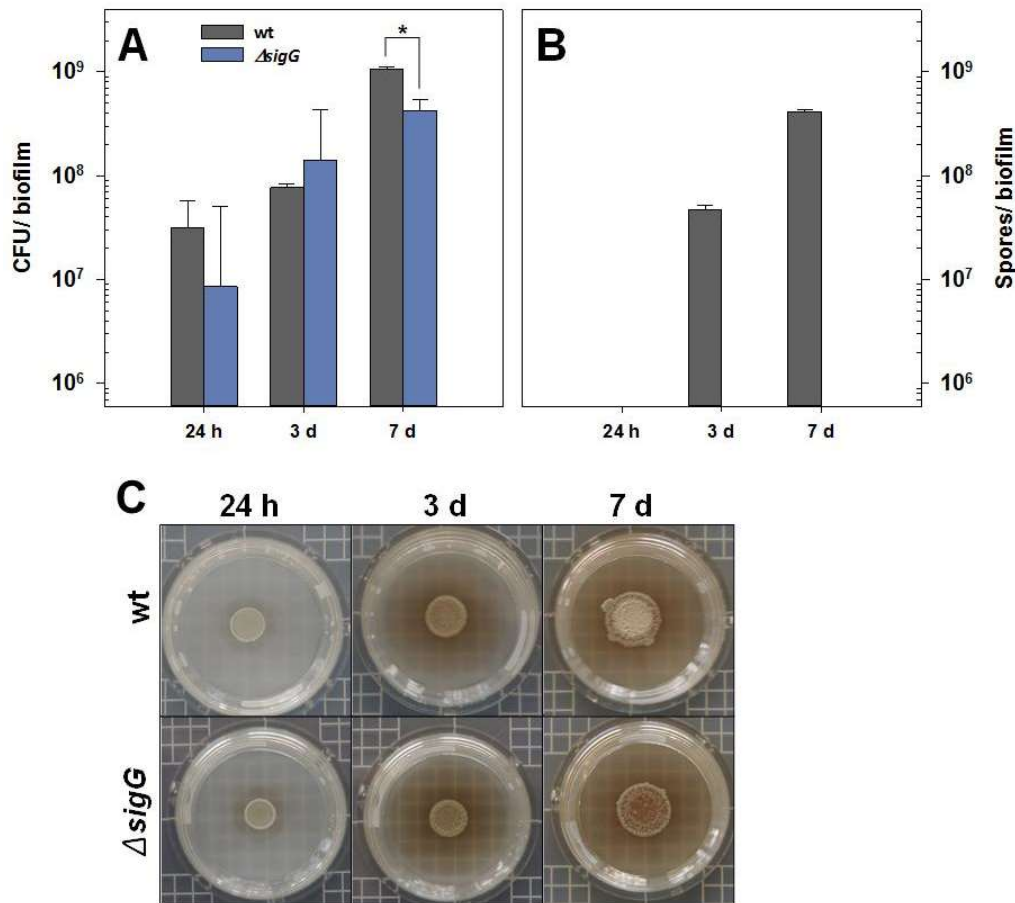


**Figure 19: CFU/spore composition of NCIB 3610 and  $\Delta sigG$  biofilms**

In order to compare the biofilm development of the *B. subtilis* non-spore-forming mutant  $\Delta sigG$  (NCIB 3610 background) and its wild-type, fresh precultures matured from a single colony were grown overnight in LB medium at 37 °C. Cells were washed in PBS-buffer and adjusted to an OD<sub>600</sub> of 0.3 (~ $1-4 \times 10^6$  cells per inoculum). For each strain, 10  $\mu$ l of the respective cell-solution were used to inoculate membrane filters, which were then incubated for 1, 3 and 7 days on MSgg-medium at 37 °C. After each time point, biofilms were photographed for phenotypical characterization and investigated regarding their CFU and spore composition by determining titers via plating serial dilutions. Graph A represents CFUs per biofilm, whereas graph B shows the total amount of spores per biofilm. The image composition in C illustrates representative biofilm phenotypes of  $\Delta sigG$  and NCIB 3610. For scaling: The length of three squares corresponds to 1 cm. Statistical analysis was performed by two-way ANOVA considering  $P < 0.05$  as significant. Data represents biological replicates (N=4 for  $\Delta sigG$  and N=6 for wt) per strain and condition, error bars represent the standard deviation.

### Vacuum exposure and desiccation experiments

To characterize the usability of membrane filters, the desiccation resistance of biofilms under vacuum conditions similar to space conditions (low Earth orbit) was investigated. Biofilms were grown on R2A, a full medium, which is used frequently in space experiments (Figure 20, A) and MSgg as a minimal medium reference (B). Ultra-high vacuum (UHV) is omnipresent in space and varies depending on the

distance to planets and celestial bodies. Low pressure leads to a radical dry environment in which *B. subtilis* spores may persist but vegetative cells are not able to survive longer periods (Horneck *et al.*, 2010, Wang *et al.*, 2006). Biofilms were incubated at 30 °C for one week by using the membrane filter method and air dried for 24 h. Control samples ( $t_0$ ) were immediately serially diluted and plated for CFU and spore determination. Another set of samples was air-dried for 2 h at room temperature by using a laminar flow hood to remove most volatile compounds, which can negatively affect the vacuum quality. Membranes harboring biofilms were transferred into glass petri-dishes and an ultra-high vacuum of  $\sim 7.2 \times 10^{-7}$  mbar was applied. Maximum pressure loss was observed after 3 h of vacuum.

The amount of CFU was reduced over time, especially for biofilms grown on MSgg ( $\sim$ one order of magnitude), due to the shift between vegetative cells and spores at the beginning of the drying phase. CFU of biofilms grown on R2A, barely decreased over the course of one week. Spores encased in biofilms grown on MSgg and R2A showed no significant changes in survival between drying at room temperature under laboratory conditions and UHV. Differences between MSgg and R2A can be explained by the amount of provided nutrients during growth, leading to higher biomass on R2A and a faster biofilm growth, which ends after most nutrients were exhausted, in spore production. Cells metabolizing MSgg grow slower, due to the nutrient limitation, therefore sporulation starts delayed in comparison to R2A-incubation. Drying of biofilms within the membrane filter system offered reproducible data, for both investigated drying methods.

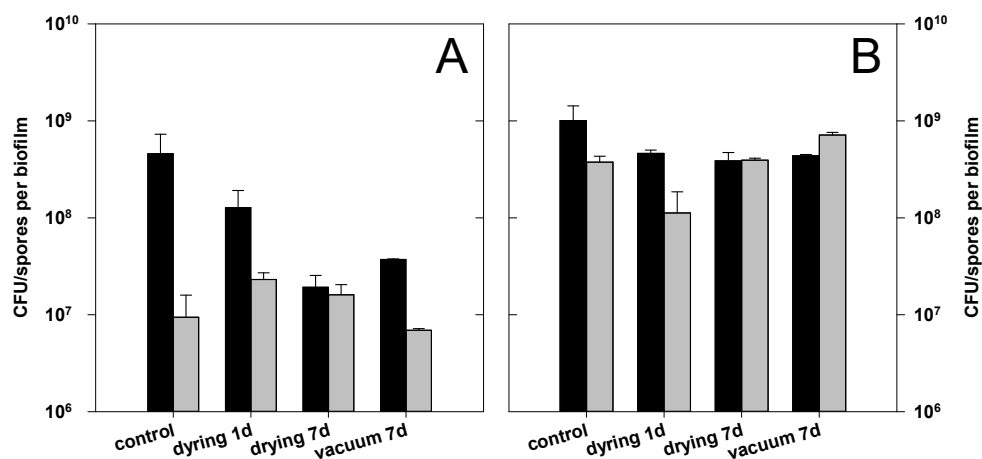


**Figure 20: *B. subtilis* biofilms exposed to vacuum**

MSgg-agar plates (A, supplemented with 10mM L-alanine, minimal medium) and R2A- agar plates (B, full medium) were inoculated each with  $1 \times 10^6$  spores of *B. subtilis* NCIB 3610 by using the membrane filter method to grow standardized biofilms. Incubation took place at 30 °C for one week. Biofilms grown in filters were removed from the medium and air-dried at room temperature for one and seven days or exposed to vacuum for seven days ( $\sim 7.2 \times 10^{-7}$  mbar). Controls ( $t_0$ ) were immediately analyzed by determining CFU (black bars) and spore composition (grey bars). Data represents biological replicates ( $N \geq 3$ ) and error bars represent the standard deviation.

### Application range of the membrane filter method

The membrane filter system proofed to be a reliable method to grow standardized biofilms. Compared to the conventional growth of biofilms on agar, the growth in the membrane filters is slightly delayed. This effect is helpful when aiming for small biofilm radii, which are needed for the simulation of microgravity. The overall manual effort for cultivation is higher compared to conventional growing methods, but a variety of subsequent downstream analyses is offered. For instance, the filter harboring biofilms can be removed after incubation and transferred to fresh nutrient media. On the other hand, the filter can also be dried after removal or be used for further experiments such as UHV, X-ray or

heavy ion treatments. For CFU and spore determination, the filter was removed from the media and placed in a sterile petri dish. By adding PBS, the biofilm was carefully dissolved by using a sterile inoculating loop. The biofilm detached from the filter membrane and was pipetted into an Eppendorf® tube for further purposes. This method was also applied for isolating DNA, RNA and proteins. By using the membrane filter method, highly reproducible standardized biofilm production was possible. The combination of incubation parameters adapted from literature and experimental results, offered the establishment of a trustworthy method which was applied for most biofilm experiments within this thesis. Varying setups were only used due to feasibility reasons or as control. The following list summarizes all parameters for biofilm production used in frame of this thesis.

**Table 8: Incubation parameters for standardized *B. subtilis* biofilm formation**

<b>Standardized biofilm formation</b>	
<b>Parameters</b>	<b>Implementation</b>
Incubation medium	MSgg + 10mM L-alanine
Incubation temperature	37 °C
Membrane filter	hydrophilized PTFE (HTTP for SEM and TEM)
Standard strain	NCIB 3610
Spore inoculum	1x10 <sup>6</sup>
Inoculum volume	10 µl
Incubation time	72 h
Harvesting media	PBS
Medium for plate count	LB-agar
<b>Limits of standardized biofilm formation</b>	
<b>Parameters</b>	<b>Range</b>
Incubation medium	All agar-based media (>1.2 % agar)
Incubation temperature	-20 °C - 55 °C
Membrane filter	hydrophilized PTFE (HTTP for SEM and TEM)
Spore inoculum	>1x10 <sup>4</sup> - ∞
Inoculum volume	min. 5 µl - 100 µl
Incubation time	0 h → ∞ h
Harvesting media	PBS, H <sub>2</sub> O, nutrient media, (...)
Medium for plate count	All nutrient media, (...)

### 3.3 Simulation of microgravity

#### Characterization of biofilm growth in simulated microgravity

##### Early biofilm development under 1g and sim-µg

To compare the growth of young *B. subtilis* (NCIB 3610) biofilms under 1g and sim-µg, samples grown under both conditions were analyzed in different growth phases (Figure 27). Live cell microscopy in time-lapse was used to investigate the growing propagation zone. Sim-µg and 1g biofilms were transferred after 10 h of incubation to a preheated microscopy chamber and were allowed to grow for 1 h. Inoculated spores germinated and the former spore ring distribution had been replaced by an elevated growth zone. Central regions remained planar (black arrows) and showed only minor elevations compared to the expanding regions on the rim. The zone expanded concentrically from the center in wave-like structures, which show different plateau levels, both in 1g and after sim-µg incubation (white arrows). Within the elevated rim region, vein-like structures were observable. Their

grey-blue appearance weakly asserted itself against the cell layers above it and are schematically highlighted for better visibility in Figure 21, C. These structures move during biofilm expansion and remain flexible, but never appeared in the outmost wave-like propagation zones. Significant structural differences among 10 h-old biofilms grown under 1g and sim- $\mu$ g were not observed, although the outer growth zone of sim- $\mu$ g samples tended to show less pronounced marginal regions.

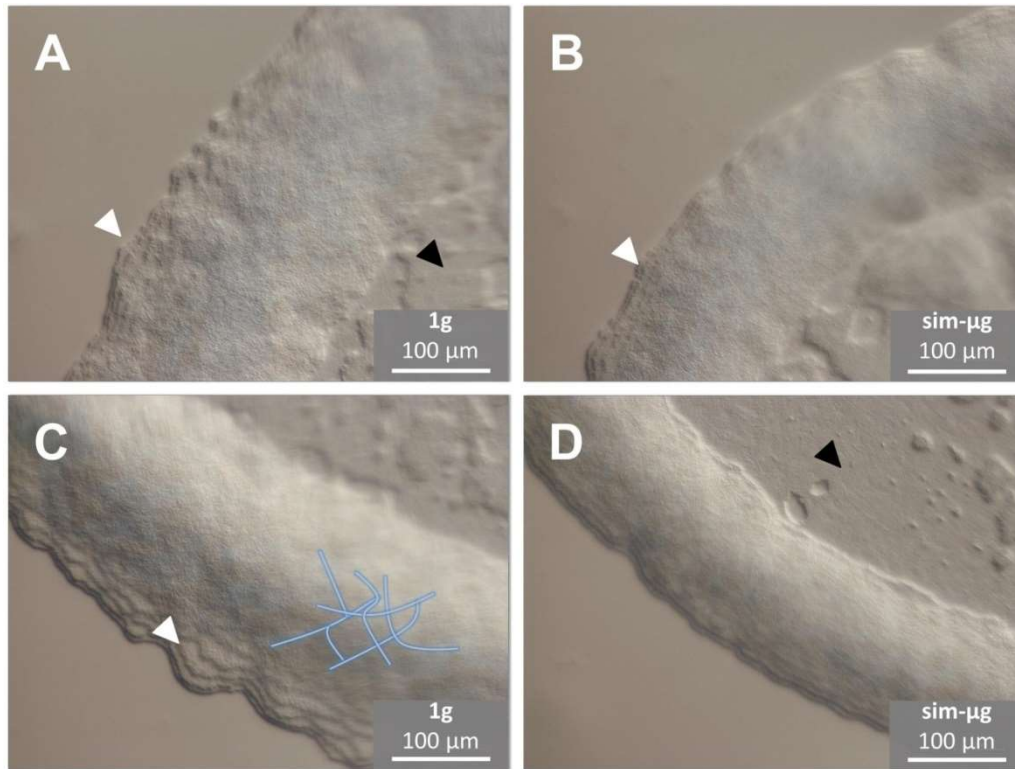


**Figure 21: Early biofilm development (1g and sim- $\mu$ g)**

Images represent *B. subtilis* NCIB 3610 biofilms grown at 37 °C on MSgg-agar for 10 h (1 mm agar thickness, supplemented with 10 mM L-alanine). Early stages of biofilm growth and expansion were analyzed by capturing images of the propagating regions. Biofilms grown under terrestrial gravity (1g, **A**, **C**) showed growth properties similar to those grown under sim- $\mu$ g (2-D clinostat, **B**, **D**). The former spore ring, an artifact from the inoculation phase, propagated in all directions in wave-like movements (visible in time-resolved recordings), which slide over each other in different plateau levels (white arrow heads). Depending on the contrast and the focus plane, grey-blue vein structures run through the outer ring and grow with it (visualized in **C**). The inner center of all biofilms remained mostly planar after 10 h incubation (black arrow heads). Scale bars represent 100  $\mu$ m.

### 1g and sim- $\mu$ g biofilm development after 20, 40 & 60 h

In the last two decades, many studies focused on understanding the properties, functions and structure of *B. subtilis* biofilms. In frame of these studies, many biofilm related genes have been identified as well as one operon, which is mainly responsible for biofilm formation in *B. subtilis*: The *epsA-O* operon. Mutants not carrying the *epsA-O* operon are not able to form typical biofilm components such as the BslA protein-layer, which intercalates extra polymeric substances (EPS) and further structural components. Colonies of  $\Delta$ *epsA-O* can barely be defined as biofilm but are mentioned as biofilm in the context of this thesis for simplification. For analysis of young biofilms another deletion mutant was used to compare the effects of growth under different gravity regimes: An absence of the *hag*-gene causes non-flagellated vegetative cells, which results in cells that are not able to move and propagate actively. Biofilm expansion can therefore only take place via passive movement and thus offers a further perspective on biofilm formation. In the following setup, a time-lapse series of macroscopic images of biofilm growth after 20, 40 and 60 h incubation are presented (Figure 23). In addition to macroscopic

image acquisition, biofilms were investigated by microscopy by using high resolution tile-scans (not shown). In order to perform microscopically analyses, biofilms were cultured by using ibidi®-dishes (grid, transparent bottom) on 1 mm thick MSgg-agar. For sim- $\mu$ g incubation, dishes were mounted within regular empty grid petri-dishes aligning the biofilm to the rotation axis of the 2-D clinostat. Biofilm incubation was stopped after acquiring images and CFU and spore titer per biofilm were determined by plating serial dilutions (Figure 22).

Biofilms grown for 20 h showed no structural characteristics or aberrations. The colonies were predominantly bright in color and except for the wild-type, the diameter of the spore inoculation ring was not exceeded. After 40 h of incubation, colonies had grown significantly and exhibited first biofilm features. The wild-type as well as the  $\Delta hag$ -mutant showed wrinkles on the surface and were frayed along the colony edge. The biofilm deficient mutant,  $\Delta epsA-O$ , appeared flatter, less pronounced in diameter and remained in similar colony dimensions after 60 h of incubation. However, it changed color from yellow/white to yellow/brown. The color of the wild-type and the  $\Delta hag$ -mutant turned darker after 60 h. Wild type biofilms appeared to be more pronounced when grown under sim- $\mu$ g, but no statistical difference was measured. In comparison to the  $\Delta hag$ -mutant, wild-type biofilms were larger in diameter and showed a more distinct wrinkle formation, but similar concentrically patterning of the colony. In general, macroscopic differences between 1g and sim- $\mu$ g could not be detected either after 20 h, 40 h or after 60 h for all investigated strains. Only differences among the mutants compared to the wild-type strain were visible.

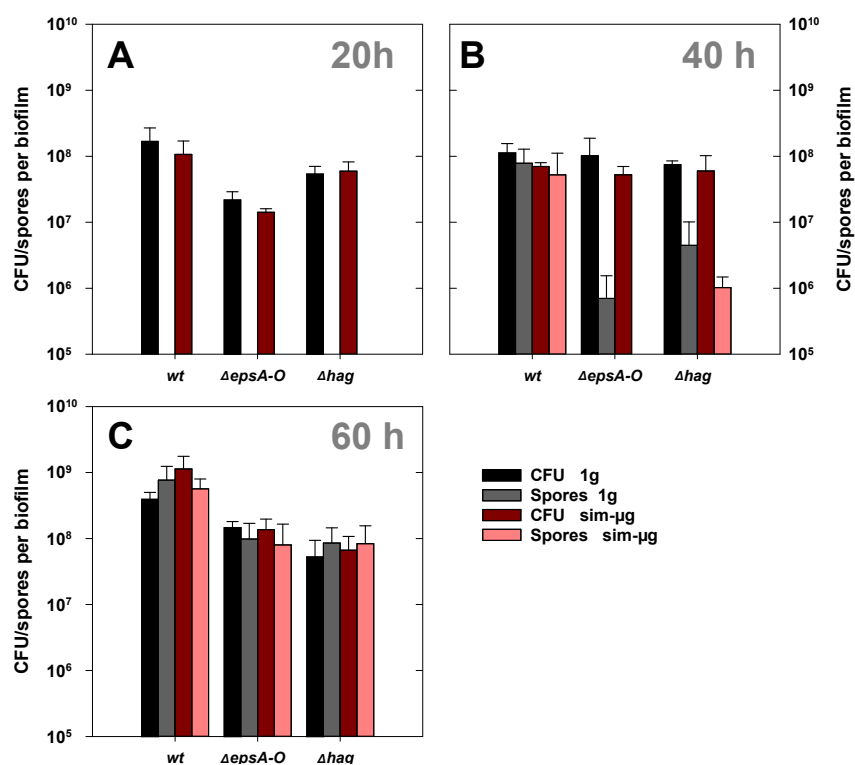


**Figure 22: CFU and spore composition of *B. subtilis* biofilms grown under 1g and sim- $\mu$ g**

For inoculation,  $1 \times 10^6$  spores of *B. subtilis* wild-type (NCIB 3610),  $\Delta epsA-O$  (biofilm deficient) and  $\Delta hag$  (no active flagella driven movement) were used. Incubation took place under standardized conditions on MSgg agar (supplemented with 10 mM L-alanine) at 37 °C by using ibidi®-dishes. For simulating microgravity, a fast rotating 2-D clinostat was used. After incubation, dissolved biofilms were analyzed by plating serial dilutions to determine the CFU and spore composition. For samples grown under 1g, CFU (black bars) and spores (grey bars) are pictured on the left side and for sim- $\mu$ g samples, CFU (red bars) and spores (rose) are shown on the right. Graphs represent different stages of biofilm development: 20 h (A), 40 h (B) and 60 h (C) of incubation. Corresponding images of biofilms are shown in Figure 23. Error bars represent the standard deviation,  $N \geq 3$ .

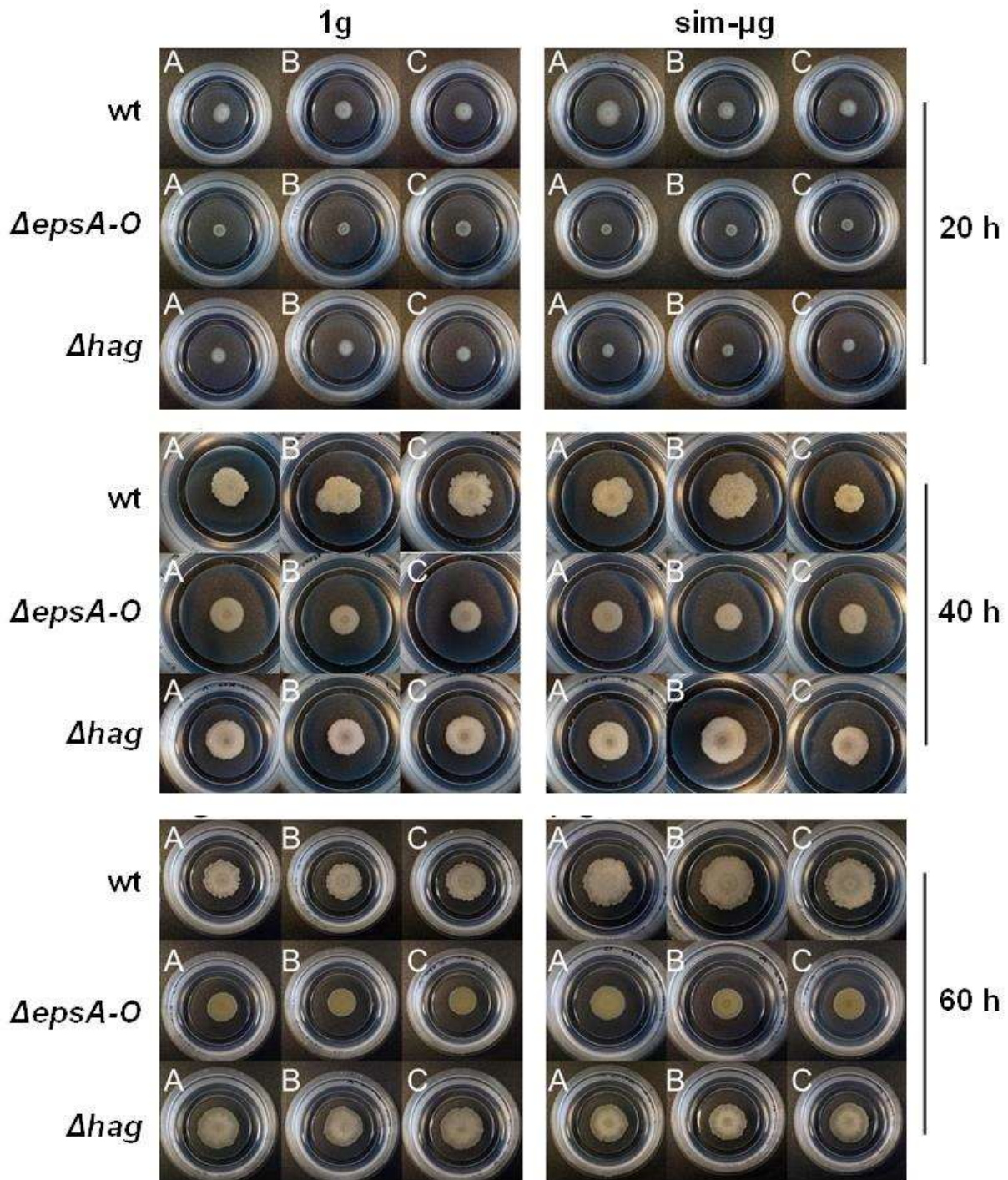


**Figure 23: Time-dependent *B. subtilis* biofilm growth under 1g and sim- $\mu$ g**

For inoculation,  $1 \times 10^6$  spores of *B. subtilis* wt,  $\Delta$ epsA-O (biofilm deficient) and  $\Delta$ hag (no active flagella driven movement) were used. Incubation took place under standardized conditions on MSgg agar (supplemented with 10 mM L-alanine) at 37 °C by using ibidi®-dishes. For simulating microgravity during the incubation, a fast rotating 2-D clinostat was used. The figure is separated into three incubation stages: 20 h, 40 h and 60 h. For each time, three biological replicates (A-C) per strain and gravity condition are depicted. Biofilm images vertically aligned of the same strain and gravity condition do not show same biofilm over time, but show representative biofilms at corresponding incubation times. This was necessary to ensure undisturbed incubation, which is particularly important for cultivation under simulated microgravity. For scale: the inner circle (appears darker) of an ibidi®-dish equals 2.5 cm.



Investigated biofilms were also analyzed regarding their CFU and spore composition after 20, 40 and 60 h incubation under 1g and sim- $\mu$ g (Figure 22). None of the three strains showed sporulation or dormant spores, which might have remained from the initial inoculum after 20 h. Growth was increased by 2 orders of magnitude for the wild-type, by 1.2 for  $\Delta epsA-O$  and by 1.8 for  $\Delta hag$ -mutant. Samples grown under sim- $\mu$ g showed slightly less growth compared to the 1g controls, but no significant differences were determined. First spores appeared after 40 h of incubation for the wild-type and  $\Delta hag$ , whereas only 1g samples of  $\Delta epsA-O$  showed sporulation, but not in sim- $\mu$ g samples. Generally, sporulation was less pronounced among sim- $\mu$ g samples compared with their controls. Growth of all strains stagnated early and reached its maximum after 60 h resulting in  $\sim 7-8 \times 10^8$  CFU/spores for the wild-type and an order of magnitude less for both mutants. Spore levels appeared to be increased in comparison to the overall CFU-proportion, which might have been caused by the heat activation of spores during the pasteurization step, which inactivated all vegetative cells.

### **Biofilm maturation under 1g and sim- $\mu$ g**

As shown before, biofilm growth started within less than 40 h to feature typical biofilm characteristics such as wrinkle formation, matrix production, coverage by BslA-protein layer and formation of aerial structures as well as rising levels in CFU and spores. Most biofilm assays within this thesis have been performed with biofilms younger than 72 h. After more than 72 h, side effects, such as nutrient depletion and water limitation due to convection might influence long term studies. The membrane filter method decelerates biofilm growth and is perfectly adapted for studying biofilms up to five days at 37 °C. For longer incubation assays as shown in Figure 24 and Figure 25, no membrane filter was used. This allowed larger colony growth with maximum nutrient uptake rates from the minimal medium (MSgg). Biofilms shown in Figure 25 do not represent images of the same colony over the course of a week, to avoid interrupting the incubation (temperature and gravitational changes) of the sample, which was particularly important for sim- $\mu$ g samples. Every 24 h over the course of one week, biofilms were photographed for macroscopical imaging, harvested, microscopied and examined with regard to their CFU/spore content.

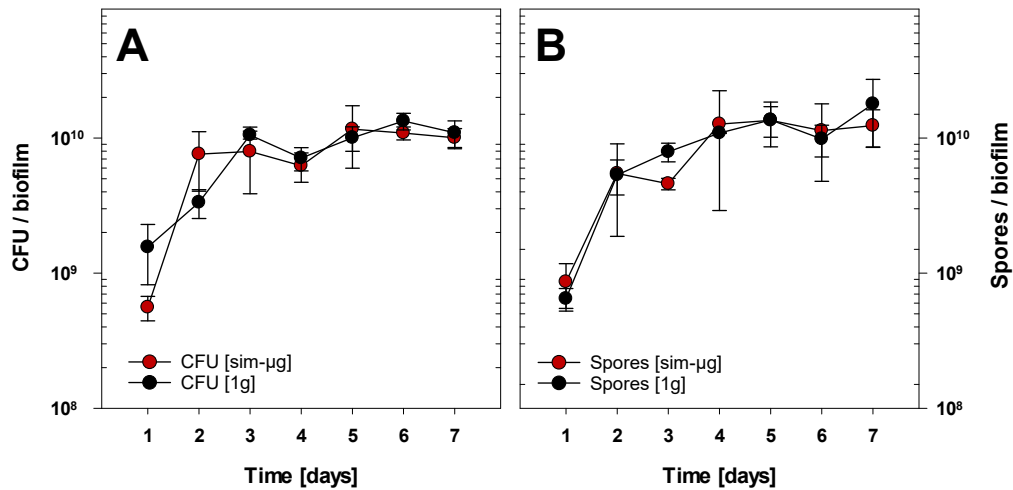


**Figure 24: Time-resolved CFU and spore composition of biofilms grown under 1g and sim-µg**

Biofilms of *B. subtilis* NCIB 3610 were grown under standardized conditions under regular gravity (1g, black circles) and simulated microgravity (sim-µg, red circles) by using a fast rotating 2-D clinostat at 60 rpm. For each biofilm,  $1 \times 10^7$  spores were used as inoculum, without using filter membranes to support larger colony growth. At intervals of 24 h, biofilms incubated on MSgg at 37 °C were harvested and analyzed by determining the CFU and spore composition. Data represents CFU (A) or spores (B) per biofilm. Y-axes are represented in a logarithmic scale,  $N \geq 3$ . Error bars represent the standard deviation.

The starting inoculum comprised  $1 \times 10^7$  spores per biofilm and raised within the first three days to a maximum of  $\sim 8 \times 10^9$ - $2 \times 10^{10}$  CFU/spores. After more than three days of incubation, the biofilm diameter (Figure 25) was still developing but no changes in CFU/spore composition were observed. Early biofilm development stopped after  $\sim 48$  h under both gravity conditions and represented similar data compared to the ibidi®-system which was previously shown (Figure 22). Biofilm specific characteristics such as wrinkle formation or aerial structures were already observable after 24 h of incubation whereas the ibidi®-system showed first wrinkle-formation after 40 h. The former spore-ring distribution (caused by droplet inoculation) was no longer visible after one day, but a circular biofilm-structure remained. First sporulation was observed after 24 h in 1g and sim-µg samples, which reached a maximum level after 3 to 4 days. Interestingly, only a small amount of mother cells was observable using microscopy.

Mature biofilms of both gravity conditions showed regions at the biofilm edges, which were characterized by different levels of colorization, size and texture. Biofilms seemed to exhibit delta-shaped branches or pioneer-zones, which evolved from the biofilm center and spread over the agar claiming unexploited nutrient sources and avoiding other leakage regions of the same biofilm. Younger biofilms did not exhibit any similar branching regions as observed for biofilms grown for more than three days. Offshoots like these were also observed for mature *B. subtilis* biofilms grown on LB-media (not shown). Microscopical images from the peripheral areas show higher concentrations of vegetative cells in contrast to the biofilm center, where spores were found more frequently (not shown).

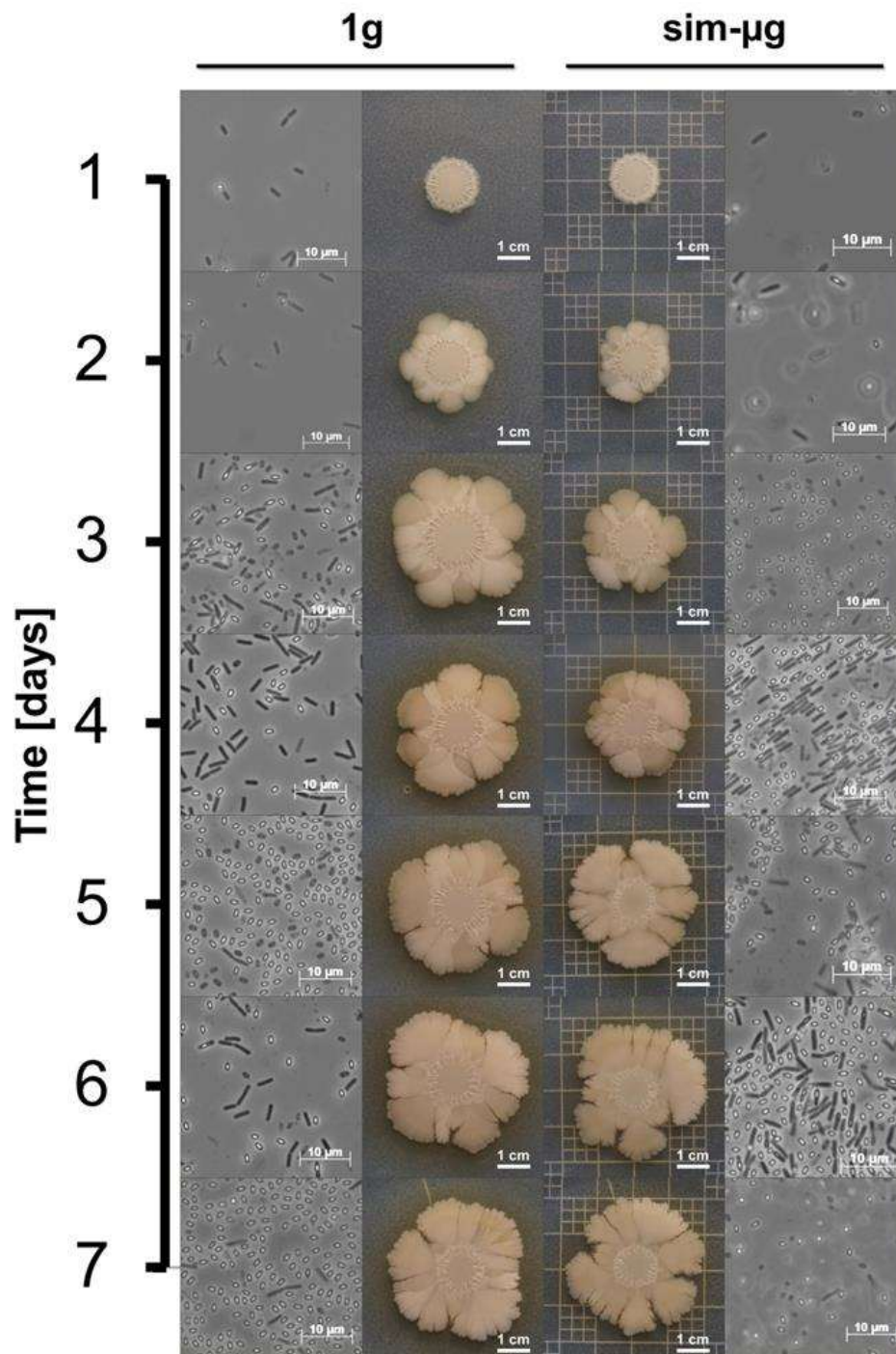


**Figure 25: Time-resolved images of biofilms grown under 1g and sim- $\mu$ g**

This figure features a composition of macroscopic and microscopic images of *B. subtilis* NCIB 3610 biofilms grown on MSgg agar (supplemented with 10 mM L-alanine) during one week under regular gravity (1g) and simulated microgravity (sim- $\mu$ g, using a fast rotating 2-D clinostat). Macroscopic images do not picture the same biofilm over time, but show representative colonies at corresponding incubation times. This was necessary to ensure undisturbed incubation, which is particularly important for cultivation under simulated microgravity. On the left side, biofilms cultivated under 1g and microscopic images of the respective dissolved biofilm are shown, whereas images on the right side represent sim- $\mu$ g biofilms. Phase microscopic images were acquired by using 10  $\mu$ l of disrupted biofilm material. These images do not provide quantitative information on the ratio between vegetative cells and spores, but give a rough overview of the spore content of the respective sample. Scale bars of microscopic images represent 10  $\mu$ m and scale bars of macroscopic images represent 1 cm.

### Types of sim- $\mu$ g simulation: RPM & 2-D clinostat

In order to simulate microgravity, several different techniques have been developed to generate a low-shear environment, which prevents or minimizes microbial recognition of directed gravity. Previously shown experiments were performed by using a fast rotating 2-D clinostat, which rotated biofilm samples along one axis. This system is very similar to rotating wall vessels (RWVs) or pipette clinostats, which also only use one rotation axis. A further possibility for  $\mu$ g-simulation is the random positioning machine (RPM). This device uses two rotation axes, which rotate biofilm samples randomly with different speed over time to produce a net gravitation of  $\sim 0$  g. Dr. Simon Wüest and his colleagues provided the RPM that was used here, on which the ibidi®-system was attached by using Velcro-tape. Per run, four biofilm samples were rotated simultaneously. After the incubation of three days at 37 °C, biofilms were harvested and examined by CFU and spore determination. Results were compared to 1g-control samples and samples which were incubated by using a fast rotating 2-D clinostat. Both, 1g controls and 2-D clinostat samples showed similar CFU ( $2\text{-}3 \times 10^9$ ) and spore levels ( $1\text{-}2 \times 10^9$ ) which were consistent with previous results. CFU and spore composition of biofilms grown under sim- $\mu$ g conditions by using an RPM, showed significantly less spores compared to 2-D clinostat biofilms ( $P=0.031$ ; 1g spores/RPM spores:  $P=0.197$ , t-test:  $P \leq 0.05$ ). RPM results exhibited a decrease in CFU compared to 1g or clinorotation, but did not exceed significant levels (1g/RPM:  $P=0.108$ ; 2-D clinostat/RPM:  $P=0.145$ ). Colony diameter and macroscopic biofilm appearance did not show any differences among all three cultivation methods (not shown).

In summary, biofilms grown for three days under 1g and both sim- $\mu$ g simulations did not exhibit significant changes in CFU, but RPM samples showed significantly less sporulation compared to biofilms formed during clinorotation.

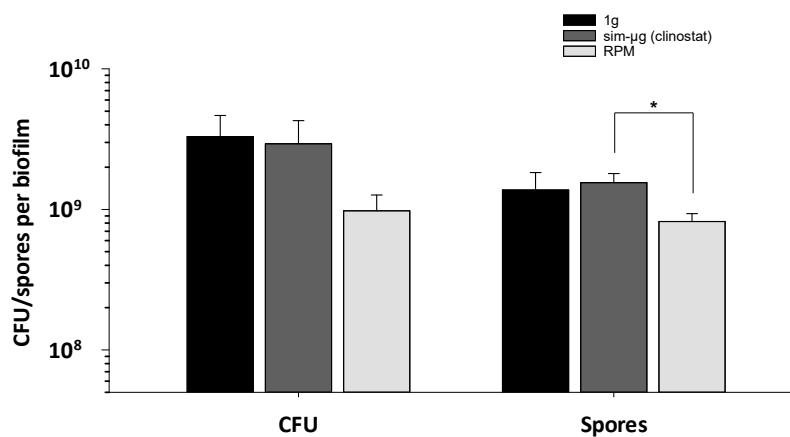


**Figure 26: 2-D clinostat and RPM cultivation of *B. subtilis* biofilms**

*B. subtilis* NCIB 3610 biofilms were grown in ibidi®-dishes (containing MSgg agar, supplemented with 10 mM L-alanine) under standardized conditions by using  $1 \times 10^6$  spores as inoculum. Incubation took place at 37 °C for 3 days by using standard incubation (upside down storage of plates, 1g, black bars), simulated microgravity (sim- $\mu$ g) by using a fast rotating 2-D clinostat (dark grey bars) and the random positioning machine (RPM, light grey bars). After incubation, CFU (left side) and spores (right side) of all biofilm samples were determined by plating serial dilutions of dissolved biofilms. Biological replicates were carried out in  $N=4$ , technical replicates in  $N \geq 3$ , error bars represent the standard deviation. For testing significant changes, data was checked for normality and analyzed by Welch's t-test ( $P \leq 0.05$ ).

### Profilometry of biofilms grown under 1g and sim- $\mu$ g

Biofilms often form highly structured surfaces, after reaching a mature state. Depending on the incubation conditions, such as time, temperature, starting inoculum and nutrient medium, biofilms may differ in size, shape and appearance. A quantification of 1g and sim- $\mu$ g biofilm surfaces was achieved by white-light profilometry, which allowed measuring heights and depths of biofilm surface architectures. Biofilms were grown under standardized conditions by using the membrane filter method and microscopically analyzed on the filter. In Figure 27, representative examples of *B. subtilis* wild-type (A, C) and  $\Delta epsA-O$  (B, D) biofilm surface-measurements are shown. Experiments were performed in the laboratories of Prof. Oliver Lieleg under supervision of Carolina Falcón García at the TUM in Munich. Elevated biofilm regions are presented in red, whereas shallow regions are shown in blue, representing the height distribution only for the respective sample. The overall height was measured compared to a reference measurement. Presented samples demonstrated total height of 285  $\mu$ m in A (1g, wild-type), 271  $\mu$ m (sim- $\mu$ g, wild-type) and 34  $\mu$ m for the biofilm deficient mutant under 1g and 129  $\mu$ m under sim- $\mu$ g.

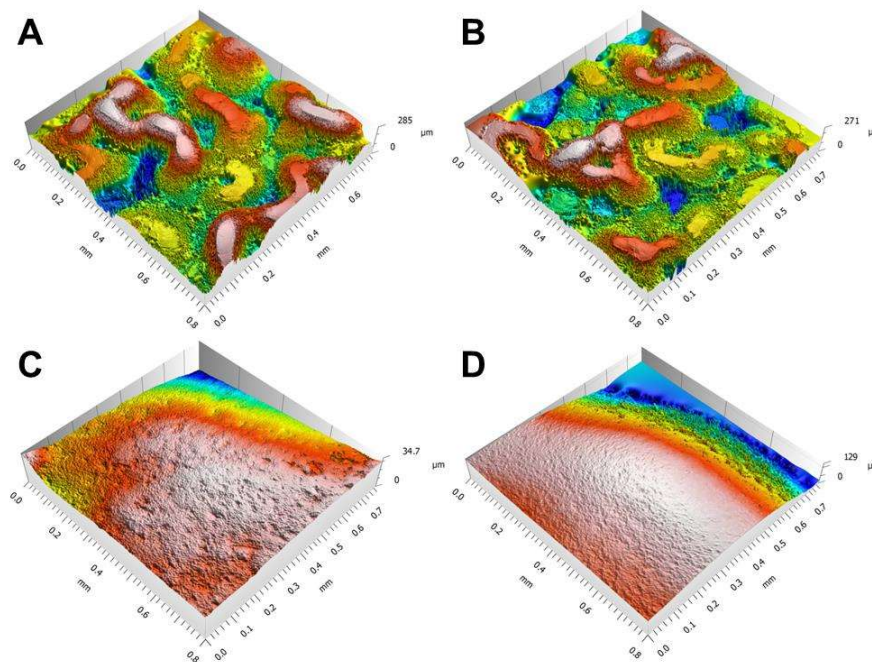


**Figure 27: Profilometry of *B. subtilis* biofilm surfaces grown under 1g and sim- $\mu$ g**

Images A-D show representative surface profiles of *B. subtilis* wild-type (A, B) and  $\Delta epsA-O$  (C, D) biofilms. For inoculation,  $1 \times 10^6$  spores of the respective strain were used. Incubation took place under standardized conditions on MSgg agar (supplemented with 10 mM L-alanine) at 37 °C by using membrane filters. Controls (1g, A, C) were grown under regular conditions and for growth under simulating microgravity (sim- $\mu$ g, B, D) a fast rotating 2-D clinostat was used. For microscopy, white light profilometry was used to calculate the surface parameters of a 0.75x0.75 mm area in the center of a biofilm. Red structures represent elevated areas which contrast with flatter regions (blue). Calculated parameters were used to compare the effects of regular gravity and simulated microgravity.

Acquired data was used to calculate several parameters which were used to compare mutants and the wild-type (Figure 28). The following mutants have been used:  $\Delta tasA$  (amyloid fiber deficient),  $\Delta bsIA$  (surface layer protein deficient),  $\Delta hag$  (flagella deficient) and  $\Delta epsA-O$  (biofilm deficient). In total five parameter have been determined but only the most important parameters were listed in Figure 28: Sq represents the biofilm surface as root mean squared average of the height deviations from a

calculated center line over the defined area. Simplified, **Sq** represents the roughness of the biofilm surface in  $[\mu\text{m}]$ , whereas **Sz** indicates the maximum biofilm height in  $[\mu\text{m}]$  and **Sdr** shows the developed interfacial area ratio [%]. Given box-plots are based on biological biofilm replicates, which were individually measured by white-light profilometry. Due to the limited amount of samples ( $n=3$ ), error bars show sporadically the heterogeneity in biofilm surface measurements among some sample sets.

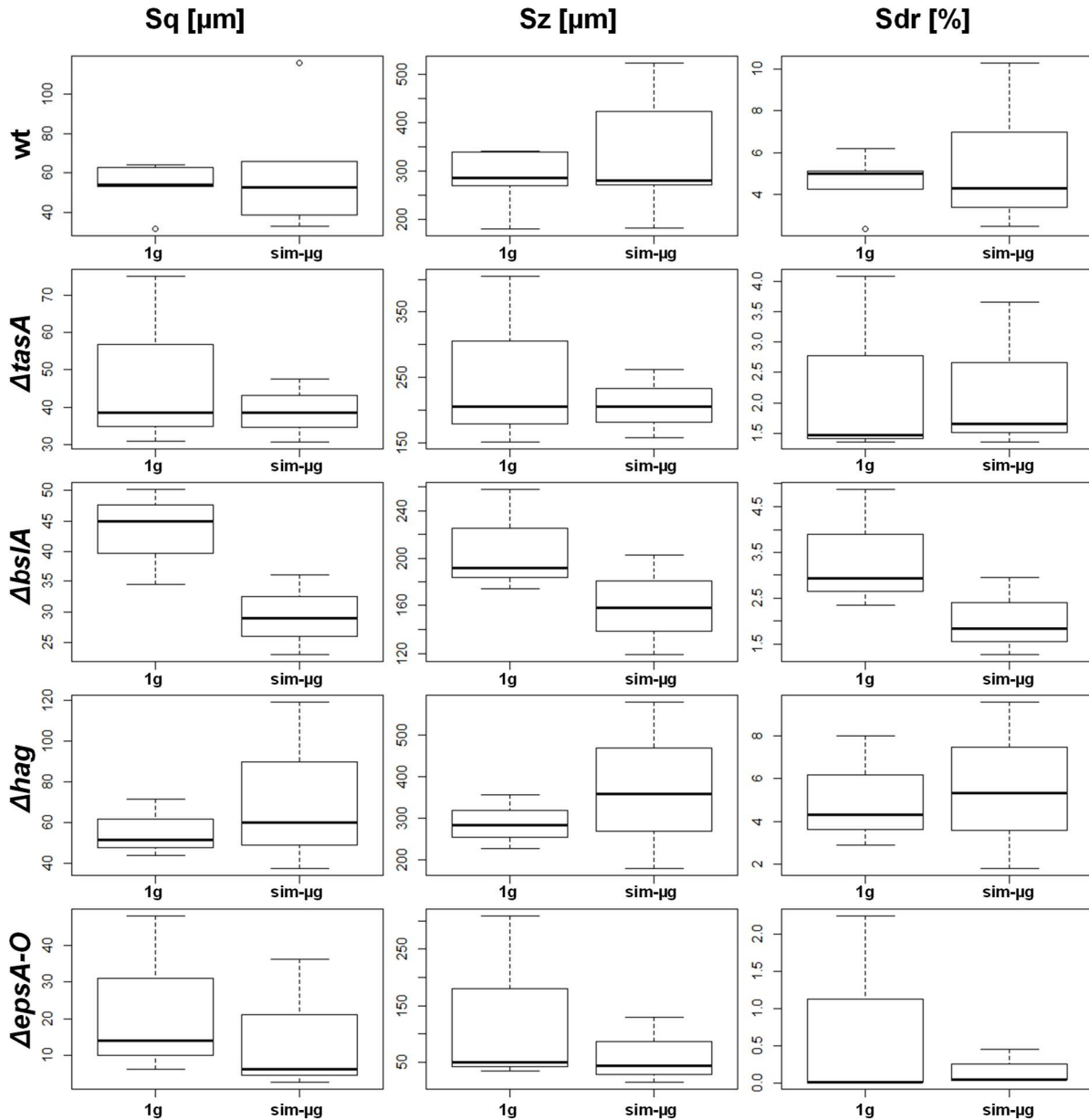


**Figure 28: Comparison of surface parameters of *B. subtilis* biofilms grown under 1g and sim- $\mu\text{g}$**

Biofilm surface parameters were acquired by measuring the surface properties via profilometry of a  $0.75 \times 0.75$  mm area of biofilms grown under 1g and sim- $\mu\text{g}$  conditions by using a fast rotating 2-D clinostat. Biofilms were grown under standardized conditions on MSgg agar (supplemented with 10 mM L-alanine) on membrane filters with an inoculum of  $1 \times 10^6$  spores. The wild-type strain *B. subtilis* NCIB 3610 (wt) and four mutants in the NCIB 3610 background were compared:  $\Delta\text{tasA}$  (amyloid fiber deficient),  $\Delta\text{bsIA}$  (surface layer protein deficient),  $\Delta\text{hag}$  (flagella deficient) and  $\Delta\text{epsA-O}$  (biofilm deficient). Analyzed surface parameters are: **Sq** (shows roughness of the biofilm surface as root mean squared average of the height deviations from a calculated center line over the defined area), **Sz** (represents maximum biofilm height) and **Sdr** (developed interfacial area ratio). The surface parameter analysis was performed individually for each strain and both gravity

conditions. Scales of Y-axes differ between experiments and measured conditions. Error bars represent the standard deviation,  $n=3$ , all data was successfully checked for normal distribution and statistically analyzed by using two-way ANOVA. No statistically relevant differences were observed.

All samples were normal distributed, and no significant differences between 1g and sim- $\mu$ g were observed. A comparison among biofilms grown under the same gravitational condition (not shown) showed only significant differences in surface parameters compared to  $\Delta epsA-O$ . All other mutants exhibited similar topographical patterning. Interestingly  $\Delta bsIA$ , showed a trend in reduced surface roughness, height and surface development if grown under sim- $\mu$ g, which also, but to a lesser extent, could be observed in  $\Delta epsA-O$ . In contrast to  $\Delta bsIA$  and  $\Delta epsA-O$ ,  $\Delta hag$  demonstrated a slightly more pronounced height, roughness and surface development when grown under sim- $\mu$ g. The two most similar results in all analyzed parameters between both gravity conditions were observed for the wild-type and  $\Delta tasA$ , which is consistent with previously performed macroscopic observations. In summary, 1g and sim- $\mu$ g biofilms did not exhibit any significant differences in surface architecture. Interestingly minor trends were observable, which should not be over interpreted due to the limited amount of analyzed samples.

### Surface hydrophobicity of biofilms grown under 1g and sim- $\mu$ g

Mature *B. subtilis* biofilms are characterized by their hydrophobic BslA-protein layer, which protects the biofilm against environmental influences and can therefore be considered as virulence factor. To measure surface hydrophobicity, only the biofilm center was investigated, as this comprises the oldest part of the colony. Peripheral biofilm regions were not suitable for hydrophobicity testing because they were still in the growth process and showed only a weakly developed protein layer. The wild-type (NCIB 3610), a *bsIA*-deficient mutant and  $\Delta epsA-O$  were investigated regarding their surface hydrophobicity with respect to growth under sim- $\mu$ g (Figure 29). Biofilms were grown for three days at 37 °C on MSgg-medium under standardized conditions (1g and sim- $\mu$ g) by using the membrane filter method. After incubation, biofilms were cut out of the agar together with the filter. By carefully pipetting a 10  $\mu$ l of ddH<sub>2</sub>O onto the center of the biofilm colony, the shape of the formed droplet was immediately photographed in profile (Figure 29, B). Depending on the contact angle of the water droplet on the biofilms surface, hydrophobicity was determined. Higher angles represent an increase in hydrophobicity, whereas biofilms with small contact angles do not exhibit any hydrophobicity.

The surface properties of the *B. subtilis* wild-type showed the most pronounced contact angles among all analyzed strains and thus the highest biofilm surface hydrophobicity. Biofilms grown under 1g exhibited a significant lower mean contact angle ( $\sim 84 \pm 5^\circ$ ) compared to biofilms grown under sim- $\mu$ g ( $\sim 99 \pm 5^\circ$ ,  $p=0.012$ , two-way ANOVA; t-test:  $p=0.006$ ). A deficiency in the BslA-protein layer resulted in contact angles of  $50 \pm 5^\circ$  (1g) and  $55 \pm 3^\circ$  (sim- $\mu$ g). Lowest hydrophobicity was exhibited by  $\Delta epsA-O$ , which showed contact angles of  $20 \pm 2^\circ$  under 1g conditions and  $26 \pm 8^\circ$  under sim- $\mu$ g. All given results show a trend, in which biofilms of all tested strains tend to form more hydrophobic biofilms when incubated under simulated microgravity. Biofilms which were grown on plain MSgg-agar under 1g conditions, without the membrane filter showed elevated levels (+10-15 %) in their contact angle and therefore their hydrophobicity (not shown).

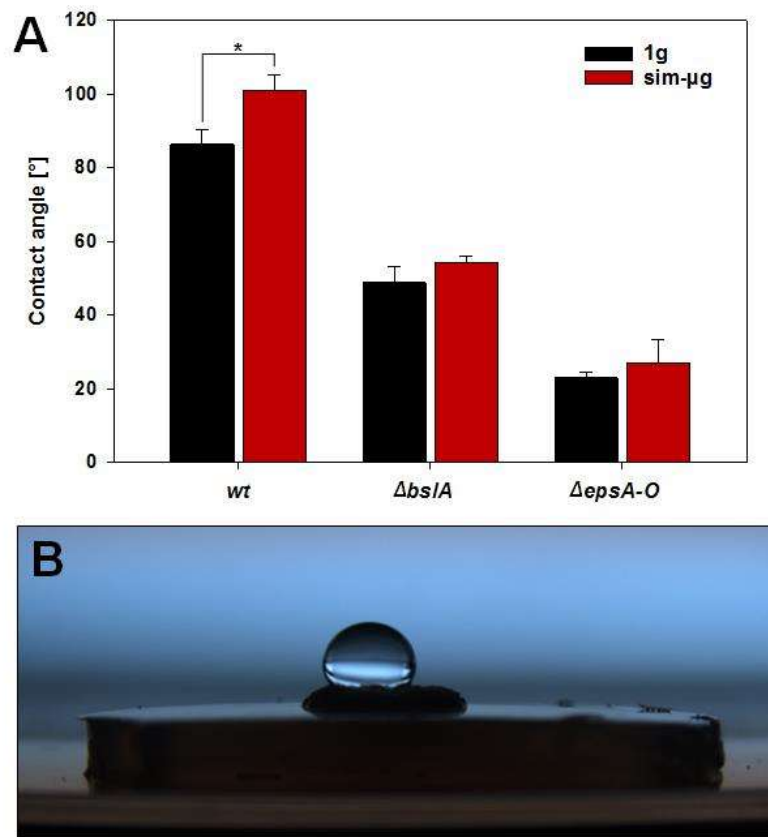


**Figure 29: Hydrophobicity of biofilms grown under 1g and sim-μg**

For determining the hydrophobicity of biofilm surfaces, contact angle measurements were performed (A). For each biofilm (n=3, per condition and strain),  $1 \times 10^6$  spores of *B. subtilis* (wt),  $\Delta bsIA$  (surface layer protein deficient) and  $\Delta epsA-O$  (biofilm deficient) were used as inoculum to incubate membrane filters. Biofilms were incubated for three days at 37 °C on MSgg agar (supplemented with 10 mM L-alanine) under regular gravity (1g) and simulated microgravity by using a fast rotating 2-D clinostat. After incubation, biofilms were cut out of the agar and transferred onto a glass slide. Biofilms were horizontally aligned with a camera system (B) and 10 μl of ddH<sub>2</sub>O were pipetted onto the center of the biofilm to capture an image which was then analyzed to determine the contact angle (A). Hydrophobicity increases with higher contact angles. Error bars represent the standard deviation, n=3, all data was successfully checked for normal distribution and statistically analyzed by using one-way ANOVAs and t-tests. Values of  $p \leq 0.05$  were considered as statistically significant. For scale, the agar piece measures 2.5 cm in diameter.

### 3.4 Cross section analysis via scanning electron microscopy (SEM)

#### Sample preparation for cross section analysis

In frame of this thesis a new standardized method was developed to generate highly reproducible biofilm cross sections from different biofilm regions. Parts of the preparation method were published by Fuchs *et al.* and representative figures are presented in the following (Figure 30-Figure 31) (Fuchs *et al.*, 2018). In contrast to the membrane filter method, which was typically performed with PTFE membranes, HTTP membranes proved to be more advantageous for the fixation and staining of biofilms using osmium tetroxide. Both filter materials were suitable to be used for the SEM-preparation, but PTFE-membranes detached from the biofilm during osmium staining and fixation, whereas HTTP-membranes detached during the dehydration series at high ethanol concentrations guaranteeing stable biofilms during the process-chain, minimizing the risk of mechanical stresses. As shown before, young 40 h-old biofilms form different growth regions if grown from a circular spore inoculum (spore-ring).



Due to the concentric form, a single biofilm can be used for the analysis of several cross section fragments of the same and different regions (Figure 30, A). After 40 h of incubation, membranes harboring biofilms were carefully removed from the nutrient agar and transferred into an osmium tetroxide staining and fixation bath. Subsequently, biofilms were washed and remaining water was substituted with ethanol by a dilution series with ascending concentration until a complete exchange had been completed. The membrane filter dissolved during the dehydration process. Macroscopic and microscopic biofilm images have already shown that young biofilms develop different growth zones. These were divided into three distinct regions for simplification: The center, as the oldest part of the biofilm in which the spore ring was originated, the intermediate/interstitial region, the second oldest region and the peripheral/rim/edge areas in which the biofilm extended until the end of incubation.

After dehydration, biofilms were submerged in ethanol, pre-cut into trapezoidal fragments' harboring the desired biofilm region (Figure 30, A). The shape of the trapezoid was aligned with the small parallel side towards the biofilm center, which allowed an identification of the fragments orientation. For surface analysis these fragments were already suitable for critical point drying, whereas the generation of cross sections required the freeze-fracture method. Biofilm samples were carefully placed on closed forceps and transferred to liquid nitrogen (B). By releasing the compression of the forceps, biofilm cross sections were created (C). Due to the force that developed when the forceps were relaxed into their original shape, biofilm fragments broke along the trapezoid longitudinal axis. Cross sectional fragments were critical point dried, sputtered with Au/Pt and mounted in order to perform SEM-imaging. Figure 30 D schematically represents different cross section regions of the biofilm modified after (Cairns *et al.*, 2014). In contrast to the schematic representation, each region showed typical biofilm characteristics such as different surface development, basal matrix mat or different cell/spore compositions. In contrast to the freeze-fracture method, conventional methods described in literature used the method of freeze sectioning. The freeze-fracture method created clean fracture edges, which run perpendicularly from the biofilm surface to the basal end. A frozen cut, on the other hand, caused a distribution of the biofilm material from the upper layers down to the lower regions and disrupted the cutting edge. Biofilm cross sections generated with both methods were compared to each other, proving that the creation of flat, uninterrupted edges cannot be achieved by the conventional cutting technique.

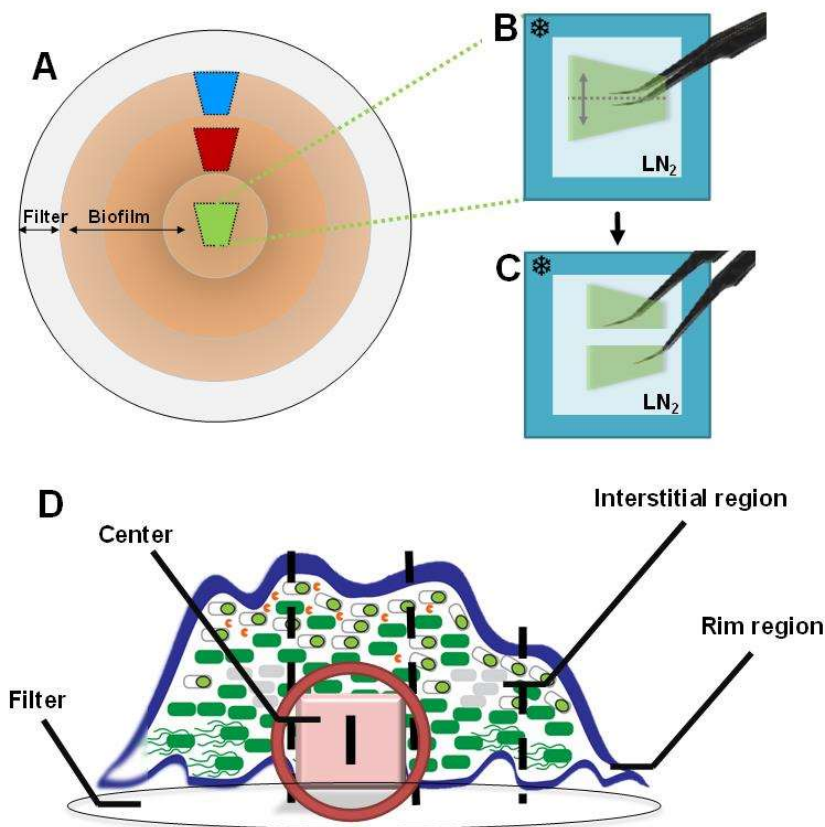


**Figure 30: Schematic freeze-fracture generation of *B. subtilis* biofilms**

*B. subtilis* biofilms were grown under standardized conditions ( $1 \times 10^6$  spores as inoculum) on MSgg agar (supplemented with 10 mM L-alanine) on filter membranes (A, outer zone,  $\phi$  4.7 cm) for 40 h at 37 °C. Due to the incubation of spores, which have been pipetted onto a filter membrane, concentric biofilm regions develop over time (A, circular biofilm regions). Each biofilm region (top view in A and side view of a cross section, D) differs along its radius depending on the distance to the center of the biofilm. Three different representative regions were analyzed: Center (green), interstitial region (red) and the rim or edge region (blue). After fixation and dehydration, biofilm regions were carefully sectioned into trapezoidal structures (~6 mm), which shared their longitudinal axis corresponding to the diameter of the biofilm. The trapezoidal structure helped to identify the original position within the biofilm after processing the sample. Fragments were placed on the tips of a partially closed forceps, aligning the longitudinal axis between the tips and transferred from an ethanol bath into liquid nitrogen (B). The frozen sample was torn apart along the axis by releasing the forceps tips (C), creating cross sections along the biofilm diameter. After freeze-fracturing, fragments were critical point dried, mounted and sputtered for SEM. Images A-C were modified after (Fuchs *et al.*, 2018) and image D is taken and modified after (Cairns *et al.*, 2014).

### Spatial distribution of cells, spores and EPS within *B. subtilis* biofilms

*B. subtilis* biofilms are known for their high diversity in structural components and that they comprise different cell types in different growth stages (Aguilar *et al.*, 2007). Especially biofilms produced by using the membrane filter method exhibited concentric structures, which were separated into different regions (Figure 30 and Figure 31). In Figure 31, regions were categorized into A (blue): peripheral/rim regions, B (red): intermediate regions and C (green) the biofilm center. The schematic illustration shows representative biofilm areas of a single biofilm along its radius. In A, cell bundles become visible (grey arrows), that were previously only loosely attached to the filter membrane. Most bundles were covered by a thin layer of the BslA-surface protein (visible in higher magnifications). With increasing distance to the biofilm center, the thickness of the protein layer decreases. At the outermost ends of the biofilm,

the protein layer could no longer be observed, which may be caused by the preparation method. In contrast to the intermediate region and biofilm center, a basal cell layer was barely or entirely absent. The intermediate regions (B) exhibited pronounced aerial structures as well as a basal cell mat. Cells within this region are interconnected by EPS matrix components and first spores can be found, whereas no spores were observable in the peripheral biofilm regions. A dense matrix mat (grey arrow) was formed in the basal end of the central region (C), which is a distinct indicator for the center and therewith oldest biofilm region. Aerial structures seemed to be collapsed and are less pronounced compared to the structures observed in cross sections of intermediate regions, which also correlate with DIC-microscopic images of young biofilm colonies. Biofilms older than 40 h often exhibited elevated concentrically aerial structures, situated within the intermediate regions, reaching almost the center of the biofilm.

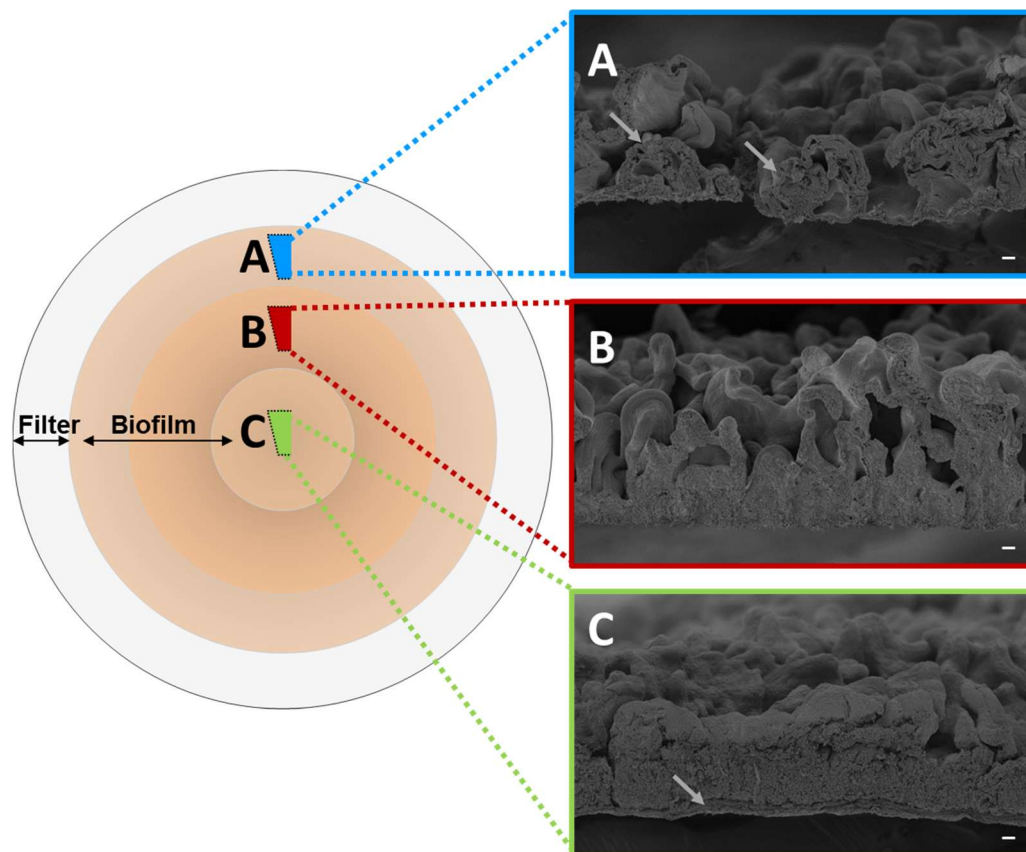


**Figure 31: Schematic overview of biofilm fragments of different regions**

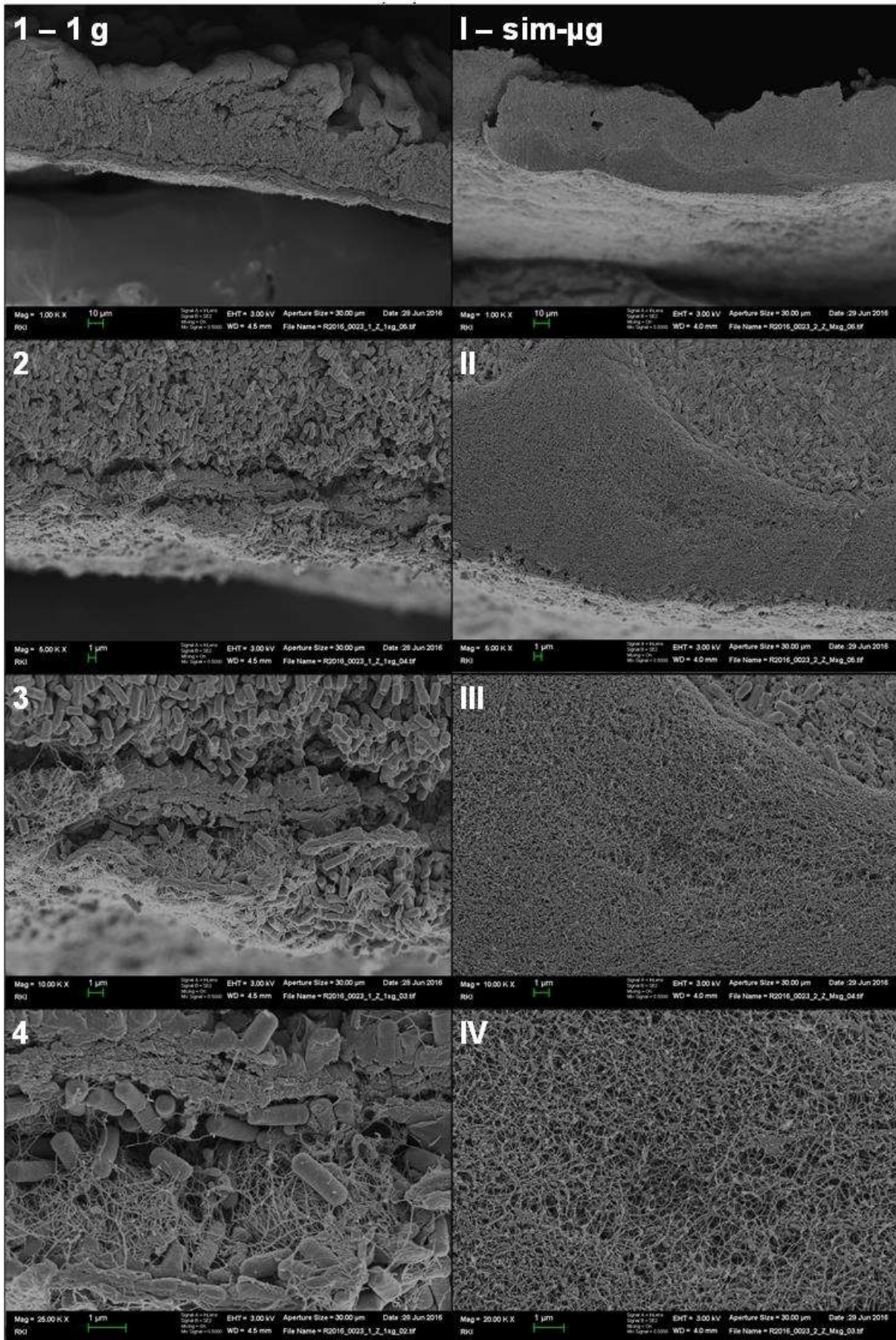
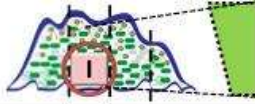
SEM-images of representative regions are shown on the right side of the scheme to visualize typical biofilm regions which were found in 40 h-old *B. subtilis* biofilms which were grown on membrane filters under standardized conditions (inoculum of  $1 \times 10^6$  spores, MSgg agar, 37 °C). Concentrically grown *B. subtilis* biofilms were separated into different biofilm regions. The center (C, shown in green) is the oldest biofilm region. Spores which have been used as inoculum started to germinate and grow here first. Descendant cells migrated in all directions (360°) and formed an intermediate area (B, shown in red) and the outer rim or edge region (A, youngest region, shown in blue). The rim region was characterized by its bundles (arrows in A) of cells which were aligned in long chains covered by a thin BslA-layer. The intermediate area showed cells and spores embedded in compact basal structure interconnected with EPS (B, see Figure 35). Above the condensed cells at the bottom of the fragments, an apical layer appeared to have similar, but more compact wavy structures including holes and valleys as shown for fragments of the rim region. A cross section of the biofilm center reveals three different layers (C): A basal matrix mat (arrow in C), which consisted of only EPS woven into a fine network, a densely packed region, filled with cells and spores (see Figure 32) as well as an apical layer structured by a few holes and valleys which seemed to be less wavy and pronounced than the surface in the intermediate surface region. Scale bars represent 10  $\mu\text{m}$ .

### 3.5 Cross sectional comparison via SEM of *B. subtilis* biofilms grown under 1g and sim- $\mu$ g

The freeze fracture method provides biofilm cross sections, which can be used to compare and analyze inner biofilm architecture ranging from a millimeter scale to nanometer scale. Individual regions of a single biofilm can be compared as well as biofilm-spanning replicas that have grown under the same or different conditions. Biofilms, for the generation of biofilm cross-sections, were cultivated on HTPP-membranes under 1g and simulated microgravity by using a fast-rotating 2-D clinostat. After the incubation, the clinostat was stopped and biofilms grown on membranes were immediately transferred into a buffered osmium solution for fixation and staining. All subsequent freeze-fracture preparation steps were identical as previously described for 1g biofilms.

To compare biofilms grown under 1g and sim- $\mu$ g, two sets of biological replicates ( $n \geq 4$ ) per condition were grown under standardized conditions. As shown before, biofilm cross sections were produced by applying the freeze-fracture method and biofilms were divided into three particular regions: Center, intermediate region and rim. Each biofilm was individually examined for each region, including the outermost, frayed regions. In the following, representative biofilm areas for both gravity conditions and regions are presented in different resolutions and magnifications ranging from 1000x to 50kx. Each of the following figures provides a schematic representation of the respective region within the biofilm which is shown underneath. On the left side of each figure, samples of 1g cross section are shown, whereas sim- $\mu$ g samples are presented on the right side. For each condition, only one biofilm fragment is presented ranging from a low magnification up to high magnifications; in Arabic numbers for 1g-samples (1-4/1-3) and Roman numbers for sim- $\mu$ g samples (I-IV/I-III, Figure 32-Figure 34).

# Region: center



Results

**Figure 32: Central cross sections of *B. subtilis* biofilms grown at 1g and sim- $\mu$ g**

SEM-images on the left side (1-4) show a representative cross section of a *B. subtilis* biofilm grown under regular gravity (1g) and a representative cross section of a biofilm grown under sim- $\mu$ g on the right side (I-IV). Due to the tilting of the 1g sample, the surface shows apical formations composed of cell bundles forming a structure of cell bundles and valleys. Similar apical structures were observed in sim- $\mu$ g samples (not pictured). The overall biofilm height is similar in both examples as well as cell length and cell/spore ratio (2 and II). A closer examination of the basal regions of the central biofilm part (3+4, III + IV) reveals changes in the EPS-mat which is located on the underside of the biofilm directed towards the filter and therefore the substrate. Under 1g, the EPS-mat is equally distributed along the biofilm diameter capturing several enclosed cells. Under sim- $\mu$ g, the EPS-layer is diverse in height and shows no intercalating cells. Scale bars represent 10  $\mu$ m for images 1+I and 1  $\mu$ m for all other displayed images (in variable dimensions).

**Cross sections of central biofilm regions grown under 1g and sim- $\mu$ g**

Cross sectional fragments of central regions of *B. subtilis* NCIB 3610 biofilms grown under 1g and sim- $\mu$ g are shown in Figure 32. The average thickness of biofilm fragments was almost identical under both gravitational conditions. Samples exhibited an apical BslA protein layer, which was sporadically disrupted. These might be potential artifacts that occurred during the preparation phase. Several cavity-like structures were observed in almost all biofilms in different quantities. Cavities or inclusions were sealed from the inside with a protecting protein layer. Due to the cell orientation, cavities could possibly be caused by overlapping of former surface structures. The curvature of the fragments can be regarded as an artifact because biofilms were grown on a planar filter. The dehydration of the samples already led to a shrinking of up to 25 % during the preparation.

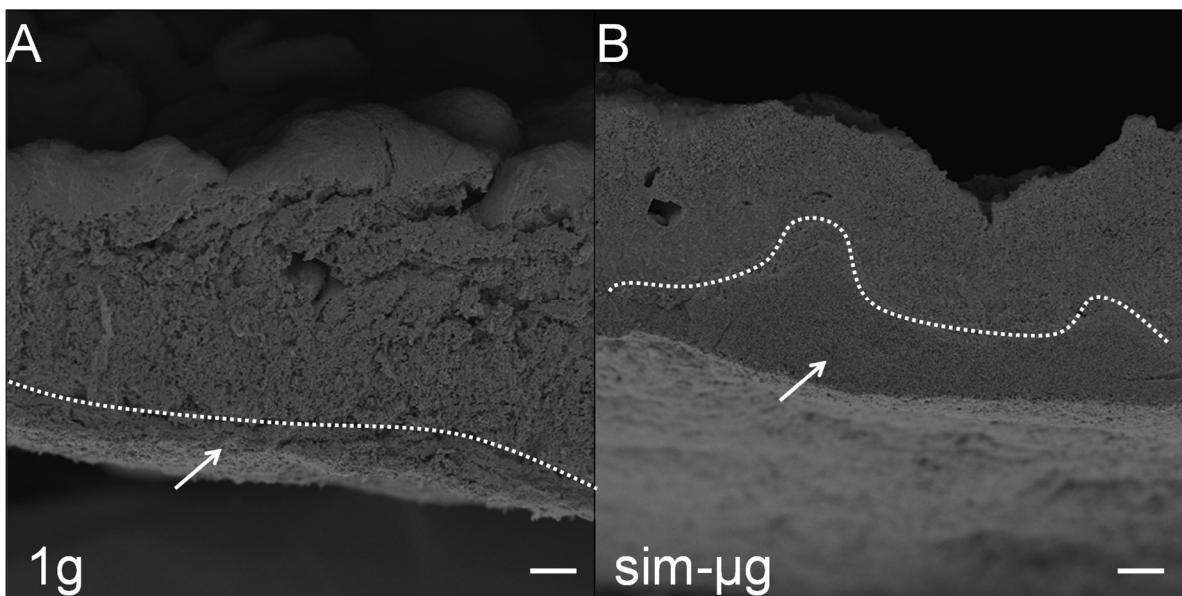


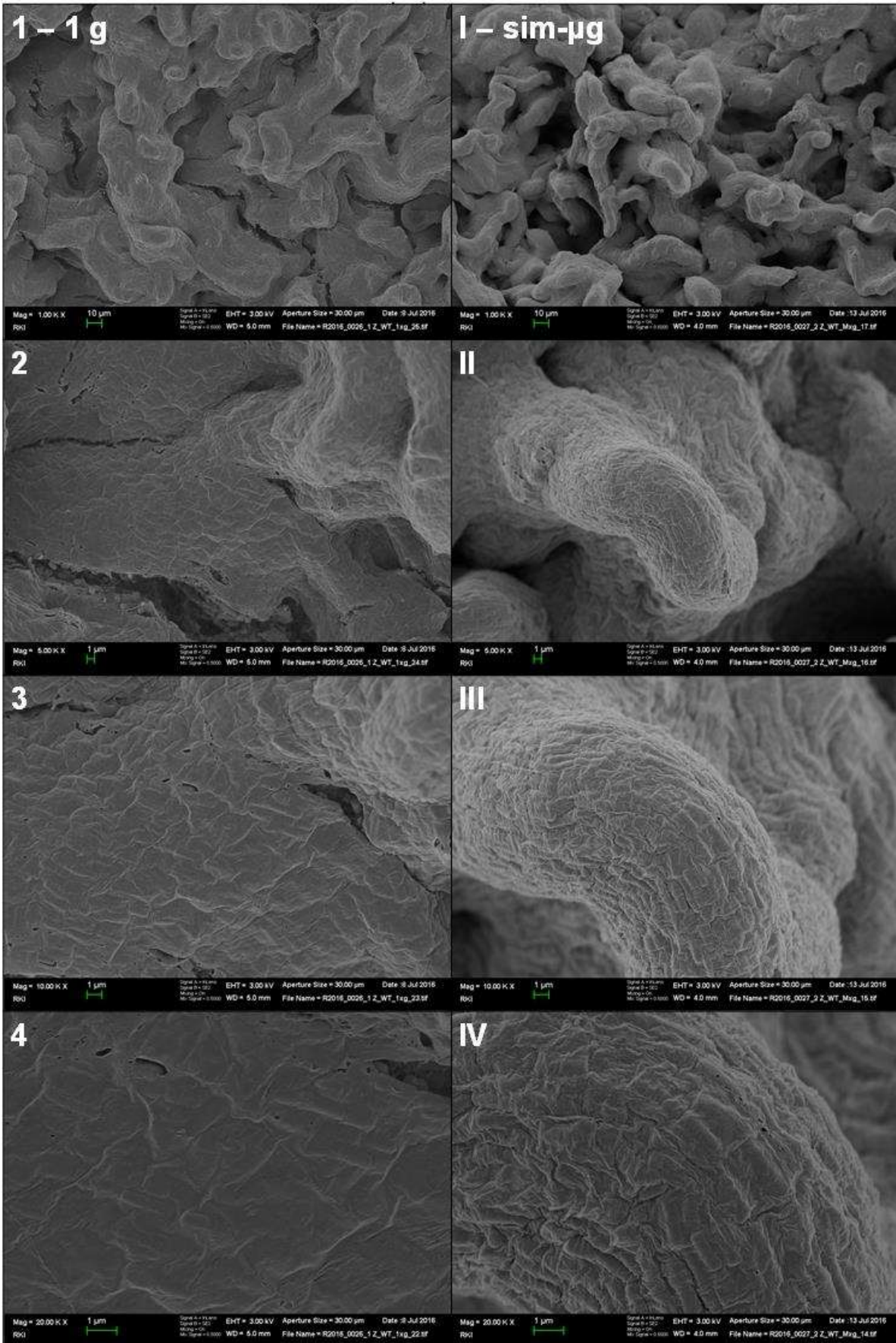
**Figure 33: Basal matrix-mat at the bottom of 1g and sim- $\mu$ g *B. subtilis* biofilms**

Both SEM-images show cross sections (freeze-fractures) of 40 h old *B. subtilis* NCIB 3610 biofilms grown under regular gravity (1g, **A**) and simulated microgravity (sim- $\mu$ g, **B**). SEM-images were taken at a magnification of 1000x. Biofilms grown under 1g and sim- $\mu$ g developed a basal matrix-mat in the center of the biofilm. The center represents the oldest part of the respective biofilm. The bottom was formerly attached to the filter, which was removed during the fixation process. The dotted lines represent the matrix-mat which was present in both samples, showing that under 1g conditions a homogeneous basal mat was formed, whereas under sim- $\mu$ g a heterogeneous, but generally thicker matrix appeared. The matrix mat at 1g was intercalated with many vegetative cells, but mostly consisting of EPS structures. Samples of sim- $\mu$ g showed a clear separation between cells and matrix components. Scale bars represent 10  $\mu$ m.

The major difference between 1g and sim- $\mu$ g samples was the basal matrix mat. In 1g biofilms, all analyzed samples exhibited a homogenous distributed matrix mat at the biofilm bottom (originally attached to the filter membrane), which narrowed towards the intermediate region (not shown). The fine-fibrous cross-linking of the EPS-matrix was occupied by single vegetative cells and spores. In contrast to this, sim- $\mu$ g samples often exhibited a highly developed basal matrix mat. It consisted of filigree EPS elements and was not intercalated with vegetative cells or spores. The sim- $\mu$ g samples (Figure 32, I-IV and Figure 33, A-B) exhibited a matrix, which was arranged in wave-like structures. However, other sim- $\mu$ g biofilms showed different matrix-mat structures in the basal regions of the central region.

In summary, biofilms formed under both conditions exhibited only sporadically spores and few empty cell membranes, also called "ghosts". Cells grown under sim- $\mu$ g were slightly smaller than the 1g cells.

# Region: center



Results



**Figure 34: Surface topography *B. subtilis* biofilms grown at 1g and sim- $\mu$ g**

SEM-images on the left side (1-4) show a representative cross section of a *B. subtilis* NCIB 3610 biofilm grown under regular gravity (1g) and a representative cross section of a biofilm grown under sim- $\mu$ g on the right side (I-IV). In 1 and I, a total view of the biofilm surface topography is presented. The perspective is an on-top view, therefore shadows represent lower regions on the surface and brighter areas represent apical structures. Images taken only compare one sample grown under 1g and sim- $\mu$ g, but represent typical surface structures observed across all central and interstitial biofilm regions. Valleys and wave-like structures alternate. Most apical structures show a uniform thickness. All surfaces are covered by a BslA protein-layer through which individual cells from the subsurface emerge (4, IV). In 2 and 3, a crack in the surface shows vegetative cells from lower structures. Scale bars represent 10  $\mu$ m for images 1+I and 1  $\mu$ m for all other displayed images (in variable dimensions).

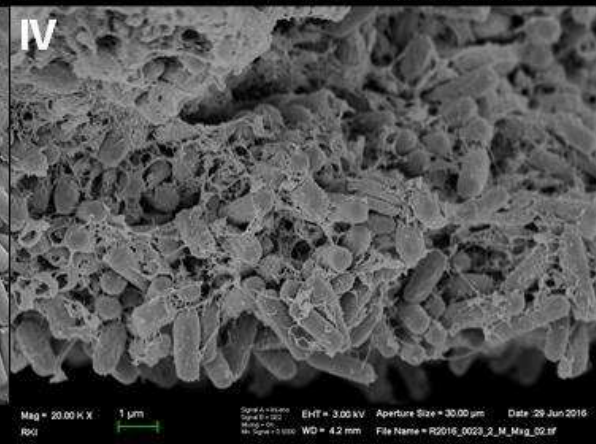
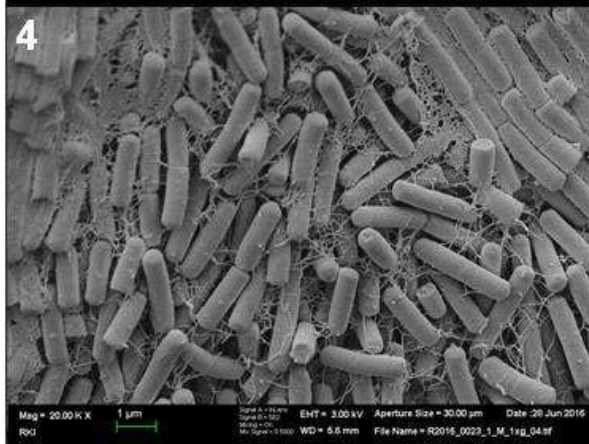
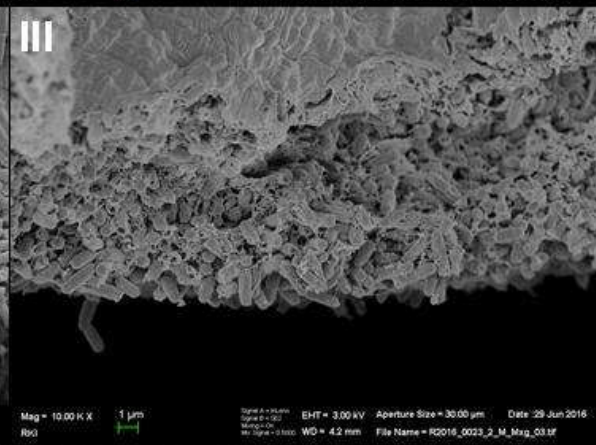
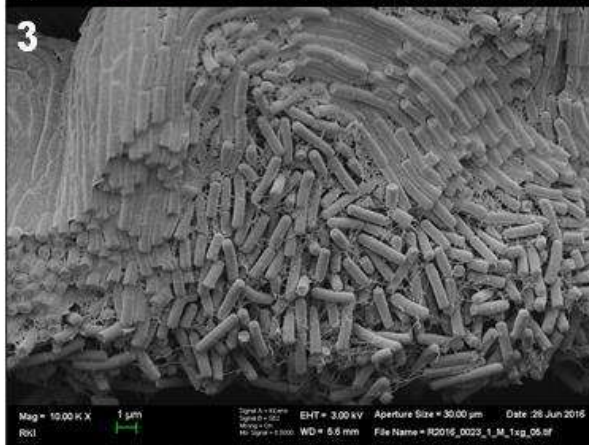
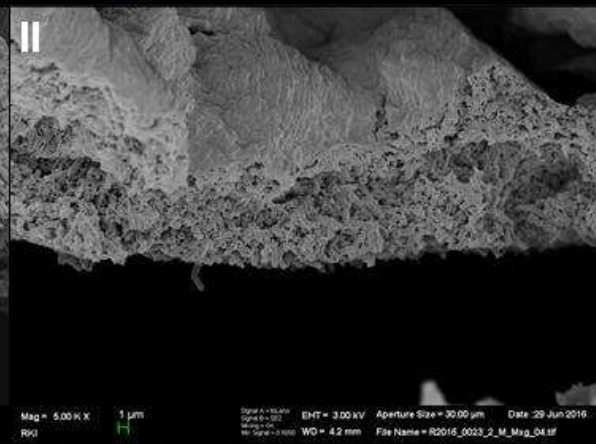
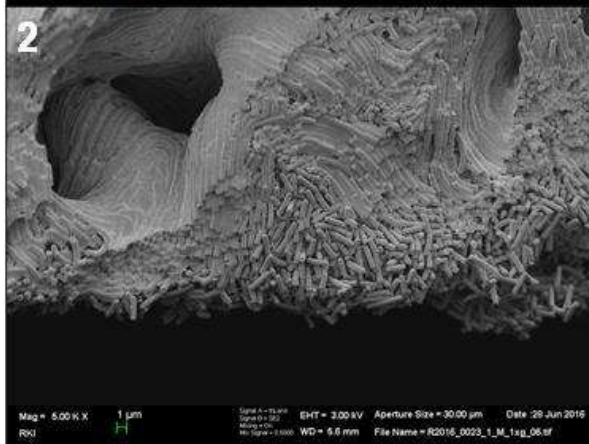
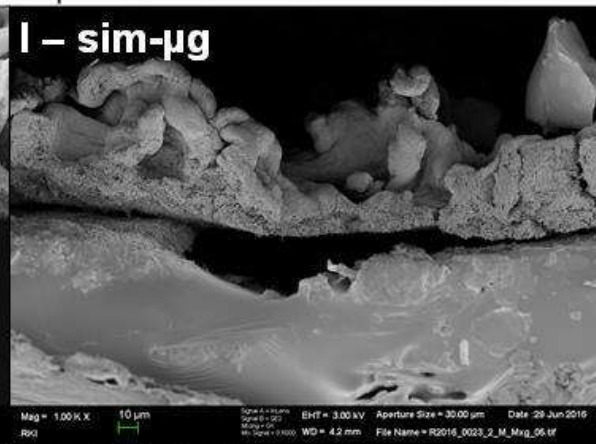
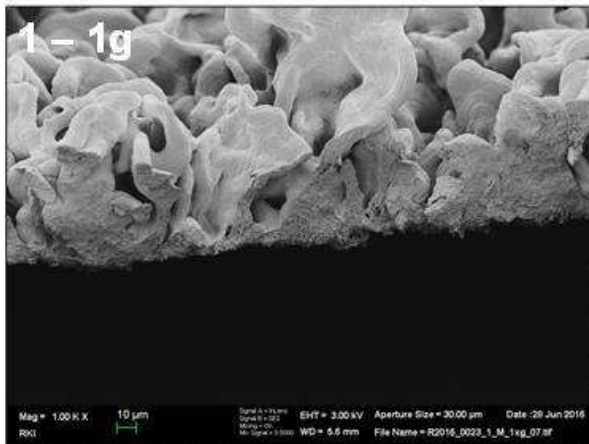
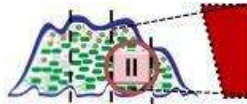
**Surface topography of *B. subtilis* biofilms grown under 1g and sim- $\mu$ g**

In Figure 34 surface characteristics of representative biofilms grown under both gravitational conditions are shown. As already described in the cross sectional analysis of the central region, biofilms were completely covered by a thick BslA surface layer. Due to its hydrophobicity, the protein layer protects the biofilm from harmful environmental influences and provides a closed biofilm environment underneath. High magnifications show sporadic small cracks in the protein layer, which were probably caused by the SEM-preparation (2, 3). On closer examination, the imprint of single cells underneath the BslA protein layer became visible (i.e. IV). This allowed determining the cell orientation through the protein layer. For example, the cell distribution in 3-4 (1g) was heterogeneous, whereas the bundle-structure as a result of cell-chain formation became apparent in III-IV (sim- $\mu$ g).

Depending on which biofilm region is observed, the aerial structures differed: The outermost biofilm edge was flat and only consisted of individual cell layers at the ends. In connection with this, transition between the flat layers and the rest of the rim region, exhibited large bundle-like structures, which were most pronounced in the intermediate regions. The central region (Figure 34) also showed elevated aerial structures, which were less branched and flatter than in the interstitial region. Differences in overall height or depth of elevated aerial structures were not observed. Due to the large individuality of the surface structures, only general comparisons can be made. The analysis of single cell bundles is not useful, because they exhibit different sizes, shapes and angles within a biofilm. Differences between 1g and sim- $\mu$ g were hardly determinable by phenotypical comparison. As profilometry results demonstrated before, biofilm topography was not significantly influenced by sim- $\mu$ g.

In summary, the comparison of surface structures showed no phenotypic differences between 1g and sim- $\mu$ g biofilms. This is consistent with the statistical analysis of the profilometric data supporting the SEM-surface analysis findings.

# Region: interstitial



Results

**Figure 35: Interstitial cross sections of *B. subtilis* biofilms grown at 1g and sim- $\mu$ g**

SEM-images on the left side (1-4) show a representative cross section of a *B. subtilis* biofilm grown under regular gravity (1g) and a representative cross section of a biofilm grown under sim- $\mu$ g on the right side (I-IV). Due to the tilting of the 1g sample, the surface shows apical formations composed of cell bundles forming a structure of cell bundles and valleys. Similar apical structures were observed in sim- $\mu$ g samples. Fragments of the interstitial region do not exhibit a basal EPS-mat as it is present in the central biofilm regions. The overall biofilm height differs in 1g and sim- $\mu$ g ranging from a few  $\mu$ m to highly developed apical structures (2 and II). The BslA surface protein layer seems to be similar for biofilms grown under both gravity conditions. By the imprint of the cells under the protein layer, the cell size of the respective condition can be estimated. A closer examination of the basal regions (3+4, III + IV) reveals changes in cell morphology and EPS composition. Cells grown under 1g seem to form long and uniform rods, whereas vegetative cells of sim- $\mu$ g samples formed short rods, which are densely packed. Fine EPS structures are visible under 1g conditions, connecting cells with each other. Sim- $\mu$ g samples showed a coagulative interconnection of EPS between the cells, less fine than in 1g-samples (4+IV). Scale bars represent 10  $\mu$ m for images 1+I and 1  $\mu$ m for all other displayed images (in variable dimensions).

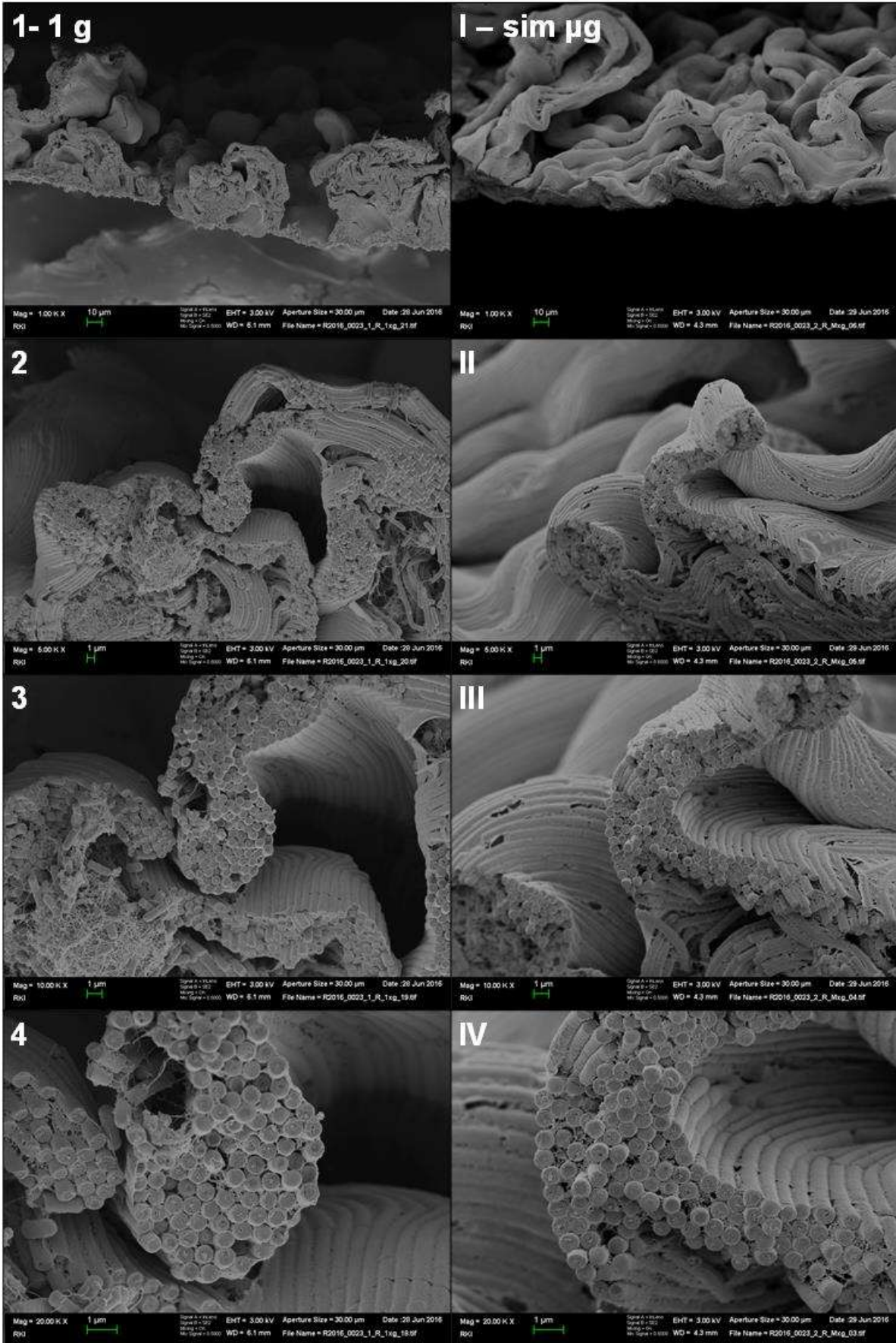
**Cross sections of interstitial biofilm regions developed under 1g and sim- $\mu$ g**

Intermediate or interstitial biofilm regions enclosed the biofilm center and were themselves surrounded by the edge/rim region. The overall thickness of the interstitial biofilm regions grown under 1g and sim- $\mu$ g exhibited no significant differences in total height (1, I), which is in accordance with previously shown profilometry results (see page - 67 -). In general, the region was characterized by its heterogeneity, which varies from apical topography structures to the basal end throughout the cross section. Due to cell elevations and valleys, spatial structures formed the biofilm surface. The upper layers were arranged in bundles, which incline towards the basal end and thus represent the surface. It seems that the bundles were formed by compression, presumably with increasing cell growth. In addition, all outer regions were covered by a pronounced BslA protein layer, showing imprints of cells from underneath.

In contrast to the central biofilm region, intermediate areas did not exhibit a basal matrix mat under both tested gravitational conditions. Instead, the basal end of the biofilm harbored only vegetative cells, which were interconnected by fine EPS-elements forming a matrix. In 1g samples (4), intercalating EPS appeared to be much finer and more filigree than in comparable regions in sim- $\mu$ g biofilms. Furthermore, the cell size and shape differed between both gravitational conditions. In biofilm regions grown under 1g, vegetative cells exhibited a long and uniformly thick appearance. Arrangements of these cells followed no pattern especially in the basal regions, whereas cells close to the surface were aligned in bundles (2), connecting cells end to end in parallel formations.

Cell growth within the interstitial biofilm region under sim- $\mu$ g showed different cell shapes and sizes in apical and basal regions. Upper regions were partially organized in cell bundles consisting of shorter cells than comparable bundles grown under 1g. At the basal end of the biofilm region, individual "ghosts" and mainly small, densely packed cells were observable, which were not subject to an orderly structure. In contrast to fine EPS-elements, as shown in 1g samples, sim- $\mu$ g samples (III, IV) exhibited a lumpy, close-meshed and heterogeneous matrix. Overall, the intermediate regions of biofilms grown under 1g and sim- $\mu$ g showed distinct differences in biofilm structure. Especially the basal region exhibited differences, which varied in matrix composition and structure as well as in cell size and thickness.

# Region: rim



Results

**Figure 36: Rim/edge region of *B. subtilis* biofilms grown at 1g and sim- $\mu$ g**

SEM-images on the left side (1-4) show a representative cross section of a *B. subtilis* biofilm grown under regular gravity (1g) and a representative cross section of a biofilm grown under sim- $\mu$ g on the right side (I-IV). For both gravity conditions, 1g and sim- $\mu$ g, the outer biofilm regions are dominated by large cell-bundles which seem to propagate in wave-like structures (1 and I). These bundles can consist of individual chains of vegetative cells, but also can comprise dozens of cell chains. At the outermost edge, artefacts may occur and small fragments may be lost due to the preparation. A steady basal cell layer is not present as it is interrupted by the curvatures of the wave like structures. Compared to biofilm preparation of other regions, the rim regions also show a predominant BslA layer covering the cell chain bundles (2, 3 and II, III). At magnifications above 20kx very fine EPS connections between the cell chains are visible (4, IV). Scale bars represent 10  $\mu$ m for images 1+I and 1  $\mu$ m for all other displayed images (in variable dimensions).

**Cross sections of biofilm edge regions developed under 1g and sim- $\mu$ g**

Apart from the central and the interstitial regions, peripheral biofilm regions proportionally cover the largest surface area. In order to prevent disruptions, preparation and mounting of biofilm rim samples were carried out carefully, due to the overall fragility of the fragments. As mentioned before, the outer biofilm region underwent an extreme shrinking during the ethanol dehydration, causing the biofilm to contract. Therefore, subsequent analysis of the edge region should be considered with caution, assuming possible artifact formation.

In contrast to central and intermediate biofilm regions, peripheral biofilm regions did not exhibit a basal cell layer (1/I). As partwise visible in the interstitial regions, the biofilm rim was mainly organized in cell bundles (2/II). At the outer edges the cell bundles seem to become thinner and less branched. All bundle-like structures as well as flatter biofilm regions were covered by a thin BslA surface protein layer. Disruptions of this layer were observed in 1g and sim- $\mu$ g samples and may have been caused by the preparation. The cross sections revealed fine intercalating matrix components within single bundles, connecting cells with each other (3, 4 /IV). In regions, divided longitudinally by cross sectioning, it can be observed that matrix components were longitudinally attached between the cells. The cell poles (rods ends) were connected to each other, thus matrix elements occurred only on the sides.

Cells grown under both gravitational conditions were uniformly in length and thickness, attached end to end in parallel alignment. "Ghosts" or spores were not observable due to the young age of this region. The overall surface area in the biofilm rim is less pronounced compared to interstitial regions.

In summary, no phenotypical differences in cell or biofilm structure between 1g and sim- $\mu$ g were characterized in the peripheral biofilm regions. This biofilm region was mainly dominated by the large bundle formations, harboring cells aligned in chains interconnected by fine matrix components.

## Region: center

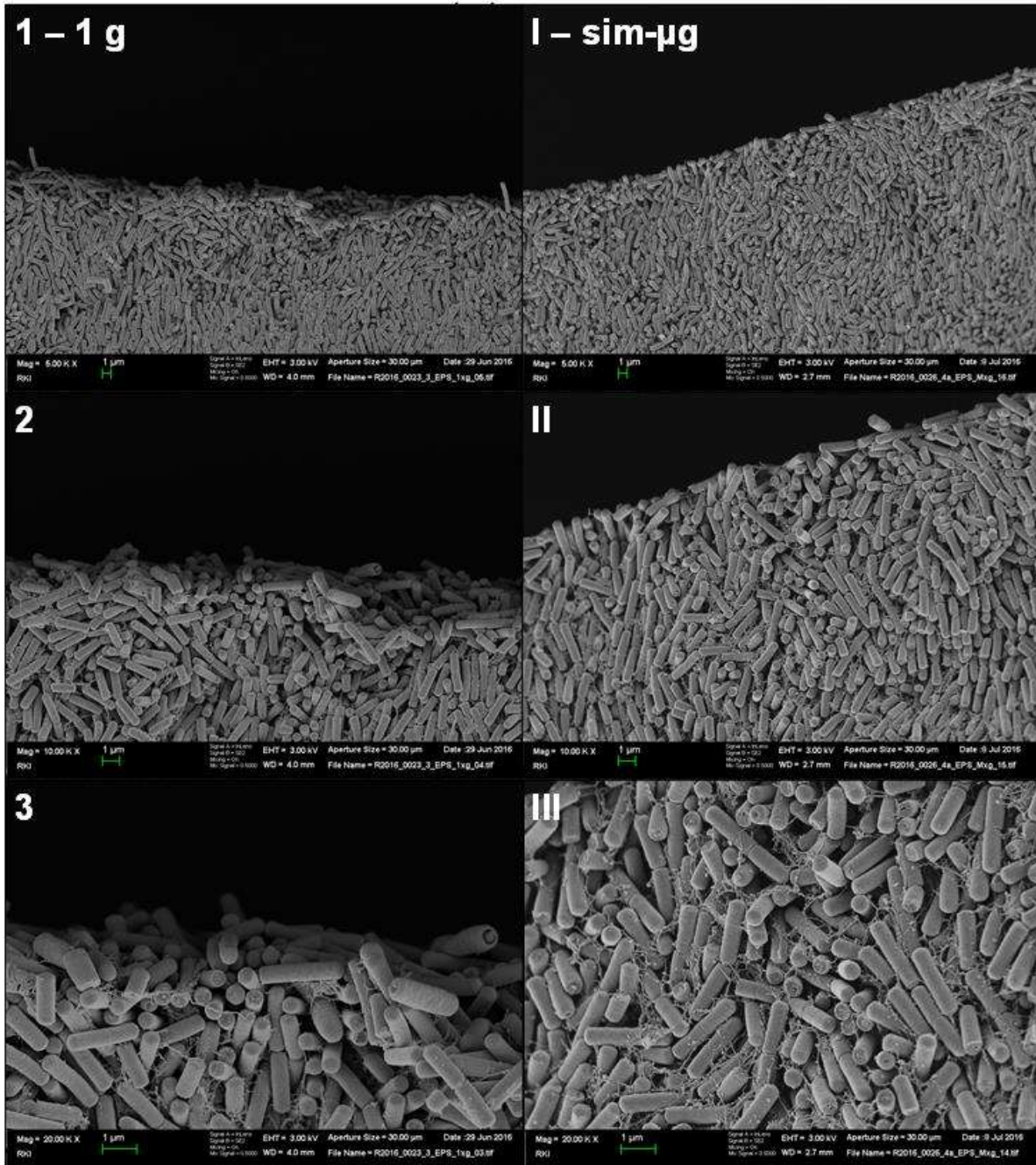
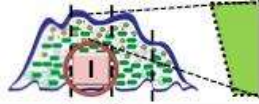


**Figure 37: Central region of *B. subtilis*  $\Delta epsA-O$  colonies grown at 1g and sim- $\mu g$**

In accordance with Figure 30, the spatial orientation, the central region of a *B. subtilis*  $\Delta epsA-O$  (biofilm-deficient) colony is shown above the figure. SEM-images on the left side (1-3) show a representative cross section of a colony grown under regular gravity (1g) and a representative cross section of a colony grown under sim- $\mu g$  on the right side (I-III). Cross sections have been created by applying the freeze fracture method of 40 h old *B. subtilis* NCIB 3610 biofilms. Each biofilm was inoculated with  $1 \times 10^6$  spores on a membrane filter (HTTP,  $\phi$  3.7cm) and incubated on MSgg agar (supplemented with 10 mM L-alanine) at 37 °C. Samples were osmium-fixated and stained, ethanol dehydrated, critical point dried and sputtered with Au/Pd. SEM-images 1+I were taken at a magnification of 5kx, 2+II: 10kx and 3+III: 20kx. In 1 and I, a total view of  $\Delta epsA-O$  colonies can be seen for both gravity conditions. In contrast to *B. subtilis* biofilms, the colonies show no BslA protein layer or any other surface structure. Cells mainly appear uniform in length and thickness and seem to be not structured in any pattern. A

minor amount of cells is still connected by polar attachment (2+II). At high magnifications fine matrix components become visible, which seem to link cells with each other (3+III). Scale bars represent 1  $\mu\text{m}$ .

### **Cross section $\Delta\text{epsA-O}$ colonies grown under 1g and sim- $\mu\text{g}$**

Previously shown results featured SEM-images of *B. subtilis* wild-type (NCIB 3610) biofilms. For cross sectional comparison, a biofilm deficient mutant,  $\Delta\text{epsA-O}$ , was incubated under 1g and sim- $\mu\text{g}$ . Characteristic biofilm components such as the surface protein layer (BslA) were not expressed and cells remained unprotected at their apical regions. Figure 41 shows a cross section from the center of an  $\Delta\text{epsA-O}$  colony. In comparison to wild-type biofilms, the surface development was almost non-existent. This is in accordance with profilometry and microscopy results. Phenotypically,  $\Delta\text{epsA-O}$  colonies appeared flat. Cell bundles or bulges on the surface were not observed. In addition, cells did not seem to be arranged in patterns, but randomly arranged. Rim regions of the mutant showed cell chains (not shown) but no rim threads as they were observed in wild-type biofilms.

In contrast to the wild-type biofilms, the biofilm deficient mutant showed no visible spore formation or ghosts after 40 h incubation. This result was supported by the CFU/spore analysis of young biofilms grown under sim- $\mu\text{g}$  (Figure 22), which showed that  $\Delta\text{epsA-O}$  did not form any spores after 40 h incubation. In contrast, colonies under 1g conditions formed spores, which were not visible in the sample section (1-3). Other sections sporadically showed spores, but as described in Figure 22, the overall spore content was less than  $1 \times 10^6$  spores per colony. Furthermore, neither “ghosts” nor vegetative cells in different lengths were observed. All cells in the biofilm center appeared to be uniformly long and thick.

At larger magnifications, minor EPS-like components became visible, interconnecting cells, despite the mutant’s disability to form most structural biofilm components. However, these structures were not as pronounced as the matrix in wild-type biofilms. The basal end is not shown in Figure 41, but the characteristic matrix mat is completely missing. The bottom cell layer, which was previously placed on the filter, was flat, but did not differ structurally from the cell layers above it.

In summary, remarkably differences between the  $\Delta\text{epsA-O}$ -mutant and the wild-type were observable by comparing cross sections of the central biofilm/colony region. Although wild-type biofilms differed in their structure under different gravitation conditions, colonies of biofilm-deficient mutants did not show any structural differences between 1g and sim- $\mu\text{g}$ . The only difference was that 1g colonies already showed spores after 40 h, which could only be observed after 60 h in sim- $\mu\text{g}$  samples.

### **Structural analysis of *B. subtilis* spores formed under 1g and sim- $\mu\text{g}$**

The analysis of single vegetative cells grown under different gravity regimes showed no significant differences in their cell morphology or phenotypic appearance. Young 40 h-old biofilms, which represent compositions of vegetative cells in different cell stages, differed, however, with regard to their composition and structure. Hereinafter, the formation of spores under 1g and sim- $\mu\text{g}$  is analyzed. A typical technique to investigate the structure of bacterial spores is TEM-imaging. By creating thin-sections of spores, the inner spore structure composed of different protein layers and the inner core became visible. In order to generate spores under sim- $\mu\text{g}$ , sporulation media was inoculated with a fresh overnight culture of *B. subtilis* NCIB 3610, which were mounted after drying in a fast rotating 2-D clinostat. Cells were allowed to form spores over a period of 5 days at 30 °C. After incubation, spores were harvested, washed, fixated and stained with ruthenium red. After embedding, thin sections of samples grown under both gravity conditions were created.

In Figure 38 (A and B), TEM-images of representative spores are shown. The inner center comprised the spore core (dark center) containing the nucleoid (brighter structures). It is surrounded by the spore cortex (white ring, well visible in A) followed by several layers of different inner spore coat proteins (grey) and the terminating outer spore coat (black). TEM-images A and B show representative examples of spores formed under both gravitational conditions. The overall composition of typical spore characteristics did not differ significantly. Size, shape and proportion of certain coat layers or spore components remained identical in spores grown under both gravitational conditions.

In addition to TEM-imaging, phenotypic characterization of spores formed under 1g and sim- $\mu$ g was performed by SEM-imaging (Figure 38: C, D). Spores were grown and harvested under the same conditions as spores used for TEM. In contrast to the TEM-preparation, spores were osmium fixated and stained. Typically, *B. subtilis* spores are rounded at their poles and exhibit a slightly oval shape along their longitudinal axis. Spores formed under 1g and in sim- $\mu$ g showed wrinkle formation along the surface of their longitudinal sides, which extended vein-wise up to the poles. Polar spore regions were relatively flat in comparison to the spore body, without exhibiting pronounced patterning or structures.

In summary, spores formed under 1g and sim- $\mu$ g demonstrated no macroscopic differences in structure, size or other morphological features via SEM and TEM-imaging.

### 3.6 TEM-imaging of biofilms and individual cells and spores

#### TEM analysis of spores within biofilms grown under 1g and sim- $\mu$ g

As previously shown, *B. subtilis* wild-type biofilms grown under 1g and sim- $\mu$ g were fragmented into cross sections using the freeze-fracture method and examined via SEM. This offered the possibility to analyze biofilm fragments from micro- to nano- scale. For examination of individual biofilm components such as single cells or spores, TEM-imaging offered an in-detail magnification for investigation. In Figure 39, representative examples of sections of vegetative cells (A, B), spore-containing mother cells (C, D) as well as spores (E, F) grown in 1g and sim- $\mu$ g biofilms are presented. Given sections for TEM were taken from the interstitial biofilm region and show extracts of individual components, between the apical biofilm surface and the basal end.



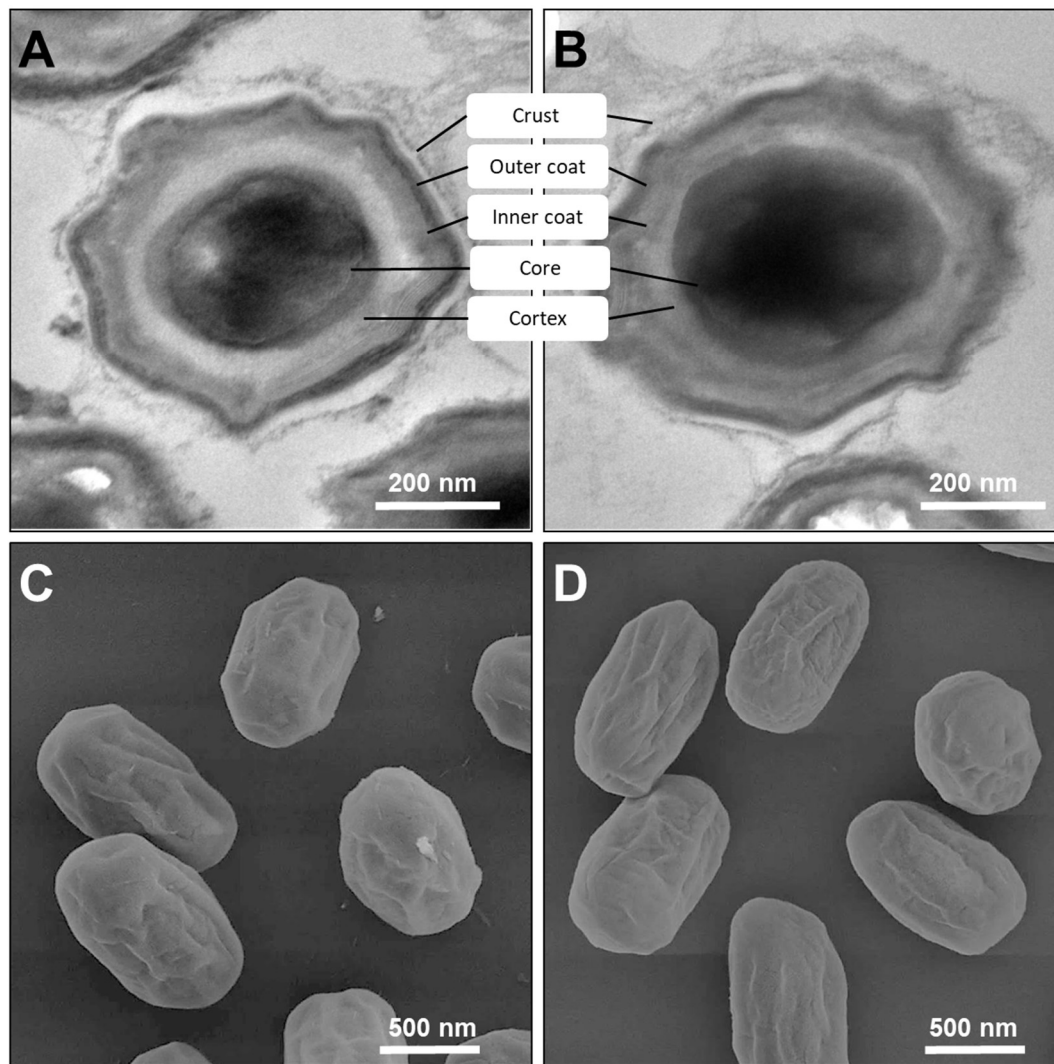


**Figure 38: TEM- and SEM-images of *B. subtilis* spores grown under 1g and sim- $\mu$ g**

Images show representative examples of *B. subtilis* NICB 3610 spores grown under regular gravity (1g, A+C) and under simulated microgravity (sim- $\mu$ g, B+D). Top row shows TEM-images (A+B) of spores which have been stained with ruthenium red. Spores were shown cut along their transverse axis. Proportional distribution of the coat layers and spore cores were similar under both gravitational conditions. SEM-images of *B. subtilis* spores showed typical spore characteristics (C+D): wrinkle- and vein-like structures, oval proportions and less structured polar regions. No morphological differences between spores grown under 1g and sim- $\mu$ g were observed by using SEM. Size bars represent 200 nm for TEM-images and 500 nm for SEM-images.

In general, cells grown under 1g and sim- $\mu$ g exhibited almost identical cell thicknesses ( $0.55 \pm 0.07 \mu\text{m}$ ) despite differences in their length. In addition, no differences in cytosol or membrane composition and thickness were observed. Compared to the majority of vegetative cells and a few ghosts, only sporadically spore-forming mother cells were present in the biofilm after 40 h incubation (C, D).

A *B. subtilis* endospore is formed at a specific cell pole within the vegetative mother cell via separating the prespore with a septum from the remaining cytosol. Depending on the status of the sporulation, a fully mature spore enclosed in the mother cell can be observed (C, D), which was present before lysis of the mother cell after final maturation. Characteristic features for spores, such as the core, cortex, as well as the inner and outer spore coats and the surrounding crust were illustrated via TEM-imaging. The angle of view varied in dependence of the sectioned plane, and therefore individual spore elements were magnified. Due to the relatively small amount of mother cells in different sporulation stages, a

reliable quantification is barely possible. However, from a macroscopic point of view, no differences between 1g and sim- $\mu$ g were observed. In contrast to previously shown TEM-images of individual isolated spores, 40 h old biofilms sporadically exhibited spores, which were released after mother cell lysis. These were mainly found within the central biofilm region or in rare cases at the basal layer within the interstitial region (E, F). The macroscopic comparison of both SEM and TEM images barely allowed conclusions to be drawn regarding the absolute abundance of spores under 1g or sim- $\mu$ g. In previous experiments, biofilms grown under both gravitational conditions showed no significant differences via CFU and spore determination. In addition, the spores formed within a biofilm did not differ in their structure compared to spores grown under different gravity regimes. Typical spore characteristics were observable, both in spores of the central region as well as in the intermediate region.

### **TEM analysis of biofilm fragments of different regions grown under 1g and sim- $\mu$ g**

In addition to TEM-images of single biofilm components, the analysis of whole biofilm fragments was achieved by applying tile scans of regions of interest. 40 h-old *B. subtilis* wild-type biofilms were fixated, stained, embedded and cut into ultra-thin sections. In rare cases, individual cells or cell fragments detached themselves from the thin sections, creating sporadic gaps. The advantage of TEM-imaging of biofilm fragments compared to SEM imaging was that ghosts, (empty cell membranes), were recognized immediately. When examining SEM images, the differentiation between vegetative cells and ghosts was hardly possible. Therefore, false-positive results regarding the vitality of biofilms had to be taken into account. A combination of TEM and SEM of biofilm fragments from the same region allowed the best possible comparison for architectonic and structural differentiation between growth in 1g and sim- $\mu$ g.

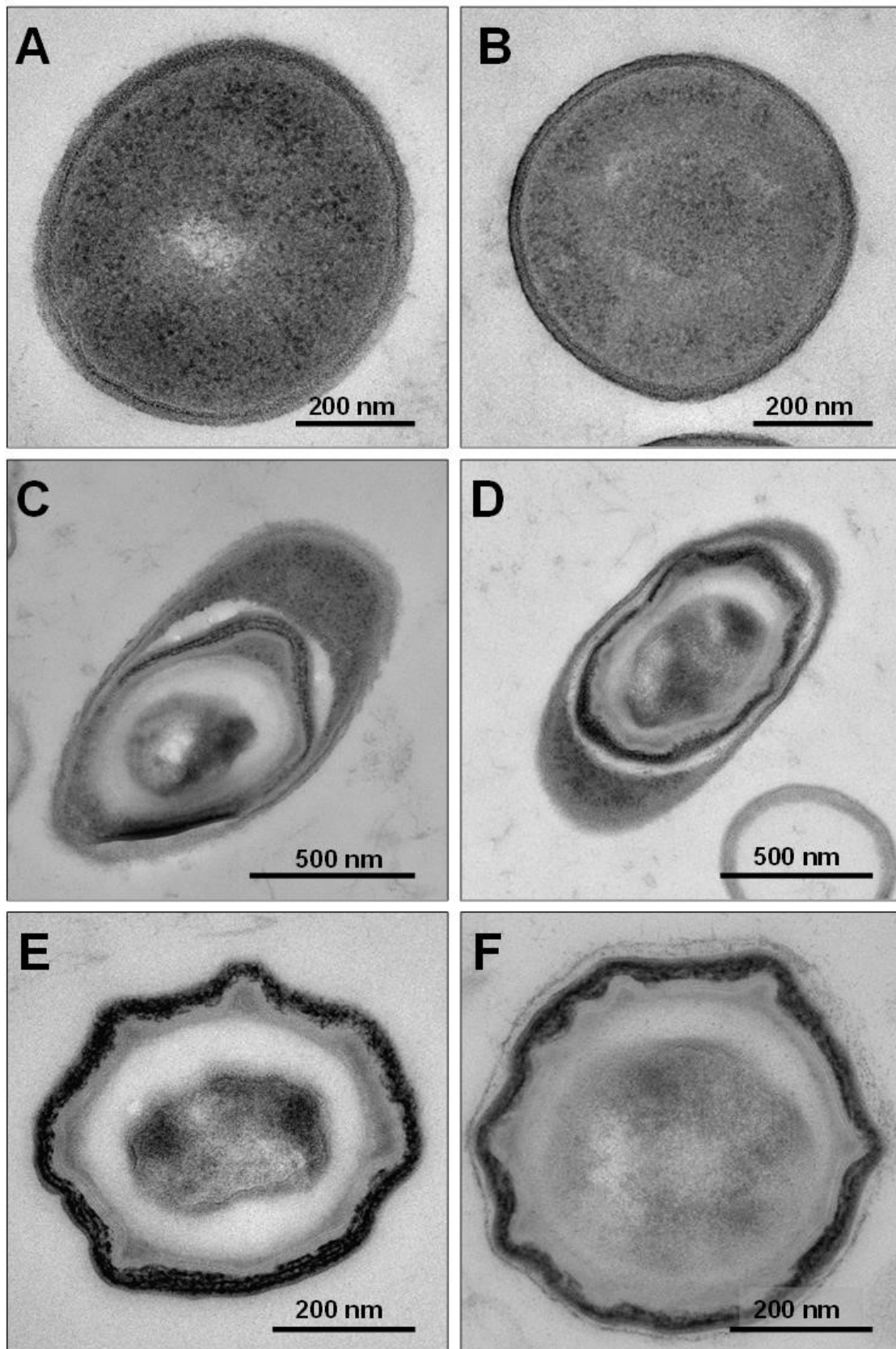


**Figure 39: TEM-images of 1g and sim-μg biofilm-embedded vegetative cells, mother cells and spores**

TEM- images demonstrate representative examples of vegetative cells (A+B), mother cells harboring a spore (C+D) and spores (E+F) embedded in 40 h old of *B. subtilis* NICB 3610 biofilms, grown under regular gravity (1g, A, C, E) and under simulated microgravity (sim-μg, B, D, F) by using a fast rotating 2-D clinostat. For inoculation,  $1 \times 10^6$  spores were spotted on membrane filters (HTTP,  $\phi$  3.7cm), which were incubated on MSgg agar (supplemented

with 10 mM L-alanine) at 37 °C. All biofilm fragments depicted here were isolated from intermediate regions. Rod shaped, vegetative *B. subtilis* were cut along their transversal axis (A+B). Membrane thickness and cytosol composition seemed not to differ between 1g and sim- $\mu$ g conditions. Depending on the biofilm area and age of biofilms, considerably more empty cell bodies appear (ghosts), which consist only of membrane components. In C and D, vegetative mother cells are harboring a spore. Both examples were cut along their longitudinal axis in different depths. In both examples the spore core and the outer spore coat layers are visible. Both spores are attached to a polar region of the respective mother cell. Spores from basal interstitial biofilm regions are shown in E and F. Most biofilms were analyzed after 40 h of incubation and at this time only a minority of vegetative cells formed spores. These transversal-cut examples show typical spore characteristics such as spore coat layers and darker spore cores. Differences in size, structural alterations or overall abundance of all three examples were not observed between 1g and sim- $\mu$ g biofilm samples. Scale bars represent 200 nm for A, B, E, F and 500 nm for C and D.

In Figure 40, representative TEM-biofilm sections from *B. subtilis* biofilms are shown. In comparison to previously shown SEM images of biofilm fragments, these were likewise incubated for 40 h under 1g (images on the left) and sim- $\mu$ g (images on the right). The following TEM-sections are aligned with their apical end pointing upwards and their basal end pointing downwards. Images A and B represent sections from the central and therefore oldest biofilm region. The density of vegetative cells (dark circular and oval shapes) was relatively low compared to all other biofilm regions. Spore-forming mother cells as well as individual spores occurred with increased frequency. Depending on the angle of the respective cell or spore during the section, different morphological properties became visible. For instance, a differentiation between early and late sporulation phase or finalized sporulation was possible. Furthermore, the central biofilm region under both gravity conditions revealed high amounts of “ghosts” as well as structural EPS-components (light-grey structures). The comparison of large sections was difficult to achieve via TEM, but offered high-resolution detail-levels for the identification and characterization of single biofilm components. Differences in central biofilm regions grown under 1g and sim- $\mu$ g were only observed in the basal matrix-mat (not shown in Figure 40 A+B) which dominated in size and structure in sim- $\mu$ g biofilms.

Intermediate biofilm regions (1g: C and sim- $\mu$ g: D) harbored only a few “ghosts” compared to central biofilm regions, which were identified despite almost completely preserved membranes by the lack of cytosol. Spores and spore-forming mother cells (dark inclusions) were rarely observed in comparison to the biofilm center. Cells appeared to be densely packed, following no structural patterning, apart from apical regions (not shown), where bundle-like cell-formations were visible. SEM cross sections of intermediate areas demonstrated, that cells grown within 1g-biofilms, were uniformly in size and thickness in contrast to heterogeneous sim- $\mu$ g biofilms. Due to the two-dimensional imaging by TEM, a less plastic resolution is given, which was however sufficient to detect differences in cell length between 1g and sim- $\mu$ g especially in the basal regions. In comparison to the biofilm center, interstitial regions grown under 1g and sim- $\mu$ g exhibited less pronounced matrix and EPS-structures (open spaces and grey shadows between veg. cells).

TEM-images E and F (Figure 40) show representative sections of biofilm rim regions grown under 1g (E) and sim- $\mu$ g (F). As shown via SEM-imaging, vegetative cells in the periphery of biofilms were aligned in large bundle structures interconnected by fine EPS and matrix elements. At the top of image F, a small part of the surface protein layer BslA can be seen, which covered the cells in this region in their early developmental stages. Both sections presented here were cut transversal through one of the cell bundles. Due to the relatively young age of the peripheral areas, neither sporulating mother cells nor spores or ghosts were observed. Overall, cells in the rim regions showed uniform cell length and thickness. As shown via SEM-imaging, no differences between 1g and sim- $\mu$ g biofilms were observed in the rim regions.

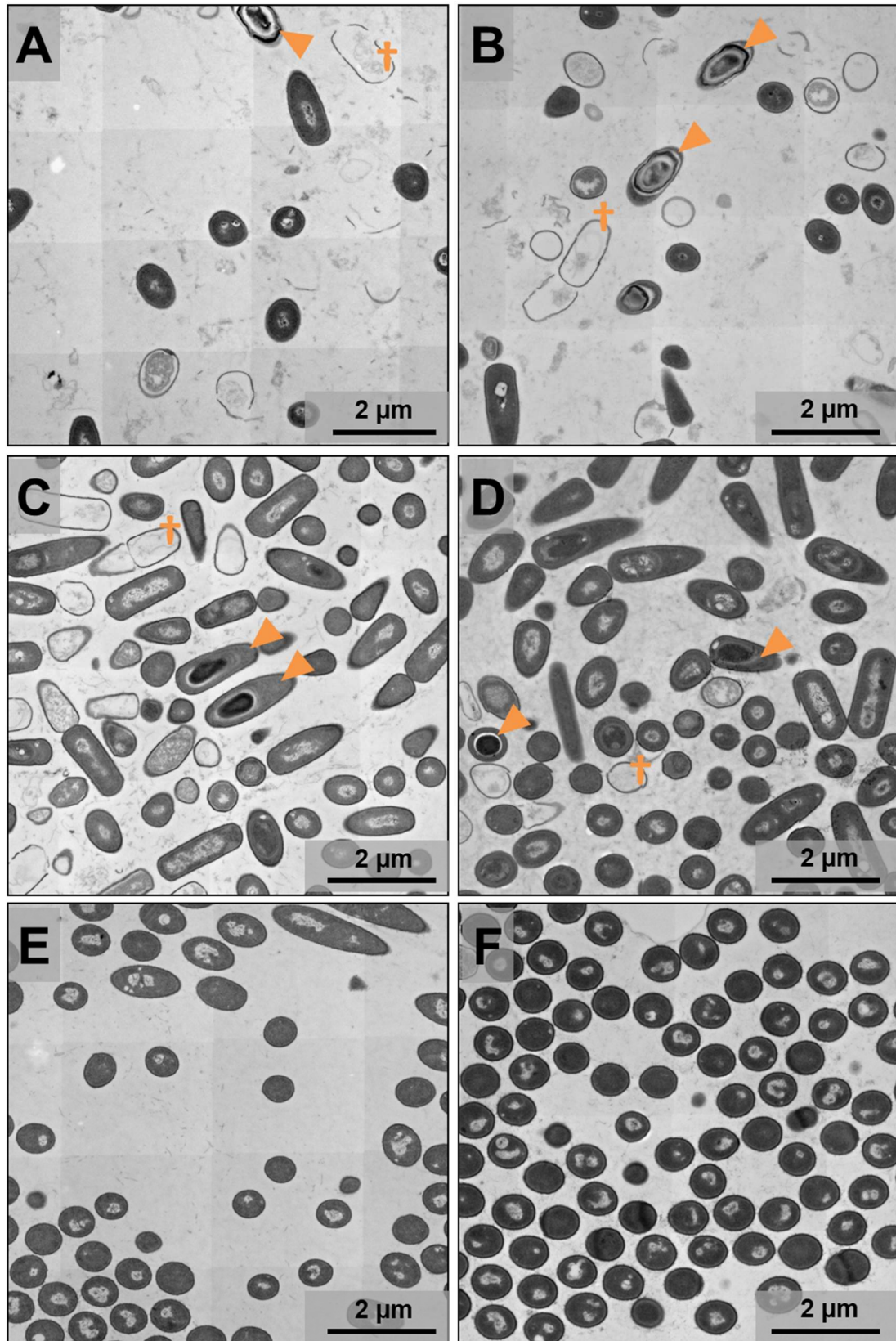


**Figure 40: TEM-images of different *B. subtilis* regions grown under 1g and sim- $\mu$ g**

Stitched TEM- images show representative examples of ultra-thin sections of 40 h old *B. subtilis* NCIB 3610 biofilms grown under regular gravity (left side, A, C, E) and simulated microgravity by using a fast rotating 2-D clinostat (right side, B, D, F). Images A and B represent fragments of the central biofilm region, C, D show examples of intermediate regions and E, F illustrate sections of the rim/edge of biofilm regions. For inoculation,

$1 \times 10^6$  spores were spotted on membrane filters (HTTP,  $\varnothing$  3.7cm), which were incubated on MSgg agar (supplemented with 10 mM L-alanine) at 37 °C. All images are arranged that apical regions are orientated upwards and basal structures are shown at the bottom. Due to the resolution, it is not possible to display the images along the entire biofilm height. The top row (A, B) shows biofilm sections from the central and therefore oldest biofilm region. A mixture of different cutting planes is visible, showing mother cells (arrow heads) harboring spores, EPS and matrix components (shadow or smear) and 'ghosts' (membrane artifacts which remain after vegetative cells died, indicated with a cross) as well as vegetative cells (all other dark oval and round objects). Living cells were less densely packed than in the intermediate (C, D) biofilm regions. In both regions cells seem to be randomly arranged in space, without distinct pattern. Almost no ghosts are visible in the intermediate regions and spore formation just started. EPS and matrix components are present, although less pronounced than in the central biofilm areas. The rim/edge regions of biofilms grown under 1g and sim- $\mu$ g (E, F) show neither mother cells, spores nor EPS and matrix components. Both images presented here illustrate sections along the transversal axis of vegetative cells. Due to the almost uniform cell distribution and alignment and comparison to SEM-images, the bundle structures of rim regions are represented. In the upper part of image F, the covering BslA protein layer is visible. Morphological or structural differences between both gravity conditions have not been observed. Scale bars represent 2  $\mu$ m.

### 3.7 Transcriptomics of young *B. subtilis* biofilms under 1g and sim- $\mu$ g

RNAseq or transcriptomic analysis offers the possibility to compare the transcriptome of two or more samples. Several previously performed biofilm experiments were incubated for 40 -72 h resulting in mature biofilms. In general, it can be assumed that mature biofilms share an equilibrium of spores, dying and growing cells, which might result in complex, misleading transcriptomic data. For comparing the influence of sim- $\mu$ g with 1g conditions during biofilm formation, time points of 4, 8 and 16 h were chosen. Young biofilms do not form spores and quorum sensing is about to take place after germination of the initial spore inoculum. Early time points provided an uninterrupted analysis on the pristine transcriptome of emerging biofilms, which were able to develop under the influence of 1g and sim- $\mu$ g.

As control and therewith time point zero ( $t_0$ ), RNA of  $1 \times 10^9$  dormant spores formed under 1g conditions were isolated and sequenced. For the investigation of both gravitational conditions, biofilms were grown using the standardized growth protocol (membrane filter method) with a starting inoculum of  $1 \times 10^7$  spores each. After incubation of 4, 8 and 16 h, biofilms were harvested ( $n=3$ , for each time point and gravitational condition) and immediately frozen in liquid nitrogen. The RNA was subsequently isolated from the samples and the RNA concentration was determined. Due to very low RNA concentrations, samples had to be pooled in order to obtain a sufficient quantity for RNAseq. Therefore, the number of samples had to be reduced from  $n=3$  to  $n=1$  per time point and condition, which did not allow a statistical comparison between sample sets.

After RNAseq, .fasta files were analyzed by using MultiQC (Ewels *et al.*, 2016), the tool set of University of Groningen (GSEA-Pro v3) and FastQC (version 0.11.7., Babraham Bioinformatics, Cambridge, UK, codes are partwise used by MultiQC). Sequence reports of all pooled samples exhibited proper "mean quality scores" (mean quality value across each base position in the read, Figure 41, A) and "per sequence quality scores" (number of reads with average quality scores, Figure 41, B) according to MultiQC. All 135,188,452 single-end reads (Figure 41, C) showed a length of exactly 76 bp.

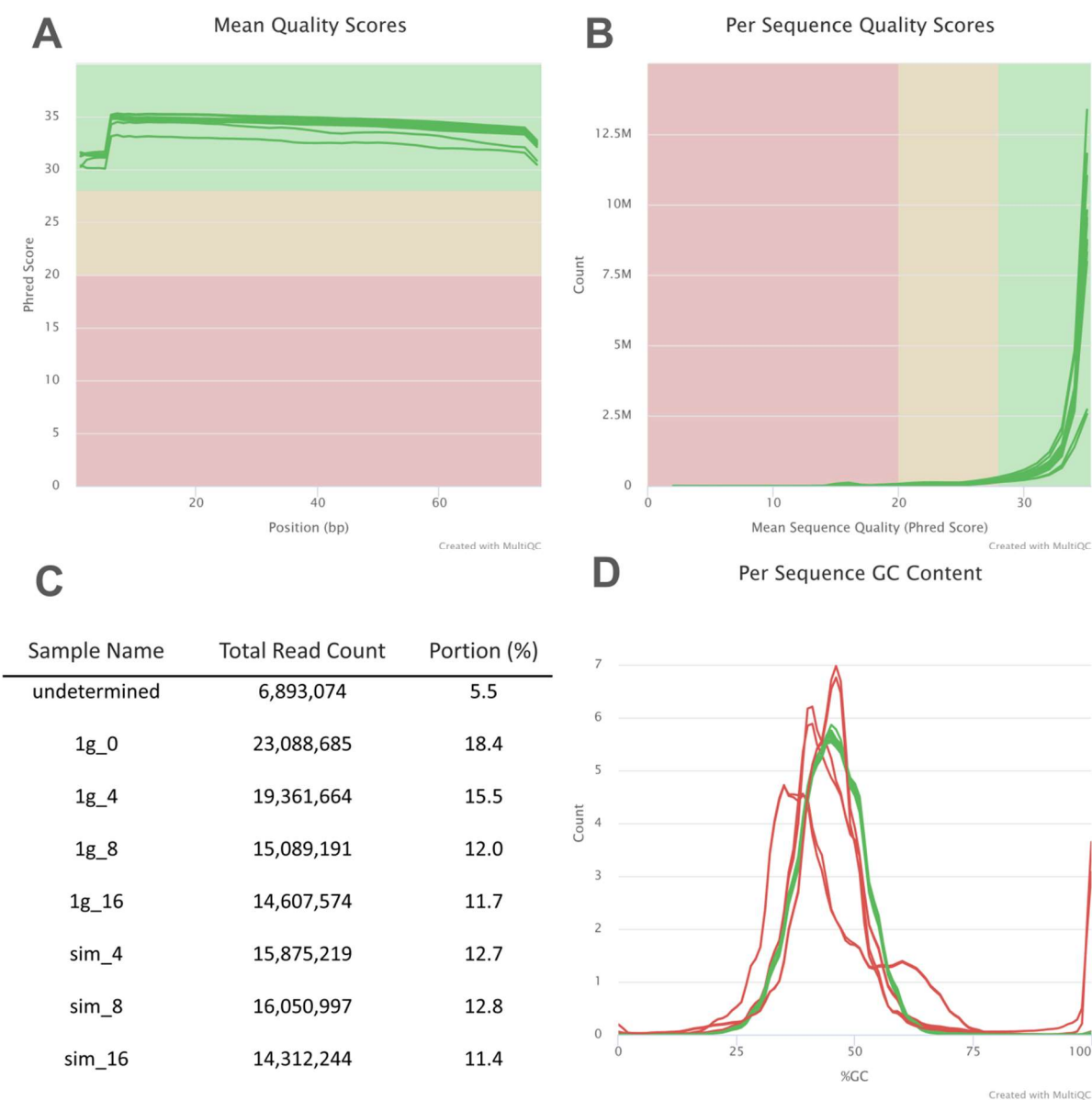


**Figure 41: RNAseq of emerging biofilms: MultiQC-reports**

RNAseq samples comprised a  $t_0$ -control (dormant *B. subtilis* spores) and young emerging biofilms grown for 4, 8 and 16 h under 1g and sim- $\mu$ g. Graph **A** represents the Phred-score (quality score of generated nucleobases during RNAseq) on the ordinate compared to each base position in the whole read for all biofilm samples shown on the abscissa. In graph **B**, the quality score per sequence (Phred-score) is shown on the abscissa for all analyzed sequences of the respective sample (ordinate). The color codes in graph **A** and **B** represent the overall Phred-score-based sequence quality: red, poor; orange, acceptable; green, good sequence quality. The chart given in **C**, summarizes the read count and the proportion of all analyzed samples including undetermined sequences. Graph **D**, represents the GC deviations (count in [%], ordinate) of individual sequences from the mean GC content. Colors of curves represent the likeliness of an assumed Gaussian normal distribution, which typically varies depending on the sample variability.

Figure 41 D represents the GC variations of individual sequences. The outmost left curve corresponds to the  $t_0$ -sample, which strongly differed from the expected Gaussian normal distribution. The main peak of the sample was below 37 % in GC content and a second peak was observed at 60 % GC-content, which suggests contamination of the  $t_0$  sample. During annotation of all samples, the control sample at  $t_0$  showed an unexpected high amount of undetermined sequences, which did not correspond to the

*B. subtilis* NCIB 3610 genome. On closer examination, the sample was found to have been contaminated by RNA from *Pseudomonas putida*, a Gram-negative rod shaped bacterium, which is ubiquitous in the environment. Interestingly, none of the other biofilm samples analyzed showed any indication for a possible contamination, although all samples were created from the same spore stock.

MultiQC-reports can be accessed via the link below:

Weblink: [http://core-fastqc.bio.nyu.edu/H5K5JAFX/merged/multiqc\\_report.html#general\\_stats](http://core-fastqc.bio.nyu.edu/H5K5JAFX/merged/multiqc_report.html#general_stats)

FastQ-Reports (FastQC) can be accessed via the link below:

Weblink: <http://ngs.molgenrug.nl/felix/>

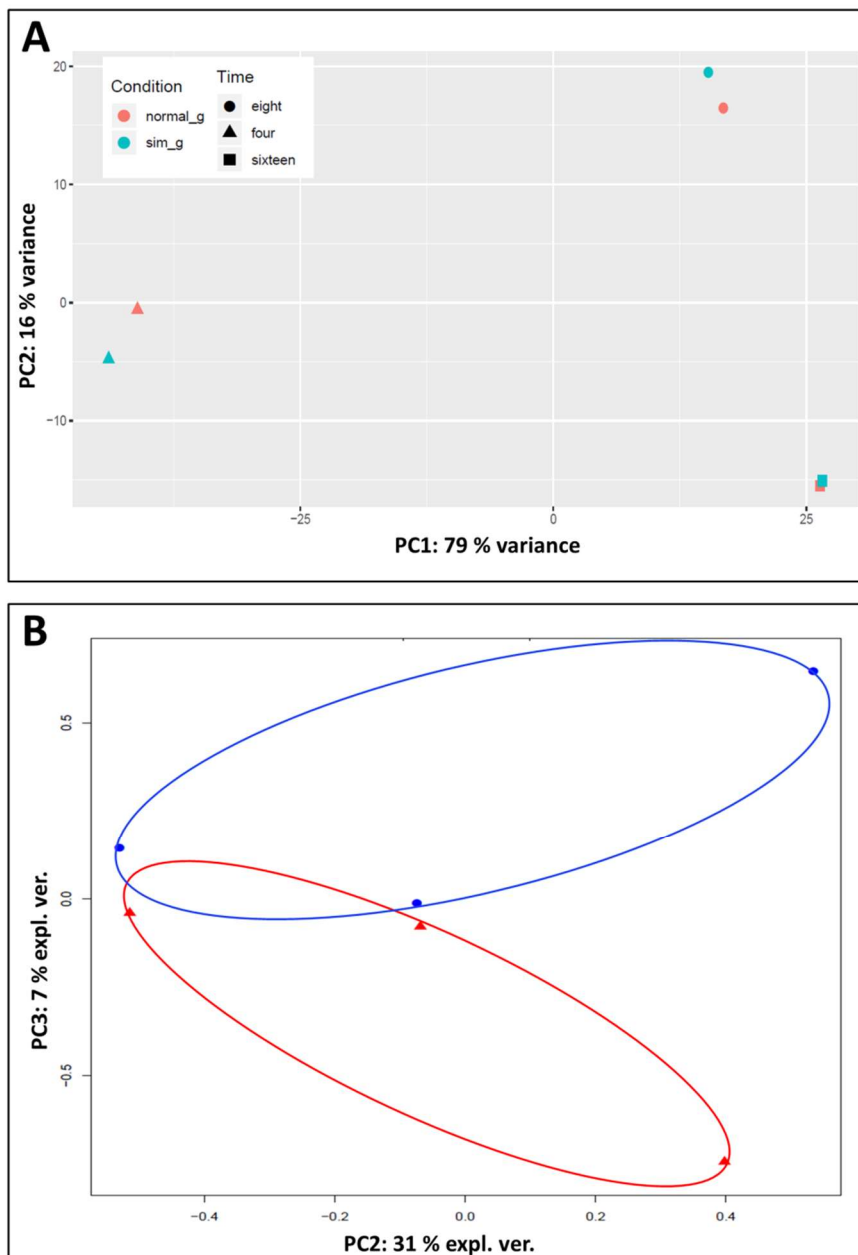


**Figure 42: Principal component analyses (PCA) of transcriptomic data**

*B. subtilis* NCIB 3610 samples were grown under standardized conditions for 4 h (triangle), 8 h (circle) and 16 h (square) under regular gravity (graph A, orange; graph B blue circles) and simulated microgravity (graph A,



turquoise; graph B red triangles). After incubation, samples were prepared for RNAseq of the whole transcriptome, whereas a single data point represents three pooled biological samples. As shown in graph A, PC1 represents the variance in the growth phase and PC2 shows the variance depending on the incubation time. PCA plot B, demonstrates the influence in variance of the gravitational condition (PC3) and variance of incubation time (PC2).

Sequence data was analyzed by using the tool sets Genome2D, GSEA-Pro (v3) and T-Rex provided by Dr. Anne de Jong (de Jong *et al.*, 2015). Annotation was performed with *B. subtilis* NCIB 3610 chromosome/complete genome data (GenBank: CP020102.1) and sequence data from the plasmid pBS32 (GenBank: CP020103.1). A principal component analysis (PCA) was performed showing that the main source of transcriptome variation is related to the growth phase (79 %, PC1, Figure 42, A). In addition, 16 % of the total variation (PC2) was related to the time points at which samples were collected. Samples grown under both gravitational conditions grouped together, showed significant differences between 4 and 16 h growth compared to 8 h growth. This could be due to the fact that the transcriptome of 4 h samples still included post-germination transcripts, in contrast to the emerging biofilm samples (8 and 16 h) which already entered the exponential growth phase. Interestingly, 4 h samples exhibited similar transcripts (closer positioning along the PC2-axis) as shown for the 16 h samples.

A second PCA focused on the difference between 1g and sim- $\mu$ g in transcriptomic variance was performed (Figure 42, B). The influence of gravity during incubation resulted in a total variance of 7 % (PC3). Furthermore, both gravitational conditions were clustered together (colored ovals) when compared to the incubation time (PC2). This result suggests that sim- $\mu$ g has a small effect on gene expression during late germination phase (4 h) and early biofilm stages (8, 16 h).

In summary, transcriptomic data of young emerging biofilms presented here should be considered with caution due to the low amount of samples, which barely allow any statistical conclusions to be drawn. In order to generate reliable data, this experiment should be repeated with a higher spore inoculum, more samples and further time points. Interestingly, the  $t_0$  sample showed a minor contamination with *P. putida*. Therefore, the sample cannot be used for any comparison between individual time points (or gravitational conditions) and endospore dormancy. Nevertheless, data gives a first hint, that the gravitational conditions might have a minor impact on the transcriptome of young emerging biofilms.

### Proteomics

In order to compare the proteome of biofilms grown under different gravitational conditions, *B. subtilis* NCIB 3610 ( $\Delta lysA$ ) was grown under 1g conditions on heavy L-lysine supplementation and on light L-lysine supplementation for sim- $\mu$ g samples. Isolated proteins were digested and peptides were analyzed by mass-spectroscopy. Results were aligned regarding their mass and cleavage time to several databases. For quality assurance a q-value was calculated to estimate the overall error probability per protein. In addition, the coverage of all analyzed peptides per protein was calculated as well as the sequence coverage, which represented the peptide coverage for each protein. Furthermore, unique peptides per protein were determined. Protein abundance ratios (fold changes, sim- $\mu$ g/1g) of biofilms grown under 1g and sim- $\mu$ g offered a semi-quantitative approach to compare the proteome under both conditions.

**Table 9: Overview of SILAC proteomics results**

Biofilm samples were aligned with two datasets, comparing the peptides to 3962 (24 h) and 4168 (72 h) known *B. subtilis* proteins. By database matching, 1102 (24 h) and 1544 (72 h) proteins could be detected, whereas the majority were not or not clearly covered by peptides. By comparing heavy L-lysine comprising peptides (1g) and light L-lysine containing peptides (sim- $\mu$ g), a fold change above 1.3 was set as cutoff and fold changes >2 were considered as relevant. After 24 h, sim- $\mu$ g biofilms showed a significant fold change in 129 proteins (11.71 % of the total expressed proteins) as well as in 93 proteins (6.02 % of the total expressed proteins) in 72 h old biofilms. In contrast sim- $\mu$ g biofilms exhibited 116 (10.53 %) significantly downregulated proteins after 24 h and 61 (3.95 %) after 72 h. The lower part of the table shows proteins and their gene symbols with a fold change >2 which were found either commonly up- or downregulated in 24 h old biofilms as well as in 72 h old biofilms. Genes are sorted in alphabetical order.

	24 h		72 h	
	total	[%]	total	[%]
<b>Peptide analysis</b>				
Compared to proteins in database	3962	-	4168	-
Undetected and incomplete protein pairs	2860	72.19	2624	62.96
Protein pairs for quantification	1102	27.81	1544	38.97
<b>Fold change</b>	total	[%]	total	[%]
<b>Upregulated</b>				
Proteins with a fold-change <1.3	773	70.15	1247	80.76
Proteins with a fold-change of 1.3-2	200	18.15	204	13.21
Proteins with a fold-change of >2	129	<b>11.71</b>	93	<b>6.02</b>
<b>Downregulated</b>				
Proteins with a fold-change <1.3	814	73.87	1283	83.1
Proteins with a fold-change of 1.3-2	172	15.61	200	12.95
Proteins with a fold-change of >2	116	<b>10.53</b>	61	<b>3.95</b>
<b>Common proteins FC&gt;2 after 24 &amp; 72 h</b>				
<b>Gene symbol</b>	<b>Description</b>			
<b>Upregulated</b>				
<i>nasE</i>	Assimilatory nitrite reductase			
<i>ntdB</i>	Kanosamine-6-phosphate phosphatase			
<i>yjcS</i>	Uncharacterized protein			
<i>ypjC</i>	Uncharacterized protein			
<i>yqiG</i>	Probable NADH-dependent flavin oxidoreductase			
<i>ytrF</i>	ABC transporter permease			
<i>yusV</i>	Probable siderophore transport system ATP-binding protein			
<b>Downregulated</b>				
<i>purR</i>	transcription repressor of the <i>pur</i> operon			
<i>rpmD</i>	Ribosomal protein L30			
<i>ywmD</i>	Uncharacterized protein			

In total, peptides of biofilm samples were compared with more than 3900 known *B. subtilis* proteins, resulting in more than 1102 found proteins of 24 h-old biofilms and 1544 proteins of 72 h-old biofilms grown under sim- $\mu$ g and 1g. Due to low or no comparative values between heavy and light L-lysine samples, fold changes of 2860 possible and presumed proteins after 24 h (72.19 %) and 2624 (62.96 %) proteins after 72 h could not be calculated. The fold change cutoff was set to 1.3 and fold changes above 2.0 were considered as significantly altered. After 24 h incubation, sim- $\mu$ g biofilms showed 11.71 % (129 proteins of 773) significantly upregulated proteins and 10.53 % significantly

downregulated proteins (116 of 814 proteins, Table 9). Incubation times of 72 h resulted in 6.02 % (93 proteins of 1247) upregulated and 3.95 % (61 of 1283) downregulated proteins. Young sim- $\mu$ g biofilms showed a greater relative difference in their proteome when exposed to sim- $\mu$ g conditions than mature biofilms, which differed only half as much. Interestingly no biofilm related genes were significantly upregulated under sim- $\mu$ g.

Comparing both time points, 24 h and 72 h biofilm incubation, only seven common upregulated proteins were found under sim- $\mu$ g (Table 9) as well as three common downregulated proteins. These proteins represent 5.43 % of all upregulated proteins after 24 h and 7.53 % after 72 h. Among these common proteins are two transport associated proteins, YtrF a substrate-binding lipoprotein and YusV, a probable siderophore transporter. Furthermore, a probable flavin oxidoreductase (YqiG), a subunit of an assimilatory nitrite reductase (NasE) and two proteins with an unknown function were found significantly increased in sim- $\mu$ g biofilms. Another protein found in at both time points was NtdB, which part of a three-protein cluster synthesizing the antibiotic kanosamine-6-phosphate. Kanosamine is constituent of kanamycin, inhibiting cell wall synthesis of certain fungi and bacteria (Milner *et al.*, 1996, Vetter *et al.*, 2013).

Regarding commonly downregulated proteins, only three proteins were identified resulting in 2.59 % of all significantly downregulated proteins after 24 h respectively in 4.92 % for the 72 h time point. The protein PurR functions as a repressor of the *pur*-operon and therewith regulates the purine biosynthesis. In addition, the essential ribosomal protein RpmD (L30) was found to be significantly downregulated at both observed time points. The last of the three commonly found downregulated proteins is YwmD, a non-essential protein with unknown function.

By annotating significantly changed proteins developed under sim- $\mu$ g to functional groups (Figure 43), the majority of upregulated and downregulated proteins was related to metabolically processes (upregulated: 57 % after 24 h and 52 % after 72 h, downregulated: 62 % after 24 h and 56 % after 72 h) as well as to cell differentiation and communication (upregulated: 9 % after and 7 %, downregulated: 7 % and 5 %), cell organization and homeostasis (upregulated: 5 % and 4 %, downregulated: 6 % and 10 %), transport related proteins (upregulated: 5 % and 1 %, downregulated: 4 % and 5%) and other proteins (upregulated: 5 % and 2 %, downregulated: 4 % and 8 %). In addition, 19 % (24 h) and 34 % (72 h) of the upregulated proteins as well as 17 % (24 h) and 16 % (72 h) of the downregulated proteins were unspecific or unknown in their function.

Among the upregulated proteins in sim- $\mu$ g, 12 found proteins involved in metabolic pathways associated with antibiotic biosynthesis were found after 24 h and 9 after 72 h. In contrast, 9 proteins associated with antibiotic biosynthesis were found to be downregulated after 24 h, but no downregulation of any protein could be detected after 72 h. Furthermore, no biofilm related proteins have been found significantly up- or downregulated. Only two proteins associated with cell motility (CheA; a chemotaxis protein and FliY; a flagellar motor switch phosphatase) movement were found significantly downregulated.

*B. subtilis* biofilms did not show any particularities with regard to their altered proteome under sim- $\mu$ g regarding the functional annotation of the significantly differently regulated proteins. However, after longer incubation times, the trend became apparent that overall fewer proteins (absolute and relative) were regulated differently (24/72 h; upregulated: 11.7%/6 %; downregulated: 10.5%/4 %). After 24 h 22.2 % of all found proteins were significantly changed in contrast to 10.0 % after 72 h. These results indicate, that during the simulation of microgravity and with increasing maturity of the biofilm, the proteome is under constant transformation and differs most in the initial incubation phase and converge to towards the proteome of the 1g samples with increasing incubation time.

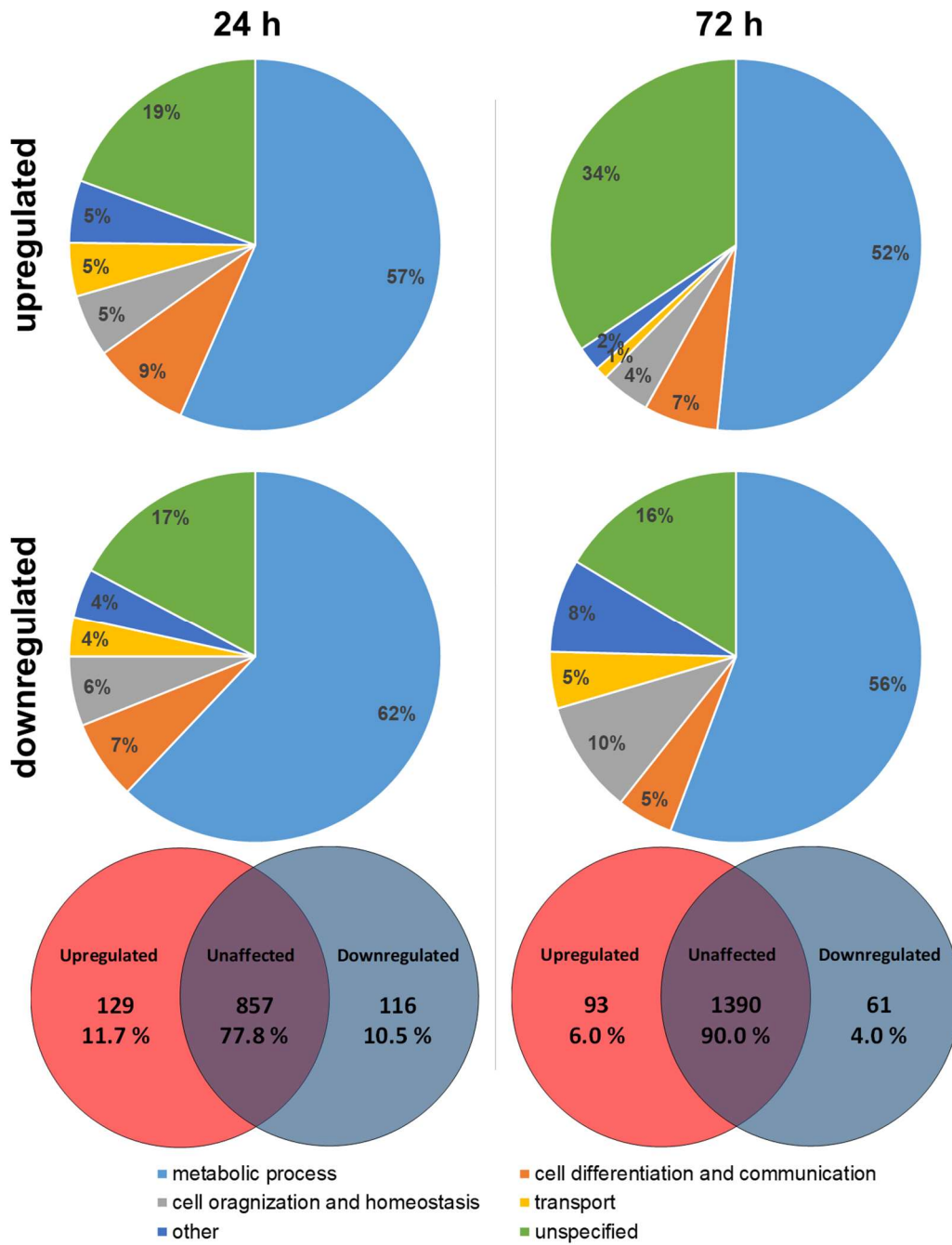


**Figure 43: Functional annotation of significantly different regulated proteins under sim-µg**

The proteome of 1g and sim-µg *B. subtilis* biofilms was investigated by SILAC. In order to compare found proteins, fold changes of all comparable proteins were calculated, where fold changes >2 were considered as significantly altered. Pie charts represent functional annotations of significantly up- and downregulated proteins under sim-µg regarding their biological processes after 24 h biofilm incubation and after 72 h. Bottom figure schematically represents absolute numbers of unaffected and significantly up- and downregulated proteins as well as their relative proportion of the total of identifiable proteins.

### 3.8 Germination of *B. subtilis* spores grown under 1g and sim-µg

Apart from morphologic and structural analysis via microscopy, the germination behavior of *B. subtilis* spores grown under 1g and sim-µg was investigated. Two different spore isolation methods or growing conditions were used to isolate *B. subtilis* spores: On the one hand, spores were extracted from biofilms grown on MSgg-medium under standardized conditions for 3 d at 37 °C, which required several

subsequent washing steps. On the other hand, spores were grown on/in sporulation medium (SSM) at 30 °C for 2-3 d in liquid culture or for 5 d on solidified SSM. Whichever method was chosen, isolated spores were washed extensively with sterile ddH<sub>2</sub>O until they were free of vegetative cells, germinated spores and cell debris. Using phase-contrast microscopy, spore solutions were examined and washed until the desired quality of more than 99 % dormant spores was achieved.

As mentioned before, dormant spores of the *B. subtilis* wild-type (NCIB 3610) appear white using phase-contrast microscopy. By observing germination using live cell microscopy, the change in the refractive index of the germinating spores from white to grey to phase dark can be monitored. This process is based on the reduction of the optical density, which is caused by the release of Ca<sup>2+</sup>-DPA from the spore during germination and begins immediately after the contact between spores and germinant (i.e. L-alanine). The effect of the refractivity index-dependent phase-shift occurred within the first minutes of germination and was measured by using photometrical methods such as optical well-plate readers. To analyze the germination of *B. subtilis* spores, a photometric kinetic at 600 nm over a time course of 20 minutes up to two hours was surveyed. As known from literature, germination effects strongly depend on the used strain, incubation medium, temperature and the synchronization status of spores. Synchronization was achieved by heating up analyzed spores for 30 min at ~70 °C. Almost all germination experiments were performed with synchronized spores to increase germination efficiency and reduce heterogeneity. Spores grown under 1g and sim- $\mu$ g conditions were treated likewise after harvesting. This is only possible because spores by definition are classified as dormant and not metabolically active, which in turn means that spores formed under sim- $\mu$ g do not change physiologically when processed and stored under 1g conditions. The germination under sim- $\mu$ g was not analyzed due to the technical limitations, which would require clinostat-photometry measurements.

Following graphs demonstrate the germination efficiency (maximum germination equals to ~60 % loss in refractivity/ OD<sub>600 nm</sub>) on the ordinate, measured by the maximum germination after 10 mM L-alanine at 37 °C, including spore synchronization. The germination kinetics are given on the abscissa, representing the time course between the addition of the spores into the preheated medium (37 °C; experiment initiation) and the end of the experiment. All following graphs and figures illustrate experiments performed with 1g spores with black symbols, whereas germination experiments performed with sim- $\mu$ g spores are indicated in red symbols.

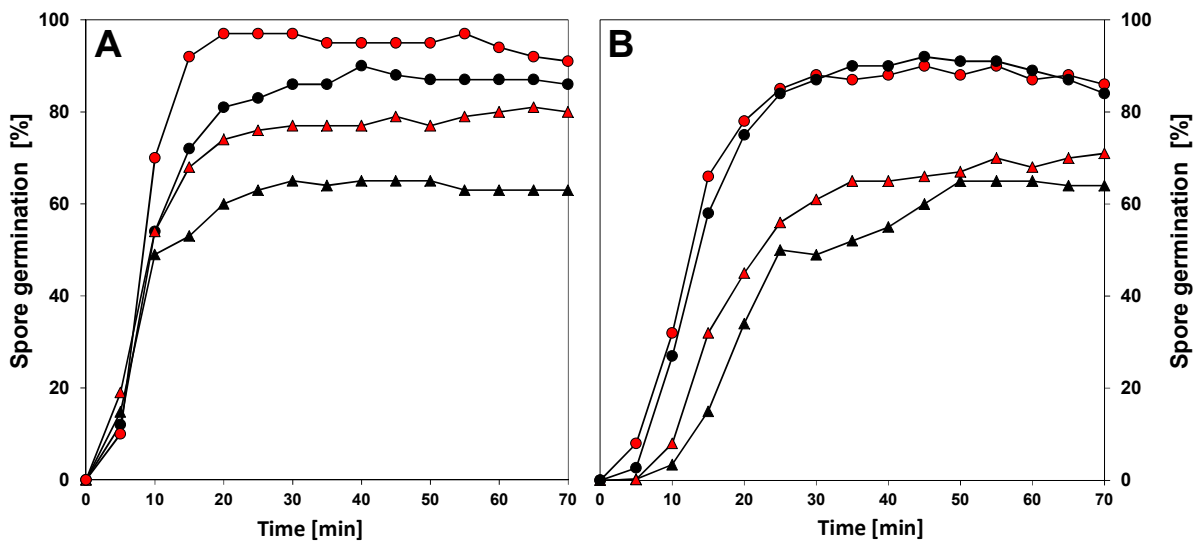
### Triggered germination of spores grown under 1g and sim- $\mu$ g

Figure 44 demonstrates the germination behavior of *B. subtilis* wild-type spores grown under 1g and sim- $\mu$ g in presence of 10 mM L-valine (A) and a germinant mix of L-asparagine, D-glucose, D-fructose and KCl (AGFK). Non-synchronized spores (triangles) showed similar germination properties within the first 10 min after the experiment started. However, the overall germination efficiency differed remarkably after 15 minutes of incubation and resulted in ~20 % increased germination in spores grown under sim- $\mu$ g compared to spores formed under regular gravity. Synchronized spores exhibited a similar pattern within the first 5 minutes of germination. Synchronized sim- $\mu$ g spores germinated faster (10 min: 68.3 %) than the 1g control (10 min: 54.6 %) and more efficient (70 min: +7.5 %) over time. The difference between germination efficiency in synchronized and non-synchronized spores resulted in ~27.2 % for 1g-spores and ~17.1 % for sim- $\mu$ g spores.

Germination effects of AGFK, are shown in B: As observed for L-valine, non-synchronized spores exhibited lower germination profiles of 63.5 % under 1g and 70.7 % under sim- $\mu$ g. Germination profiles of synchronized spores exhibited almost identical germination kinetics (1g: 84.6 %; sim- $\mu$ g: 87.7 %). However, 1g spores seemed to be slightly delayed in their germination speed compared to sim- $\mu$ g

spores, but not as pronounced as under the influence of L-valine. The total germination efficiency barely varied under the influence of AGFK, neither with synchronized ( $\pm 3.1\%$ ) or non-synchronized spores ( $\pm 7.2\%$ ). In comparison to L-valine as germinant, germination kinetics were delayed under the influence of AGFK, which showed a shift of  $\sim 5$  min in the end of the exponential germination phase.

By using AGFK, germination of 1g and sim- $\mu$ g spores seemed to be slightly delayed in comparison to L-valine germination. Interestingly 1g spores germinated more efficient in AGFK compared to L-valine. Sim- $\mu$ g spores generally showed faster germination kinetics in contrast to 1g spores, but germinated less efficient in AGFK. As shown in literature, synchronization of spores grown under both gravitational conditions had a significant impact on germination kinetics and efficiency.



**Figure 44: Triggered germination of 1g and sim- $\mu$ g *B. subtilis* spores**

Graphs **A** and **B** demonstrate the germination behavior of *B. subtilis* NCIB 3610 spores grown under regular gravity conditions (1g, black symbols) and simulated microgravity (sim- $\mu$ g, red symbols) by using a fast rotating 2-D clinostat. For each individual experiment  $1 \times 10^8$  synchronized (circles; **A**, **B**: 30 min at 70 °C) or non-synchronized (triangles, spores after storage at 4 °C) spores were used. Single measurements ( $n \geq 5$ ) at OD<sub>600</sub> (at 37 °C) were taken at 5 min intervals up to 70 min and data is represented as  $N/N_0$  assuming a maximum germination at 60 % refractivity loss. Graph **A** represents the germination behavior of spores under the influence of 10 mM L-valine in 25 mM Tris-HCl buffer. Spores grown under sim- $\mu$ g show higher and faster germination ratios in both, synchronized and unsynchronized setups compared to spores grown under 1g. The final germination efficiency after 70 min was slightly increased for sim- $\mu$ g spores. Graph **B**, shows germination ratios of spores under the influence of 10 mM AGFK (L-asparagine, D-glucose, D-fructose and  $K^+$  / KCl in 25 mM Tris-HCl buffer). Germination profiles of spores grown under 1g and sim- $\mu$ g seemed to be identical, whereas unsynchronized sim- $\mu$ g spores seemed to germinate faster and more efficient after 70 min. Both experiments were performed in the laboratory of Prof. P. Setlow, UConn Health, Farmington, USA.

### Germination profiles von individual *B. subtilis* spores grown under 1g and sim- $\mu$ g

As already shown in Figure 44, the germination profiles of 1g and sim- $\mu$ g spores differed in their kinetics as well as in their germination efficiency. It was also shown, that germination is strongly influenced by heat synchronization. Based on these results, the germination kinetics on the basis of individual synchronized spores instead of pooled spores were examined (

Figure 45). Single spores were observed during germination via differential interface contrast microscopy and spectral patterns were recorded during a time course of 30 min. Y-axes represent the relative germination status: bright, dormant spores (1.0, dormancy), grey spores during germination start ( $\sim 0.9-0.3$ ,  $Ca^{2+}$ -DPA release) and black spores during finalized germination ( $\sim 0.3-0.0$ ). In graph A,

germination profiles of individual spores grown under 1g conditions germinating in 10 mM L-valine are shown. Given examples germinated over a time course of ~3-15 min, which correlated with germination data of pooled spore samples shown in Figure 44. Individual spores which were formed under the influence of sim- $\mu$ g germinated within ~2-7.5 min (B), which was an increase of approximately ~50 % for the fastest and an increase of 100 % for the slowest germinating spores. However, the time span between first and last observed germinated spore showed a high degree of heterogeneity in 1g samples (~12 min) compared to a relatively homogenous germination distribution in sim- $\mu$ g spores (~5.5 min).

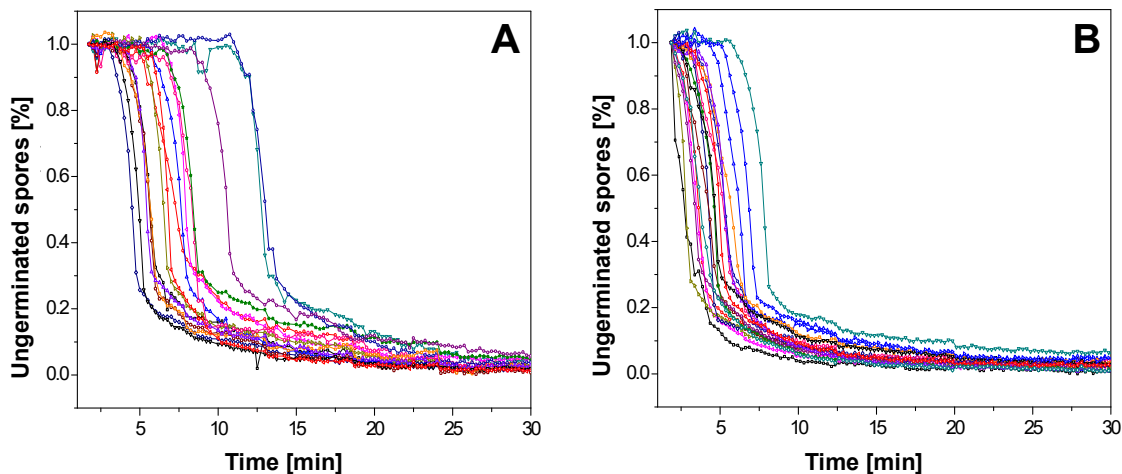


**Figure 45: Germination profiles of individual 1g and sim- $\mu$ g spores of *B. subtilis***

Graphs demonstrate the germination behavior of *B. subtilis* NCIB 3610 spores grown under regular gravity conditions (A, 1g) and simulated microgravity (B, sim- $\mu$ g) by using a fast rotating 2-D clinostat. Different colors represent the germination behavior of single individual spores. Culturing of spores was conducted on SSM-agar for 5 days at 30 °C followed by harvesting, washing in ddH<sub>2</sub>O and storage at 4 °C. Prior to germination, spores were synchronized at 70 °C for 30 min and stored on ice prior incubation. Germination took place in pre-warmed 10 mM L-valine in 25 mM HEPES (pH 7.4) for 30 min at 37 °C. Measurements of single cells were achieved by analyzing spectral patterns during germination by differential interference contrast microscopy (DIC). Kinetics are presented as  $N/N_0$  (grey values), assuming a maximum germination after one hour. 1g spores (A) exhibited a heterogeneous distribution ranging from 3-15 min, whereas sim- $\mu$ g spores (B) germinated more homogeneously and faster (2-7.5 min). Experiments were performed in the lab of Prof. Y.-Q. Li, BSOM, Greenville, USA. Due to the individual spore germination curves, no error bars are given.

### Germination of 1g and sim- $\mu$ g spores in various temperatures and media

Germination experiments using 10 mM L-valine and AGFK as germinants showed differences in germination efficiency and homogeneity between *B. subtilis* spores grown under 1g and sim- $\mu$ g. For analyzing the influence of the incubation medium and the temperature during germination, spores grown under both gravitational conditions were examined with regard to their germination behavior. Tris-HCl-buffer including 10 mM L-alanine was used as positive control to demonstrate the most efficient germination possible. Two nutrient media, the full-medium LB both, and the biofilm promoting medium MSgg in addition with 10 mM L-alanine, were used to compare germination under typical laboratory conditions. Sterile water, in which spores were stored at 4 °C prior to the experiment, was used as negative control. Due to the technical limitations of used well-plate readers, a minimum temperature below 26 °C could not be maintained. Therefore, experiments were conducted at following temperatures: 30 °C (sporulation temperature); 37 °C (standard incubation temperature) and 45 °C (high temperature within the tolerated range of *B. subtilis*).

In Figure 46, the germination of *B. subtilis* wild-type spores (1g and sim- $\mu$ g) is shown in dependence on medium and temperature. Values given on the ordinate are given in rel. OD<sub>600 nm</sub>, wherein the initial value minus the optical density of the used medium has been defined as 100 % (initial rel. OD<sub>600 nm</sub>). Previous experiments in showed, that a decrease of  $\sim 60$  % rel. OD, compared to the initially measured OD, represented a total germination of  $\sim 1 \times 10^8$  *B. subtilis* spores in 300  $\mu$ l medium. This indicates that all spores germinated at values of  $\sim 40$  % ( $\pm 4$  %) rel. OD. Thus, the lowest point of each curve represents the maximum germination efficiency. All subsequent elevated values (mainly occurring after 60 min) demonstrated the beginning of vegetative growth.

Graphs A-C represent the germination properties of spores grown in 1g and sim- $\mu$ g in buffered 10 mM L-alanine. At 30 and 37 °C, spores grown under sim- $\mu$ g conditions germinated slightly faster, compared to 1g spores, but exhibited identical germination rates at 45 °C. The maximum of germinated spores, grown under both gravity conditions, demonstrated similar values at 30 and 37 °C. However, sim- $\mu$ g spores showed a decrease in the total amount of germinated spores of up to 15 % ( $\pm 2$  %) at 45 °C, whereas 1g spores remained unaffected. Based on graph B, all other graphs were calculated as described above, since in accordance with literature and previous experiments a reduction of OD<sub>600</sub> by  $\sim 60$  % was given (Fuchs *et al.*, 2017a, Nagler *et al.*, 2015).

1g-spores that germinated in LB-broth (graphs D-F), showed similar germination rates at 37 and 45 °C as observed with L-alanine and germinated faster at 30 °C, whereas sim- $\mu$ g spores were delayed compared to the positive control. Up to 17 % ( $\pm 3$  %) of sim- $\mu$ g spores did not germinate or germinated delayed in LB-broth (cannot be excluded by OD-measurements). The strongest growth among all experiments was observed for both gravity conditions at 30 °C (1g and sim- $\mu$ g) and 45 °C (1g). Graphs E and F show that 1g spores, although they shared almost identical germination rates with sim- $\mu$ g spores, matured faster into vegetative cells. Although LB-broth is a full medium and contained various germinants in alternating proportions, the same germination efficiency as under the influence of 10 mM L-alanine was not achieved. This was consistent with the results given in Figure 44, where the germinant mix AGFK also led to slightly lower germination efficiency.



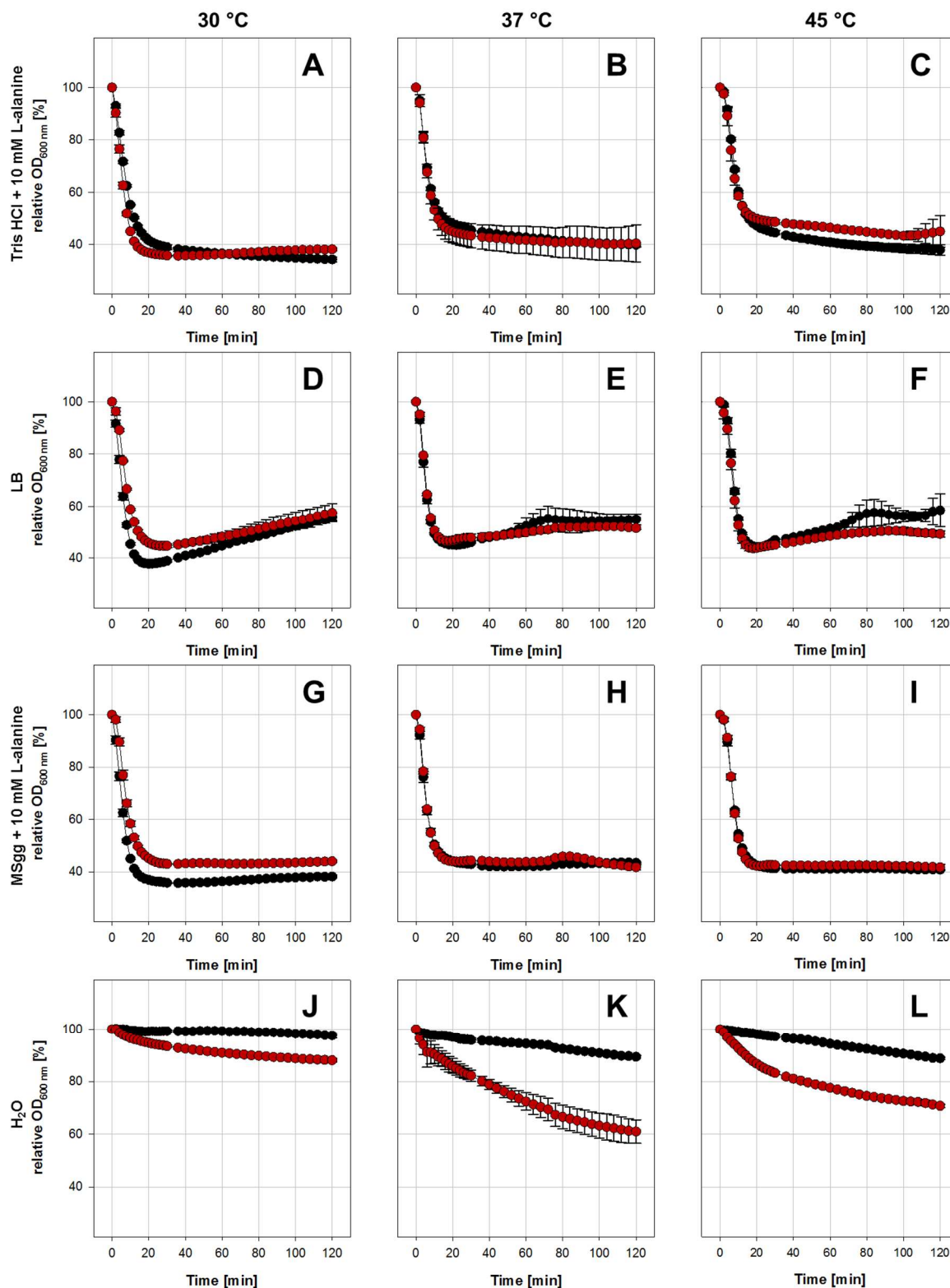


**Figure 46: Temperature, media, gravity and time dependent germination of *B. subtilis* spores**

Graph represents germination behavior of  $5 \times 10^7$  *B. subtilis* NCIB 3610 spores grown under regular gravity conditions (black circles, 1g) and simulated microgravity (red circles, sim- $\mu$ g) by using a fast rotating 2-D clinostat. Culturing of spores was conducted on SSM-agar for 5 days at 30 °C followed by harvesting, washing in ddH<sub>2</sub>O and storage at 4 °C. Prior to germination, spores were heat synchronized. Germination occurred in pre-warmed Tris HCl + 10 mM L-alanine (A, B, C), LB-broth (D, E, F), MSgg + 10 mM L-alanine (G, H, I) and ddH<sub>2</sub>O (J, K, L). Spectroscopic measurements of all samples groups were achieved by analyzing the OD<sub>600 nm</sub> during germination. Kinetics are presented as quotient of  $N/N_0$  where  $N_0$  represents the OD<sub>600 nm</sub> at  $T_{0 \text{ min}}$  and  $N$  the OD<sub>600 nm</sub> at the

respective time point. Germination experiments were conducted at 30 °C (left side), 37 °C (middle) and 45 °C (right side). Germination behavior mostly showed no significant changes between 1g and sim- $\mu$ g spores. At 30 °C, 1g samples germinated faster and more efficient than sim- $\mu$ g samples (A, D and G). No changes were observed at 37 °C (B, E and H). At 45 °C, germination of sim- $\mu$ g spores was less efficient in Tris-HCl (+L-alanine), but slightly more efficient in LB broth and identical in MSgg (+L-ala) compared to 1g spores. A rise in OD<sub>600</sub> indicates cell growth, therefore best growth was observed in LB broth samples compared to MSgg media (D, E and F). Germination in sterile water occurred at all three investigated temperatures. Strongest spontaneous germination of up to 57 % of spores grown under sim- $\mu$ g was observed at 37 °C (K) and 25 % at 30 °C (J) as well as 51 % at 45 °C (L). Spores, cultivated under 1g, germinated less than 6 % (J) at 30 °C and 17-19 % at 37 and 45 °C (K, L). N<sub>≥</sub>5, error bars represent the standard deviation.

MSgg was originally developed to promote *B. subtilis* biofilm formation under minimal nutrient supplementation and did not comprise a germinant. By addition of 10 mM L-alanine, inoculated spores were triggered to germinate in order to form standardized biofilms. To investigate the germination of spores in MSgg broth, graphs G-I represent germination profiles under the influence of different temperatures. At 30 °C, germination rates as well as the germination efficiency were identical as observed in LB-broth. Spores grown under 1g, were more efficient ( $\sim$ 18 $\pm$ 3 %) and slightly faster ( $\sim$ 3.5 $\pm$ 0.45 min) in germination, compared to sim- $\mu$ g spores. However, these effects could not be observed at 37 °C or 45 °C, since the germination curves of spores grown under 1g and sim- $\mu$ g were congruent. Therefore, no differences in germination rate, germination efficiency or growth were observed in MSgg-broth at 37 and 45 °C.

### Spontaneous germination in H<sub>2</sub>O

In comparison to the positive control as well as the two tested nutrient media, double-deionized water was used as negative control (graphs J-L). Prior to the germination experiments, spores were washed in  $\sim$  22 °C water and were stored in water over longer periods at 4 °C. Microscopic routine examinations of spores were carried out ahead of each experiment in order to verify spore quality and to detect any germinated spores. Only samples containing more than 99 % dormant spores were used for biofilm or germination experiments. Spores treated with 30 °C warm water were not expected to germinate, but sim- $\mu$ g spores germinated up to 25 % ( $\pm$  3 %) in contrast to 1g spores, which germinated up to 6 $\pm$ 1 %. Interestingly, sim- $\mu$ g spores showed a germination efficiency of 57  $\pm$  8 % at 37 °C (1g spores: 17  $\pm$  2 %) and 51  $\pm$  3 % at 45 °C (1g spores: 19  $\pm$  2 %). The germination rates in 37 and 45 °C warm water were very low compared to the positive control and nutrient media and complete germination did not seem to be complete after two hours of incubation.

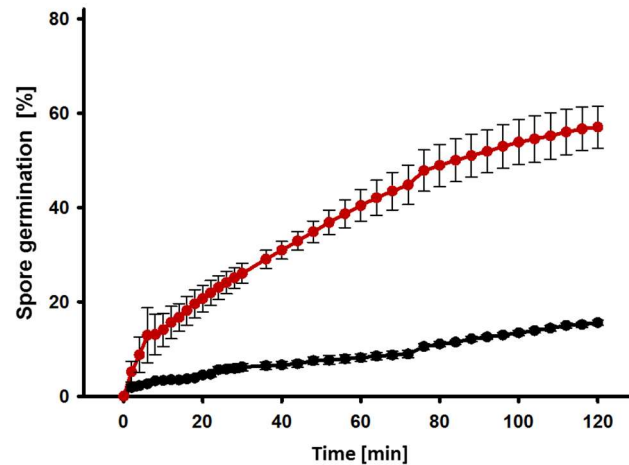


**Figure 47: Spontaneous germination of 1g and sim-µg *B. subtilis* spores**

Graph represents the germination behavior of  $5 \times 10^7$  *B. subtilis* NCIB 3610 spores grown under regular gravity conditions (black circles, 1g) and simulated microgravity (red circles, sim-µg) by using a fast rotating 2-D clinostat. Prior to germination, spores were not synchronized. Germination occurred in pre-warmed ddH<sub>2</sub>O at 37°C. Spectroscopic measurements of both samples groups were achieved by analyzing the OD<sub>600 nm</sub> during germination. Kinetics are presented as  $N/N_0$  assuming a refractivity loss of 60 % during germination by using 10 mM L-alanine in 25 mM Tris-HCl buffer (not shown). Spores grown under sim-µg germinated in warm water up to 60 % of their maximum germination capacity during the incubation time of 2 h. 1g controls germinated up to 17 % of their total germination potential after 2 h.  $N \geq 5$ , error bars represent the standard deviation.

Due to the extraordinarily germination of sim-µg and 1g spores in warm water, this effect can be described as enhanced spontaneous germination. For a better visualization of this effect, Graph K (H<sub>2</sub>O at 37 °C) was plotted as germination over time (Figure 47). As shown before, both spore batches, which were cultivated under 1g and sim-µg, partially germinated in warm water. The germination rate of the first  $10 \pm 2$  % sim-µg spores showed a similar exponential behavior compared to germination in nutrient media. However, germination slowed down after 5 min, but continuously progressed up to ~57 %. On the contrary, 1g spores exhibited a very low germination rate, but an almost linear germination process, which was not completed after two hours of incubation at 37°C.

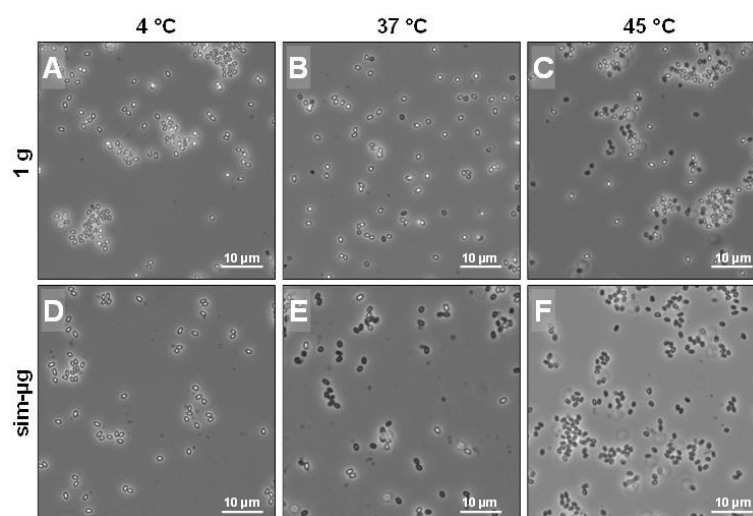


**Figure 48: Spontaneous germination of 1g and sim-µg *B. subtilis* spores**

Phase contrast images represent the germination behavior of  $5 \times 10^7$  *B. subtilis* NCIB 3610 spores grown under regular gravity conditions (1g, top row) and simulated microgravity (sim-µg, bottom row) by using a fast rotating 2-D clinostat. Culturing of spores was conducted on SSM-agar for 5 days at 30 °C followed by harvesting, washing

in ddH<sub>2</sub>O and storage at 4 °C. Prior to germination, spores were not synchronized. Germination occurred in pre-cooled (4 °C left column) or pre-warmed (37 °C: middle column and 45 °C: right column) ddH<sub>2</sub>O. Images were captured after 30 min exposure. At 4 °C, no germination of 1g and sim- $\mu$ g spores was observed. Spores remained phase bright. With increasing exposure times, single spores (<5 %) started to germinate (not pictured). At 37 °C, single germinated 1g spores were observable, which occurred with increased frequency at 45 °C. In comparison, sim- $\mu$ g spores showed high levels of germinated spores at 37 °C and almost no dormant spores at 45 °C. Scale bars represent 10  $\mu$ m.

Germinated vegetative *B. subtilis* cells were not able to survive longer periods (>2-4 h) in pure water (not shown). Therefore, spontaneous germination in water was fatal for the spore. Once germinated, there is no mechanism to re-enter the protective dormant spore form. This could be a considerable survival disadvantage in the germination behavior of sim- $\mu$ g spores compared to spores formed under 1g. In the case of water as a solvent, spontaneous germination is temperature-dependent. At 4 °C, hardly any spores germinate even after months of storage. At 37 °C, however, the number of germinated spores increased significantly, as well as in 45 °C.

Phase contrast microscopy (Figure 48) allowed a non-quantitative, phenotypical differentiation between germinated and dormant 1g (A-C) and sim- $\mu$ g (D-F) spores after exposure to tempered water. Spores grown under both gravity conditions were transferred from their 4 °C cold stock into 37 °C and 45 °C warm water. After 30 min of incubation, spores were fixated and microscopically analyzed. As expected, spores stored at 4 °C did not germinate. Similar to data generated via OD<sub>600nm</sub>, 1g spores sporadically germinated at 37 °C, whereas only a small minority of sim- $\mu$ g spores remained dormant. With increasing temperature, 1g spores germinated up to ~50 % at 45 °C. Compared to previous experiments, more than twice as many 1g spores germinated at 45°C. However, sim- $\mu$ g spores incubated at 45 °C exhibited rarely a dormant spore, indicating, that almost all spores germinated, which is in contradiction to former well-plate reader results, claiming germination efficiencies of around 51 % at 45 °C (Figure 46). The increased germination of both spore experiments at 37 °C and 45 °C is presumably due to the different methods used. Unfortunately, 1g and sim- $\mu$ g spores tended to germinate spontaneously (<2 %) during microscopy (not shown). Nevertheless, the trend in different germination behavior between 1g and sim- $\mu$ g spores was supported by using phase contrast microscopy.

#### Determination of SASP during spontaneous germination of 1g and sim- $\mu$ g spores

In dormant spores, small acid soluble proteins (SASP) protect the DNA from UV-light, radicals and heat by intercalation and encapsulation. SASP can constitute up to 20 % of the total amount of all proteins occurring in the spore. Shortly after germination, SASP are no longer required for DNA-binding and are therefore released into the surrounding medium. These can be measured by spectrophotometric methods such as MALDI-TOF. As previous experiments showed, warm water influences the spontaneous germination of *B. subtilis* wild-type spores, especially when grown under sim- $\mu$ g. In the following experiment, spores, grown under 1g and sim- $\mu$ g were incubated each in 37 °C water for up to two hours in order to examine the medium for SASP after 0, 60 and 120 min and thus for the germination of the spores (Figure 49). The X-axis represents a mass/charge ratio (m/z) and Y-axis maps the intensity in arbitrary units (a. u.). Typical mass charges of major SASP were found at 6849.8 (SASP- $\beta$ ) and 6941.5 (SASP- $\alpha$ ) as well as 9138.3 for the minor SASP- $\gamma$ , indicated grey auxiliary lines (Ryzhov *et al.*, 2000, Hathout *et al.*, 2003).

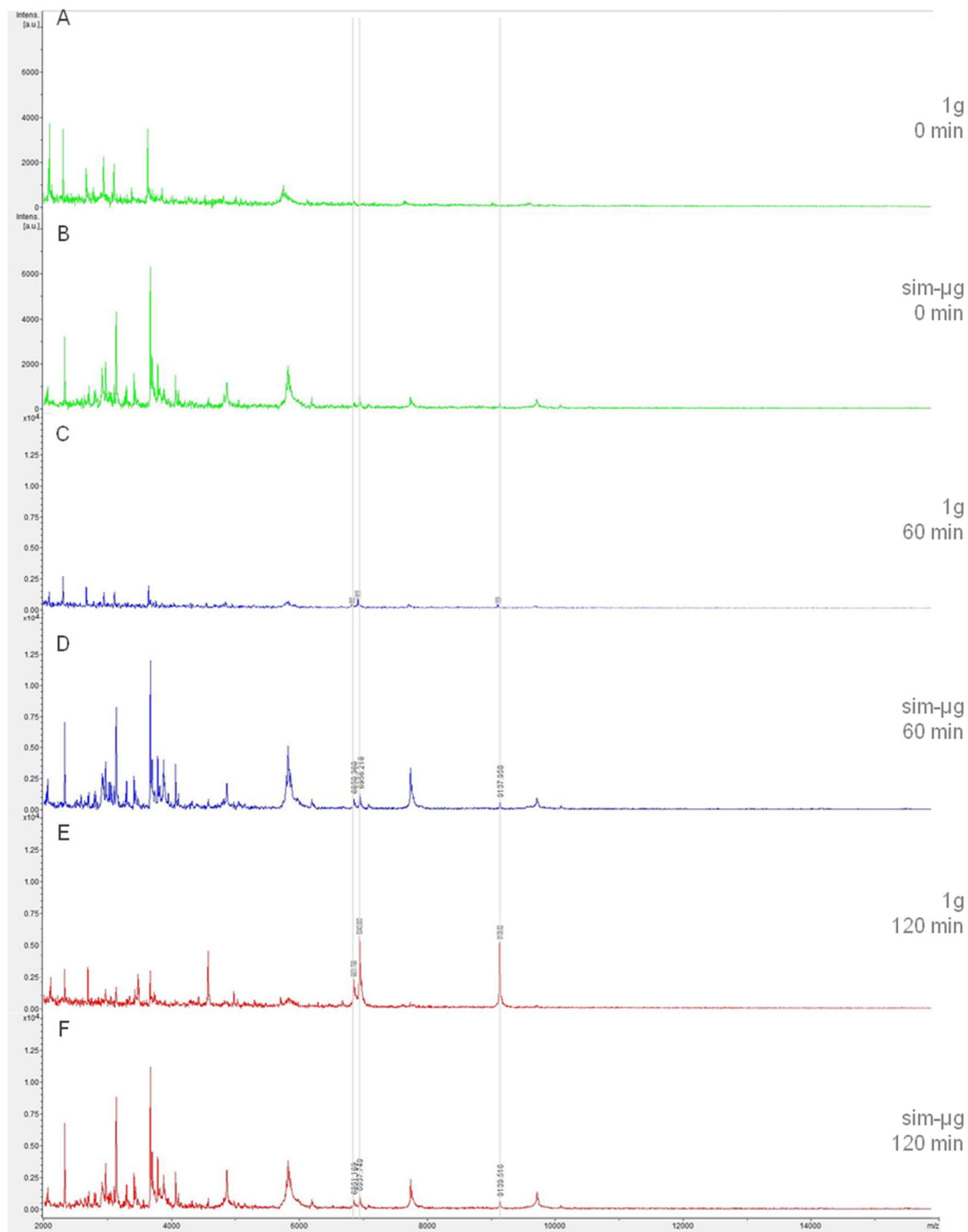


**Figure 49: SASP release of *B. subtilis* spores grown under 1g and sim- $\mu$ g**

*B. subtilis* NCIB 3610 spores were grown on SSM-media for 5 days at 30 °C under regular gravity conditions (1g) and simulated microgravity by using a fast rotating 2-D clinostat (sim- $\mu$ g). Harvested spores were washed and adjusted to  $1 \times 10^8$  spores per ml of which 500  $\mu$ l were used as inoculum in 1 ml 37 °C ddH<sub>2</sub>O to investigate spontaneous germination. After 0, 60 and 120 min, a formic acid protein extraction of the supernatant was carried out to isolate small acid-soluble proteins (SASP), which were analyzed by molecular weight determination using MALDI-TOF. SASP are present in the core region of dormant spores and bound to the spore DNA. After germination, SASP are released. The quantification capabilities of MALDI-TOF are limited and therefore only provide information on the presence of SASP. X-axis represents mass/charge ratio (m/z) and Y-axis is given in arbitrary units (a. u.). Mass charges of SASP are 6849.8 ( $\beta$ ), 6941.5 ( $\alpha$ ) and 9138.3 ( $\gamma$ ). After 0 min no SASP were present in the supernatant of spores grown under 1g and sim- $\mu$ g conditions. After 60 min sim- $\mu$ g samples showed a SASP-release above the threshold compared to 1g samples. Both, 1g and sim- $\mu$ g samples exhibited a SASP release after 120 min incubation in 37 °C ddH<sub>2</sub>O. Auxiliary grids are used to support m/z peaks of SASP.

During germination, the change in refractivity of spores can be measured or analyzed via phase contrast microscopy or well-plate reader assays. In order to quantify excreted SASP, regardless of whether spores germinated spontaneously or germinant-driven, proteins of the supernatant of spore containing solutions were isolated. As control, the supernatant of spores stored at 4 °C was prepared via formic acid protein extraction and analyzed via MALDI-TOF (0 min; graphs A and B). No SASPs were detected in neither 1g or in sim- $\mu$ g samples, which indicated that no spontaneous germination occurred during storage of the spores. After 60 min of incubation in warm water, first SASP were detectable. 1g samples barely exhibited germination (C) compared to sim- $\mu$ g samples which showed increased levels of three different SASP (major: SASP- $\alpha/\beta$  and minor SASP- $\gamma$ ). These results correlate with previous experiments, showing that spores grown under sim- $\mu$ g tend to germinate spontaneously in warm water in higher amounts than spores grown under 1g-conditions. After 120 min of incubation, both sample-sets showed elevated levels of SASP in the surrounding medium. The abundance of SASP in the medium of 1g-spores was increased in contrast to sim- $\mu$ g samples. This may be due to the fact that germination occurs in 1g samples with a considerable delay in time. Results were supported by OD-measurements, which showed that spontaneous germination in sim- $\mu$ g spores, if it took place, progressed faster than in 1g samples. However, the results of the SASP measurement via MALDI-TOF demonstrated that spores formed under 1g and sim- $\mu$ g spontaneously germinated in 37 °C warm water. In addition, this experiment supported the observed germination kinetics of sim- $\mu$ g spores, which tend to germinate faster than 1g spores.

### **Sporulation efficiency of *B. subtilis* biofilms**

Previous experiments demonstrated that spores grown under different gravitational conditions showed dissimilar germination properties depending on the incubation media and temperature. In contrast to differences in gravity-related germination properties, the influence of sim- $\mu$ g on the sporulation in biofilms remained unknown. To investigate the sporulation efficiency (absolute number of spores formed) after an incubation of 7 days on sporulation medium, the number of spores was evaluated by CFU-determination. In addition to the wild-type strains, NCIB 3610, B1 and PS 216, the following biofilm deficient mutants in the background of NCIB 3610 have been investigated:  $\Delta epsA-O$ ,  $\Delta bslA$  and  $\Delta tasA$ . In order to produce high amounts of spores and to enhance sporulation efficiency, most sporulation protocols in literature suggest high levels of D-glucose. Thus SSM-agar was enriched with 1, 2.5 and 5 % D-glucose to investigate the influence of sim- $\mu$ g on *B. subtilis* NCIB 3610 sporulation.

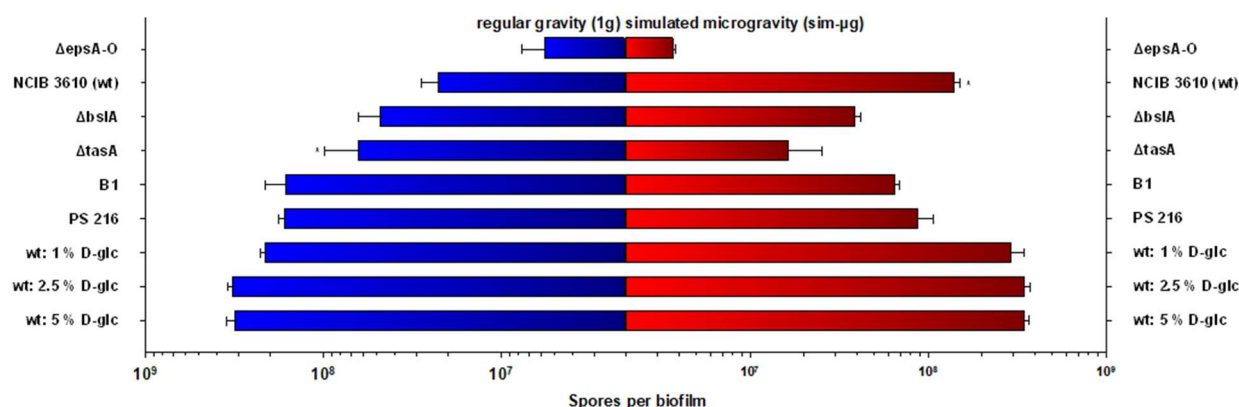


**Figure 50: Differences in spore formation in *B. subtilis* biofilms grown under 1g and sim-µg**

Biofilms of *B. subtilis* NCIB 3610 (wt, and  $\Delta epsA-O$ ,  $\Delta bslA$ ,  $\Delta tasA$ ), PS 216 and B1 were grown under standardized conditions at 30 °C by using membrane filters. Strains were grown on SSM-medium (partly supplemented with 1, 2.5 and 5% D-glucose) under regular gravity (1g, blue bars) and simulated microgravity by using a fast rotating 2-D clinostat (sim-µg, red bars). Each experiment was inoculated with  $1 \times 10^6$  spores ( $N \geq 3$  per strain/condition). Bars indicate the absolute amount of spores produced during the incubation time of 7 days. Results were sorted based of the maximum spore yield under 1g conditions. Least spore production was yielded by the biofilm deficient mutant  $\Delta epsA-O$  and high spore yields were achieved by the wild type in sporulation media with D-glucose. *B. subtilis* wild-type strains B1, PS 216 and NCIB 3610 resulted in 1.2-2 orders of magnitude increase in spore growth under 1g compared to 1.8-2.1 orders of magnitude. Except for NCIB 3610 and the amyloid fiber deficient mutant ( $\Delta tasA$ ) no significant differences in sporulation were observed. Asterisks represent significant differences between gravity condition ( $P \leq 0.05$ , t-test). Error bars represent the standard deviation

The sporulation efficiency of investigated strains is shown in Figure 50, in which the spores per biofilm are displayed on the abscissa. The center of the abscissa marks the inoculum of each individual experiment, which comprised  $1 \times 10^6$  spores per biofilm. Sporulation data was sorted from lowest to highest sporulation efficiency under 1g-conditions (blue bars) after 7 days of incubation on SSM-agar. On the right side of the figure, sharing the Y-axis, corresponding sim-µg sporulation efficiency (red bars) is shown. The experiment was carried out in triplicates (wt,  $n=5$ ) by using the membrane filter method, limiting the biofilm diameter and maximum growth for better comparison.

The biofilm deficient mutant  $\Delta epsA-O$  exhibited the lowest sporulation efficiency of all the other strains. Spore growth did not exceed an increase of one order of magnitude under 1g and sim-µg. In contrast to the biofilm deficient mutant, the wild-type strain NCIB 3610 showed a sporulation efficiency of  $1 \times 10^7$  under 1g and  $1 \times 10^8$  under sim-µg per biofilm ( $P=0.000047$ ;  $P \leq 0.05$ , t-test). This result should be considered with caution, as neither the colony size nor the morphology (not shown) differed between both gravitational conditions. In addition, previous experiments for the *B. subtilis* wild-type strain (NCIB 3610, i.e. Figure 24) showed similar values for sporulation efficiency in biofilms grown on MSgg-agar for seven days. Therefore, it can be assumed that the wild-type should exhibit higher sporulation efficiency than its biofilm deficient mutants in the same background, as shown in sim-µg biofilms. However, PS 216 and B1, both *B. subtilis* wild-type strains showed no significant differences in sporulation efficiency between 1g and sim-µg.

Biofilms formed without the BslA surface layer protein ( $\Delta bslA$ ) exhibited similar sporulation levels under both gravitational conditions, whereas mutants lacking amyloid-like fibers ( $\Delta tasA$ ) within biofilms showed a significant increase in sporulation under 1g conditions ( $P=0.044$ ;  $P \leq 0.05$ , t-test). However, since the p-value was close to the significance level and the standard deviation of both data sets was relatively high, this value should not be over interpreted, but may support the idea, that a stable matrix supports sporulation efficiency – especially when grown under less stressful, 1g conditions. As

expected, the addition of D-glucose to the SSM-medium enhanced the sporulation efficiency under both tested gravity conditions by a factor of x30 in 1g and x2 in sim- $\mu$ g. Again, 1g results for the wild-type must be considered with caution. The overall effect between the addition of 1, 2.5 and 5 % of D-glucose was barely distinguishable, but raised sporulation by  $\sim$ 2.1-2.3 orders of magnitude compared to the spore inoculum.

### 3.9 Survival and resistance properties of 1g and sim- $\mu$ g biofilms and spores

#### X-ray irradiation of biofilms grown under 1g and sim- $\mu$ g

*B. subtilis* biofilms are known to be particularly resilient to extreme environmental influences. These include resistance to UV radiation, desiccation, protection towards chemical treatments and high mechanical stability. When considering biofilm growth under space conditions, radiation plays an important role. A large part of the composition of cosmic rays is gamma radiation ( $\sim$ X-ray), which represents more than 90 % of the total spectrum. Although radiation is largely shielded even in the interior of the ISS, missions outside our electromagnetic shield could potentially result in higher radiation doses. This raises the question of whether biofilms grown under sim- $\mu$ g may exhibit altered resistances to extreme X-ray doses. To investigate this question, biofilms grown under 1g and sim- $\mu$ g were incubated for three days at 37 °C on MSgg medium under standardized conditions. Subsequently, biofilms were dried for a short time and subsequently irradiated with X-ray doses of up to 1000 Gy (Figure 51). Afterwards the CFU (A) and spores (B) were determined by serial dilutions of biofilm samples. On the ordinate, survival is shown as a quotient of the CFU or spores compared to their non-irradiated controls ( $N/N_0$ ). Samples were determined in triplicates at doses of 100, 500 and 1000 Gy.

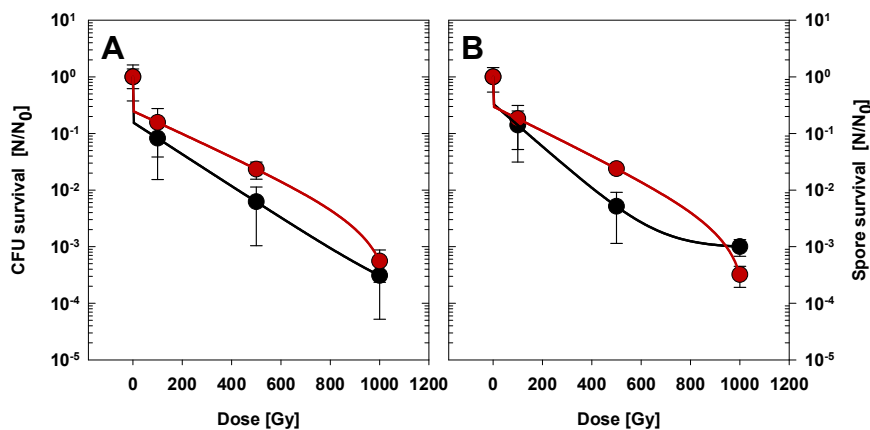


**Figure 51: Survival of *B. subtilis* biofilms grown under 1g and sim- $\mu$ g after irradiation with X-ray**

Graphs represent survival fractions of dried *B. subtilis* NCIB 3610 biofilms grown under regular gravity (1g, black circles) and simulated microgravity by using a fast rotating 2-D clinostat (sim- $\mu$ g, red circles). After incubation, biofilms were air-dried and irradiated with X-rays. Graph A represents survival fractions of total CFU and B represents survival fractions of spores. All samples were irradiated with 100, 500 and 1000 Gy. Both, CFU and spores showed a reduction in survivability of four orders of magnitude after irradiation with 1000 Gy X-ray. No significant differences between 1g and sim- $\mu$ g samples were observed. Experiments were carried out in triplicates ( $N \geq 3$ ) and compared to the  $T_0$ -control (survival fraction:  $N/N_0$ ). Error bars represent the standard deviation.

Irradiation of 100 Gy led to  $\sim$ 80 % decrease in CFU survivability of sim- $\mu$ g biofilms and  $\sim$ 98.3 % decrease for 1g biofilms (A). The number of spores in both groups was likewise reduced by  $\sim$ 80-90 % after treatment with 100 Gy. Doses of 500 Gy X-ray led to a survival of  $\sim$ 3 % in sim- $\mu$ g biofilms and  $\sim$ 0.7 % in 1g biofilms. Similar data was observed for spore survival, exhibiting similar survival. Biofilms grown



under both gravitational conditions demonstrated a decrease in survival by more than three orders of magnitude, for CFU as well as spores after the treatment with 1000 Gy. Regarding the survival of CFU, sim- $\mu$ g biofilms showed a slightly elevated survival rate compared to 1g samples. However, the survival of spores after 1000 Gy X-ray showed that 1g spores were reduced by  $\sim 3$  orders of magnitude, whereas spores from sim- $\mu$ g biofilms were reduced more than two-three times in number compared to 1g samples. When irradiating biofilms with X-ray doses of 100-500 Gy, sim- $\mu$ g biofilms showed a slightly increased resistance compared to 1g biofilms. This trend was only observed at doses of up to 1000 Gy for CFU and 500 Gy for the examination of spores. However, doses of 1000 Gy seemed to affect the survivability of sim- $\mu$ g spores more than spores isolated from 1g biofilms. The lethal dose at which 90 % of the analyzed spores were inactivated (LD90) of CFU and spores was calculated and that spores embedded in biofilms have an LD90 of  $\sim 668 \pm 46$  Gy under 1g conditions compared to  $\sim 655 \pm 32$  Gy under sim- $\mu$ g. Whereas vegetative cells demonstrated LD90 values of  $\sim 586 \pm 117$  Gy under 1g and  $\sim 691 \pm 165$  Gy under sim- $\mu$ g. These results represent a high dynamic range of a probable LD90 distribution, but might be explained by the biofilm structure itself. The superficial layers of mature biofilms are comprised of spores, whereas the layers underneath harbor more vegetative cells. Significant differences in the calculated LD90 between 1g and sim- $\mu$ g were not observed.

### Heavy ion irradiation of biofilms grown under 1g and sim- $\mu$ g

For the investigation of the biological effect and the resulting viability against alpha particles and HZE-ions, biofilms were grown under standardized conditions under 1g and sim- $\mu$ g. Prior to the transport, biofilms were removed from the medium by detaching the filter membrane and air-dried. Figure 52 comprises two graphs representing the survival of CFU and spores after argon-ion (A) and helium-ion (B) treatments with doses up to 1000 Gy for He-ions and 1400 Gy for Ar-ions. The Y-axis represents the relative survival rate as quotient of the remaining CFU or spores after treatment over the absolute CFU and spores of the transport control ( $N/N_0$ ). Spores were depicted as triangles and CFU data as circles.

Biofilms grown under 1g (black symbols) and sim- $\mu$ g (red symbols) showed a reduction of  $\sim 90$  % (1g) and 93 % in survival (CFU and spores) after the treatment with 100 Gy Ar-ions (A). This contradicts the survival rates at higher irradiation treatments such as doses of 250 Gy Ar-ions, which resulted in  $\sim 50$  % survival of CFU/spores of sim- $\mu$ g biofilms and  $\sim 15$  % survival of 1g biofilms. Interestingly, a similar effect was observed for the treatment with 100 Gy He-ions (B). Biofilms grown under both gravitational conditions exhibited only 4-9 % survival (spores and CFU) after 100 Gy He, but 40-70 % survival rates at 250 Gy He-ion treatments. The lethal influence of low radiation doses (100 Gy of Ar- and He-ions) is remarkable, because a doubling of the dose ( $\times 2.5$ ) showed less reduction in survival. Irradiated biofilms grown under sim- $\mu$ g conditions differed in survival at doses of 500 Gy Ar-ions from 1g samples. 1g biofilms were reduced by  $\sim 30$ -40 %, whereas sim- $\mu$ g CFU and spores exhibited only 4-5 % survival. The irradiation with 1000 Gy Ar-ions led to a reduction of CFU and spores of almost two orders of magnitude in both sample sets. Due to the significantly fluctuating survival rates of both samples, interpretation should be performed with caution. This also applies to the results given by He-ion treatments, which also showed increased survival after higher dose treatments (transition between 100 Gy and 250 Gy). Doses of 1000 Gy He-ions led to 50 % survival in spores and 10 % in CFU, whereas sim- $\mu$ g samples represented 20 % spore survival and 7 % CFU survival. The highest dose of 1400 Gy He-ions resulted in almost 10 % survival of CFU and spores in 1g biofilms and 5 % survival in spores as well as 1 % survival of all CFU in sim- $\mu$ g biofilms.

As expected, irradiation with Ar-ions showed a greater lethal effect on the survival of biofilms than He-ions. In contrast to irradiation with X-Ray (Figure 51), the results of heavy ion irradiation differed for each individual ion. In addition, the survival rates after X-ray treatment are lower than after treatment

with similar doses with Ar- or He-ions. The strongest effect was observed after irradiation with 100 Gy Ar or He-ions each. However, biofilms were only reduced to two orders of magnitude after 1000 Gy Ar-ion treatments and 1400 Gy He-ion treatments. Significant differences in survival after heavy ion treatments between 1g and sim- $\mu$ g biofilms were not observed. LD90 doses were calculated for both Helium and Argon ions. Due to the high variances in survival data, the LD90 for Helium does not offer any useful information and should be viewed carefully: For CFU  $4.27 \pm 1.9$  kGy (1g) and  $2.18 \pm 0.98$  kGy (sim- $\mu$ g) and for spores  $7.83 \pm 0.94$  kGy (1g) and  $3.50 \pm 0.28$  kGy (sim- $\mu$ g). Calculated LD90 values for Argon seem more reliable and represent data within a more expected range: For CFU  $1.42 \pm 0.08$  kGy (1g) and  $1.21 \pm 0.08$  kGy (sim- $\mu$ g) and for spores  $1.42 \pm 0.15$  kGy (1g) and  $1.27 \pm 0.05$  kGy (sim- $\mu$ g). Significant differences in LD90 for Argon ion treatment (neglecting the helium LD90 data) between 1g and sim- $\mu$ g *B. subtilis* biofilm cultivation were not observed.

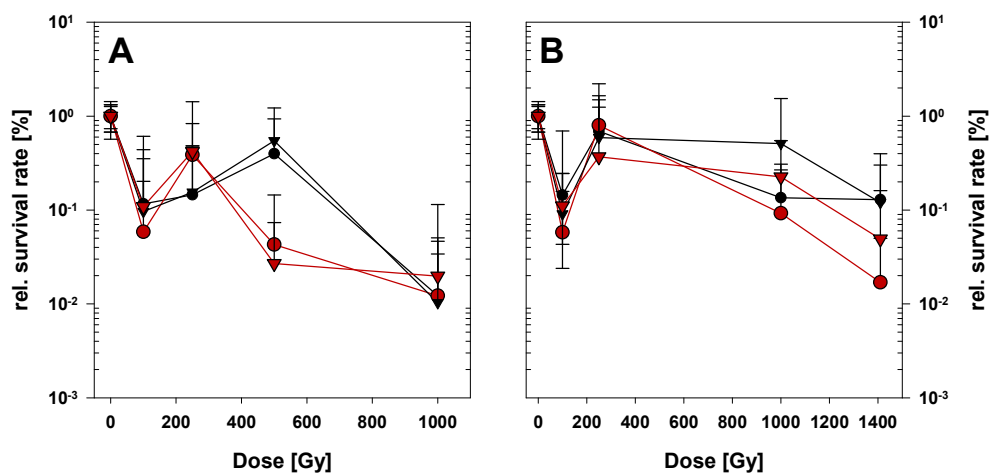


**Figure 52: Helium and argon ion treatment of 1g and sim- $\mu$ g *B. subtilis* biofilms**

Graphs represent survival fractions of dried *B. subtilis* NCIB 3610 biofilms grown under regular gravity (1g, black symbols) and simulated microgravity by using a fast rotating 2-D clinostat (sim- $\mu$ g, red symbols). After incubation, biofilms were air-dried and shipped to Japan in order to perform heavy ion irradiation experiments with argon ions (A) and helium ions (B). Circles represent survival fractions of total CFU and triangles represent survival fractions of spores. All samples were irradiated with 100, 250, 500 and 1000 Gy of the respective radiation source. Argon-ion treatment (1000 Gy) resulted in a decrease in survivability of two orders of magnitude compared to biofilms treated with helium-ions, which did not exceed a decrease of 2 orders of magnitude after 1400 Gy. Biofilms grown under sim- $\mu$ g seem to be more susceptible compared to 1g biofilms – especially when treated with helium ions. Generally high variances in survival at lower doses were observed. Experiments were carried out in triplicates ( $N \geq 3$ ) and compared to the transport control (survival fraction:  $N/N_0$ ). Error bars represent the standard deviation.

### X-ray and heavy ion irradiation of *B. subtilis* spores grown under 1g and sim- $\mu$ g

As previously mentioned, galactic cosmic rays are composed of gamma radiation (X-ray), alpha particles ( $\sim^4\text{He}$ -ions) and HZE-ions such as argon ions. Simulations of high-dose treatments do not correspond to the radiation exposure on the ISS or satellites, but may reveal differences between the radiation types and the influence between growth under 1g and sim- $\mu$ g. Biofilms grown under 1g and sim- $\mu$ g have been analyzed regarding the effects of the main components of cosmic radiation. Apart from biofilms, spores can be found on every spacecraft and the effect of simulated cosmic radiation on spores grown or formed under sim- $\mu$ g conditions was analyzed in following experiments.

*B. subtilis* spores were grown in biofilms under standardized conditions under 1g and sim- $\mu$ g conditions. After harvesting and washing, the titer of spore solutions was adjusted to  $1 \times 10^9$  spores/ml, of which 100  $\mu$ l ( $\sim 1 \times 10^8$  spores) were used as inoculum for the radiation experiments ( $n \geq 3$ ). Besides the wild-type strains NCIB 3610 (*wt*) and B1, the biofilm deficient mutants  $\Delta epsA-O$ ,  $\Delta tasA$ ,  $\Delta bslA$  were examined

regarding their survivability against X-rays (black triangles), Ar-ions (black circles) and He-ions (white circles),

Figure 53 and Figure 54). Survival fractions are presented as quotient of cultivable spores after treatment over the untreated transport controls ( $N/N_0$ ). On the left side of both figures, the survival of 1g spores is shown, whereas on the right side the survival of spores grown under sim- $\mu$ g is demonstrated. For the following doses applied, CFU data was determined for each strain (1g and sim- $\mu$ g) and each radiation source: 0 Gy (transport control), 100, 250, 500 and 1000 Gy.

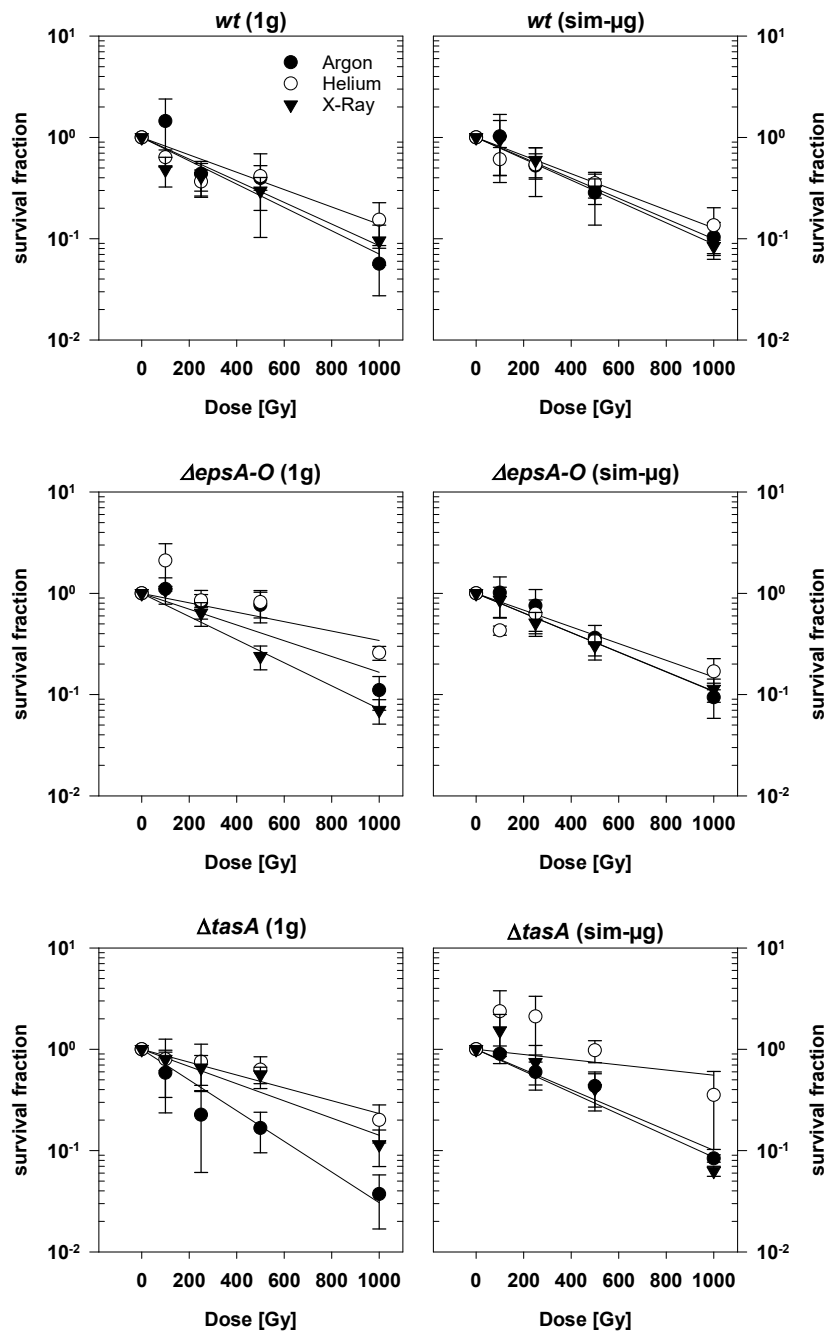


**Figure 53: Irradiation of *B. subtilis* spores grown under 1g and sim- $\mu$ g (I)**

*B. subtilis* NCIB 3610 spores (wt,  $\Delta epsA-O$  and  $\Delta tasA$ ) were grown on SSM-media for 5 days at 30 °C under regular gravity conditions (1g) and simulated microgravity by using a fast rotating 2-D clinostat (sim- $\mu$ g). Harvested spores were washed and adjusted to  $1 \times 10^8$  spores per 100  $\mu$ l which were used for irradiation treatments. Black circles

represent irradiation with Argon ions, white circles Helium ions and black triangles show survival fractions after X-ray ionization. All samples were irradiated with 100, 250, 500 and 1000 Gy of the respective radiation source. Graphs on the left side show survival fractions of spores grown under 1g and sim- $\mu$ g on the right side. Helium ions seemed to have lower inactivation ratios compared to Argon ions and X-ray. *ΔtasA* spores were slightly more susceptible to radiation compared to wt and *ΔepsA-O* spores. Experiments were carried out in triplicates ( $N \geq 3$ ) and compared to the transport control (survival fraction:  $N/N_0$ ). Error bars represent the standard deviation.

Wild-type spores (NCIB 3610; 1g and sim- $\mu$ g) exhibited almost identical survival fractions for each radiation source. At doses of 1000 Gy, the overall survivability was reduced by almost one order of magnitude (10 % survival), wherein the influence of He-ions was least lethal (~15-20 % survival). This was shown as a tendency in all investigated samples of all strains. X-rays on the other hand reduced the survivability of CFU and spores by almost three orders of magnitude in previous experiments after irradiation of 1000 Gy (Figure 51), but showed similar or slightly enhanced levels of inactivation to comparable doses of Ar-ions on spores. Spores of the biofilm-deficient mutant *ΔepsA-O*, exhibited an identical survival pattern (survival of ~10 % after 1000 Gy Ar-ions and X-ray) as their wild-type strain for both investigated gravitational conditions. The influence of He-ions in *ΔtasA* and *ΔbslA* in sim- $\mu$ g spores should be treated with caution due to the wide dispersion of data. However, both strains exhibited similar survival of ~4-10 % after the exposure of 1000 Gy with Ar-ions and X-rays. Interestingly, spores of the wild-type strain B1, which is known for its extremely structured biofilms and high sporulation rates, demonstrated survival fractions of only ~ 4 % in comparison to NCIB 3610, which exhibited survival rates of ~10 %. In summary, the sole influence of X-rays on spores isolated from biofilms was significantly (almost two orders of magnitude) less lethal compared to spores within biofilms. The influence of Ar-ions and X-rays in similar doses showed mostly identical survival fractions, as the survivability was reduced by more than one order of magnitude. As expected, He- ions showed the least critical reduction in spore survival. Differences in survival between spores grown under 1g and sim- $\mu$ g were not observed. Furthermore, calculated LD90 values for every condition and strain can be found in a separate table attached to the appendix (section 7.5). LD90 values tend to become unreliable with large data scatter, but still did not show significant differences between 1g and sim- $\mu$ g spores.

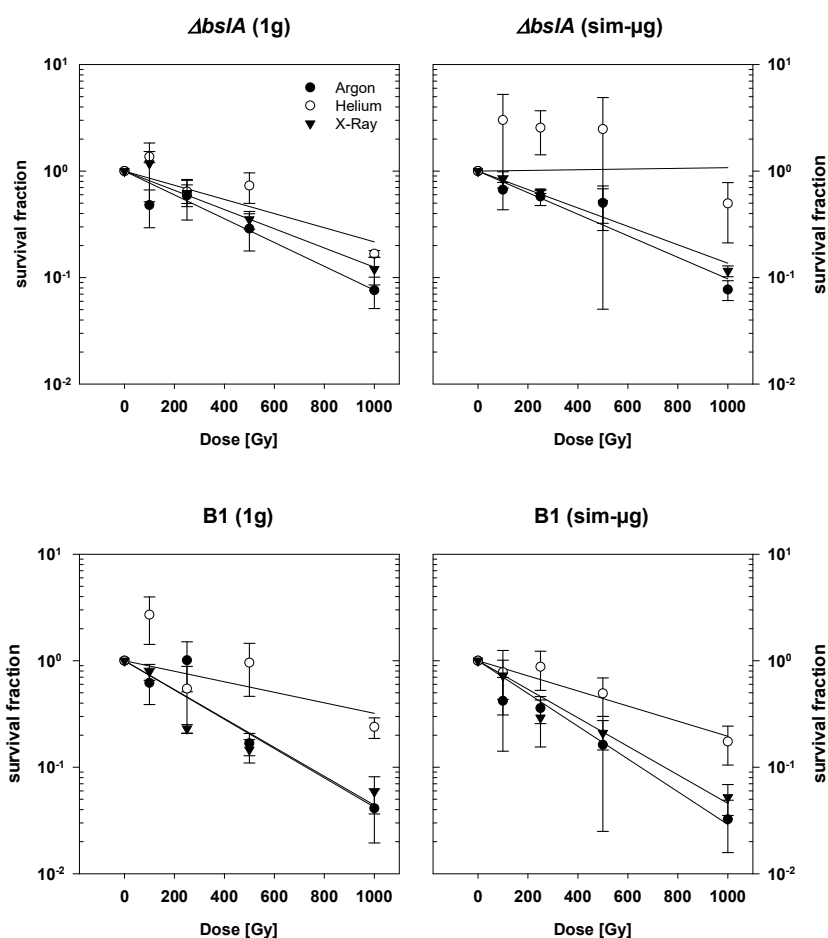


**Figure 54: Irradiation of *B. subtilis* spores grown under 1g and sim- $\mu$ g (II)**

*B. subtilis* B1 and NCIB 3610 spores ( $\Delta bsIA$ ) were grown on SSM-media for 5 days at 30 °C under regular gravity conditions (1g) and simulated microgravity by using a fast rotating 2-D clinostat (sim- $\mu$ g). Harvested spores were washed and adjusted to  $1 \times 10^8$  spores per 100  $\mu$ l which were used for irradiation treatments. Black circles represent irradiation with argon ions, white circles helium ions and black triangles show survival fractions after X-ray ionization. All samples were irradiated with 100, 250, 500 and 1000 Gy of the respective radiation source. Graphs on the left side show survival fractions of spores grown under 1g and sim- $\mu$ g on the right side. Helium ions seemed to have lower inactivation ratios compared to Argon ions and X-ray. No statistical significant differences were observed between 1g sim- $\mu$ g spores of the respective strains. Experiments were carried out in triplicates ( $N \geq 3$ ) and compared to the transport control (survival fraction:  $N/N_0$ ). Error bars represent the standard deviation.

#### **Dry and wet heat: Survivability of *B. subtilis* spores grown under 1g and sim- $\mu$ g**

A classical approach to investigate the resistance properties of bacterial strains, is the determination of survivability after exposure to dry and wet heat. Both methods are typical decontamination methods applied in food industry, to prevent or delay bacterial food spoilage. Within the following experimental setup, *B. subtilis* spores were grown under 1g and sim- $\mu$ g conditions, harvested, washed and adjusted to  $1 \times 10^9$  spores/ml. Spore solutions of 100  $\mu$ l were used as inoculum for the wet heat experiments (Figure 55, B). In order to investigate the resistance properties of dry heat, 100  $\mu$ l of the respective spore solution was allowed to dry in a reaction vessel under sterile conditions and subsequently used for the thermal treatment (A). The ordinate represents the quotient between the CFU after treatment over the untreated control group ( $N/N_0$ ). Dry heat samples were analyzed after 0, 10, 20, 40 and 60 min exposure to 120 °C, whereas spores exposed in wet heat were exposed to 90 °C for 0, 2.5, 5, 7.5 and 10 min. Previous experiments demonstrated, that dry heat needs more time to inactivate *B. subtilis* spores compared to wet heat (not shown). After 10 min exposure to dry heat, survival rates of ~40-50 % were

observed for 1g and sim- $\mu$ g spore. Due to the high variability of the samples, 20 min treated spores exhibited similar (1g) or slightly decreased survival parameter (sim- $\mu$ g). Incubation times of 40 min resulted in  $\sim 8\%$  survival of 1g spores and  $\sim 4\%$  survival of sim- $\mu$ g spores. The maximum exposure time of 1 h, reduced the viability of sim- $\mu$ g samples by more than two orders of magnitude, whereas 1g samples exhibited more than 2 % survival.

To investigate the resistance to wet heat at 90 °C, also known as mild pasteurisation, spores were kept in water in contrast to dry heat. Spores are known to be very heat resistant, which is typically used to determine the spore titer of a mixed sample (veg. cells and spores), by heating the sample at 80 °C for 10-15 min to inactivate any vegetative cells. Spores remain viable after the treatment and their titer can be determined by plating serial dilutions. Exposure to higher temperatures (90 °C) reduced the spore viability (1g and sim- $\mu$ g) after 5 min wet heat treatment (B) to  $\sim 50\%$ . Only 20 % of all tested spore sets remained viable after 7.5 min exposure. After 10 min, a reduction of more than one order of magnitude was observed in 1g spore samples (5 % survival) compared to  $\sim 15\%$  survival of sim- $\mu$ g spores.

LD90 values of wet heat in activation ranged around  $19.5 \pm 2.3$  min under 1g and  $26.8 \pm 6.4$  min under sim- $\mu$ g, whereas the calculated LD90 for dry heat reached  $84.5 \pm 5.1$  min (1g) and  $65.3 \pm 8.7$  min (sim- $\mu$ g). Again, with an increase in data scatter, the LD90 calculation becomes more unreliable. According to the LD90, spores grown under 1g tend to be more sensitive to wet heat but withstand dry heat better than spores formed under sim- $\mu$ g.

The effects of dry and wet heat on the survival of *B. subtilis* spores, regardless of their gravitational incubation method, resulted in a steady decrease in viability, which was strongly affected by a high variability in cell counts (standard deviation). Wet heat tends to inactivate spores faster at lower temperatures compared to dry heat. Differences between spores grown under 1g and sim- $\mu$ g were not observed for neither of the two methods applied.

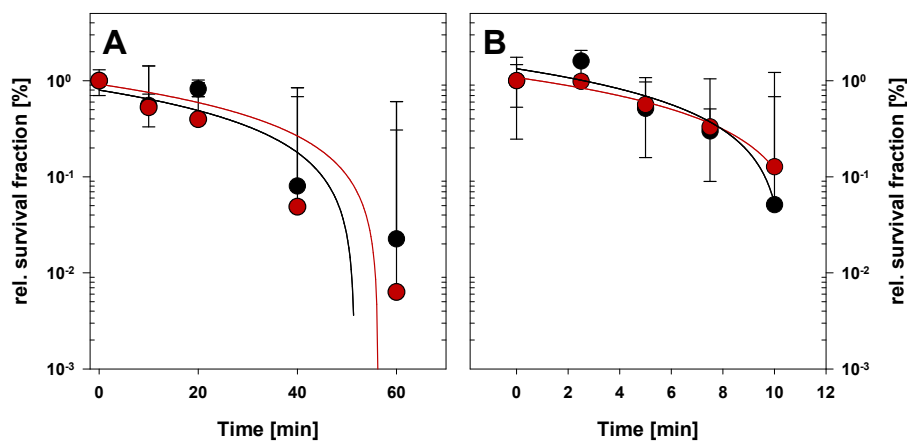


**Figure 55: Dry heat and wet heat survival of 1g and sim- $\mu$ g *B. subtilis* spores**

Graphs represent survival fractions of *B. subtilis* NCIB 3610 spores grown under regular gravity (1g, black circles) and simulated microgravity by using a fast rotating 2-D clinostat (sim- $\mu$ g, red circles). Dry heat resistance is shown in graph A. Graph B represents survival fractions of spores treated with wet heat. Dried spore samples ( $\sim 1 \times 10^8$  spores) were treated at 120 °C up to 60 min and wet samples ( $\sim 1 \times 10^8$  spores) were treated at 90 °C for up to 10 min. Both, 1g and sim- $\mu$ g exhibited a reduction in survivability of two orders of magnitude after 60 min dry heat treatment, whereas wet heat caused a one-log reduction in spore survival after 10 min. No significant differences between 1g and sim- $\mu$ g samples were observed. Experiments were carried out in triplicates ( $N \geq 5$ ) and compared to the  $T_0$ -control (survival fraction:  $N/N_0$ ). Error bars represent the standard deviation.

### Desiccation resistance of *B. subtilis* biofilms grown under 1g and sim- $\mu$ g

*B. subtilis* spores are known for their extraordinary resistance towards desiccation. Biofilms, on the other hand, contain a large proportion of vegetative cells, which are less resistant to water deprivation. In the following experiment, biofilms grown under 1g and sim- $\mu$ g conditions were analyzed regarding their resistance towards desiccation after 1, 7, 14 and 30 days (Figure 56). Prior to drying, biofilms were incubated at 37 °C for 3 d on membrane filters under standardized conditions. After incubation, biofilms were immediately removed from their medium and air-dried under sterile conditions.

The abscissa represents the survival fraction composed of the quotient of the CFU/spore data over the CFU/spore content of biofilms prior desiccation ( $N/N_0$ ). Black and dark red bars represent the survival fractions of vegetative cells grown under 1g and sim- $\mu$ g. Spore survival or growth is shown in grey for 1g and in red for sim- $\mu$ g biofilms. 1g and sim- $\mu$ g biofilms desiccated for one day showed a reduction of vegetative cells by two orders of magnitude. The amount of spores within both sample sets raised after one day by the factor of five, and remained stable during the tested time span (7, 14 and 30 days). After one week of drying, the proportions of vegetative cells (1g and sim- $\mu$ g) had decreased by more than four orders of magnitude, which was likewise observable after 14 and 30 days of desiccation.

In summary, biofilms grown under 1g and sim- $\mu$ g conditions showed no differences in survival patterns of vegetative cells during desiccation. Both sample sets were reduced by four orders of magnitude in vegetative cells and increased their spore fractions.

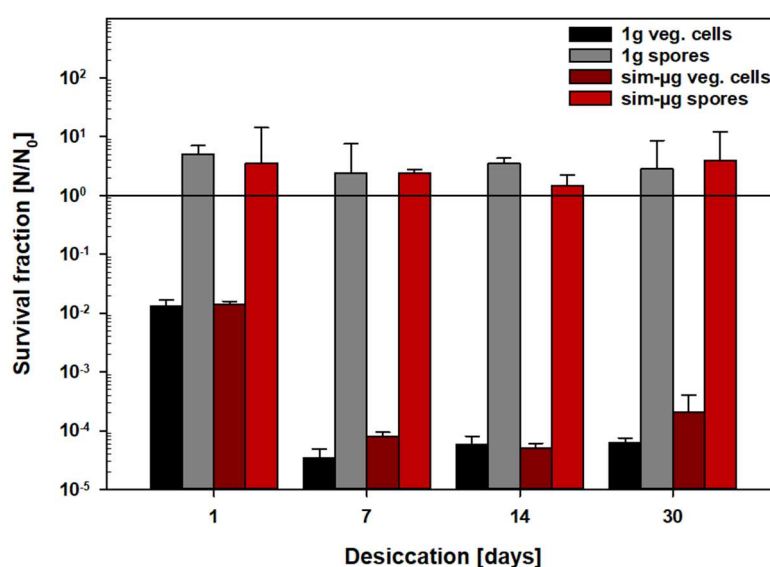


**Figure 56: Survival of *B. subtilis* biofilms grown under 1g and sim- $\mu$ g after desiccation**

*B. subtilis* NCIB 3610 biofilms were grown under standardized conditions under regular gravity (1g, black and grey bars) and simulated microgravity by using a fast rotating 2-D clinostat (sim- $\mu$ g, red and dark red bars). For inoculation,  $1 \times 10^6$  spores were spotted on membrane filters (PTFE,  $\phi$  2.7 cm), which were incubated on MSgg agar (supplemented with 10 mM L-alanine) at 37 °C. After incubation, biofilms were air-dried for one, 7, 14 and 30 days at room temperature under constant relative air-humidity of 40 %. Darker colors (black/1g and dark red/sim- $\mu$ g) represent vegetative cells, whereas spores are shown in brighter colors (grey/1g and red/sim- $\mu$ g). After one day the amount of vegetative cells was reduced by two orders of magnitude. The number of spores in biofilms increased by half an order of magnitude and remained constant during the experiment length. After one week the amount of vegetative cells in 1g and sim- $\mu$ g samples was reduced by four orders of magnitude. No significant differences between 1g and sim- $\mu$ g samples were observed. Experiments were carried out in triplicates ( $N \geq 3$ ) and compared to the  $T_0$ -control (survival fraction:  $N/N_0$ ). Error bars represent the standard deviation.

### Effect of antibiotics on *B. subtilis* biofilms grown under 1g and sim- $\mu$ g

Biofilms proved to be resistant to many different environmental stresses. So far, the influence of simulated microgravity on the resistance properties of *B. subtilis* biofilms towards chemical or antibiotic treatments remained largely unknown. In the following experiments, the resistance properties of the *B. subtilis* wild-type (NCIB 3610) and  $\Delta$ *epsA-O* as biofilm-deficient mutant were tested for their minimal inhibitory concentration (MIC) towards doripenem (positive control), rifampicin, nalidixic acid, trimethoprim and bacitracin (negative control, not shown). The minimal inhibitory concentration ( $\mu$ g/ml) is considered as antibiotic concentration affecting visible bacterial growth on nutrient media under laboratory conditions.

MSgg-agar plates were inoculated with spores of the respective strain in the center within a 1.5 cm radius. To determine the MIC, E-tests according to the manufacturer's instructions were used (bioMérieux). Incubation was performed under 1g and sim- $\mu$ g at 37 °C for three days. Subsequently, the minimal inhibitory concentration was calculated by the determination of the mean value of quadruplicates (wt) and triplicates ( $\Delta$ *epsA-O*). Black (wt) and grey ( $\Delta$ *epsA-O*) bars represent the MIC of the respective antibiotic of biofilms grown under 1g conditions, whereas dark red bars (wt) and red ( $\Delta$ *epsA-O*) represent sim- $\mu$ g data (Figure 57).

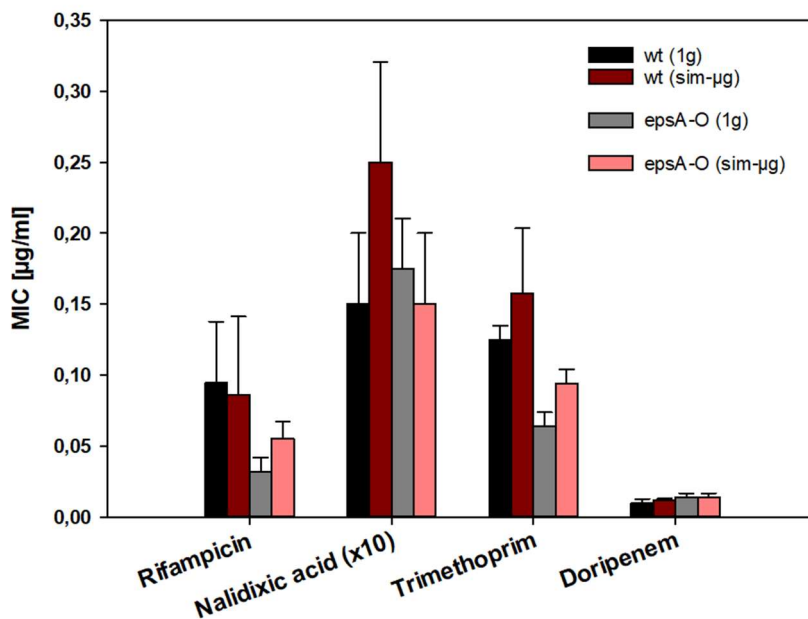


**Figure 57: Antibiotic susceptibility of *B. subtilis* biofilms grown under 1g and sim- $\mu$ g**

*B. subtilis* NCIB 3610 biofilms (wt and  $\Delta$ *epsA-O*) were grown for 3 days on MSgg agar (supplemented with 10 mM L-alanine) at 37 °C under regular gravity (1g, black and grey bars) and under simulated microgravity by using a fast rotating 2-D clinostat (sim- $\mu$ g, dark red and red bars). Antibiotic susceptibility of rifampicin, nalidixic acid, trimethoprim, doripenem (positive control) and bacitracin (negative control, not shown) were tested by determining the minimal inhibitory concentration (MIC) using E-tests. MICs of rifampicin and doripenem showed no significant differences between 1g and sim- $\mu$ g. Wild-type biofilms grown under sim- $\mu$ g were significantly more resistant to nalidixic acid ( $P=0.024$ ) and trimethoprim ( $P=0.043$ ) compared to 1g samples. The  $\Delta$ *epsA-O*-mutant showed no significant differences between both tested gravity conditions. Statistical significance was tested by t-test ( $P \leq 0.05$ ). Experiments were carried out in triplicates ( $N \geq 3$ ) and MIC was determined after manufacturer's instructions. Error bars represent the standard deviation.

Rifampicin, inhibits DNA-dependant RNA polymerases and showed a MIC of  $\sim 0.09 \pm 0.04$   $\mu$ g/ml for wt-biofilms grown under 1g and sim- $\mu$ g. The biofilm deficient mutant was more susceptible, showing MICs of  $0.35 \pm 0.5$   $\mu$ g/ml (1g) and  $0.05 \pm 0.005$   $\mu$ g/ml (sim- $\mu$ g). Nalidixic acid is inhibiting primarily the gyrase in



Gram negative bacteria, but also inhibits the the gyrase functions in Gram positive bacteria. Therefore  $\sim 1.5 \pm 0.5$   $\mu\text{g/ml}$  (1g) and  $2.5 \pm 0.6$   $\mu\text{g/ml}$  (sim- $\mu\text{g}$ ,  $P=0.024$ ; t-test,  $P \leq 0.05$ ) of nalidixic acid were needed to reach the MIC for the wild-type strain as well as  $1.7 \pm 0.3$   $\mu\text{g/ml}$  (1g) and  $1.5 \pm 4$   $\mu\text{g/ml}$  (sim- $\mu\text{g}$ ) for  $\Delta\text{epsA-O}$ . Trimethoprim binds to the dihydrofolate reductase and thus inactivates the folic acid metabolism. Wild-type biofilms grown under 1g conditions were inhibited at  $0.13 \pm 0.01$   $\mu\text{g/ml}$  Trimethoprim ( $0.16 \pm 0.04$   $\mu\text{g/ml}$  for sim- $\mu\text{g}$ ;  $P=0.043$ ; t-test,  $P \leq 0.05$ ) and 1g  $\Delta\text{epsA-O}$  biofilms were susceptible at concentrations of  $0.07 \pm 0.01$   $\mu\text{g/ml}$  ( $0.09 \pm 0.01$   $\mu\text{g/ml}$ ).

Doripenem was used as positive control to show inhibitory effects at very low concentrations and is known for its ability to inhibit cell wall synthesis. The minimal inhibitory concentration of doripenem was  $\sim 1-2$   $\mu\text{g/ml}$  for biofilms of both tested strains grown under 1g and sim- $\mu\text{g}$ . Bacitracin, which is produced by *B. subtilis* was used as negative control and showed no biofilm inhibition for any tested condition.

In conclusion, sim- $\mu\text{g}$  biofilms were more resistant to the nalidixic acid and trimethoprim than biofilms grown under 1g conditions. A similar trend was observed for  $\Delta\text{epsA-O}$ -biofilms for rifampicin and trimethoprim, but showed no statistical significance.

## 4. Discussion

### 4.1 Development of standardized biofilms

In contrast to the planktonic growth of cells, biofilms are extremely complex structures which differ from each other both phenotypically and genetically even under laboratory conditions (Brehm-Stecher & Johnson, 2004, Vlamakis *et al.*, 2013). For almost two decades, intensive research has been carried out on *B. subtilis* biofilms using a plethora of different biofilm cultivation methods, making it very difficult to compare the results. For example, one of the most used incubation media, MSgg was introduced by Branda *et al.* in 2001 and took part in many studies (Branda *et al.*, 2001, Arnaouteli *et al.*, 2019, Dervaux *et al.*, 2014b). But on the other side, other biofilm studies were conducted by using LB-medium (Gingichashvili *et al.*, 2017, Kesel *et al.*, 2017) or other media containing glycerol, manganese or other biofilm promoting ingredients (Kobayashi & Ikemoto, 2019, Gingichashvili *et al.*, 2017). Glycerol is a favored energy source of *B. subtilis* and signal molecule for KinD, a kinase that takes part in the initiation of biofilm and spore formation via phosphorylating Spo0A (Shemesh & Chai, 2013). The incubation temperature, which strongly affects the growth rate, differs among the studies and the amount of cells or spores used for inoculation of the respective experiment is not or insufficiently given (Kumar & Libchaber, 2013, Fuchs *et al.*, 2017a). Although it was shown by different studies that the way the incubation takes place can result in massive physiological differences with regard to spore and/or biofilm formation (Kesel *et al.*, 2017). Several different methods within the biofilm community exist, but a general meta-standard for best comparison among studies is missing.

The experiments within this work should be comparable with the existing literature, whereby typical *B. subtilis* cultural conditions were selected, which were consistently applied for all experiments. Since agar-based colonies may differ despite identical incubation parameters, the membrane filter method was developed within the framework of this thesis in order to reproduce standardized biofilms as far as possible. By using defined amounts of spores and the separation between membrane and culture medium, biofilms could be produced, which shared almost identical phenotypic characteristics and hardly differed in their CFU and spore composition (Fuchs *et al.*, 2017a). Preliminary experiments showed that the germination kinetics depend on the spore heat activation and the actual germination temperature (Knaysi, 1964, Black *et al.*, 2005, Setlow, 2013). Accordingly, growth is also strongly temperature dependent, but shows consistent results when using the membrane filter method. The dimensions of the filter and the inner diameter limit the biofilm growth at high temperatures (above 40 °C) or mature biofilms (older than one week) (Fuchs *et al.*, 2017a). These incubation conditions have so far been little studied, as the temperatures were mostly outside the physiological optimum (Warth, 1978) or exceed the log phase. However, growth is generally slowed down by the membrane filter, since all the necessary nutrients have to be transported through the fine-pored membrane, which due to the size of the pores can only be achieved by diffusion. In contrast to most commercial filters, filters used in frame of this thesis were factory-made hydrophilized to promote passive diffusion rates. With increasing biofilm size and biomass, a nutrient scarcity occurs after three days of incubation on the nutrient-poor nutrient medium. A direct consequence is the spore formation, especially in the biofilm center, as well as the loss of vegetative cells (Allocati *et al.*, 2015, Gingichashvili *et al.*, 2017). Nutrient limitation causes in many ways different stress responses in *B. subtilis* cells, which leads to increased sporulation rates and increasing cell lethality (Kohlstedt *et al.*, 2014, Ter Beek *et al.*, 2008, Hecker & Völker, 1990).

Partial nutrient limitation depends on the growth speed and the colony size. Therefore, one week-old biofilms grown at 37 °C reached higher cell densities and showed an increase in sporulation of more than one order of magnitude in contrast to biofilms grown at 30 °C. By using standardized growth conditions, *B. subtilis* biofilms were incubated on membrane filters for a maximum of three days to avoid a potential nutrient shortage (Fuchs *et al.*, 2017a). Nevertheless, preliminary experiments demonstrated that increased sporulation rates in the biofilm center were independent from the nutrient limitation. This was tested by placing the biofilm-carrying filter on fresh medium after 24 and 48 h of incubation (data not shown). Despite a medium change, self-regulatory processes within the biofilm led to an initiation of spore formation, indicating that the influence of fresh nutrients barely had any effect on the cell population (Allocati *et al.*, 2015, Gingichashvili *et al.*, 2017).

In addition, experiments with the sporulation-deficient mutant ( $\Delta sigG$ ; early sporulation, sigma factor  $\sigma^G$  deficient) (Mearls *et al.*, 2018) demonstrated that in 24 h old biofilms, no differences in CFU to the wild type were observed, whereas in mature biofilms, CFU decreased significantly compared to the wild type. This could be due to the fact that the natural reaction to a nutrient deficiency in biofilms is regulated almost binary: By either sporulation or starvation (Gray *et al.*, 2019). Under normal physiological conditions, but also under moderate nutrient deficiencies, certain cells within the biofilm produce and secrete proteases which can dissolve and digest other cells to the benefit of the whole biofilm community, (Marlow *et al.*, 2014a, Veening *et al.*, 2008) or to dissolve the matrix proteins and dissolve the biofilm (Verhamme *et al.*, 2007). So called cannibal cells secrete toxins (Skf and Sdp) to inactivate susceptible cells in order to digest those for nutrients or to restructure the biofilm (Lopez *et al.*, 2009, Gonzalez-Pastor *et al.*, 2003, Hofler *et al.*, 2016). In contrast to environmental conditions, biofilms show no dispersion or release of cells if grown under agar-based laboratory conditions. Due to the filter-based method, cells were exposed to only minor shear forces compared to conventional agar incubation methods (Fuchs *et al.*, 2017a). Furthermore, the MSgg-medium of both strains turned from a milky-white/transparent color to a light brown after 72 hours. Interestingly, 7 d-old topographically elevated regions of biofilms of the wild-type were significantly brighter in color compared to biofilms of the sporulation-deficient mutant. This could be due to the fact that spores have a relatively high refractive index due to their density and consistency and therefore appear beige/white (Gomez-Aguado *et al.*, 2013, Branda *et al.*, 2001). It has not yet been possible to clearly identify which metabolites are involved (Vlamakis *et al.*, 2013). This effect also occurred in liquid cultures. HPLC-analyses of filtered liquid MSgg medium after culturing *B. subtilis* 168 for 7 days showed elevated levels of  $\alpha$ -ketoglutaric acid (6 M) and  $\beta$ -methylbutyric acid (1.1 M), which might have caused the discoloration of the medium (unpublished data from R. Moeller, 2012).

## 4.2 Microgravity simulation

As previously shown, the inoculation strongly affects the later biofilm size and structure (Fuchs *et al.*, 2017a, Ghanbari *et al.*, 2016, Huang *et al.*, 2019). For the best phenotypic comparison of biofilms, a circular drop shape proved to be a reasonable option (Dervaux *et al.*, 2014a, Fuchs *et al.*, 2017a) Fuchs 2017. This offers several advantages: The spores are evenly distributed, with an increased concentration at the edges, which in turn forms the biofilm center. With increasing incubation time, growth takes place concentrically. The center is thus the oldest part of the biofilm and all the surrounding regions are younger with increasing radius (Dervaux *et al.*, 2014a, Srinivasan *et al.*, 2018). Especially the simulation of microgravity takes advantage of this incubation method, due to the fact, that the most accurate simulation of microgravity takes place along the rotation axis (Herranz *et al.*, 2013a). For standardized biofilm formation, membrane filters were usually placed in

the middle of an agar plate, aligning the dried spores at the center (Garschagen *et al.*, 2019, Ott *et al.*, 2019). Therefore, the biofilm center represents the oldest part of the biofilm and comprises the area, where the best quality of microgravity was simulated. According to the calculation model, the center comprised  $\sim 0.01g$  ( $r=2.5$  mm) compared to the outer boundaries of a three days-old biofilm which was exposed to  $\sim 0.02g$  ( $r=5.00$  mm).

### Growth rates under sim- $\mu g$

*B. subtilis* growth behavior in microgravity was analyzed during the STS-63 mission, analyzing the lag-phase duration, the growth rate as well as cell concentration and overall biomass (Kacena *et al.*, 1999b). Incubation was achieved using a fluid processing apparatus for both, flight and ground experiment. Microgravity affected the growth in liquid by an increase in cell mass of 125 % at 23 °C and by 474 % under 37 °C and showed a critical to determine elevated growth rate of more than 23 % at 23 °C as well as identical levels in lag-phase duration (Kacena *et al.*, 1999b). In frame of this thesis, by using 2-D clinostats on solid media, slightly increased growth rates in sim- $\mu g$  and identical levels in the lag phase were also observed (as far as evaluable). In contrast to the STS-63 results, sim- $\mu g$  samples and their 1g-reference showed no differences in the total cell count. This probably depends to a great extent on the used incubation method that might cause sedimentation, reduced waste product disposal and local oxygen and nutrient limitations. In contrast, microgravity seems not to lead to spatial nutrient deficiencies in liquid media (Morrison *et al.*, 2019, Kacena *et al.*, 1999a). Menningham and Lange showed similar observations regarding the overall biomass production of *B. subtilis* during a flight experiment and also reported that under  $\mu g$ , spore formation in the late stationary stage was drastically reduced compared to the ground experiment (Mennigmann & Lange, 1986), which could not be shown with comparable sim- $\mu g$  simulations and their controls. Kacena *et al.* demonstrated in several experiments, that solid incubation media does not promote enhanced biomass levels of *B. subtilis* grown under  $\mu g$ , which corresponds to the results within this thesis (Kacena *et al.*, 1997b). This is an indication that growth in liquid media under the influence of microgravity is more influenced by fluid dynamics than by cellular response (Huang *et al.*, 2018).

### RPM and 2-D clinostat in comparison

Both microgravity simulations used in this work function the same way by rotating the object to be examined along one (2-D clinostat) or two axes (3-D clinostat, or RPM) (Herranz *et al.*, 2013a). In the past, the 2-D clinostat was first used to perform gravitational experiments with plants and was then adapted to study cell cultures and microbial behavior under simulated microgravity (Newcombe, 1904, Zhang *et al.*, 2014). Both methods have already been investigated several times with regard to their biological effects and often demonstrated different results – at least for samples in liquid cultures (Svejgaard *et al.*, 2015, Brungs *et al.*, 2019). There is an ongoing discussion among scientists which of the two methods is better suited to simulate microgravity. It should be noted that whichever organism is used, the incubation parameters need to be adjusted as they have a very strong impact on the experiment (Brungs *et al.*, 2019, Wuest *et al.*, 2015). So far, there are only two studies which analyzed agar-based microgravity simulation via use of a 2-D clinostat of *B. subtilis* (Kacena *et al.*, 1997b, Kacena *et al.*, 1997a). Comparative results between RPM and 2-D clinostat regarding the growth of *B. subtilis* or its biofilm formation have not yet been performed. The results of this thesis demonstrated that the biofilm formation under identical growth conditions but different microgravity simulations can differ significantly. CFU levels under 1g and sim- $\mu g$  (clinostat) barely differed, whereas a trend was observed, that sim- $\mu g$  by using a RPM showed a reduction in

CFU by almost 50 % and therewith significantly less spores. Unfortunately, there is barely any literature which has investigated both methods with regard to agar-based cultivation (other than plant experiments), but several other investigations showed differing results between their tested samples (Brungs *et al.*, 2019, Svejgaard *et al.*, 2015). During the incubation of the sample in the RPM, it can often experience partial gravitation, since the gravitational vector only zeroes itself computationally distributed over time. In contrast to this, the 2-D clinostat is constantly rotated around an axis, thus excluding the reception of the gravitational vector. Therefore, it cannot be excluded that both simulation techniques differ regarding their effect on biofilm growth. Depending on the experimental setup, the simulation method must be selected to be appropriate for each experiment.

### 4.3 Biofilm formation under sim- $\mu$ g

#### Biofilm surface properties

Biofilm-forming *Bacillus* sp., *Enteriobacteriaceae*, *Propionebacterium* spp., *Clostridium* and *Staphylococcus* spp. have been found on the ISS as well as several filamentous fungi such as *Penicillium* and *Aspergillus* (Venkateswaran *et al.*, 2014, Checinska *et al.*, 2015b, Mora *et al.*, 2019, Schiwon *et al.*, 2013, Novikova *et al.*, 2006). Schiwon *et al.* reported, that 83 % of 29 isolated strains found on the International space station were able to form biofilms (Schiwon *et al.*, 2013) and Sobisch *et al.* demonstrated, that nine *B. cereus* isolates from the ISS formed phenotypically heterogeneous biofilms on Earth (Sobisch *et al.*, 2019). Both studies as well as the aforementioned publications show, that biofilm-formers are quite abundant on spacecraft and are still able to form robust biofilms after isolation and re-cultivation under terrestrial conditions. Biofilm formation is initiated by adherence of individual cells to an interface such as a solid surface. During the growth- and expansion phase, the cells begin to divide and with increased cell mass and associated excreted signal molecules, quorum sensing takes place which organizes and restructures the cell community. So far the process of early biofilm-formation on solid media has never been investigated, neither under real  $\mu$ g conditions nor under sim- $\mu$ g. Most biofilm-related research conducted under space conditions was endpoint-driven and not focused on early stages of biofilm development. By using the 2D-clinostat, early biofilm formation of up to 24 h was investigated using DIC-microscopy, but no macroscopic or phenotypic differences between 1g and sim- $\mu$ g were observed. All experiments showed equal levels of vegetative cells of all tested strains after 20 h - without any detectable sporulation. After 40 h of incubation, 1g and sim- $\mu$ g samples of the wild type and the motility deficient mutant ( $\Delta$ hag) exhibited sporulation. Interestingly, the biofilm deficient mutant ( $\Delta$ epsA-O) only formed spores under 1g in contrast to the sim- $\mu$ g, where no sporulation occurred. So far several systems are known, that might delay sporulation, such as the sigma factor  $\sigma^F$  (Karmazyn-Campelli *et al.*, 2008) or kinC and kinD, two kinases, which are involved in phosphorylation of Spo0A (López *et al.*, 2009). Both sensor kinases are activated by potassium leakage caused by membrane interactions of surfactins (Lopez, 2015, López *et al.*, 2009). Kinsinger *et al.* assumed that the surface motility of *B. subtilis* is dependent on extracellular surfactins as well as on potassium (Kinsinger *et al.*, 2003). Young  $\Delta$ epsA-O colonies grown under sim- $\mu$ g might produce less surfactins in contrast to 1g samples, due to the clinorotation, which might support the distribution of vegetative cells. This would explain why sporulation under sim- $\mu$ g is delayed by approximately ~10+20 h. However, this effect was not observed in any other mutant. Instead, wild type *B. subtilis* biofilms grown under both gravitational conditions demonstrated no significant differences regarding their CFU and spore composition.

In addition, 1g and sim- $\mu$ g biofilms were examined regarding their surface topography using profilometric analyses. Biofilms of the wild type,  $\Delta$ *tasA*,  $\Delta$ *bslA*,  $\Delta$ *hag* and  $\Delta$ *epsA-O* showed no significant differences in their maximum height or depth, their overall roughness and their interfacial area ratio when comparing both gravitational settings. Kim *et al.* showed that motile *Pseudomonas aeruginosa* in liquid-cultures formed column-and-canopy-shaped biofilms in microgravity in contrast to mushroom-shaped biofilms under 1g (Kim *et al.*, 2013). A similar study of Orsini *et al.* by simulating  $\mu$ g using HARVs, demonstrated that *Streptococcus mutans* biofilms form compact round aggregates, whereas 1g controls were less compact (Orsini *et al.*, 2017). Also using HARVs, *Candida albicans* showed phenotypic differences towards an irregular-wrinkle formation in its biofilm structure under sim  $\mu$ g (Searles *et al.*, 2011). These experiments were performed in liquid media and showed completely different phenotypic biofilm results. As mentioned before, differences between liquid and solid media can be significant when comparing the effects of different gravitational regimes (Brungs *et al.*, 2019, Svejgaard *et al.*, 2015). Given the current state of literature, no comparable sim- $\mu$ g or  $\mu$ g-studies on the surface of agar-based biofilms have been conducted. Interestingly, the surface hydrophobicity analysis, which is directly linked to the surface layer protein BslA, demonstrated that *B. subtilis* biofilms tend to be more hydrophobic when grown under sim- $\mu$ g conditions. Biofilms of wild type exhibited a significant increase (~15 %) in hydrophobicity compared to the respective 1g-control. BslA is one of the most important structural components within *B. subtilis* biofilms protecting the community from several harmful environmental influences (Hobley *et al.*, 2013, Kobayashi & Iwano, 2012). In frame of a transcriptome analysis of *B. subtilis* grown under  $\mu$ g, Morrison *et al.* found out that *bslA* was significantly upregulated compared to the ground control (Morrison *et al.*, 2019). BslA is self-assembled and an increase of its transcripts under  $\mu$ g or sim- $\mu$ g conditions might be an indication for higher levels of the final protein within biofilms that could result in an elevated hydrophobicity (Morris *et al.*, 2017, Arnaouteli *et al.*, 2016). In contrast to the space experiment, in Morrison's study, which was analyzed after 36 h, transcriptomic analyses of 72 h-old biofilms (this study) showed no significant upregulations in *bslA*. This might be due to the fact that after an incubation period of three days the BslA protein layer has completely formed or due to the incubation method of the space experiment, which was performed in liquid culture. A further explanation of this phenomenon could be hydrodynamic shear forces occurring especially in the space experiment, which are known to promote protein secretion during biofilm formation (Ramasamy & Zhang, 2005, Liu & Tay, 2002). However, this would not explain an increase of hydrophobicity under agar-based sim- $\mu$ g cultivation or the trend of higher hydrophobicity observed for the BslA-deficient mutant.

### **Biofilm architecture under sim- $\mu$ g**

Concentrically formed biofilms allowed the classification into three different biofilm areas, which were intensively examined by SEM and TEM cross-section analysis (Fuchs 2018). During the evaluation of the biofilm cross-sections, particular attention was paid to the spatial distribution of cells, spores and EPS/matrix elements. As mentioned before, the center represents the oldest part of the biofilm as well as the position in which the lowest shear forces during microgravity simulation occur. With increasing radius of the colony, a shear force gradient towards the biofilm edge developed by using 2-D clinostats. The biofilm center of sim- $\mu$ g samples showed significantly more EPS at the bottom of the colony compared to 1g controls. Partwise the matrix seemed to function as a sponge, without harboring any vegetative cells or spores. 1g samples demonstrated a homogenous basal matrix-mat, which was intercalated with individual cells and spores. For comparison, *Micrococcus luteus* was found to produce larger amounts of EPS in sim- $\mu$ g compared to samples

grown under 1g (Mauclaire & Egli, 2010). *M. luteus* Strains isolated from the ISS showed even higher levels of EPS when cultivated under sim- $\mu$ g and 1g. Cheng *et al.* investigated the biofilm structure of *S. mutans* and found that EPS production and formation was enhanced and heterogeneously distributed among sim- $\mu$ g (Cheng *et al.*, 2014). Huang and colleagues reviewed several  $\mu$ g and sim- $\mu$ g studies and concluded, that agar-based  $\mu$ g-studies of different strains, exhibited identical or reduced growth compared to 1g controls (Huang *et al.*, 2018).

Apart from the changed EPS-formation, cells under sim- $\mu$ g were smaller and randomly distributed in contrast to long rods embedded in fine matrix elements as observed in 1g samples. This result is consistent with a study of Zea *et al.*, which cultured *E. coli* in space and showed, that cells are smaller when cultured under  $\mu$ g (Zea *et al.*, 2017). For *B. subtilis*, cells at the basal end up to the apical regions demonstrated smaller phenotypic appearances when analyzed via SEM. But many of those observed cells were only cell membrane remnants ('ghosts') as visualized via TEM. Samples formed under both gravitational conditions exhibited elevated levels of "ghosts" and obviously destroyed cells in the central biofilm region with in agreement with other biofilm studies (Gingichashvili *et al.*, 2017). Growth in the biofilm center is strongly dependent on the nutrition from the agar underneath, but it also represents the exact position of the initial inoculation of the respective sample. Therefore, the center is probably the most nutrient-depleted region of the biofilm and this explains the loss of intact viable cells in the center. A decrease of intact bacteria was found in the biofilm center by TEM-imaging, which was also demonstrated by (Gingichashvili *et al.*, 2017). Both results indicate, that the increased detection of spores in the upper biofilm regions as well as the increased matrix in sim- $\mu$ g and cells in 1g, affect the whole biofilm center, which could be part of programmed cell death to facilitate biofilm dispersion via spore release (Gingichashvili *et al.*, 2017, Allocati *et al.*, 2015). However, spores were observed equally under both gravitational conditions. In contrast to literature (Branda *et al.*, 2001, Vlamakis *et al.*, 2013), spores were not only (but primary) found in the apical regions, but could also be detected via TEM in the middle (longitudinal) and basal regions. Cross sections (TEM) and morphological analyses of spores and mother cells revealed no structural differences between both gravitational conditions, which correlates with observations of *B. pumilus* spores exposed to  $\mu$ g (Vaishampayan *et al.*, 2012).

In contrast to the central regions, intermediate biofilm regions showed no extended basal matrix mat. Instead, differences in cell length and intercalating matrix elements occurred between 1g and sim- $\mu$ g biofilms. Sim- $\mu$ g cells appeared smaller and the EPS and matrix was less filigree, compared to 1g samples. Although, agar-based  $\mu$ g simulation offers less shear-forces in contrast to liquid media, occurring forces might impact cell size and matrix comparable to the biofilm center (Cheng *et al.*, 2014). Depending on the mechanical forces and age of the respective biofilm region, elastic, plastic and viscous properties in biofilms constantly change (Persat *et al.*, 2015) and therefore EPS and its composition can be seen as indicator for a variety of different environmental influences (Wilking *et al.*, 2011). Interestingly,  $\Delta$ *bslA* biofilms, which were not able to form most EPS components, did not exhibit morphological differences in any investigated biofilm region. Highly structured biofilms react to a change in shear forces or due to the loss of gravity perception, while the biofilm-deficient mutant was unaffected. Mauclaire and Egli hypothesize that that relation of shear stress and EPS-formation directly influences the 3-D structure of biofilms (Mauclaire & Egli, 2010), which partially matches with results of this study, showing, that the inner biofilm architecture rather than the biofilm surface is influenced by changing shear force levels. The biofilm surface structure is subject to other regulation systems such as localized cell death (Asally *et al.*, 2012).

However, the biofilm rim demonstrated identical structural features of biofilms grown under both gravitational conditions. This might be due to the fact, that only 40 h-old biofilms were analyzed.

Young cells at the biofilm edges are motile cells, not differentiated into immobile EPS-producing phenotypes (Mielich-Suss & Lopez, 2015, Cairns *et al.*, 2014). Biofilm samples under 1g and sim- $\mu$ g exhibited typical wave-forming propagation zones, which were also called “van Gogh” bundles, describing the synergistic interaction of surfactin production (motile cells) and immobile matrix-producing cells (van Gestel *et al.*, 2015). At the outmost edges of these bundles are flat, whereas with increasing proximity to the biofilm center they slowly rise and form aerial structures. Differences in cell size were not observed and TEM cross sections of individual cells of all regions, showed, that the cell wall thickness of vegetative cells was not influenced by sim- $\mu$ g. Biofilm growth and therewith raise in CFU takes place mainly in the peripheral areas and only to a small extent in the center and intermediate regions (Gingichashvili *et al.*, 2017).

The results of this study show no differences in the biofilm surface, apart from the fact that the hydrophobicity was increased under sim- $\mu$ g. The internal biofilm architecture demonstrated clear differences between sim- $\mu$ g and 1g, probably induced by shear force differences between both simulation methods. Depending on the biofilm region, they differ more (center) or less (edges) in structure.

#### 4.4 Impact of sim- $\mu$ g on spores

##### Sporulation and structure

Flight experiments demonstrated that spore size and structural characteristics were not affected by  $\mu$ g (Mennigmann & Lange, 1986). These findings match with SEM and TEM results of spores formed under sim- $\mu$ g. Spores were examined both within biofilms and individually after washing them in water. Phenotypical (SEM-images) and structural imaging via cross-sections revealed no differences between both gravitational conditions. Spores of different *Bacillus* spp. other than *B. subtilis* tend to clump during washing, which complicates isolation of individual spores. Although biofilms under sim- $\mu$ g showed increased EPS, no clumping of spores could be observed during isolation. As with all spore isolations from biofilms, spores had to be washed very often, especially when incubated on MSgg, due to an enhanced biofilm and therewith EPS production. Spores of the  $\Delta$ *bsIA* mutant and the  $\Delta$ *epsA-O* mutant were significantly easier to separate from cell debris. Sporulation levels and efficiency correlated with the amount of CFUs based on the maturity of the biofilm, demonstrating no differences between 1g and sim- $\mu$ g. In addition, monitoring by live cell microscopy of the germination of spores produced under sim- $\mu$ g showed identical results as 1g controls during and after germination.

##### Germination of sim- $\mu$ g spores

For studying germination and outgrowth, properties of *B. subtilis* spores were determined by analyzing several parameters like the germination efficiency as well as germination and growth kinetics. Optical measurements of a population of spores, forced to germinate by facing a germinant like L-valine, L-alanine or AGFK provided information on an averaged germination behavior regarding the efficiency and the kinetic (Nagler *et al.*, 2015). On single cell level these parameters may differ and demonstrate, that all spore populations are intrinsic heterogeneous to a certain extend (Pandey *et al.*, 2013, Zhang *et al.*, 2009) and sometimes harbor individual super-dormant spores (Ghosh & Setlow, 2009). By combining both methodical approaches by averaging the germination parameters and analyzing the individual germination properties, the physiological properties of the spores formed under sim- $\mu$ g were analyzed. In contrast to 1g spores, sim- $\mu$ g spores showed significantly



different germination behavior towards L-valine and LB (faster germination, more efficient) as well as towards L-alanine (slower germination, less efficient). Raman-spectroscopy of individual germinating spores in L-valine showed, that sim- $\mu$ g spores germinated significantly more homogenous and faster compared to spores formed under 1g. Spores are often characterized by their heterogeneity with regard to their germination behavior, which is influenced by various factors: The composition of germination receptors (GRs) and associated proteins form the "germinosome", which differs individually for each spore and is strongly influenced by environmental parameters and stresses (e.g. temperature, water and cation availability) during sporulation (Chen *et al.*, 2014, Ghosh *et al.*, 2012, Troiano *et al.*, 2015, Melly *et al.*, 2002). Germination properties can be correlated with the amount and composition of GRs and associated (spore coat-) proteins (Yi *et al.*, 2011, Troiano *et al.*, 2015). In contrast to sporulation under 1g conditions, the influence of shear forces during the simulation of  $\mu$ g is changed, which might result in an altered germinosome. Zhou *et al.* investigated the effects of adhesion and shear forces stress of spores and found that the pH, temperature and inorganic salt levels modify the surface during sporulation and thus probably the germination properties of spores (Xu Zhou *et al.*, 2017). Differences observed in germination between 1g and sim- $\mu$ g spores, which were partly heat- synchronized could also be explained by a change within the germinosome. An altered germinosome, would react differently in terms of a heat-induced conformational change of the GRs during synchronization receptors (Zhang *et al.*, 2009). Regarding the germination results, it cannot be generally said whether sim- $\mu$ g spores germinate more effectively or faster than their 1g control, only that they differ significantly from each other. Germinants affect germination differently depending on the composition of GRs and associated proteins (Troiano *et al.*, 2015, Stewart & Setlow, 2013, Moir & Cooper, 2015). Therefore, given results indicate the possibility that the germinosome composition has changed due to sim- $\mu$ g.

A further indication to support this hypothesis is shown by the germination behavior of sim- $\mu$ g spores in demineralized water at 37 °C, in which spores germinated spontaneously up to 60 %. The term "spontaneously" is used because no germinant was used during the experiment and washed spores do not exhibit such high germination rates in (warm) water (Sturm & Dworkin, 2015). Furthermore, spontaneous germination of spores formed under sim- $\mu$ g was analyzed by determining the SASP concentration via MALDI-TOF in the supernatant of spores exposed to 37 °C warm water. In accordance with photo spectrometric results, sim- $\mu$ g samples showed enhanced levels of SASP in the supernatant after one hour in contrast to 1g spores, which showed no SASP and therefore no germination. Van Vliet reviewed current literature and hypothesized that GerE, a transcriptional regulator of spore coat genes (McKenney *et al.*, 2013), plays the major role in spontaneous germination and is related to the spore coat structure and/or composition and influences therewith affects the germination behavior already during sporulation (van Vliet, 2015). Sturm and Dworkin showed that lower *gerE*-expression supports spontaneous germination (Sturm & Dworkin, 2015). This indicates, that sim- $\mu$ g might affect the transcription of *gerE* during sporulation and therewith affect the expression of more than 50 proteins (Eichenberger *et al.*, 2004). Mutants lacking *gerE* are able to form spores, but exhibit phenotypic structural differences (Ghosh *et al.*, 2008), which spores grown under sim- $\mu$ g did not demonstrated. Therefore, *gerE* is not completely suppressed, because spores grown under sim- $\mu$ g exhibited no phenotypical alterations, compared to  $\Delta$ *gerE*-mutants.

## 4.5 Impact of microgravity on survival of biofilms and spores

### Antibiotics

Increased microbial virulence under space flight conditions and the weakened immune system of astronauts could endanger future space missions (Taylor, 2015, Gueguinou *et al.*, 2009, Sonnenfeld *et al.*, 2003) wherein one of the most important strategies of bacteria and fungi is persisting via biofilm formation. Vaishampayan and Grohmann reviewed various papers regarding spacecraft isolates and biofilms with regard to their antibiotic resistance and came to the conclusion that antibiotic resistances are more prevalent among bacteria found on the space station (Vaishampayan & Grohmann, 2019). In their review article, Horneck *et al.* hypothesized, that the effects of reduced susceptibility could be caused by reduced antibiotic uptake of antibiotics or by increased bacterial resistance (Horneck *et al.*, 2010). However, not all studies showed that increased virulence was a generalized phenomenon. For example, several experiments showed an increase in antibiotic resistance under  $\mu\text{g}$  (Sobisch *et al.*, 2019, Lapchine *et al.*, 1986, Tixador *et al.*, 1985), while others were not affected (Sieradzki & Tomasz, 2003). Up to now, the experimental design of almost all conducted studies was focusing on finding enhanced virulence rather than testing for susceptibilities.

So far, the exact mechanisms for increased antibiotic resistance in microgravity are unknown. In frame of this thesis, the influence of several antibiotics during *B. subtilis* growth under 1g and sim- $\mu\text{g}$  were analyzed. The biofilm forming wild type as well as the biofilm deficient mutant  $\Delta\text{epsA-O}$  demonstrated no elevated or reduced resistances towards any tested antibiotic. These experiments indicate that the simulation of microgravity has no significant effect on the antibiotic resistance of *B. subtilis* biofilms, regardless of whether they can form biofilms. Morrison *et al.* investigated the susceptibility of *B. subtilis* on more than 70 different antibiotics and growth inhibiting substances (Morrison *et al.*, 2017). Their overall results conclude, that spaceflight conditions did not impact nor antibiotic resistance or susceptibility of *B. subtilis*, which is consistent with the results of this work, which were obtained under sim- $\mu\text{g}$ . Tirumalai *et al.* exposed *E. coli* for thousand generations to sim- $\mu\text{g}$  by using HARVs and found out, that in presence of chloramphenicol, antibiotic resistance towards several other antibiotics was enhanced under sim- $\mu\text{g}$  (Tirumalai *et al.*, 2019). Their results contradicted those of their previous study, which showed no antibiotic resistance during sim- $\mu\text{g}$  in the absence of chloramphenicol (Tirumalai *et al.*, 2017). Interestingly, the production of antibiotics such as cephalosporin (*Streptomyces clavuligerus*), rapamycin and others was shown to be reduced in Gram positive strains exposed to sim- $\mu\text{g}$  (Fang *et al.*, 1997, Fang *et al.*, 2000) and other in turn showed an increased antibiotic production of e.g. actinomycin D or avermectin (Lam *et al.*, 2002, Liu *et al.*, 2011). This implicates, that both antibiotic production and their effects on other organisms may be altered under microgravity, but bacteria react differently to it. For *B. subtilis*, results similar to those obtained under microgravity could be simulated experimentally, but transferability to other microorganisms is not possible due to the individual properties of each strain.

### Sim- $\mu\text{g}$ has no influence on spore resistance properties

Spores of *Geobacillus stearothermophilus* or *B. subtilis* are often used to verify and challenge the effectiveness of commercial sterilization procedures such as autoclaves (Finley & Fields, 1962, Wells-Bennik *et al.*, 2019, Lin *et al.*, 2018). Spores are bio-indicators due to their enormous resistance to various environmental influences. As mentioned before, spores are able to withstand physical stresses like radiation, heat, vacuum, shear forces and chemical stresses like detergents (changes in pH), osmotic imbalance and antibiotic treatments (Horneck *et al.*, 2010, Setlow, 2006b, Moeller *et al.*, 2007a, Melly *et al.*, 2002, Rose *et al.*, 2007). To investigate whether the resistance properties of

spores produced under sim- $\mu$ g differ or remain the same, 1g and sim- $\mu$ g spores were exposed to desiccation, X-rays, heavy ion radiation as well as to wet and dry heat.

Wet heat inactivation is a typical method to verify the resistance properties of bacteria and their spores (Melly & Setlow, 2001, Melly *et al.*, 2002, Coleman *et al.*, 2007). Spores formed under 1g and sim- $\mu$ g demonstrated almost identical survival rates after wet heat treatments. These results agree with those of the dry heat resistance assays, which are less effective on *B. subtilis* spores compared wet heat, but exhibit similar inactivation pattern of 1g and sim- $\mu$ g spores. Unfortunately, no comparable studies on the heat resistance of  $\mu$ g or sim- $\mu$ g spores have been published so far, so that comparability is not given. This also applies to the investigation of the dry heat resistance of *B. subtilis* spores, which also showed no differences in survival between 1g and sim- $\mu$ g spores. *B. subtilis* as soil-dwelling bacterium is often confronted with harmful conditions such as desiccation and UV-radiation. Due to the enormous desiccation resistance of spores, they can persist for many years to match a suitable moment for germination (Ulrich *et al.*, 2018). The results of the dry resistance of 1g and sim- $\mu$ g spores showed no differences during the investigated periods. In order to check long-term effects, they would probably have to be desiccated for a much longer period of time. The desiccation resistance of spores converts them into well-protected transmission vectors that support the spread of the species even to inhospitable places (Swick *et al.*, 2016, Horneck *et al.*, 1994). The transmission path from *B. subtilis* spores to the International Space Station consists simply of surviving the pre-decontamination procedures and then reaching the ISS as an opportunist as part of a supply delivery (Horneck *et al.*, 2010).

Apart from *Bacillus* spp., several other fungal and bacterial spores formed under  $\mu$ g were found and identified on the ISS (Knox *et al.*, 2016, Checinska *et al.*, 2015b, Checinska *et al.*, 2015a, Vaishampayan & Grohmann, 2019). Spore formation usually takes place under a stressful situations, such as nutrient deprivation (Tan & Ramamurthi, 2014), but results of sim- $\mu$ g experiments showed similar sporulation levels compared to 1g samples, which indicates, that sporulation was not enhanced due to altered shear force (stress) levels. Although differences in germination were observed, 1g and sim- $\mu$ g spores showed no difference in their resistance behavior. These results suggest that the spore morphology, which is essentially responsible for the resistance properties, is fully functional within spores formed under sim- $\mu$ g, but the composition or sensitivity of germination receptors might be altered by sim- $\mu$ g.

Space is a hostile place for all organisms due to the increased radiation levels. Radiation doses within the space station vary widely, dependent on the respective module and the shielding. Experiments with suspended *B. subtilis* spores exposed to space radiation (mainly solar UV filtered to  $\sim 254$  nm of a total UV range of 10-400 nm) showed high survival rates even at high doses in contrast to dried spores exposed vacuum and solar UV (Buecker *et al.*, 1974). For testing the effects of GCR on spore survival, *B. subtilis* spores were shielded within space hardware, only allowing HZE particles to penetrate. Sample carriers were then exposed to space, but no differences in survival rates compared to untreated samples were found (Buecker *et al.*, 1972). These and other studies demonstrated that in order to observe a reduction in survival, high doses are needed. Therefore, doses tested on *B. subtilis* spores in frame of this thesis resemble extreme radiation levels to illustrate the resistance properties.

To investigate the effects of space radiation (X-ray and heavy ions) on the survival of 1g and sim- $\mu$ g spores, spores (wild type and various mutants) were isolated from biofilms, suspended and subsequently irradiated. The aim of the experiments was to determine whether there are resistance differences between 1g and sim- $\mu$ g spores regarding X-ray and GCR treatments and whether the absence of biofilm relevant genes during sporulation has an influence on the resistance behavior.

Overall, no differences in survival between 1g and sim- $\mu$ g spores and biofilms were observed. Furthermore, the lack of specific biofilm genes and therewith altered growth and sporulation conditions did not influence the survival. As expected, spores were less strongly inactivated by helium ions. Argon ions and gamma radiation showed almost identical spore inactivation levels at comparable doses. These results support the findings from other resistance and survival assays performed in frame of this thesis: That sim- $\mu$ g seems to have no influence on the spore structure and the subsequent DNA-repair mechanisms, which are needed during spore revival in the germination phase (Fuchs *et al.*, 2017b, Vlašić *et al.*, 2014). Moeller *et al.* analyzed the influence of spores lacking certain spore characteristic properties, such as SASP and DPA (Moeller *et al.*, 2012a). They concluded, that both proteins are essential for the survival after HZE-treatments (or simulated GCR), which supports the hypothesis that there are no significant differences in SASP- or DPA concentration during the simulation of  $\mu$ g, which might influence the resistance properties. Unfortunately, investigating the resistance of spores by CFU-determination can be seen critically: Extreme doses of heavy ions and gamma radiation may completely inhibit spores from germination (Gould, 1970), but often spores germinate and are not able to form a vegetative cell. Some cells are unable to divide themselves and from exceptional long rods, stay small or burst (Fuchs *et al.*, 2017b). These cells are still viable but non-cultivable also known as VBNCs (Li *et al.*, 2014). Therefore, results of resistance and survival assays must be considered with caution, as the number of still viable cells can be underestimated. Viable cells may not be able to divide any more, but they may serve as donors of DNA and thus provide potential virulence factors to other microorganisms.

#### 4.6 Transcriptomics and proteomics

In contrast to transcriptomic analysis of samples grown under different gravity regimes, quantitative proteomics offered the comparison of the overall protein abundance. Results of transcriptomics and proteomics often differ, due to the various post-translational processes and the overall short half-life of mRNA. By combining both methods, potential alterations between different growth conditions of biofilms can be better detected and compared. Unfortunately, the transcriptomic results within this thesis were based on individual pooled samples in order to acquire a sufficient amount of RNA and therefore only one sample per condition and time point could be analyzed and results in general should be considered with caution. Nevertheless, five samples were combined into a single sample thus providing a stable mean value. Simulated microgravity showed to impact  $\sim 7$  % of the overall transcriptome within young biofilms, which matches with observations from the proteome, which exhibited a significantly upregulation of 11.71 % of all expressed proteins after 24 h and 6.02 % after 72 h. A general response on the proteomic and transcriptomic level to microgravity was not observed, which corresponds results from a meta-analysis of eight spaceflight data sets performed by Morrison and Nicholson (Morrison & Nicholson, 2018). They concluded that the main variance within the experiments occurred due to the experimental design.

Only seven common proteins were found to be upregulated at both investigated time points, a relatively small number considering that 129 (24 h) and 93 (72 h) different proteins were significantly upregulated. The most interesting common protein was NtdB, which acts as a kanosamine-6-phosphate phosphatase, an antibiotic which is a constituent of kanamycin (Milner *et al.*, 1996, Vetter *et al.*, 2013). Kanosamine inhibits the cell wall synthesis of certain fungi such as oomycetes, ascomycetes, basidiomycetes and deuteromycetes as well as other bacteria (Milner *et al.*, 1996). The production of antibiotics is often related to the recognition of different environmental stresses (Stein, 2005), which might be related to potential stresses occurring during the simulation of  $\mu$ g. In total, 12 respectively 9 proteins associated with antibiotic biosynthesis exhibited significantly

enhanced levels in sim- $\mu$ g biofilms after 24 and 72 h incubation. A general increase or decrease of antibiotic production under  $\mu$ g or sim- $\mu$ g is controversially discussed in the literature (Horneck *et al.*, 2010) and could be less due to microgravity than to the stress to which the cells were exposed to (Benoit *et al.*, 2006, Huang *et al.*, 2018). Interestingly, no biofilm related proteins were found to be upregulated in sim- $\mu$ g biofilms, contrasting the results from Morrison *et al.* which demonstrated elevated transcript levels of e.g. *bslA*, *ycaA* and *luxS* in *B. subtilis* flight samples (liquid culturing in trypticase soy yeast extract medium at room temperature) (Morrison *et al.*, 2019). Chiang and colleagues were the first research group investigating the proteome of *B. pumilus* exposed to outer space conditions (Chiang *et al.*, 2019). Their results are barely comparable, because they exposed spores to different pressure levels (up to  $10^{-4}$  Pa), solar and Mars UV as well as to extreme temperature fluxes and germinated them on Earth. Since all factors probably have an effect on the germination behavior and the subsequent vegetative cell type, gravitation-specific aspects probably cannot be identified. Nevertheless, *B. pumilus* cells showed a partwise upregulated secondary metabolism, indicating that vegetative cells respond to the stress they have experienced in the spore form, which supports the findings of Morrison *et al.* and the results of this thesis (Morrison *et al.*, 2019).

Among the downregulated proteins, only three were identified to be repressed at both investigated time points. One of them, the essential ribosomal protein RpmD (L30), was found to be significantly downregulated after 24 h and 72 h. This is interesting because after only 24 h the biofilm and thus the protein biosynthesis and therewith the associated ribosome quantity is still in growth. A reduction of L30 was previously reported to be caused by carbon starvation stress (de Jong *et al.*, 2012). Yet it seems to be unlikely, that sim- $\mu$ g causes a significant nutrient limitation for biofilms growing on agar-based media, because no significant changes in CFU or sporulation have been observed in identical experimental setups. In contrast to upregulated proteins involved in antibiotic production, 9 proteins also associated with antibiotic biosynthesis were significantly downregulated after 24 h, whereas after 72 h no downregulated proteins involved in the production of antibiotics were found. This would support the findings of other bacterial strains, which showed increased antibiotic production under long time exposure to microgravity (Benoit *et al.*, 2006). Although *B. subtilis* biofilms seem to show an increase in antibiotic synthesis associated proteins, experiments on antibiotic susceptibility showed no differences in survival.

#### 4.7 Summary: Effect of sim- $\mu$ g on biofilms and spores

So far, the field of research investigating simulated gravity on *B. subtilis* biofilms is still in its infancy and with this thesis, standardized *B. subtilis* biofilms under sim- $\mu$ g were investigated in detail for the first time. Almost all experiments conducted unveiled novel insights in the field which often overlapped with comparable space studies or other sim- $\mu$ g experiments. In order to test the hypotheses previously formulated, biofilms were examined with regard to their structure and composition, their resistance properties and their proteome and transcriptome. As result, sim- $\mu$ g seemed to affect the inner biofilm architecture, but did not alter the biofilm topography, which proved to be more hydrophobic under sim- $\mu$ g. Within the biofilm, depending on the region observed, cell phenotypes changes and the amount and structure of EPS differed between both investigated gravitational conditions. Differences in the cell or spore composition could not be detected and resistance properties towards ionizing radiation, desiccation and antibiotics remained unchanged. Interestingly, sim- $\mu$ g seemed to affect ~7 % of the transcriptome as well as 6-11 % of the proteome. Thus the first hypothesis could be confirmed, in which differences in the biofilm structure and composition under sim- $\mu$ g could be clarified. In the second hypothesis it was assumed, based on the given literature, that differences in the resistance behavior between 1g and sim- $\mu$ g could be observed. This could not be confirmed by the experiments conducted in the context of this thesis. The resistance properties of both complex biofilms and spores did not seem to be influenced by sim- $\mu$ g. However, potential resistance properties, such as increased hydrophobicity or increased antibiotic production, appeared to be more pronounced under sim- $\mu$ g.

In addition to all conducted biofilm experiments, spores grown under sim- $\mu$ g were investigated regarding their resistances as well as germination properties. Structural and phenotypic differences were not observed and resistance properties remained unchanged. The only properties, which seemed to be affected by sim- $\mu$ g was the more homologous germination reaching higher germination efficiencies as well as the observed spontaneous germination. Therefore, the third hypothesis was at least partially confirmed in which it was assumed that sim- $\mu$ g influences sporulation and germination. Changes in sporulation efficiency could not be proven experimentally.

**Table 10: Overview of investigated biological parameters affected or unaffected by sim- $\mu$ g**

In frame of this thesis spore resistance, germination and outgrowth (upper table) and biofilms (bottom table) of *B. subtilis* have been investigated regarding their properties after sim- $\mu$ g exposure. The most important parameters, which were experimentally proved to be either unaffected (left side, blue) or affected (right side, green) by sim- $\mu$ g are given underneath the spore and biofilm section.

##### Spores

Unaffected in sim- $\mu$ g	Affected by sim- $\mu$ g
Spore structure	Homogenous germination
Desiccation resistance	Germination efficiency
X-ray resistance	Spontaneous germination
Heavy ion resistance	
Dry & wet heat resistance	
Sporulation efficiency	

## Biofilms

Unaffected in sim- $\mu$ g	Affected by sim- $\mu$ g
Topography	Inner architecture
Desiccation resistance	Size and phenotype of cells
X-ray resistance	EPS composition and structure
Heavy ion resistance	Hydrophobicity
Composition (CFU/spores)	~7 % of the transcriptome
Antibiotic resistance	~6-11 % of the proteome
Motility and swarming	

In summary, several changes between 1g and sim- $\mu$ g in *B. subtilis* biofilms were experimentally identified and determined. Given results should be considered with the knowledge that the simulation method used is only a mathematical approximation of a shear force reduction and therefore probably cannot reflect the conditions under real microgravity. Nevertheless, the 2-D clinostat is scientifically recognized and has been used for decades. Interestingly, many of the observed features only expressed under sim- $\mu$ g often correlate with the typical stress response of *B. subtilis* cells and biofilms. This actually was also shown in several independent space experiments, which were able to demonstrate these (found changes in frame of this thesis) and other stress responses under microgravity. Therefore, any results obtained under both sim- $\mu$ g and real microgravity should always be considered under the aspect of a general stress response. Presumably, the stress caused by shear-force reduction/microgravity leads to most changes in biofilms and may even have a lasting effect on the germination properties of *B. subtilis*. Thus the simulation of microgravity with the help of 2-D clinostats proved to be a suitable method to simulate comparable space experiments on earth at low cost. Of course they cannot replace space research, but the method can still provide preliminary information to investigate microbiological samples for possible changes under sim- $\mu$ g and thus prepare space experiments. As ground control clinostats could also be used in parallel to experiments in space to refine and expand the method. For further experiments, the RPM would also be recommended, which can serve as a third pillar of research in the field of microbial behavior under microgravity.

## 5. Outlook

In order to investigate the effects of space related parameters on bacterial samples, ground based simulation facilities and techniques provide a variety of possibilities. In space, all parameters occur together, but to investigate the extent to which a single parameter affects complex biological systems such as *B. subtilis* biofilms, this parameter must be considered individually. As shown before, depending on whether the 2-D clinostat or the RPM, biological results differed and will be most likely differ, if grown under real microgravity. Therefore, it would be interesting to verify the observed gravitational effects on spores and biofilms under further RPM experiments. It would be interesting to see whether, despite different results between the two simulation methods, the same trends could be observed which differ in contrast to 1g incubation. The focus of this thesis was mainly concentrating on agar-based biofilm cultivation. For the approximation to space conditions the biofilm formation in liquid culture could also be interesting, which was excluded in the context of this thesis due to the technical limitations of sim- $\mu$ g devices. In order to answer the question to what extent the simulation corresponds to real microgravity, only a space experiment under similar conditions would provide the final answer. But most of the methods, e.g. contact angle measurements or imaging methods cannot be applied in space. Therefore, suitable experiments and methods could be used to compare biofilm formation under  $\mu$ g (e.g. on the ISS) and ground-based sim- $\mu$ g. In space, samples can be centrifuged to achieve terrestrial g-forces and it would be interesting to compare 1g controls from Earth to those achieved in space via centrifugation. Comparing the results, both from space and terrestrial biofilm/spore formation, would provide insight to what extent the respective simulation method is suitable to simulate results of the respective other condition.

In the near future, further long-term missions are to be carried out and thus, the interest in the investigation of potentially altered microbial virulence under space conditions is growing. In frame of this thesis, only *B. subtilis* virulence factors such as spore formation and several resistance parameters have been investigated. Although barely any changes in resistance properties were found in *B. subtilis* under sim- $\mu$ g, this is not representative for all microorganisms. Therefore, the investigation of further (biofilm-forming) microorganisms with regard to their virulence or pathogenicity under space conditions would help to understand and counteract bacterial and fungal behavior.

In addition, it would be interesting to study the adherence and dispersal properties of *B. subtilis* spores, which might be affected by the influence of changing shear forces during sim- $\mu$ g incubation. The germinosome of spore formed under sim- $\mu$ g could be compared in detail with the germinosome of 1g spores to find potential differences in the composition or find a proof, that the composition of GRs is not changed under different gravitational levels. All previously performed studies regarding the germination properties of spores were performed under 1g conditions, but information about germination under  $\mu$ g or sim- $\mu$ g is missing and was not subjected in space research yet.

Even after more than sixty years of manned spaceflight, we still know little about the impact of space conditions on both eukaryotic and prokaryotes. In order to understand the cellular behavior in space, more (Long-term) space missions have to be conducted to ensure that the future of manned space missions can be carried out safely and in a controlled manner. In contrast to risks, microorganisms can also possess positive properties, which in addition to biotechnological approaches bring further advantages such as biomining, oxygen production, nitrogen recycling and bioremediation. Whatever our path in the future of space travel will be, we will always travel together with microorganisms - so we should never stop trying to understand them.



## 6. Bibliography

- Agarwal, R. (2009) Allergic bronchopulmonary aspergillosis. *Chest* **135**: 805-826.
- Aguilar, C., Vlamakis, H., Losick, R., and Kolter, R. (2007) Thinking about *Bacillus subtilis* as a multicellular organism. *Current Opinion in Microbiology* **10**: 638-643.
- Alekhoa, T.A., Zakharchuk, L.M., Tatarinova, N.Y., Kadnikov, V.V., Mardanov, A.V., Ravin, N.V., and Skryabin, K.G. (2015) Diversity of bacteria of the genus *Bacillus* on board of international space station. *Biochemistry and biophysics* **465**: 347-350.
- Allard-Massicotte, R., Tessier, L., Lécuyer, F., Lakshmanan, V., Lucier, J.-F., Garneau, D., Caudwell, L., Vlamakis, H., Bais, H.P., and Beauregard, P.B. (2016) *Bacillus subtilis* early colonization of *Arabidopsis thaliana* roots involves multiple chemotaxis receptors. *mBio* **7**: e01664-01616.
- Allocati, N., Masulli, M., Di Ilio, C., and De Laurenzi, V. (2015) Die for the community: An overview of programmed cell death in bacteria. *Cell death & disease* **6**: e1609.
- Alzahrani, O.M., and Moir, A. (2014) Spore germination and germinant receptor genes in wild strains of *Bacillus subtilis*. *Journal of applied microbiology* **117**: 741-749.
- Andersson, A., Ronner, U., and Granum, P.E. (1995) What problems does the food industry have with the spore-forming pathogens *Bacillus cereus* and *Clostridium perfringens*? *International Journal of Food Microbiology* **28**: 145-155.
- Anken, R., and Rahmann, H., (2002) *Gravitational Zoology: How Animals Use and Cope with Gravity*.
- Arnauteli, S., MacPhee, C.E., and Stanley-Wall, N.R. (2016) Just in case it rains: building a hydrophobic biofilm the *Bacillus subtilis* way. *Current Opinion in Microbiology* **34**: 7-12.
- Arnauteli, S., Matoz-Fernandez, D.A., Porter, M., Kalamara, M., Abbott, J., MacPhee, C.E., Davidson, F.A., and Stanley-Wall, N.R. (2019) Pulcherrimin formation controls growth arrest of the *Bacillus subtilis* biofilm. *Proceedings of the National Academy of Sciences of the United States of America* **116**: 13553-13562.
- Arweiler, N.B., and Netuschil, L. (2016) The Oral Microbiota. *Advances in experimental medicine and biology* **902**: 45-60.
- Asally, M., Kittisopikul, M., Rue, P., Du, Y., Hu, Z., Cagatay, T., Robinson, A.B., Lu, H., Garcia-Ojalvo, J., and Suel, G.M. (2012) Localized cell death focuses mechanical forces during 3D patterning in a biofilm. *Proceedings of the National Academy of Sciences of the United States of America* **109**: 18891-18896.
- Atluri, S., Ragkousi, K., Cortezzo, D.E., and Setlow, P. (2006) Cooperativity between different nutrient receptors in germination of spores of *Bacillus subtilis* and reduction of this cooperativity by alterations in the GerB receptor. *Journal of Bacteriology* **188**: 28-36.
- Bagliani, P., Sabbatini, M., and Horneck, G., (2008) Astrobiology experiments in low Earth orbit: facilities, instrumentation, and results. In *Complete Course in Astrobiology*, pp. 273-319.
- Bai, J., Chao, Y., Chen, Y., Wang, S., and Qiu, R. (2019) The effect of interaction between *Bacillus subtilis* DBM and soil minerals on Cu(II) and Pb(II) adsorption. *Journal of Environmental Sciences* **78**: 328-337.
- Bais, H.P., Fall, R., and Vivanco, J.M. (2004) Biocontrol of *Bacillus subtilis* against infection of *Arabidopsis* roots by *Pseudomonas syringae* is facilitated by biofilm formation and surfactin production. *Plant physiology* **134**: 307-319.
- Baker, P.W., Meyer, M.L., and Leff, L.G. (2004) *Escherichia coli* growth under modeled reduced gravity. *Microgravity science and technology* **15**: 39-44.
- Barrila, J., Ott, C.M., LeBlanc, C., Mehta, S.K., Crabbe, A., Stafford, P., Pierson, D.L., and Nickerson, C.A. (2016) Spaceflight modulates gene expression in the whole blood of astronauts. *NPJ microgravity* **2**: 16039.
- Beauregard, P.B., Chai, Y., Vlamakis, H., Losick, R., and Kolter, R. (2013) *Bacillus subtilis* biofilm induction by plant polysaccharides. *Proceedings of the National Academy of Sciences of the United States of America* **110**: E1621-E1630.
- Bell, T.E., (2007) Preventing "sick" spaceships. In. T. Phillips (ed). [https://science.nasa.gov/science-news/science-at-nasa/2007/11may\\_locad3](https://science.nasa.gov/science-news/science-at-nasa/2007/11may_locad3)
- Benner, S.A. (2010) Defining life. *Astrobiology* **10**: 1021-1030.
- Benoit, M.R., Li, W., Stodieck, L.S., Lam, K.S., Winther, C.L., Roane, T.M., and Klaus, D.M. (2006) Microbial antibiotic production aboard the International Space Station. *Applied Microbiology and Biotechnology* **70**: 403-411.
- Blachowicz, A., Chiang, A.J., Romsdahl, J., Kalkum, M., Wang, C.C.C., and Venkateswaran, K. (2019) Proteomic characterization of *Aspergillus fumigatus* isolated from air and surfaces of the International Space Station. *Fungal genetics and biology : FG & B* **124**: 39-46.

- Black, E.P., Koziol-Dube, K., Guan, D., Wei, J., Setlow, B., Cortezzo, D.E., Hoover, D.G., and Setlow, P. (2005) Factors influencing germination of *Bacillus subtilis* spores via activation of nutrient receptors by high pressure. *Applied and environmental microbiology* **71**: 5879-5887.
- Blanchette, K.A., and Wenke, J.C. (2018) Current therapies in treatment and prevention of fracture wound biofilms: why a multifaceted approach is essential for resolving persistent infections. *Journal of Bone and Joint Infection* **3**: 50-67.
- Blumberg, B.S. (2003) The NASA Astrobiology Institute: early history and organization. *Astrobiology* **3**: 463-470.
- Bornemann, G., Waßer, K., Tonat, T., Moeller, R., Bohmeier, M., and Hauslage, J. (2015) Natural microbial populations in a water-based biowaste management system for space life support. *Life sciences in space research* **7**: 39-52.
- Borst, A.G., and van Loon, J.J.W.A. (2008) Technology and Developments for the random positioning machine, RPM. *Microgravity science and technology* **21**: 287.
- Bozzola, J.J. (2007) Conventional specimen preparation techniques for transmission electron microscopy of cultured cells. *Methods in Molecular Biology* **369**: 1-18.
- Brack, A., (2008) Astrobiology: From the origin of life on Earth to life in the universe. In *Complete Course in Astrobiology*, pp. 1-22.
- Branda, S.S., Chu, F., Kearns, D.B., Losick, R., and Kolter, R. (2006) A major protein component of the *Bacillus subtilis* biofilm matrix. *Molecular microbiology* **59**: 1229-1238.
- Branda, S.S., Gonzalez-Pastor, J.E., Ben-Yehuda, S., Losick, R., and Kolter, R. (2001) Fruiting body formation by *Bacillus subtilis*. *Proceedings of the National Academy of Sciences of the United States of America* **98**: 11621-11626.
- Branda, S.S., Gonzalez-Pastor, J.E., Dervyn, E., Ehrlich, S.D., Losick, R., and Kolter, R. (2004) Genes involved in formation of structured multicellular communities by *Bacillus subtilis*. *Journal of Bacteriology* **186**: 3970-3979.
- Branda, S.S., Vik, S., Friedman, L., and Kolter, R. (2005) Biofilms: the matrix revisited. *Trends in microbiology* **13**: 20-26.
- Brehm-Stecher, B.F., and Johnson, E.A. (2004) Single-cell microbiology: tools, technologies, and applications. *Microbiology and Molecular Biology Reviews* **68**: 538-559
- Bridier, A., Briandet, R., Thomas, V., and Dubois-Brissonnet, F. (2011) Resistance of bacterial biofilms to disinfectants: a review. *Biofouling* **27**: 1017-1032.
- Bridier, A., Sanchez-Vizueté, P., Guilbaud, M., Piard, J.C., Naitali, M., and Briandet, R. (2015) Biofilm-associated persistence of food-borne pathogens. *Food microbiology* **45**: 167-178.
- Briegleb, W. (1992) Some qualitative and quantitative aspects of the fast-rotating clinostat as a research tool. *ASGSB Bulletin* **5**: 23-30.
- Brungs, S., Egli, M., Wuest, S.L., M. Christianen, P.C., W. A. van Loon, J.J., Ngo Anh, T.J., Hemmersbach, R. (2016) Facilities for simulation of microgravity in the ESA ground-based facility programme. *Microgravity Science and Technology* **28**: 191-203.
- Brungs, S., Hauslage, J., and Hemmersbach, R. (2019) Validation of random positioning versus clinorotation using a macrophage model system. *Microgravity science and technology* **31**: 223-230.
- Brungs, S., Hauslage, J., Hilbig, R., Hemmersbach, R., and Anken, R. (2011) Effects of simulated weightlessness on fish otolith growth: Clinostat versus Rotating-Wall Vessel. *Advances in Space Research* **48**: 792-798.
- Brungs, S., Kolanus, W., and Hemmersbach, R. (2015) Syk phosphorylation - a gravisensitive step in macrophage signalling. *Cell communication and signaling* **13**: 9.
- Buecker, H., and Horneck, G. (1975) The biological effectiveness of HZE-particles of cosmic radiation studied in the Apollo 16 and 17 Biostack experiments. *Acta Astronautica* **2**: 247-264.
- Buecker, H., Horneck, G., Reinholz, E., Scheuermann, W., Ruether, W., Graul, E., Planel, H., Soleilhavoup, J., Cuer, P., and Kaiser, R. (1972) Biomedical Experiments. Part A: Biostack Experiment. <https://ntrs.nasa.gov/search.jsp?R=19730013034>
- Buecker, H., Horneck, G., Wollenhaupt, H., Schwager, M., and Taylor, G.R., (1974) Viability of *Bacillus subtilis* spores exposed to space environment in the M191 experiment system aboard Apollo 16. In: *Life sciences and space research*. P.H.A. Sneath (ed). Pergamon, pp. 209-213.
- Burgess, C., and Dubbs, C., (2007) *Animals in Space: From Research Rockets to the Space Shuttle*.
- Byloos, B., Coninx, I., Van Hoey, O., Cockell, C., Nicholson, N., Ilyin, V., Van Houdt, R., Boon, N., and Leys, N. (2017) The impact of space flight on survival and interaction of *Cupriavidus metallidurans* CH34 with basalt, a volcanic moon analog rock. *Frontiers in microbiology* **8**: 671.
- Cairns, L.S., Hopley, L., and Stanley-Wall, N.R. (2014) Biofilm formation by *Bacillus subtilis*: new insights into regulatory strategies and assembly mechanisms. *Molecular microbiology* **93**: 587-598.

- Calfee, M.W., Rose, L.J., Tufts, J., Morse, S., Clayton, M., Touati, A., Griffin-Gatchalian, N., Slone, C., and McSweeney, N. (2014) Evaluation of sampling methods for *Bacillus* spore-contaminated HVAC filters. *Journal of microbiological methods* **96**: 1-5.
- Carrera, M., Zandomeni, R.O., Fitzgibbon, J., and Sagripanti, J.-L. (2007) Difference between the spore sizes of *Bacillus anthracis* and other *Bacillus* species. *Journal of Applied Microbiology* **102**: 303-312.
- Castro, V.A., Thrasher, A.N., Healy, M., Ott, C.M., and Pierson, D.L. (2004) Microbial characterization during the early habitation of the International Space Station. *Microbial ecology* **47**: 119-126.
- Chai, Y., Chu, F., Kolter, R., and Losick, R. (2008) Bistability and biofilm formation in *Bacillus subtilis*. *Molecular microbiology* **67**: 254-263.
- Chai, Y., Norman, T., Kolter, R., and Losick, R. (2010) An epigenetic switch governing daughter cell separation in *Bacillus subtilis*. *Genes & development* **24**: 754-765.
- Chaudhary, N., and Marr, K.A. (2011) Impact of *Aspergillus fumigatus* in allergic airway diseases. *Clinical and Translational Allergy* **1**: 4-4.
- Checinska, A., Paszczynski, A., and Burbank, M. (2015a) *Bacillus* and other spore-forming genera: variations in responses and mechanisms for survival. *Annual review of food science and technology* **6**: 351-369.
- Checinska, A., Probst, A.J., Vaishampayan, P., White, J.R., Kumar, D., Stepanov, V.G., Fox, G.E., Nilsson, H.R., Pierson, D.L., Perry, J., and Venkateswaran, K. (2015b) Microbiomes of the dust particles collected from the International Space Station and Spacecraft Assembly Facilities. *Microbiome* **3**: 50.
- Checinska Sielaff, A., Kumar, R., Pal, D., Mayilraj, S., and Venkateswaran, K. (2016) *Solibacillus kalamii* sp. nov., isolated from the International Space Station HEPA filter system. *International Journal of Systematic and Evolutionary Microbiology*. **4**:896-90
- Checinska Sielaff, A., Urbaniak, C., Mohan, G.B.M., Stepanov, V.G., Tran, Q., Wood, J.M., Minich, J., McDonald, D., Mayer, T., Knight, R., Karouia, F., Fox, G.E., and Venkateswaran, K. (2019) Characterization of the total and viable bacterial and fungal communities associated with the International Space Station surfaces. *Microbiome* **7**: 50.
- Chen, Y., Ray, W.K., Helm, R.F., Melville, S.B., and Popham, D.L. (2014) Levels of germination proteins in *Bacillus subtilis* dormant, superdormant, and germinating spores. *PloS one* **9**: e95781.
- Cheng, X., Xu, X., Chen, J., Zhou, X., Cheng, L., Li, M., Li, J., Wang, R., Jia, W., and Li, Y.-Q. (2014) Effects of simulated microgravity on *Streptococcus mutans* physiology and biofilm structure. *FEMS microbiology letters* **359**: 94-101.
- Chiang, A.J., Malli Mohan, G.B., Singh, N.K., Vaishampayan, P.A., Kalkum, M., and Venkateswaran, K. (2019) Alteration of proteomes in first-generation cultures of *Bacillus pumilus* spores exposed to outer space. *mSystems* **4**: e00195-00119.
- Cleland, C.E., and Chyba, C.F. (2002) Defining 'Life'. *Origins of life and evolution of the biosphere* **32**: 387-393.
- Cockell, C.S., (2015) *Astrobiology: understanding life in the universe*. John Wiley & Sons.
- Cockell, C.S. (2016) The similarity of life across the universe. *Molecular biology of the cell* **27**: 1553-1555.
- Cockell, C.S., Hecht, L., Landenmark, H., Payler, S.J., and Snape, M. (2018) Rapid colonization of artificial endolithic uninhabited habitats. *International Journal of Astrobiology* **17**: 386-401.
- Coleman, W.H., Chen, D., Li, Y.-q., Cowan, A.E., and Setlow, P. (2007) How moist heat kills spores of *Bacillus subtilis*. *Journal of Bacteriology* **189**: 8458.
- Commichau, F.M., Blötz, C., and Stülke, J., (2015) Methods in molecular biology of bacteria. In *Method collection*. pp. 16-18.
- Conn, H.J. (1930) The Identity of *Bacillus subtilis*. *The Journal of Infectious Diseases* **46**: 341-350.
- Cook, A.M., and Brown, M.R. (1965) Relationship between heat activation and percentage colony formation for *Bacillus stearothermophilus* spores: effects of storage and pH of the recovery medium. *Journal of Applied Bacteriology* **28**: 361-364.
- Cooper, D.G., Macdonald, C.R., Duff, S.J., and Kosaric, N. (1981) Enhanced production of surfactin from *Bacillus subtilis* by continuous product removal and metal cation additions. *Applied and environmental microbiology* **42**: 408-412.
- Cortezão, M., Fuchs, F.M., Commichau, F.M., Eichenberger, P., Schuerger, A.C., Nicholson, W.L., Setlow, P., and Moeller, R. (2019) *Bacillus subtilis* spore resistance to simulated Mars surface conditions. *Frontiers in microbiology* **10**.
- Corydon, T.J., Kopp, S., Wehland, M., Braun, M., Schutte, A., Mayer, T., Hulsing, T., Oltmann, H., Schmitz, B., Hemmersbach, R., and Grimm, D. (2016) Alterations of the cytoskeleton in human cells in space proved by life-cell imaging. *Scientific reports* **6**: 20043.
- COSPAR, (2012) Committee on space research (COSPAR). In: *COSPAR Annual Meeting 2012*.

- Costerton, J.W., Cheng, K.J., Geesey, G.G., Ladd, T.I., Nickel, J.C., Dasgupta, M., and Marrie, T.J. (1987) Bacterial biofilms in nature and disease. *Annual review of microbiology* **41**: 435-464.
- Costerton, J.W., Stewart, P.S., and Greenberg, E.P. (1999) Bacterial biofilms: a common cause of persistent infections. *Science (New York, N.Y.)* **284**: 1318-1322.
- Costerton, W., Veeh, R., Shirtliff, M., Pasmore, M., Post, C., and Ehrlich, G. (2003) The application of biofilm science to the study and control of chronic bacterial infections. *The Journal of Clinical Investigation* **112**: 1466-1477.
- Council, N.R., (2006) *Preventing the forward contamination of Mars*, p. 166. The National Academies Press, Washington, DC.
- Crick, F. (1970) Central dogma of molecular biology. *Nature* **227**: 561-563.
- Dang, H., and Lovell, C.R. (2015) Microbial surface colonization and biofilm development in marine environments. *Microbiology and Molecular Biology Reviews* **80**: 91-138.
- Darouiche, R.O. (2004) Treatment of infections associated with surgical implants. *The New England journal of medicine* **350**: 1422-1429.
- Dawes, I.W., Kay, D., and Mandelstam, J. (1969) Sporulation in *Bacillus subtilis*. Establishment of a time scale for the morphological events. *Journal of general microbiology* **56**: 171-179.
- de Carvalho, C. (2017) Biofilms: Microbial strategies for surviving UV exposure. *Advances in experimental medicine and biology* **996**: 233-239.
- de Jong, A., van der Meulen, S., Kuipers, O.P., and Kok, J. (2015) T-REx: Transcriptome analysis webserver for RNA-seq Expression data. *BMC Genomics* **16**: 663.
- de Jong, I.G., Veening, J.W., and Kuipers, O.P. (2012) Single cell analysis of gene expression patterns during carbon starvation in *Bacillus subtilis* reveals large phenotypic variation. *Environmental microbiology* **14**: 3110-3121.
- de Vos, W.M. (2015) Microbial biofilms and the human intestinal microbiome. *NPJ Biofilms Microbiomes* **1**: 15005-15005.
- Decho, A.W. (2000) Microbial biofilms in intertidal systems: an overview. *Continental Shelf Research* **20**: 1257-1273.
- Deegan, R.D., Bakajin, O., Dupont, T.F., Huber, G., Nagel, S.R., and Witten, T.A. (1997) Capillary flow as the cause of ring stains from dried liquid drops. *Nature* **389**: 827-829.
- Dervaux, J., Magniez, J.C., and Libchaber, A. (2014a) On growth and form of *Bacillus subtilis* biofilms. *Interface Focus* **4**: 20130051.
- Di Giulio, M. (2010) Biological evidence against the panspermia theory. *Journal of theoretical biology* **266**: 569-572.
- Diethmaier, C., Pietack, N., Gunka, K., Wrede, C., Lehnik-Habrink, M., Herzberg, C., Hubner, S., and Stulke, J. (2011) A novel factor controlling bistability in *Bacillus subtilis*: the YmdB protein affects flagellin expression and biofilm formation. *Journal of Bacteriology* **193**: 5997-6007.
- Dittmann, C., Han, H.M., Grabenbauer, M., and Laue, M. (2015) Dormant *Bacillus* spores protect their DNA in crystalline nucleoids against environmental stress. *Journal of structural biology* **191**: 156-164.
- Dix, D.E. (2002) What is life? Prerequisites for a definition. *The Yale journal of biology and medicine* **75**: 313-321.
- Dobrowolski, R., Krzyszczyk, A., Dobrzyńska, J., Podkościelna, B., Zięba, E., Czemińska, M., Jarosz-Wilkotłazka, A., and Stefaniak, E.A. (2019) Extracellular polymeric substances immobilized on microspheres for removal of heavy metals from aqueous environment. *Biochemical Engineering Journal* **143**: 202-211.
- Dragoš, A., Kiesewalter, H., Martin, M., Hsu, C.-Y., Hartmann, R., Wechsler, T., Eriksen, C., Brix, S., Drescher, K., Stanley-Wall, N., Kümmerli, R., and Kovács, Á.T. Division of labor during biofilm matrix production. *Current Biology*. **12**:1903-1913.e5.
- Driks, A. (1999) *Bacillus subtilis* spore coat. *Microbiology and Molecular Biology Reviews* **63**: 1-20.
- Durrett, R., Miras, M., Mirouze, N., Narechania, A., Mandic-Mulec, I., and Dubnau, D. (2013a) Genome sequence of the *Bacillus subtilis* biofilm-forming transformable strain PS216. *Genome Announcements* **1**: e00288-00213.
- Earley, B., Buckham Sporer, K., and Gupta, S. (2017) Invited review: Relationship between cattle transport, immunity and respiratory disease. *Animal: an international journal of animal bioscience* **11**: 486-492.
- Edwards, A.N., Suárez, J.M., and McBride, S.M. (2013) Culturing and maintaining *Clostridium difficile* in an anaerobic environment. *Journal of visualized experiments : JoVE*: e50787-e50787.
- Eichenberger, P., Fujita, M., Jensen, S.T., Conlon, E.M., Rudner, D.Z., Wang, S.T., Ferguson, C., Haga, K., Sato, T., Liu, J.S., and Losick, R. (2004) The program of gene transcription for a single differentiating cell type during sporulation in *Bacillus subtilis*. *PLoS Biology* **2**: e328.

- Errington, J. (2003) Regulation of endospore formation in *Bacillus subtilis*. *Nature reviews. Microbiology* **1**: 117-126.
- Ewels, P., Magnusson, M., Lundin, S., and Källér, M. (2016) MultiQC: summarize analysis results for multiple tools and samples in a single report. *Bioinformatics* **32**: 3047-3048.
- Facijs, R., Bucker, H., Horneck, G., Reitz, G., and Schafer, M. (1979) Dosimetric and biological results from the *Bacillus subtilis* Biostack experiment with the Apollo-Soyuz Test Project. *Life sciences and space research* **17**: 123-128.
- Fang, A., Pierson, D.L., Mishra, S.K., and Demain, A.L. (2000) Growth of *Streptomyces hygroscopicus* in rotating-wall bioreactor under simulated microgravity inhibits rapamycin production. *Applied Microbiology and Biotechnology* **54**: 33-36.
- Fang, A., Pierson, D.L., Mishra, S.K., Koenig, D.W., and Demain, A.L. (1997) Secondary metabolism in simulated microgravity: beta-lactam production by *Streptomyces clavuligerus*. *Journal of industrial microbiology & biotechnology* **18**: 22-25.
- Fernandes, S., Simoes, L.C., Lima, N., and Simoes, M. (2019) Adhesion of filamentous fungi isolated from drinking water under different process conditions. *Water research* **164**: 114951.
- Fernández, C.R., (2019) To Reach Mars, We Need Biotechnology. <https://bioprinting.ru/en/press-center/publications/to-reach-mars-we-need-biotechnology>
- Feucht, A., Evans, L., and Errington, J. (2003) Identification of sporulation genes by genome-wide analysis of the sigmaE regulon of *Bacillus subtilis*. *Microbiology* **149**: 3023-3034.
- Feuerbacher, B., and Stoewer, H., (2006) *Utilization of Space*. Springer-Verlag Berlin Heidelberg. pp. 280-289
- Finley, N., and Fields, M.L. (1962) Heat activation and heat-induced dormancy of *Bacillus stearothermophilus* spores. *Applied microbiology* **10**: 231-236.
- Fischer, E.R., Hansen, B.T., Nair, V., Hoyt, F.H., and Dorward, D.W. (2012) Scanning electron microscopy. *Current Protocols in Microbiology* **Chapter 2**: Unit 2B 2.
- Flemming, H.C., and Wingender, J. (2010) The biofilm matrix. *Nature reviews. Microbiology* **8**: 623-633.
- Flemming, H.C., Wingender, J., Szewzyk, U., Steinberg, P., Rice, S.A., and Kjelleberg, S. (2016) Biofilms: an emergent form of bacterial life. *Nature reviews. Microbiology* **14**: 563-575.
- Flemming, H.C., and Wuertz, S. (2019) Bacteria and archaea on Earth and their abundance in biofilms. *Nature reviews. Microbiology* **17**: 247-260.
- Fong, J.N.C., and Yildiz, F.H. (2015) Biofilm matrix proteins. *Microbiology Spectrum* **3**: 10.1128/microbiolspec.MB-0004-2014.
- Fordtran, J.S. (2006) Colitis due to *Clostridium difficile* toxins: underdiagnosed, highly virulent, and nosocomial. *Proceedings (Baylor University. Medical Center)* **19**: 3-12.
- Foster, S.J., and Johnstone, K. (1990) Pulling the trigger: the mechanism of bacterial spore germination. *Molecular microbiology* **4**: 137-141.
- Fuchs, F.M., Driks, A., Setlow, P., and Moeller, R. (2017a) An improved protocol for harvesting *Bacillus subtilis* colony biofilms. *Journal of Microbiological Methods* **134**: 7-13.
- Fuchs, F.M., Holland, G., Moeller, R., and Laue, M. (2018) Directed freeze-fracturing of *Bacillus subtilis* biofilms for conventional scanning electron microscopy. *Journal of Microbiological Methods* **152**: 165-172.
- Fuchs, F.M., Raguse, M., Fiebrandt, M., Madela, K., Awakowicz, P., Laue, M., Stapelmann, K., and Moeller, R. (2017b) Investigating the detrimental effects of low pressure plasma sterilization on the survival of *Bacillus subtilis* spores using live cell microscopy. *Journal of visualized experiments : JoVE*. e56666
- Fujita, M., and Losick, R. (2005) Evidence that entry into sporulation in *Bacillus subtilis* is governed by a gradual increase in the level and activity of the master regulator Spo0A. *Genes & development* **19**: 2236-2244.
- Garrick-Silversmith, L., and Torriani, A. (1973) Macromolecular Syntheses During Germination and Outgrowth of *Bacillus subtilis* Spores. *Journal of Bacteriology* **114**: 507-516.
- Garschagen, L.S., Mancinelli, R.L., and Moeller, R. (2019) Introducing *Vibrio natriegens* as a Microbial Model Organism for Microgravity Research. *Astrobiology* **19**: 1211-1220.
- Gerwig, J., Kiley, T.B., Gunka, K., Stanley-Wall, N., and Stülke, J. (2014) The protein tyrosine kinases EpsB and PtkA differentially affect biofilm formation in *Bacillus subtilis*. *Microbiology* **160**: 682-691.
- Gerzer, R., Hemmersbach, R., and Horneck, G., (2006) Life Sciences. In: *Utilization of Space: Today and Tomorrow*. B. Feuerbacher & H. Stoewer (eds). Berlin, Heidelberg: Springer Berlin Heidelberg, pp. 341-373.
- Ghanbari, A., Dehghany, J., Schwabs, T., Müsken, M., Häußler, S., and Meyer-Hermann, M. (2016) Inoculation density and nutrient level determine the formation of mushroom-shaped structures in *Pseudomonas aeruginosa* biofilms. *Scientific reports* **6**: 32097.

- Ghosh, S., Scotland, M., and Setlow, P. (2012) Levels of germination proteins in dormant and superdormant spores of *Bacillus subtilis*. *Journal of Bacteriology* **194**: 2221-2227.
- Ghosh, S., Setlow, B., Wahome, P.G., Cowan, A.E., Plomp, M., Malkin, A.J., and Setlow, P. (2008) Characterization of spores of *Bacillus subtilis* that lack most coat layers. *Journal of Bacteriology* **190**: 6741-6748.
- Ghosh, S., and Setlow, P. (2009) Isolation and characterization of superdormant spores of *Bacillus* species. *Journal of Bacteriology* **191**: 1787-1797.
- Gingichashvili, S., Duanis-Assaf, D., Shemesh, M., Featherstone, J.D.B., Feuerstein, O., and Steinberg, D. (2017) *Bacillus subtilis* biofilm development – A computerized study of morphology and kinetics. *Frontiers in Microbiology* **8** : 2072.
- Gomez-Aguado, F., Corcuera, M.T., Gomez-Lus, M.L., de la Parte, M.A., Ramos, C., Garcia-Rey, C., Alonso, M.J., and Prieto, J. (2013) Histological approach to *Bacillus subtilis* colony-biofilm: evolving internal architecture and sporulation dynamics. *Histology and Histopathology* **28**: 1351-1360.
- Gonzalez-Pastor, J.E. (2011) Cannibalism: a social behavior in sporulating *Bacillus subtilis*. *FEMS Microbiology Reviews* **35**: 415-424.
- Gonzalez-Pastor, J.E., Hobbs, E.C., and Losick, R. (2003) Cannibalism by sporulating bacteria. *Science* **301**: 510-513.
- Gould, G.W. (1970) Mechanism of the inhibition of germination of bacterial spores by gamma-irradiation in the presence of iodoacetamide and iodate. *Journal of general microbiology* **64**: 301-309.
- Gray, D.A., Dugar, G., Gamba, P., Strahl, H., Jonker, M.J., and Hamoen, L.W. (2019) Extreme slow growth as alternative strategy to survive deep starvation in bacteria. *Nature Communications* **10**: 890.
- Grimm, D., Grosse, J., Wehland, M., Mann, V., Reseland, J.E., Sundaresan, A., and Corydon, T.J. (2016) The impact of microgravity on bone in humans. *Bone* **87**: 44-56.
- Grumbein, S., Opitz, M., and Lieleg, O. (2014) Selected metal ions protect *Bacillus subtilis* biofilms from erosion. *Metallomics : integrated biometal science* **6**: 1441-1450.
- Gueguinou, N., Huin-Schohn, C., Bascove, M., Bueb, J.L., Tschirhart, E., Legrand-Frossi, C., and Fripiat, J.P. (2009) Could spaceflight-associated immune system weakening preclude the expansion of human presence beyond Earth's orbit? *Journal of leukocyte biology* **86**: 1027-1038.
- Guggenbichler, J.P., Assadian, O., Boeswald, M., and Kramer, A. (2011) Incidence and clinical implication of nosocomial infections associated with implantable biomaterials - catheters, ventilator-associated pneumonia, urinary tract infections. *GMS Krankenhaushygiene interdisziplinär* **6**: Doc18.
- Gulimova, V., Proshchina, A., Kharlamova, A., Krivova, Y., Barabanov, V., Berdiev, R., Asadchikov, V., Buzmakov, A., Zolotov, D., and Saveliev, S. (2019) Reptiles in space missions: Results and perspectives. *International Journal of Molecular Sciences* **20**: 3019.
- Guttenplan, S.B., and Kearns, D.B. (2013) Regulation of flagellar motility during biofilm formation. *FEMS Microbiology Reviews* **37**: 849-871.
- Haines, S.R., Bope, A., Horack, J.M., Meyer, M.E., and Dannemiller, K.C. (2019) Quantitative evaluation of bioaerosols in different particle size fractions in dust collected on the International Space Station (ISS). *Applied Microbiology and Biotechnology*. **18**:7767-7782
- Halan, B., Buehler, K., and Schmid, A. (2012) Biofilms as living catalysts in continuous chemical syntheses. *Trends in biotechnology* **30**: 453-465.
- Hamon, M.A., and Lazazzera, B.A. (2001) The sporulation transcription factor Spo0A is required for biofilm development in *Bacillus subtilis*. *Molecular microbiology* **42**: 1199-1209.
- Hathout, Y., Setlow, B., Cabrera-Martinez, R.M., Fenselau, C., and Setlow, P. (2003) Small, acid-soluble proteins as biomarkers in mass spectrometry analysis of *Bacillus* spores. *Applied and environmental microbiology* **69**: 1100-1107.
- Hauslage, J., Strauch, S.M., Eßmann, O., Haag, F.W.M., Richter, P., Krüger, J., Stoltze, J., Becker, I., Nasir, A., Bornemann, G., Müller, H., Delovski, T., Berger, T., Rutzynska, A., Marsalek, K. (2018) Eu:CROPIS – “Euglena gracilis: Combined regenerative organic-food production in space” - A space experiment testing biological life support systems under Lunar and Martian gravity. *Microgravity Science and Technology* **30**: 933-942.
- Hayyan, M., Hashim, M.A., and AlNashef, I.M. (2016) Superoxide Ion: Generation and chemical implications. *Chemical reviews* **116**: 3029-3085.
- Hecker, M., and Völker, U. (1990) General stress proteins in *Bacillus subtilis*. *FEMS microbiology letters* **74**: 197-213.

- Hemmersbach, R., Ngo-Anh, J., Zell, (2016) Topical Issue on Ground-Based Facilities (GBF): Results and experiences from ESA's ground-based facilities programme in space life sciences. *Microgravity Science and Technology* **28**: 189-189.
- Hemmersbach, R., Voormanns, R., Bromeis, B., Schmidt, N., Rabien, H., and Ivanova, K. (1998) Comparative studies of the graviresponses of *Paramecium* and *Loxodes*. *Advances in Space Research* **21**: 1285-1289.
- Herranz, R., Anken, R., Boonstra, J., Braun, M., Christianen, P.C., de Geest, M., Hauslage, J., Hilbig, R., Hill, R.J., Lebert, M., Medina, F.J., Vagt, N., Ullrich, O., van Loon, J.J., and Hemmersbach, R. (2013a) Ground-based facilities for simulation of microgravity: organism-specific recommendations for their use, and recommended terminology. *Astrobiology* **13**: 1-17.
- Heyndrickx, M. (2011) The importance of endospore-forming bacteria originating from soil for contamination of industrial food processing. *Journal of Applied and Environmental Soil Science*. **2011**: 11.
- Higgins, D., and Dworkin, J. (2012) Recent progress in *Bacillus subtilis* sporulation. *FEMS Microbiology Reviews* **36**: 131-148.
- Hilbert, D.W., and Piggot, P.J. (2004) Compartmentalization of gene expression during *Bacillus subtilis* spore formation. *Microbiology and Molecular Biology Reviews* **68**: 234-262.
- Ho, T.T., Duc, L.H., Isticato, R., Baccigalupi, L., Ricca, E., Van, P.H., and Cutting, S.M. (2001) Fate and dissemination of *Bacillus subtilis* spores in a murine model. *Applied and environmental microbiology* **67**: 3819-3823.
- Hobley, L., Ostrowski, A., Rao, F.V., Bromley, K.M., Porter, M., Prescott, A.R., MacPhee, C.E., van Aalten, D.M., and Stanley-Wall, N.R. (2013) BslA is a self-assembling bacterial hydrophobin that coats the *Bacillus subtilis* biofilm. *Proceedings of the National Academy of Sciences of the United States of America* **110**: 13600-13605.
- Hofler, C., Heckmann, J., Fritsch, A., Popp, P., Gebhard, S., Fritz, G., and Mascher, T. (2016) Cannibalism stress response in *Bacillus subtilis*. *Microbiology (Reading, England)* **162**: 164-176.
- Hoiby, N. (2017) A short history of microbial biofilms and biofilm infections. *APMIS : acta pathologica, microbiologica, et immunologica Scandinavica* **125**: 272-275.
- Hölscher, T., Bartels, B., Lin, Y.-C., Gallegos-Monterrosa, R., Price-Whelan, A., Kolter, R., Dietrich, L.E.P., and Kovács, Á.T. (2015) Motility, chemotaxis and aerotaxis contribute to competitiveness during bacterial pellicle biofilm development. *Journal of molecular biology* **427**: 3695-3708.
- Holscher, T., Schiklang, T., Dragos, A., Dietel, A.K., Kost, C., and Kovacs, A.T. (2018) Impaired competence in flagellar mutants of *Bacillus subtilis* is connected to the regulatory network governed by DegU. *Environmental microbiology reports* **10**: 23-32.
- Hong, H.A., Khaneja, R., Tam, N.M., Cazzato, A., Tan, S., Urdaci, M., Brisson, A., Gasbarrini, A., Barnes, I., and Cutting, S.M. (2009) *Bacillus subtilis* isolated from the human gastrointestinal tract. *Research in microbiology* **160**: 134-143.
- Horneck, G. (1993) Responses of *Bacillus subtilis* spores to space environment: results from experiments in space. *Origins of life and evolution of the biosphere : the journal of the International Society for the Study of the Origin of Life* **23**: 37-52.
- Horneck, G. (2008) The microbial case for Mars and its implication for human expeditions to Mars. *Acta Astronautica* **63**: 1015-1024.
- Horneck, G., (2015) Encyclopedia of Astrobiology. Springer Berlin Heidelberg, pp. 157-158.
- Horneck, G., Baumstark-Khan, C., and Facius, R., (2006) Radiation Biology. In: Fundamentals of Space Biology: Research on Cells, Animals, and Plants in Space. G. Clément & K. Slenzka (eds). Springer New York, pp. 291-336.
- Horneck, G., Bucker, H., and Reitz, G. (1994) Long-term survival of bacterial spores in space. *Advances in space research : the official journal of the Committee on Space Research (COSPAR)* **14**: 41-45.
- Horneck, G., Facius, R., Enge, W., Beaujean, R., and Bartholoma, K.P. (1974) Microbial studies in the Biostack experiment of the Apollo 16 mission: germination and outgrowth of single *Bacillus subtilis* spores hit by cosmic HZE particles. *Life sciences and space research* **12**: 75-83.
- Horneck, G., Klaus, D.M., and Mancinelli, R.L. (2010) Space microbiology. *Microbiology and Molecular Biology Reviews* **74**: 121-156.
- Horneck, G., Moeller, R., Cadet, J., Douki, T., Mancinelli, R.L., Nicholson, W.L., Panitz, C., Rabbow, E., Rettberg, P., Spry, A., Stackebrandt, E., Vaishampayan, P., and Venkateswaran, K.J. (2012) Resistance of bacterial endospores to outer space for planetary protection purposes--experiment PROTECT of the EXPOSE-E mission. *Astrobiology* **12**: 445-456.
- Horneck, G., and Rettberg, P., (2007) *Complete Course in Astrobiology*.

- Hoson, T., Kamisaka, S., Masuda, Y., Yamashita, M., and Buchen, B. (1997) Evaluation of the three-dimensional clinostat as a simulator of weightlessness. *Planta* **203 Suppl**: pp.187-197.
- Hotchin, J., Lorenz, P., and Hemenway, C. (1965) Survival of microorganisms in space. *Nature* **206**: 442-445.
- Huang, B., Li, D.-G., Huang, Y., and Liu, C.-T. (2018) Effects of spaceflight and simulated microgravity on microbial growth and secondary metabolism. *Military Medical Research* **5**: 18-18.
- Huang, J., Liu, S., Zhang, C., Wang, X., Pu, J., Ba, F., Xue, S., Ye, H., Zhao, T., Li, K., Wang, Y., Zhang, J., Wang, L., Fan, C., Lu, T.K., and Zhong, C. (2019) Programmable and printable *Bacillus subtilis* biofilms as engineered living materials. *Nature Chemical Biology* **15**: 34-41.
- Huang, S.-s., Chen, D., Pelczar, P.L., Vepachedu, V.R., Setlow, P., and Li, Y.-q. (2007) Levels of Ca<sup>2+</sup>-dipicolinic acid in individual *Bacillus* spores determined using microfluidic Raman tweezers. *Journal of Bacteriology* **189**: 4681-4687.
- Hughson, R.L., Helm, A., and Durante, M. (2018) Heart in space: effect of the extraterrestrial environment on the cardiovascular system. *Nature reviews. Cardiology* **15**: 167-180.
- Ishii, Y., Hoson, T., Kamisaka, S., Miyamoto, K., Ueda, J., Mantani, S., Fujii, S., Masuda, Y., and Yamamoto, R. (1996) Plant growth processes in *Arabidopsis* under microgravity conditions simulated by a clinostat. *Biological Sciences in Space* **10**: 3-7.
- Jamal, M., Ahmad, W., Andleeb, S., Jalil, F., Imran, M., Nawaz, M.A., Hussain, T., Ali, M., Rafiq, M., and Kamil, M.A. (2018) Bacterial biofilm and associated infections. *Journal of the Chinese Medical Association* **81**: 7-11.
- Jamily, A.S., and Toyota, K. (2019) Effects of inoculation with a commercial microbial inoculant *Bacillus subtilis* C-3102 mixture on rice and barley growth and its possible mechanism in the plant growth stimulatory effect. *Journal of Plant Protection Research* **59**: 193-205
- Jedrzejewski, M.J., and Setlow, P. (2001) Comparison of the binuclear metalloenzymes diphosphoglycerate-independent phosphoglycerate mutase and alkaline phosphatase: their mechanism of catalysis via a phosphoserine intermediate. *Chemical reviews* **101**: 607-618.
- Jonsson, K.I. (2007) Tardigrades as a potential model organism in space research. *Astrobiology* **7**: 757-766.
- Kacena, M., Todd, P.J.M.S., and Technology (1997a) Growth characteristics of *E. coli* and *B. subtilis* cultured on an agar substrate in microgravity. *Microgravity Science and Technology* **10**: 58-62.
- Kacena, M.A., Leonard, P.E., Todd, P., and Luttgies, M.W. (1997b) Low gravity and inertial effects on the growth of *E. coli* and *B. subtilis* in semi-solid media. *Aviation, space, and environmental medicine* **68**: 1104-1108.
- Kacena, M.A., Manfredi, B., and Todd, P. (1999a) Effects of space flight and mixing on bacterial growth in low volume cultures. *Microgravity Science and technology* **12**: 74-77.
- Kacena, M.A., Merrell, G.A., Manfredi, B., Smith, E.E., Klaus, D.M., and Todd, P. (1999b) Bacterial growth in space flight: logistic growth curve parameters for *Escherichia coli* and *Bacillus subtilis*. *Applied Microbiology and Biotechnology* **51**: 229-234.
- Kaieda, S., Setlow, B., Setlow, P., and Halle, B. (2013) Mobility of core water in *Bacillus subtilis* spores by 2H NMR. *Biophysical journal* **105**: 2016-2023.
- Kampf, J., Gerwig, J., Kruse, K., Cleverley, R., Dormeyer, M., Grunberger, A., Kohlheyer, D., Commichau, F.M., Lewis, R.J., and Stulke, J. (2018) Selective pressure for biofilm formation in *Bacillus subtilis*: Differential effect of mutations in the master regulator SinR on bistability. *mBio* **9**. e01464-18
- Karmazyn-Campelli, C., Rhayat, L., Carballido-Lopez, R., Duperrier, S., Frandsen, N., and Stragier, P. (2008) How the early sporulation sigma factor sigmaF delays the switch to late development in *Bacillus subtilis*. *Molecular microbiology* **67**: 1169-1180.
- Kawaguchi, Y., Yokobori, S., Hashimoto, H., Yano, H., Tabata, M., Kawai, H., and Yamagishi, A. (2016) Investigation of the interplanetary transfer of microbes in the Tanpopo mission at the exposed facility of the International Space Station. *Astrobiology* **16**: 363-376.
- Kearns, D.B., Chu, F., Branda, S.S., Kolter, R., and Losick, R. (2005) A master regulator for biofilm formation by *Bacillus subtilis*. *Molecular microbiology* **55**: 739-749.
- Keijsers, B.J.F., Ter Beek, A., Rauwerda, H., Schuren, F., Montijn, R., van der Spek, H., and Brul, S. (2007) Analysis of temporal gene expression during *Bacillus subtilis* spore germination and outgrowth. *Journal of Bacteriology* **189**: 3624-3634.
- Kesel, S., Grumbein, S., Gumperlein, I., Tallawi, M., Marel, A.K., Lieleg, O., and Opitz, M. (2016) Direct comparison of physical properties of *Bacillus subtilis* NCIB 3610 and B-1 biofilms. *Applied and environmental microbiology*: 2424-2432.



- Kesel, S., von Bronk, B., Falcón García, C., Götz, A., Lieleg, O., and Opitz, M. (2017) Matrix composition determines the dimensions of *Bacillus subtilis* NCIB 3610 biofilm colonies grown on LB agar. *RSC Advances* **7**: 31886-31898.
- Khatoun, Z., McTiernan, C.D., Suuronen, E.J., Mah, T.-F., and Alarcon, E.I. (2018) Bacterial biofilm formation on implantable devices and approaches to its treatment and prevention. *Heliyon* **4**: e01067-e01067.
- Kim, W., Tengra, F.K., Young, Z., Shong, J., Marchand, N., Chan, H.K., Pangule, R.C., Parra, M., Dordick, J.S., Plawsky, J.L., and Collins, C.H. (2013) Spaceflight promotes biofilm formation by *Pseudomonas aeruginosa*. *PLoS one* **8**: e62437.
- Kinsinger, R.F., Shirk, M.C., and Fall, R. (2003) Rapid surface motility in *Bacillus subtilis* is dependent on extracellular surfactin and potassium ions. *Journal of Bacteriology* **185**: 5627.
- Klaus, D.M. (2001) Clinostats and bioreactors. *Gravitational and space biology bulletin : publication of the American Society for Gravitational and Space Biology* **14**: 55-64.
- Klein, T., Wollseiffen, P., Sanders, M., Claassen, J., Carnahan, H., Abeln, V., Vogt, T., Struder, H.K., and Schneider, S. (2019) The influence of microgravity on cerebral blood flow and electrocortical activity. *Experimental brain research* **237**: 1057-1062.
- Klintworth, R., Reher, H.J., Viktorov, A.N., and Bohle, D. (1999) Biological induced corrosion of materials II: New test methods and experiences from mir station. *Acta Astronautica* **44**: 569-578.
- Knaysi, G. (1964) Effect of temperature on the rate of germination in *Bacillus cereus*. *Journal of Bacteriology* **87**: 619-622.
- Knox, B.P., Blachowicz, A., Palmer, J.M., Romsdahl, J., Huttenlocher, A., Wang, C.C., Keller, N.P., and Venkateswaran, K. (2016) Characterization of *Aspergillus fumigatus* isolates from air and surfaces of the International Space Station. *mSphere* **1**: e00227-16.
- Kobayashi, K., and Ikemoto, Y. (2019) Biofilm-associated toxin and extracellular protease cooperatively suppress competitors in *Bacillus subtilis* biofilms. *PLOS Genetics* **15**: e1008232.
- Kobayashi, K., and Iwano, M. (2012) BslA(YuaB) forms a hydrophobic layer on the surface of *Bacillus subtilis* biofilms. *Molecular microbiology* **85**: 51-66.
- Koenig, D.W., Mishra, S.K., and Pierson, D.L. (1995) Removal of Burkholderia cepacia biofilms with oxidants. *Biofouling* **9**: 51-62.
- Kohlstedt, M., Sappa, P.K., Meyer, H., Maass, S., Zapras, A., Hoffmann, T., Becker, J., Steil, L., Hecker, M., van Dijk, J.M., Lalk, M., Mader, U., Stulke, J., Bremer, E., Volker, U., and Wittmann, C. (2014) Adaptation of *Bacillus subtilis* carbon core metabolism to simultaneous nutrient limitation and osmotic challenge: a multi-omics perspective. *Environmental microbiology* **16**: 1898-1917.
- Konkol, M.A., Blair, K.M., and Kearns, D.B. (2013) Plasmid-encoded ComI inhibits competence in the ancestral 3610 strain of *Bacillus subtilis*. *Journal of Bacteriology* **195**: 4085-4093.
- Koo, H., Allan, R.N., Howlin, R.P., Stoodley, P., and Hall-Stoodley, L. (2017a) Targeting microbial biofilms: current and prospective therapeutic strategies. *Nature reviews. Microbiology* **15**: 740-755.
- Koo, H., Allan, R.N., Howlin, R.P., Stoodley, P., and Hall-Stoodley, L. (2017b) Targeting microbial biofilms: current and prospective therapeutic strategies. *Nature reviews. Microbiology* **15**: 740-755.
- Koshland, D.E. (2002) The Seven Pillars of Life. *Science (New York, N.Y.)* **295**: 2215-2216.
- Krisko, A., and Radman, M. (2013) Biology of extreme radiation resistance: the way of *Deinococcus radiodurans*. *Cold Spring Harbor perspectives in biology* **5**: pii: a012765.
- Kumar, P., and Libchaber, A. (2013) Pressure and temperature dependence of growth and morphology of *Escherichia coli*: experiments and stochastic model. *Biophysical journal* **105**: 783-793.
- Kunst, F., Ogasawara, N., Moszer, I., Albertini, A.M., Alloni, G., Azevedo, V., Bertero, M.G., Bessieres, P., Bolotin, A., Borchert, S., Borriss, R., Boursier, L., Brans, A., Braun, M., Brignell, S.C., Bron, S., Brouillet, S., Bruschi, C.V., Caldwell, B., Capuano, V., Carter, N.M., Choi, S.K., Cordani, J.J., Connerton, I.F., Cummings, N.J., Daniel, R.A., Denzot, F., Devine, K.M., Dusterhoft, A., Ehrlich, S.D., Emmerson, P.T., Entian, K.D., Errington, J., Fabret, C., Ferrari, E., Foulger, D., Fritz, C., Fujita, M., Fujita, Y., Fuma, S., Galizzi, A., Galleron, N., Ghim, S.Y., Glaser, P., Goffeau, A., Golightly, E.J., Grandi, G., Guiseppi, G., Guy, B.J., Haga, K., Haiech, J., Harwood, C.R., Henaut, A., Hilbert, H., Holsappel, S., Hosono, S., Hullo, M.F., Itaya, M., Jones, L., Joris, B., Karamata, D., Kasahara, Y., Klaerr-Blanchard, M., Klein, C., Kobayashi, Y., Koetter, P., Koningstein, G., Krogh, S., Kumano, M., Kurita, K., Lapidus, A., Lardinois, S., Lauber, J., Lazarevic, V., Lee, S.M., Levine, A., Liu, H., Masuda, S., Mauel, C., Medigue, C., Medina, N., Mellado, R.P., Mizuno, M., Moestl, D., Nakai, S., Noback, M., Noone, D., O'Reilly, M., Ogawa, K., Ogiwara, A., Oudega, B., Park, S.H., Parro, V., Pohl, T.M., Portelle, D., Porwollik, S., Prescott, A.M., Presecan, E., Pujic, P., Purnelle, B., et al. (1997) The complete genome sequence of the gram-positive bacterium *Bacillus subtilis*. *Nature* **390**: 249-256.

- Lam, K.S., Gustavson, D.R., Pirnik, D.L., Pack, E., Bulanahgui, C., Mamber, S.W., Forenza, S., Stodieck, L.S., and Klaus, D.M. (2002) The effect of space flight on the production of actinomycin D by *Streptomyces plicatus*. *Journal of industrial microbiology & biotechnology* **29**: 299-302.
- Lang, J.M., Coil, D.A., Neches, R.Y., Brown, W.E., Cavalier, D., Severance, M., Hampton-Marcell, J.T., Gilbert, J.A., and Eisen, J.A. (2017) A microbial survey of the International Space Station (ISS). *PeerJ* **5**: e4029.
- Lapchine, L., Moatti, N., Gasset, G., Richoille, G., Templier, J., and Tixador, R. (1986) Antibiotic activity in space. *Drugs under experimental and clinical research* **12**: 933-938.
- Larimer, C., Suter, J.D., Bonheyo, G., and Addleman, R.S. (2016) In situ non-destructive measurement of biofilm thickness and topology in an interferometric optical microscope. *Journal of Biophotonics* **9**: 656-666.
- Laue, M. (2010) Electron microscopy of viruses. *Methods Cell Biol* **96**: 1-20.
- Leggett, M.J., McDonnell, G., Denyer, S.P., Setlow, P., and Maillard, J.Y. (2012) Bacterial spore structures and their protective role in biocide resistance. *Journal of applied microbiology* **113**: 485-498.
- Lenhart, T.R., Duncan, K.E., Beech, I.B., Sunner, J.A., Smith, W., Bonifay, V., Biri, B., and Suflita, J.M. (2014) Identification and characterization of microbial biofilm communities associated with corroded oil pipeline surfaces. *Biofouling* **30**: 823-835.
- Lewandowski, Z., and Boltz, J.P., (2011) 4.15 - Biofilms in water and wastewater treatment. In: Treatise on Water Science. P. Wilderer (ed). Oxford: Elsevier, pp. 529-570.
- Leys, N.M., Hendrickx, L., De Boever, P., Baatout, S., and Mergeay, M. (2004) Space flight effects on bacterial physiology. *Journal of biological regulators and homeostatic agents* **18**: 193-199.
- Li, K., Whitfield, M., and Van Vliet Krystyn, J., (2013a) Beating the bugs: roles of microbial biofilms in corrosion. In: Corrosion Reviews. pp. 73.
- Li, L., Mendis, N., Trigui, H., Oliver, J.D., and Faucher, S.P. (2014) The importance of the viable but non-culturable state in human bacterial pathogens. *Frontiers in microbiology* **5**: 258.
- Li, S., Peng, C., Cheng, T., Wang, C., Guo, L., and Li, D. (2019a) Nitrogen-cycling microbial community functional potential and enzyme activities in cultured biofilms with response to inorganic nitrogen availability. *Journal of Environmental Sciences* **76**: 89-99.
- Li, W., Zheng, T., Ma, Y., and Liu, J. (2019b) Current status and future prospects of sewer biofilms: Their structure, influencing factors, and substance transformations. *The Science of the total environment* **695**: 133815.
- Li, Y., Butzin, X.Y., Davis, A., Setlow, B., Korza, G., Ustok, F.I., Christie, G., Setlow, P., and Hao, B. (2013b) Activity and regulation of various forms of CwlJ, SleB, and YpeB proteins in degrading cortex peptidoglycan of spores of *Bacillus* species in vitro and during spore germination. *Journal of Bacteriology* **195**: 2530-2540.
- Lin, T.H., Tang, F.C., Hung, P.C., Hua, Z.C., and Lai, C.Y. (2018) Relative survival of *Bacillus subtilis* spores loaded on filtering facepiece respirators after five decontamination methods. *Indoor air* **28**: 754-762
- Lindsay, D., Brozel, V.S., and von Holy, A. (2005) Spore formation in *Bacillus subtilis* biofilms. *Journal of food protection* **68**: 860-865.
- Little, B., Wagner, P., and Mansfeld, F. (1992) An overview of microbiologically influenced corrosion. *Electrochimica Acta* **37**: 2185-2194.
- Liu, M., Gao, H., Shang, P., Zhou, X., Ashforth, E., Zhuo, Y., Chen, D., Ren, B., Liu, Z., and Zhang, L. (2011) Magnetic field is the dominant factor to induce the response of *Streptomyces avermitilis* in altered gravity simulated by diamagnetic levitation. *PloS one* **6**: e24697.
- Liu, Y., and Tay, J.H. (2002) The essential role of hydrodynamic shear force in the formation of biofilm and granular sludge. *Water research* **36**: 1653-1665.
- Loison, P., Hosny, N.A., Gervais, P., Champion, D., Kuimova, M.K., and Perrier-Cornet, J.M. (2013) Direct investigation of viscosity of an atypical inner membrane of *Bacillus* spores: a molecular rotor/FLIM study. *Biochimica et biophysica acta* **1828**: 2436-2443.
- Lopez, D. (2015) Connection of KinC to flotillins and potassium leakage in *Bacillus subtilis*. *Microbiology* **161**: 1180-1181.
- López, D., Fischbach, M.A., Chu, F., Losick, R., and Kolter, R. (2009) Structurally diverse natural products that cause potassium leakage trigger multicellularity in *Bacillus subtilis*. *Proceedings of the National Academy of Sciences of the United States of America* **106**: 280-285.
- Lopez, D., and Kolter, R. (2010) Extracellular signals that define distinct and coexisting cell fates in *Bacillus subtilis*. *FEMS Microbiology Reviews* **34**: 134-149.
- Lopez, D., Vlamakis, H., Losick, R., and Kolter, R. (2009) Cannibalism enhances biofilm development in *Bacillus subtilis*. *Molecular microbiology* **74**: 609-618.

- Loudon, C.-M., Nicholson, N., Finster, K., Leys, N., Byloos, B., Van Houdt, R., Rettberg, P., Moeller, R., Fuchs, F.M., Demets, R., Krause, J., Vukich, M., Mariani, A., and Cockell, C. (2018) BioRock: new experiments and hardware to investigate microbe–mineral interactions in space. *International Journal of Astrobiology* **17**: 303-313.
- Lovelock, J. (1995) Gaia: A new look at life on Earth. by James Lovelock. Oxford University Press, 1995. *Quarterly Journal of the Royal Meteorological Society* **122**: 563-563.
- Luu, S., Cruz-Mora, J., Setlow, B., Feeherry, F.E., Doona, C.J., and Setlow, P. (2015) The effects of heat activation on *Bacillus* spore germination, with nutrients or under high pressure, with or without various germination proteins. *Applied and environmental microbiology* **81**: 2927-2938.
- Luu, S., and Setlow, P. (2014) Analysis of the loss in heat and acid resistance during germination of spores of *Bacillus* species. *Journal of Bacteriology* **196**: 1733-1740.
- Mader, U., Antelmann, H., Buder, T., Dahl, M.K., Hecker, M., and Homuth, G. (2002) *Bacillus subtilis* functional genomics: genome-wide analysis of the DegS-DegU regulon by transcriptomics and proteomics. *Molecular genetics and genomics* **268**: 455-467.
- Mahnert, A., Vaishampayan, P., Probst, A.J., Auerbach, A., Moissl-Eichinger, C., Venkateswaran, K., and Berg, G. (2015) Cleanroom maintenance significantly reduces abundance but not diversity of indoor microbiomes. *PLoS one* **10**: e0134848-e0134848.
- Makimura, K., Hanazawa, R., Takatori, K., Tamura, Y., Fujisaki, R., Nishiyama, Y., Abe, S., Uchida, K., Kawamura, Y., Ezaki, T., and Yamaguchi, H. (2001) Fungal flora on board the Mir-Space Station, identification by morphological features and ribosomal DNA sequences. *Microbiology and Immunology* **45**: 357-363.
- Marlow, V.L., Cianfanelli, F.R., Porter, M., Cairns, L.S., Dale, J.K., and Stanley-Wall, N.R. (2014a) The prevalence and origin of exoprotease-producing cells in the *Bacillus subtilis* biofilm. *Microbiology* **160**: 56-66.
- Marlow, V.L., Porter, M., Hobley, L., Kiley, T.B., Swedlow, J.R., Davidson, F.A., and Stanley-Wall, N.R. (2014b) Phosphorylated DegU manipulates cell fate differentiation in the *Bacillus subtilis* biofilm. *Journal of Bacteriology* **196**: 16-27.
- Masachis, S., Segorbe, D., Turra, D., Leon-Ruiz, M., Furst, U., El Ghalid, M., Leonard, G., Lopez-Berges, M.S., Richards, T.A., Felix, G., and Di Pietro, A. (2016) A fungal pathogen secretes plant alkalizing peptides to increase infection. *Nature microbiology* **1**: 16043.
- Matin, A., and Lynch, S.J.A.N. (2005) Investigating the threat of bacteria grown in space. *ASM News* **71**: 235-240.
- Mauclaire, L., and Egli, M. (2010) Effect of simulated microgravity on growth and production of exopolymeric substances of *Micrococcus luteus* space and earth isolates. *FEMS immunology and medical microbiology* **59**: 350-356.
- McKay, C.P. (1991) Urey prize lecture: Planetary evolution and the origin of life. *Icarus* **91**: 93-100.
- McKenney, P.T., Driks, A., and Eichenberger, P. (2013) The *Bacillus subtilis* endospore: assembly and functions of the multilayered coat. *Nature reviews. Microbiology* **11**: 33-44.
- McKenney, P.T., Driks, A., Eskandarian, H.A., Grabowski, P., Guberman, J., Wang, K.H., Gitai, Z., and Eichenberger, P. (2010) A distance-weighted interaction map reveals a previously uncharacterized layer of the *Bacillus subtilis* spore coat. *Current biology : CB* **20**: 934-938.
- McLoon, A.L., Guttenplan, S.B., Kearns, D.B., Kolter, R., and Losick, R. (2011) Tracing the domestication of a biofilm-forming bacterium. *Journal of Bacteriology* **193**: 2027-2034.
- Mearls, E.B., Jackter, J., Colquhoun, J.M., Farmer, V., Matthews, A.J., Murphy, L.S., Fenton, C., and Camp, A.H. (2018) Transcription and translation of the sigG gene is tuned for proper execution of the switch from early to late gene expression in the developing *Bacillus subtilis* spore. *PLoS Genetics* **14**: e1007350.
- Melly, E., Genest, P.C., Gilmore, M.E., Little, S., Popham, D.L., Driks, A., and Setlow, P. (2002) Analysis of the properties of spores of *Bacillus subtilis* prepared at different temperatures. *Journal of applied microbiology* **92**: 1105-1115.
- Melly, E., and Setlow, P. (2001) Heat shock proteins do not influence wet heat resistance of *Bacillus subtilis* spores. *Journal of Bacteriology* **183**: 779-784.
- Menezes, A.A., Cumbers, J., Hogan, J.A., and Arkin, A.P. (2015a) Towards synthetic biological approaches to resource utilization on space missions. *Journal of the Royal Society. Interface* **12**: 20140715.
- Menezes, A.A., Montague, M.G., Cumbers, J., Hogan, J.A., and Arkin, A.P. (2015b) Grand challenges in space synthetic biology. *Journal of the Royal Society. Interface* **12**: 20150803-20150803.
- Mennigmann, H.D., and Lange, M. (1986) Growth and differentiation of *Bacillus subtilis* under microgravity. *Naturwissenschaften* **73**: 415-417.
- Michna, R.H., Zhu, B., Mäder, U., and Stülke, J. (2016) SubtiWiki 2.0 - an integrated database for the model organism *Bacillus subtilis*. *Nucleic acids research* **44**: D654-D662.

- Mielich-Suss, B., and Lopez, D. (2015) Molecular mechanisms involved in *Bacillus subtilis* biofilm formation. *Environmental microbiology* **17**: 555-565.
- Mileikowsky, C., Cucinotta, F.A., Wilson, J.W., Gladman, B., Horneck, G., Lindegren, L., Melosh, J., Rickman, H., Valtonen, M., and Zheng, J.Q. (2000) Natural transfer of viable microbes in space. *Icarus* **145**: 391-427.
- Miller, M.B., and Bassler, B.L. (2001) Quorum sensing in bacteria. *Annual review of microbiology* **55**: 165-199.
- Milner, J.L., Silo-Suh, L., Lee, J.C., He, H., Clardy, J., and Handelsman, J. (1996) Production of kanosamine by *Bacillus cereus* UW85. *Applied and environmental microbiology* **62**: 3061-3065.
- Mittal, A. (2012) Self-generated and reproducible dynamics in “gene years” represent life. *Journal of Biomolecular Structure and Dynamics* **29**: 609-611.
- Moeller, R., Douki, T., Cadet, J., Stackebrandt, E., Nicholson, W.L., Rettberg, P., Reitz, G., and Horneck, G. (2007a) UV-radiation-induced formation of DNA bipyrimidine photoproducts in *Bacillus subtilis* endospores and their repair during germination. *International microbiology : the official journal of the Spanish Society for Microbiology* **10**: 39-46.
- Moeller, R., Raguse, M., Reitz, G., Okayasu, R., Li, Z., Klein, S., Setlow, P., and Nicholson, W.L. (2014) Resistance of *Bacillus subtilis* spore DNA to lethal ionizing radiation damage relies primarily on spore core components and DNA repair, with minor effects of oxygen radical detoxification. *Applied and environmental microbiology* **80**: 104-109.
- Moeller, R., Reitz, G., Li, Z., Klein, S., and Nicholson, W.L. (2012a) Multifactorial resistance of *Bacillus subtilis* spores to high-energy proton radiation: role of spore structural components and the homologous recombination and non-homologous end joining DNA repair pathways. *Astrobiology* **12**: 1069-1077.
- Moeller, R., Reitz, G., Nicholson The Protect Team, W.L., and Horneck, G. (2012b) Mutagenesis in bacterial spores exposed to space and simulated martian conditions: data from the EXPOSE-E spaceflight experiment PROTECT. *Astrobiology* **12**: 457-468.
- Moeller, R., Setlow, P., Horneck, G., Berger, T., Reitz, G., Rettberg, P., Doherty, A.J., Okayasu, R., and Nicholson, W.L. (2008) Roles of the major, small, acid-soluble spore proteins and spore-specific and universal DNA repair mechanisms in resistance of *Bacillus subtilis* spores to ionizing radiation from X rays and high-energy charged-particle bombardment. *Journal of Bacteriology* **190**: 1134-1140.
- Moeller, R., Setlow, P., Reitz, G., and Nicholson, W.L. (2009) Roles of small, acid-soluble spore proteins and core water content in survival of *Bacillus subtilis* spores exposed to environmental solar UV radiation. *Applied and environmental microbiology* **75**: 5202-5208.
- Moeller, R., Stackebrandt, E., Reitz, G., Berger, T., Rettberg, P., Doherty, A.J., Horneck, G., and Nicholson, W.L. (2007b) Role of DNA repair by nonhomologous-end joining in *Bacillus subtilis* spore resistance to extreme dryness, mono- and polychromatic UV, and ionizing radiation. *Journal of Bacteriology* **189**: 3306-3311.
- Mohr, S.C., Sokolov, N.V., He, C.M., and Setlow, P. (1991) Binding of small acid-soluble spore proteins from *Bacillus subtilis* changes the conformation of DNA from B to A. *Proceedings of the National Academy of Sciences of the United States of America* **88**: 77-81.
- Moir, A. (2006) How do spores germinate? *Journal of Applied Microbiology* **101**: 526-530.
- Moir, A., and Cooper, G. (2015) Spore germination. *Microbiol Spectrum* **3**: 6.
- Molle, V., Fujita, M., Jensen, S.T., Eichenberger, P., Gonzalez-Pastor, J.E., Liu, J.S., and Losick, R. (2003) The Spo0A regulon of *Bacillus subtilis*. *Molecular microbiology* **50**: 1683-1701.
- Monds, R.D., and O'Toole, G.A. (2009) The developmental model of microbial biofilms: ten years of a paradigm up for review. *Trends in microbiology* **17**: 73-87.
- Monnard, P.-A., and Walde, P. (2015) Current ideas about prebiological compartmentalization. *Life* **5**: 1239-1263.
- Mora, M., Wink, L., Kögler, I., Mahnert, A., Rettberg, P., Schwendner, P., Demets, R., Cockell, C., Alekhova, T., Klingl, A., Krause, R., Zolotariof, A., Alexandrova, A., and Moissl-Eichinger, C. (2019) Space Station conditions are selective but do not alter microbial characteristics relevant to human health. *Nature Communications* **10**: 3990.
- Moreno-Villanueva, M., Wong, M., Lu, T., Zhang, Y., and Wu, H. (2017) Interplay of space radiation and microgravity in DNA damage and DNA damage response. *NPJ microgravity* **3**: 14.
- Morikawa, M., Ito, M., and Imanaka, T. (1992) Isolation of a new surfactin producer *Bacillus pumilus* A-1, and cloning and nucleotide sequence of the regulator gene, psf-1. *Journal of Fermentation and Bioengineering* **74**: 255-261.
- Morikawa, M., Kagihiro, S., Haruki, M., Takano, K., Branda, S., Kolter, R., and Kanaya, S. (2006) Biofilm formation by a *Bacillus subtilis* strain that produces gamma-polyglutamate. *Microbiology* **152**: 2801-2807.

- Morita, M.T. (2010) Directional gravity sensing in gravitropism. *Annual review of plant biology* **61**: 705-720.
- Morris, R.J., Schor, M., Gillespie, R.M.C., Ferreira, A.S., Baldauf, L., Earl, C., Ostrowski, A., Hogley, L., Bromley, K.M., Sukhodub, T., Arnaouteli, S., Stanley-Wall, N.R., and MacPhee, C.E. (2017) Natural variations in the biofilm-associated protein BslA from the genus *Bacillus*. *Scientific reports* **7**: 6730-6730.
- Morrison, M.D., Fajardo-Cavazos, P., and Nicholson, W.L. (2017) Cultivation in space flight produces minimal alterations in the susceptibility of *Bacillus subtilis* cells to 72 different antibiotics and growth-inhibiting compounds. *Applied and environmental microbiology* **83**: e01584-01517.
- Morrison, M.D., Fajardo-Cavazos, P., and Nicholson, W.L. (2019) Comparison of *Bacillus subtilis* transcriptome profiles from two separate missions to the International Space Station. *NPJ microgravity* **5**: 1.
- Morrison, M.D., and Nicholson, W.L. (2018) Meta-analysis of data from spaceflight transcriptome experiments does not support the idea of a common bacterial “spaceflight response”. *Scientific reports* **8**: 14403.
- Nagler, K., Setlow, P., Reineke, K., Driks, A., and Moeller, R. (2015) Involvement of coat proteins in *Bacillus subtilis* spore germination in high-salinity environments. *Applied and environmental microbiology* **81**: 6725-6735.
- Nakano, M.M., Magnuson, R., Myers, A., Curry, J., Grossman, A.D., and Zuber, P. (1991) srfA is an operon required for surfactin production, competence development, and efficient sporulation in *Bacillus subtilis*. *Journal of Bacteriology* **173**: 1770-1778.
- Newcombe, F.C. (1904) Limitations of the klinostat as an instrument for scientific research. *Science* **20**: 376-379.
- Newman, D.K., and Banfield, J.F. (2002) Geomicrobiology: how molecular-scale interactions underpin biogeochemical systems. *Science* **296**: 1071-1077.
- Nicholson, W.L., Moeller, R., and Horneck, G. (2012) Transcriptomic responses of germinating *Bacillus subtilis* spores exposed to 1.5 years of space and simulated martian conditions on the EXPOSE-E experiment PROTECT. *Astrobiology* **12**: 469-486.
- Nicholson, W.L., Munakata, N., Horneck, G., Melosh, H.J., and Setlow, P. (2000) Resistance of *Bacillus* endospores to extreme terrestrial and extraterrestrial environments. *Microbiology and Molecular Biology Reviews* **64**: 548-572.
- Nickerson, C.A., Ott, C.M., Wilson, J.W., Ramamurthy, R., and Pierson, D.L. (2004) Microbial responses to microgravity and other low-shear environments. *Microbiology and Molecular Biology Reviews* **68**: 345-361.
- Nikawa, J., and Kawabata, M. (1998) PCR- and ligation-mediated synthesis of marker cassettes with long flanking homology regions for gene disruption in *Saccharomyces cerevisiae*. *Nucleic acids research* **26**: 860-861.
- Novikova, N., De Boever, P., Poddubko, S., Deshevaya, E., Polikarpov, N., Rakova, N., Coninx, I., and Mergeay, M. (2006) Survey of environmental biocontamination on board the International Space Station. *Research in microbiology* **157**: 5-12.
- Novikova, N.D. (2004) Review of the knowledge of microbial contamination of the Russian manned spacecraft. *Microbial ecology* **47**: 127-132.
- Orsini, S.S., Lewis, A.M., and Rice, K.C. (2017) Investigation of simulated microgravity effects on *Streptococcus mutans* physiology and global gene expression. *NPJ microgravity* **3**: 4.
- Ostrowski, A., Mehert, A., Prescott, A., Kiley, T.B., and Stanley-Wall, N.R. (2011) YuaB functions synergistically with the exopolysaccharide and TasA amyloid fibers to allow biofilm formation by *Bacillus subtilis*. *Journal of Bacteriology* **193**: 4821-4831.
- Ott, E., Fuchs, F., Moeller, R., Hemmersbach, R., Kawaguchi, Y., Yamagishi, A., Weckwerth, W., and Milojevic, T. (2019) Molecular response of *Deinococcus radiodurans* to simulated microgravity explored by proteometabolomic approach. *Scientific reports* **1**:18462
- Ott, E., Kawaguchi, Y., Kolbl, D., Chaturvedi, P., Nakagawa, K., Yamagishi, A., Weckwerth, W., and Milojevic, T. (2017) Proteometabolomic response of *Deinococcus radiodurans* exposed to UVC and vacuum conditions: Initial studies prior to the Tanpopo space mission. *PloS one* **12**: e0189381.
- Pace, N.R. (2001) The universal nature of biochemistry. *Proceedings of the National Academy of Sciences of the United States of America* **98**: 805-808.
- Pandey, R., Ter Beek, A., Vischer, N.O., Smelt, J.P., Brul, S., and Manders, E.M. (2013) Live cell imaging of germination and outgrowth of individual *Bacillus subtilis* spores; the effect of heat stress quantitatively analyzed with SporeTracker. *PloS one* **8**: e58972.
- Paredes-Sabja, D., Setlow, P., and Sarker, M.R. (2011) Germination of spores of Bacillales and Clostridiales species: mechanisms and proteins involved. *Trends in microbiology* **19**: 85-94.

- Perrin, E., Bacci, G., Garrelly, L., Canganella, F., Bianconi, G., Fani, R., and Mengoni, A. (2018) Furnishing spaceship environment: evaluation of bacterial biofilms on different materials used inside International Space Station. *Research in microbiology* **169**: 289-295.
- Persat, A., Nadell, C.D., Kim, M.K., Ingremeau, F., Siryaporn, A., Drescher, K., Wingreen, N.S., Bassler, B.L., Gitai, Z., and Stone, H.A. (2015) The mechanical world of bacteria. *Cell* **161**: 988-997.
- Pierson, D.L. (2001) Microbial contamination of spacecraft. *Gravitational and space biology bulletin : publication of the American Society for Gravitational and Space Biology* **14**: 1-6.
- Pillinger, J.M., Pillinger, C.T., Sancisi-Frey, S., and Spry, J.A. (2006) The microbiology of spacecraft hardware: Lessons learned from the planetary protection activities on the Beagle 2 spacecraft. *Research in microbiology* **157**: 19-24.
- Pletser, V. (2004) Short duration microgravity experiments in physical and life sciences during parabolic flights: the first 30 ESA campaigns. *Acta Astronautica* **55**: 829-854.
- Plomp, M., Leighton, T.J., Wheeler, K.E., Hill, H.D., and Malkin, A.J. (2007) In vitro high-resolution structural dynamics of single germinating bacterial spores. *Proceedings of the National Academy of Sciences of the United States of America* **104**: 9644-9649.
- Popham, D.L. (2002) Specialized peptidoglycan of the bacterial endospore: the inner wall of the lockbox. *Cellular and molecular life sciences* **59**: 426-433.
- PubMed, (2019) PubMed. In.: National Center for Biotechnology Information, pp.
- Rabbow, E., Rettberg, P., Parpart, A., Panitz, C., Schulte, W., Molter, F., Jaramillo, E., Demets, R., Weiss, P., and Willnecker, R. (2017) EXPOSE-R2: The ystrobiological ESA mission on board of the International Space Station. *Frontiers in microbiology* **8**: 1533.
- Raguse, M., Fiebrandt, M., Denis, M., Stapelmann, K., Eichenberger, P., Driks, A., Eaton, P., Awakowicz, P., and Moeller, R. (2016a) Understanding of the importance of the spore coat structure and pigmentation in the *Bacillus subtilis* spore resistance to low-pressure plasma sterilization. *Journal of Physics D* **49**: 285401.
- Raguse, M., Fiebrandt, M., Stapelmann, K., Madela, K., Laue, M., Lackmann, J.-W., Thwaite, J.E., Setlow, P., Awakowicz, P., and Moeller, R. (2016b) Improvement of biological indicators by uniformly distributing *Bacillus subtilis* spores in monolayers to evaluate enhanced spore decontamination technologies. *Applied and environmental microbiology* **82**: 2031-2038.
- Ramanan, R., Kim, B.-H., Cho, D.-H., Oh, H.-M., and Kim, H.-S. (2016) Algae–bacteria interactions: Evolution, ecology and emerging applications. *Biotechnology Advances* **34**: 14-29.
- Ramasamy, P., and Zhang, X. (2005) Effects of shear stress on the secretion of extracellular polymeric substances in biofilms. *Water Science and Technology* **52**: 217-223.
- Ran, F.A., Hsu, P.D., Wright, J., Agarwala, V., Scott, D.A., and Zhang, F. (2013) Genome engineering using the CRISPR-Cas9 system. *Nature protocols* **8**: 2281-2308.
- Reasoner, D.J., and Geldreich, E.E. (1985) A new medium for the enumeration and subculture of bacteria from potable water. *Applied and environmental microbiology* **49**: 1-7.
- Reineke, K., Mathys, A., Heinz, V., and Knorr, D. (2013) Mechanisms of endospore inactivation under high pressure. *Trends in microbiology* **21**: 296-304.
- Rettberg, P., Fritze, D., Verbarq, S., Nellen, J., Horneck, G., Stackebrandt, E., and Kminek, G. (2006) Determination of the microbial diversity of spacecraft assembly, testing and launch facilities: First results of the ESA project MiDiv. *Advances in Space Research* **38**: 1260-1265.
- Reynolds, E.S. (1963) The use of lead citrate at high pH as an electron-opaque stain in electron microscopy. *The Journal of cell biology* **17**: 208-212.
- Richter, A., Hölscher, T., Pausch, P., Sehrt, T., Brockhaus, F., Bange, G., and Kovács, Á.T. (2018) Hampered motility promotes the evolution of wrinkly phenotype in *Bacillus subtilis*. *BMC Evolutionary Biology* **18**: 155.
- Riley, E.P., Trinquier, A., Reilly, M.L., Durchon, M., Perera, V.R., Pogliano, K., and Lopez-Garrido, J. (2018) Spatiotemporally regulated proteolysis to dissect the role of vegetative proteins during *Bacillus subtilis* sporulation: cell-specific requirement of sigma(H) and sigma(A). *Molecular microbiology* **108**: 45-62.
- Rismondo, J., Moller, L., Aldridge, C., Gray, J., Vollmer, W., and Halbedel, S. (2015) Discrete and overlapping functions of peptidoglycan synthases in growth, cell division and virulence of *Listeria monocytogenes*. *Molecular microbiology* **95**: 332-351.
- Romero, D., Aguilar, C., Losick, R., and Kolter, R. (2010) Amyloid fibers provide structural integrity to *Bacillus subtilis* biofilms. *Proceedings of the National Academy of Sciences of the United States of America* **107**: 2230-2234.

- Romero, D., Vlamakis, H., Losick, R., and Kolter, R. (2014) Functional analysis of the accessory protein TapA in *Bacillus subtilis* amyloid fiber assembly. *Journal of Bacteriology* **196**: 1505-1513.
- Rosado, H., Doyle, M., Hinds, J., and Taylor, P.W. (2010) Low-shear modelled microgravity alters expression of virulence determinants of *Staphylococcus aureus*. *Acta Astronautica* **66**: 408-413.
- Rose, R., Setlow, B., Monroe, A., Mallozzi, M., Driks, A., and Setlow, P. (2007) Comparison of the properties of *Bacillus subtilis* spores made in liquid or on agar plates. *Journal of applied microbiology* **103**: 691-699.
- Rosenzweig, J.A., Ahmed, S., Eunson, J., Jr., and Chopra, A.K. (2014) Low-shear force associated with modeled microgravity and spaceflight does not similarly impact the virulence of notable bacterial pathogens. *Applied Microbiology and Biotechnology* **98**: 8797-8807.
- Rummel, J.D. (2000) Implementing planetary protection requirements for sample return missions. *Advances in space research* **26**: 1893-1899.
- Rummel, J.D. (2019) From Planetary Quarantine to Planetary Protection: A NASA and International Story. *Astrobiology* **19**: 624-627.
- Rychen, G., Aquilina, G., Azimonti, G., Bampidis, V., Bastos, M.d.L., Bories, G., Chesson, A., Flachowsky, G., Gropp, J., Kolar, B., Kouba, M., López-Alonso, M., López Puente, S., Mantovani, A., Mayo, B., Ramos, F., Saarela, M., Villa, R.E., Wallace, R.J., Wester, P., Herman, L., Glandorf, B., Kärenlampi, S., Aguilera, J., and Cocconcelli, P.S. (2018) Safety of vitamin B2 (80%) as riboflavin produced by *Bacillus subtilis* KCCM-10445 for all animal species. *EFSA Panel on Additives* **16**: e05223.
- Ryzhov, V., Hathout, Y., and Fenselau, C. (2000) Rapid characterization of spores of *Bacillus cereus* group bacteria by matrix-assisted laser desorption-ionization time-of-flight mass spectrometry. *Applied and environmental microbiology* **66**: 3828-3834.
- Schaeffer, P., Millet, J., and Aubert, J.P. (1965) Catabolic repression of bacterial sporulation. *Proceedings of the National Academy of Sciences of the United States of America* **54**: 704-711.
- Schindelin, J., Arganda-Carreras, I., Frise, E., Kaynig, V., Longair, M., Pietzsch, T., Preibisch, S., Rueden, C., Saalfeld, S., Schmid, B., Tinevez, J.Y., White, D.J., Hartenstein, V., Eliceiri, K., Tomancak, P., and Cardona, A. (2012) Fiji: an open-source platform for biological-image analysis. *Nature Methods* **9**: 676-682.
- Schiwon, K., Arends, K., Rogowski, K.M., Furch, S., Prescha, K., Sakinc, T., Van Houdt, R., Werner, G., and Grohmann, E. (2013) Comparison of antibiotic resistance, biofilm formation and conjugative transfer of *Staphylococcus* and *Enterococcus* isolates from International Space Station and Antarctic Research Station Concordia. *Microbial ecology* **65**: 638-651.
- Schrödinger, E., (1944) *What is Life?* Cambridge University Press, Cambridge, UK.
- Schwarz, R.P., Goodwin, T.J., and Wolf, D.A. (1992) Cell culture for three-dimensional modeling in rotating-wall vessels: an application of simulated microgravity. *Journal of tissue culture methods : Tissue Culture Association manual of cell, tissue, and organ culture procedures* **14**: 51-57.
- Searles, S.C., Woolley, C.M., Petersen, R.A., Hyman, L.E., and Nielsen-Preiss, S.M. (2011) Modeled microgravity increases filamentation, biofilm formation, phenotypic switching, and antimicrobial resistance in *Candida albicans*. *Astrobiology* **11**: 825-836.
- Seccareccia, I., Kovács, Á.T., Gallegos-Monterrosa, R., and Nett, M. (2016) Unraveling the predator-prey relationship of *Cupriavidus necator* and *Bacillus subtilis*. *Microbiological Research* **192**: 231-238.
- Segev, E., Rosenberg, A., Mamou, G., Sinai, L., and Ben-Yehuda, S. (2013) Molecular kinetics of reviving bacterial spores. *Journal of Bacteriology* **195**: 1875-1882.
- Senatore, G., Mastroleo, F., Leys, N., and Mauriello, G. (2018) Effect of microgravity & space radiation on microbes. *Future Microbiology*, **7**: 831-847.
- Serra, D.O., Richter, A.M., Klauack, G., Mika, F., and Hengge, R. (2013) Microanatomy at cellular resolution and spatial order of physiological differentiation in a bacterial biofilm. *mBio* **4**: e00103-00113.
- Setlow, B., Cowan, A.E., and Setlow, P. (2003) Germination of spores of *Bacillus subtilis* with dodecylamine. *Journal of applied microbiology* **95**: 637-648.
- Setlow, B., and Setlow, P. (1995) Small, acid-soluble proteins bound to DNA protect *Bacillus subtilis* spores from killing by dry heat. *Applied and environmental microbiology* **61**: 2787-2790.
- Setlow, B., and Setlow, P. (1996) Role of DNA repair in *Bacillus subtilis* spore resistance. *Journal of Bacteriology* **178**: 3486-3495.
- Setlow, P. (2003) Spore germination. *Current Opinion in Microbiology* **6**: 550-556.
- Setlow, P. (2006) Spores of *Bacillus subtilis*: their resistance to and killing by radiation, heat and chemicals. *Journal of Applied Microbiology* **101**: 514-525.
- Setlow, P. (2014) Germination of spores of *Bacillus* species: what we know and do not know. *Journal of Bacteriology* **196**: 1297-1305.

- Setlow, P. (2016) Spore resistance properties. *The bacterial spore*: 201-216.
- Setlow, P., and Kornberg, A. (1970) Biochemical studies of bacterial sporulation and germination. Nucleotide metabolism during spore germination. *The Journal of biological chemistry* **245**: 3645-3652.
- Setlow, P., Wang, S., and Li, Y.Q. (2017) Germination of Spores of the Orders *Bacillales* and *Clostridiales*. *Annual review of microbiology* **71**: 459-477.
- Setlow, P.J.J.o.a.m. (2013) When the sleepers wake: the germination of spores of *Bacillus* species. *Journal of Applied Microbiology* **115**: 1251-1268.
- Shah, I.M., Laaberki, M.H., Popham, D.L., and Dworkin, J. (2008) A eukaryotic-like Ser/Thr kinase signals bacteria to exit dormancy in response to peptidoglycan fragments. *Cell* **135**: 486-496.
- Shakhnovich, B.E., and Shakhnovich, E.I. (2008) Improvisation in evolution of genes and genomes: whose structure is it anyway? *Current opinion in structural biology* **18**: 375-381.
- Shemesh, M., and Chai, Y. (2013) A combination of glycerol and manganese promotes biofilm formation in *Bacillus subtilis* via histidine kinase KinD signaling. *Journal of Bacteriology* **195**: 2747-2754.
- Sieradzki, K., and Tomasz, A. (2003) Alterations of cell wall structure and metabolism accompany reduced susceptibility to vancomycin in an isogenic series of clinical isolates of *Staphylococcus aureus*. *Journal of Bacteriology* **185**: 7103-7110.
- Sinai, L., Rosenberg, A., Smith, Y., Segev, E., and Ben-Yehuda, S. (2015) The molecular timeline of a reviving bacterial spore. *Molecular Cell* **57**: 695-707.
- Singh, R., Paul, D., and Jain, R.K. (2006) Biofilms: implications in bioremediation. *Trends in microbiology* **14**: 389-397.
- Singh, R.P., and Setlow, P. (1979) Regulation of phosphoglycerate phosphomutase in developing forespores and dormant and germinated spores of *Bacillus megaterium* by the level of free manganous ions. *Journal of Bacteriology* **139**: 889-898.
- Skuratov, V.M., Zagibalova, L.B., and Pushkin, V.P. (2002) Species composition and microbial contamination of atmospheric humidity condensate and potable water from the Mir water supply systems during Mir main missions 4 through 27. *Aerospace and environmental medicine* **36**: 28-32.
- Slieman, T.A., and Nicholson, W.L. (2001) Role of dipicolinic acid in survival of *Bacillus subtilis* spores exposed to artificial and solar UV radiation. *Applied and environmental microbiology* **67**: 1274-1279.
- Slieman, T.A., Rebeil, R., and Nicholson, W.L. (2000) Spore photoproduct (SP) lyase from *Bacillus subtilis* specifically binds to and cleaves SP (5-Thymine-5,6-Dihydrothymine) but not cyclobutane pyrimidine dimers in UV-Irradiated DNA. *Journal of Bacteriology* **182**: 6412-6417.
- Sobisch, L.Y., Rogowski, K.M., Fuchs, J., Schmieder, W., Vaishampayan, A., Oles, P., Novikova, N., and Grohmann, E. (2019) Biofilm forming antibiotic resistant Gram-positive pathogens isolated from surfaces on the International Space Station. *Frontiers in microbiology* **10**: 543.
- Soffen, G.A., and Snyder, C.W. (1976) The First Viking Mission to Mars. *Science* **193**: 759.
- Sondag, A., and Dittus, H. (2016) Electrostatic positioning system for a free fall test at drop tower Bremen and an overview of tests for the weak equivalence principle in past, present and future. *Advances in Space Research* **58**: 644-677.
- Soni, A., Oey, I., Silcock, P., and Bremer, P. (2016) *Bacillus* spores in the food industry: A review on resistance and response to novel inactivation technologies. *Comprehensive Reviews in Food Science and Food Safety* **15**: 1139-1148.
- Sonnenfeld, G., Butel, J.S., and Shearer, W.T. (2003) Effects of the space flight environment on the immune system. *Reviews on environmental health* **18**: 1-17.
- Soto, G.E., and Hultgren, S.J. (1999) Bacterial adhesins: common themes and variations in architecture and assembly. *Journal of Bacteriology* **181**: 1059-1071.
- Soufi, B., Kumar, C., Gnad, F., Mann, M., Mijakovic, I., and Macek, B. (2010) Stable isotope labeling by amino acids in cell culture (SILAC) applied to quantitative proteomics of *Bacillus subtilis*. *Journal of Proteome Research* **9**: 3638-3646.
- Soufi, B., and Macek, B. (2014) Stable isotope labeling by amino acids applied to bacterial cell culture. *Methods in Molecular Biology* **1188**: 9-22.
- Soule, M.H. (1932) Identity of *Bacillus subtilis*, Cohn 1872. *The Journal of Infectious Diseases* **51**: 191-215.
- Srinivasan, S., Vladescu, I.D., Koehler, S.A., Wang, X., Mani, M., and Rubinstein, S.M. (2018) Matrix production and sporulation in *Bacillus subtilis* biofilms localize to propagating wave fronts. *Biophysical journal* **114**: 1490-1498.
- Srivastava, A., Gupta, J., Kumar, S., and Kumar, A. (2017) Gut biofilm forming bacteria in inflammatory bowel disease. *Microbial pathogenesis* **112**: 5-14.



- Stalder, A.F., Kulik, G., Sage, D., Barbieri, L., and Hoffmann, P. (2006) A snake-based approach to accurate determination of both contact points and contact angles. *Colloids and Surfaces A: Physicochemical and Engineering Aspects* **286**: 92-103.
- Steil, L., Serrano, M., Henriques, A.O., and Volker, U. (2005) Genome-wide analysis of temporally regulated and compartment-specific gene expression in sporulating cells of *Bacillus subtilis*. *Microbiology* **151**: 399-420.
- Stein, T. (2005) *Bacillus subtilis* antibiotics: structures, syntheses and specific functions. *Molecular Microbiology* **56**: 845-857.
- Stewart, K.A., and Setlow, P. (2013) Numbers of individual nutrient germinant receptors and other germination proteins in spores of *Bacillus subtilis*. *Journal of Bacteriology* **195**: 3575-3582.
- Stöffler, D., Horneck, G., Ott, S., Hornemann, U., Cockell, C.S., Moeller, R., Meyer, C., de Vera, J.-P., Fritz, J., and Artemieva, N.A. (2007) Experimental evidence for the potential impact ejection of viable microorganisms from Mars and Mars-like planets. *Icarus* **186**: 585-588.
- Stoodley, P., Sauer, K., Davies, D.G., and Costerton, J.W. (2002) Biofilms as complex differentiated communities. *Annual review of microbiology* **56**: 187-209.
- Stragier, P., and Losick, R. (1996) Molecular genetics of sporulation in *Bacillus subtilis*. *Annual review of genetics* **30**: 297-241.
- Sturm, A., and Dworkin, J. (2015) Phenotypic diversity as a mechanism to exit cellular dormancy. *Current biology* **25**: 2272-2277.
- Su, L., Chang, D., and Liu, C. (2013) The development of space microbiology in the future: the value and significance of space microbiology research. *Future microbiology* **8**: 5-8.
- Sun, D., Accavitti, M.A., and Bryers, J.D. (2005) Inhibition of biofilm formation by monoclonal antibodies against *Staphylococcus epidermidis* RP62A accumulation-associated protein. **12**: 93-100.
- Sunde, E.P., Setlow, P., Hederstedt, L., and Halle, B. (2009) The physical state of water in bacterial spores. *Proceedings of the National Academy of Sciences* **106**: 19334.
- Sutherland, I.W. (2001) The biofilm matrix – an immobilized but dynamic microbial environment. *Trends in microbiology* **9**: 222-227.
- Svejgaard, B., Wehland, M., Ma, X., Kopp, S., Sahana, J., Warnke, E., Aleshcheva, G., Hemmersbach, R., Hauslage, J., Grosse, J., Bauer, J., Corydon, T.J., Islam, T., Infanger, M., and Grimm, D. (2015) Common effects on cancer cells exerted by a random positioning machine and a 2D Clinostat. *PloS one* **10**: e0135157.
- Swerdlow, B.M., Setlow, B., and Setlow, P. (1981) Levels of H<sup>+</sup> and other monovalent cations in dormant and germinating spores of *Bacillus megaterium*. *Journal of Bacteriology* **148**: 20-29.
- Swick, M.C., Koehler, T.M., and Driks, A. (2016) Surviving between hosts: Sporulation and Transmission. *Microbiology Spectrum* **4**: 10.1128
- Tan, I.S., and Ramamurthi, K.S. (2014) Spore formation in *Bacillus subtilis*. *Environmental microbiology reports* **6**: 212-225.
- Taylor, P.W. (2015) Impact of space flight on bacterial virulence and antibiotic susceptibility. *Infection and Drug Resistance* **8**: 249-262.
- Teitzel, G.M., Geddie, A., De Long, S.K., Kirisits, M.J., Whiteley, M., and Parsek, M.R. (2006) Survival and growth in the presence of elevated copper: transcriptional profiling of copper-stressed *Pseudomonas aeruginosa*. *Journal of Bacteriology* **188**: 7242-7256.
- Tena, D., Martínez-Torres, J.á., Pérez-Pomata, M.T., Sáez-Nieto, J.A., Rubio, V., and Bisquert, J. (2007) Cutaneous infection due to *Bacillus pumilus*: Report of 3 cases. *Clinical Infectious Diseases* **44**: e40-e42.
- Ter Beek, A., Keijser, B.J.F., Boersma, A., Zakrzewska, A., Orij, R., Smits, G.J., and Brul, S. (2008) Transcriptome analysis of sorbic acid-stressed *Bacillus subtilis* reveals a nutrient limitation response and indicates plasma membrane remodeling. *Journal of Bacteriology* **190**: 1751-1761.
- Thornhill, S.G., and Kumar, M. (2018) Biological filters and their use in potable water filtration systems in spaceflight conditions. *Life sciences in space research* **17**: 40-43.
- Tirumalai, M.R., Karouia, F., Tran, Q., Stepanov, V.G., Bruce, R.J., Ott, C.M., Pierson, D.L., and Fox, G.E. (2017) The adaptation of *Escherichia coli* cells grown in simulated microgravity for an extended period is both phenotypic and genomic. *NPJ microgravity* **3**: 15.
- Tirumalai, M.R., Karouia, F., Tran, Q., Stepanov, V.G., Bruce, R.J., Ott, C.M., Pierson, D.L., and Fox, G.E. (2019) Evaluation of acquired antibiotic resistance in *Escherichia coli* exposed to long-term low-shear modeled microgravity and background antibiotic exposure. *mBio* **10**: e02637-02618.

- Tixador, R., Richoille, G., Gasset, G., Planel, H., Moatti, N., Lapchine, L., Enjalbert, L., Raffin, J., Bost, R., Zaloguev, S.N., Bragina, M.P., Moroz, A.F., Antsiferova, N.G., and Kirilova, F.M. (1985) Preliminary results of Cytos 2 experiment. *Acta Astronautica* **12**: 131-134.
- Tovar-Rojo, F., Chander, M., Setlow, B., and Setlow, P. (2002) The products of the spoVA operon are involved in dipicolinic acid uptake into developing spores of *Bacillus subtilis*. *Journal of Bacteriology* **184**: 584-587.
- Traag, B.A., Pugliese, A., Setlow, B., Setlow, P., and Losick, R. (2013) A conserved ClpP-like protease involved in spore outgrowth in *Bacillus subtilis*. *Molecular microbiology* **90**: 160-166.
- Troiano, A.J., Jr., Zhang, J., Cowan, A.E., Yu, J., and Setlow, P. (2015) Analysis of the dynamics of a *Bacillus subtilis* spore germination protein complex during spore germination and outgrowth. *Journal of Bacteriology* **197**: 252-261.
- Tsokolov, S.A. (2009) Why is the definition of life so elusive? Epistemological considerations. *Astrobiology* **9**: 401-412.
- Ulrich, N., Nagler, K., Laue, M., Cockell, C.S., Setlow, P., and Moeller, R. (2018) Experimental studies addressing the longevity of *Bacillus subtilis* spores - The first data from a 500-year experiment. *PLoS one* **13**: e0208425-e0208425.
- Urbaniak, C., Sielaff, A.C., Frey, K.G., Allen, J.E., Singh, N., Jaing, C., Wheeler, K., and Venkateswaran, K. (2018) Detection of antimicrobial resistance genes associated with the International Space Station environmental surfaces. *Scientific reports* **8**: 814.
- Vaishampayan, A., and Grohmann, E. (2019) Multi-resistant biofilm-forming pathogens on the International Space Station. *Journal of biosciences* **44**: 125.
- Vaishampayan, P.A., Rabbow, E., Horneck, G., and Venkateswaran, K.J. (2012) Survival of *Bacillus pumilus* spores for a prolonged period of time in real space conditions. *Astrobiology* **12**: 487-497.
- van de Vossenberg, J.L.C.M., Driessen, A.J.M., da Costa, M.S., and Konings, W.N. (1999) Homeostasis of the membrane proton permeability in *Bacillus subtilis* grown at different temperatures. *Biomembranes* **1419**: 97-104.
- van Dijk, J.M., and Hecker, M. (2013) *Bacillus subtilis*: from soil bacterium to super-secreting cell factory. *Microbial cell factories* **12**: 3-3.
- van Gestel, J., Vlamakis, H., and Kolter, R. (2015) From cell differentiation to cell collectives: *Bacillus subtilis* uses division of labor to migrate. *PLoS Biol* **13**: e1002141-e1002141.
- van Gestel, J., Weissing, F.J., Kuipers, O.P., and Kovacs, A.T. (2014) Density of founder cells affects spatial pattern formation and cooperation in *Bacillus subtilis* biofilms. *The ISME Journal* **8**: 2069-2079.
- van Loon, J.J.W.A. (2007) Some history and use of the random positioning machine, RPM, in gravity related research. *Advances in Space Research* **39**: 1161-1165.
- Van Mulders, S.E., Stassen, C., Daenen, L., Devreese, B., Siewers, V., van Eijsden, R.G., Nielsen, J., Delvaux, F.R., and Willaert, R. (2011) The influence of microgravity on invasive growth in *Saccharomyces cerevisiae*. *Astrobiology* **11**: 45-55.
- van Wolferen, M., Orell, A., and Albers, S.-V. (2018) Archaeal biofilm formation. *Nature Reviews Microbiology* **16**: 699-713.
- van Vliet, S. (2015) Bacterial dormancy: How to decide when to wake up. *Current Biology* **25**: R753-R755.
- Veening, J.-W., Igoshin, O.A., Eijlander, R.T., Nijland, R., Hamoen, L.W., and Kuipers, O.P. (2008) Transient heterogeneity in extracellular protease production by *Bacillus subtilis*. *Molecular Systems Biology* **4**: 184-184.
- Veening, J.W., Kuipers, O.P., Brul, S., Hellingwerf, K.J., and Kort, R. (2006) Effects of phosphorelay perturbations on architecture, sporulation, and spore resistance in biofilms of *Bacillus subtilis*. *Journal of Bacteriology* **188**: 3099-3109.
- Velmourougane, K., Prasanna, R., and Saxena, A.K. (2017) Agriculturally important microbial biofilms: Present status and future prospects. *Journal of basic microbiology* **57**: 548-573.
- Venkateswaran, K., Hattori, N., La Duc, M.T., and Kern, R. (2003) ATP as a biomarker of viable microorganisms in clean-room facilities. *Journal of Microbiological Methods* **52**: 367-377.
- Venkateswaran, K., Vaishampayan, P., Cisneros, J., Pierson, D.L., Rogers, S.O., and Perry, J. (2014) International Space Station environmental microbiome - microbial inventories of ISS filter debris. *Applied Microbiology and Biotechnology* **98**: 6453-6466.
- Verhamme, D.T., Kiley, T.B., and Stanley-Wall, N.R. (2007) DegU co-ordinates multicellular behaviour exhibited by *Bacillus subtilis*. *Molecular microbiology* **65**: 554-568.
- Verhamme, D.T., Murray, E.J., and Stanley-Wall, N.R. (2009) DegU and Spo0A jointly control transcription of two loci required for complex colony development by *Bacillus subtilis*. *Journal of Bacteriology* **191**: 100-108.

- Vetter, N.D., Langill, D.M., Anjum, S., Boisvert-Martel, J., Jagdhane, R.C., Omene, E., Zheng, H., van Straaten, K.E., Asiamah, I., Krol, E.S., Sanders, D.A., and Palmer, D.R. (2013) A previously unrecognized kanosamine biosynthesis pathway in *Bacillus subtilis*. *Journal of the American Chemical Society* **135**: 5970-5973.
- Videla, H.A., and Herrera, L.K. (2005) Microbiologically influenced corrosion: looking to the future. *International microbiology* **8**: 169-180.
- Vlamakis, H., Aguilar, C., Losick, R., and Kolter, R. (2008) Control of cell fate by the formation of an architecturally complex bacterial community. *Genes & development* **22**: 945-953.
- Vlamakis, H., Chai, Y., Beaugregard, P., Losick, R., and Kolter, R. (2013) Sticking together: building a biofilm the *Bacillus subtilis* way. *Nature Reviews Microbiology* **11**: 157-168.
- Vlasic, I., Mertens, R., Seco, E.M., Carrasco, B., Ayora, S., Reitz, G., Commichau, F.M., Alonso, J.C., and Moeller, R. (2014) *Bacillus subtilis* RecA and its accessory factors, RecF, RecO, RecR and RecX, are required for spore resistance to DNA double-strand break. *Nucleic acids research* **42**: 2295-2307.
- Vlašić, I., Mertens, R., Seco, E.M., Carrasco, B., Ayora, S., Reitz, G., Commichau, F.M., Alonso, J.C., and Moeller, R. (2014) *Bacillus subtilis* RecA and its accessory factors, RecF, RecO, RecR and RecX, are required for spore resistance to DNA double-strand break. *Nucleic acids research* **42**: 2295-2307.
- Vogl, T., Hartner, F.S., and Glieder, A. (2013) New opportunities by synthetic biology for biopharmaceutical production in *Pichia pastoris*. *Current opinion in biotechnology* **24**: 1094-1101.
- Voorhies, A.A., Mark Ott, C., Mehta, S., Pierson, D.L., Crucian, B.E., Feiveson, A., Oubre, C.M., Torralba, M., Moncera, K., Zhang, Y., Zurek, E., and Lorenzi, H.A. (2019) Study of the impact of long-duration space missions at the International Space Station on the astronaut microbiome. *Scientific reports* **9**: 9911.
- Wagner-Dobler, I. (2016) Biofilm transplantation in the deep sea. *Molecular ecology* **25**: 1905-1907.
- Waller, L.N., Fox, N., Fox, K.F., Fox, A., and Price, R.L. (2004) Ruthenium red staining for ultrastructural visualization of a glycoprotein layer surrounding the spore of *Bacillus anthracis* and *Bacillus subtilis*. *Journal of Microbiological Methods* **58**: 23-30.
- Wang, H., Yan, Y., Rong, D., Wang, J., Wang, H., Liu, Z., Wang, J., Yang, R., and Han, Y. (2016) Increased biofilm formation ability in *Klebsiella pneumoniae* after short-term exposure to a simulated microgravity environment. *MicrobiologyOpen* **5**: 793-801.
- Wang, S.T., Setlow, B., Conlon, E.M., Lyon, J.L., Imamura, D., Sato, T., Setlow, P., Losick, R., and Eichenberger, P. (2006) The Forespore Line of Gene Expression in *Bacillus subtilis*. *Journal of molecular biology* **358**: 16-37.
- Wang, T., Liang, Y., Wu, M., Chen, Z., Lin, J., and Yang, L. (2015) Natural products from *Bacillus subtilis* with antimicrobial properties. *Chinese Journal of Chemical Engineering* **23**: 744-754.
- Ward, M.D., Chung, Y.J., Copeland, L.B., and Doerfler, D.L. (2010) A comparison of the allergic responses induced by *Penicillium chrysogenum* and house dust mite extracts in a mouse model. *Indoor air* **20**: 380-391.
- Warth, A.D. (1978) Relationship between the heat resistance of spores and the optimum and maximum growth temperatures of *Bacillus* species. *Journal of Bacteriology* **134**: 699-705.
- Wassmann, M., Moeller, R., Rabbow, E., Panitz, C., Horneck, G., Reitz, G., Douki, T., Cadet, J., Stan-Lotter, H., Cockell, C.S., and Rettberg, P. (2012) Survival of spores of the UV-resistant *Bacillus subtilis* strain MW01 after exposure to low-earth orbit and simulated martian conditions: data from the space experiment ADAPT on EXPOSE-E. *Astrobiology* **12**: 498-507.
- Watanabe, F., Yoshimura, K., and Shigeoka, S. (2017) Biochemistry and physiology of vitamins in *Euglena*. *Advances in experimental medicine and biology* **979**: 65-90.
- Weber, P., and Greenberg, J.M. (1985) Can spores survive in interstellar space? *Nature* **316**: 403-407.
- Wells-Bennik, M.H.J., Janssen, P.W.M., Klaus, V., Yang, C., Zwietering, M.H., and Den Besten, H.M.W. (2019) Heat resistance of spores of 18 strains of *Geobacillus stearothermophilus* and impact of culturing conditions. *International Journal of Food Microbiology* **291**: 161-172.
- Werb, M., García, C.F., Bach, N.C., Grumbein, S., Sieber, S.A., Opitz, M., and Lieleg, O. (2017) Surface topology affects wetting behavior of *Bacillus subtilis* biofilms. *NPJ Biofilms Microbiomes* **3**: 11.
- West, J.B. (2001) Historical aspects of the early Soviet/Russian manned space program. *Journal of applied physiology* **91**: 1501-1511.
- Wilking, J.N., Angelini, T.E., Seminara, A., Brenner, M.P., and Weitz, D.A.J.M.b. (2011) Biofilms as complex fluids. *MRS Bulletin* **36**: 385-391.
- Wolf, D.A., and Schwarz, R.P. (1991) Analysis of gravity-induced particle motion and fluid perfusion flow in the NASA-designed rotating zero-head-space tissue culture vessel. <https://ntrs.nasa.gov/search.jsp?R=19920004122>

- Wuest, S.L., Richard, S., Kopp, S., Grimm, D., and Egli, M. (2015) Simulated microgravity: critical review on the use of random positioning machines for mammalian cell culture. *BioMed Research International* **2015**: 971474-971474.
- Wuest, S.L., Richard, S., Walther, I., Furrer, R., Anderegg, R., Sekler, J., and Egli, M. (2014) A Novel Microgravity Simulator Applicable for Three-Dimensional Cell Culturing. *Microgravity science and technology* **26**: 77-88.
- Wuest, S.L., Stern, P., Casartelli, E., and Egli, M. (2017) Fluid dynamics appearing during simulated microgravity using random positioning machines. *PLoS one* **12**: e0170826.
- Xu Zhou, K., Li, N., Christie, G., and Wilson, D.I. (2017) Assessing the impact of germination and sporulation conditions on the adhesion of *Bacillus* spores to glass and stainless steel by fluid dynamic gauging. *Journal of Food Science* **82**: 2614-2625.
- Yamaguchi, N., Roberts, M., Castro, S., Oubre, C., Makimura, K., Leys, N., Grohmann, E., Sugita, T., Ichijo, T., and Nasu, M. (2014) Microbial monitoring of crewed habitats in space-current status and future perspectives. *Microbes and environments* **29**: 250-260.
- Yang, J., Thornhill, S.G., Barrila, J., Nickerson, C.A., Ott, C.M., and McLean, R.J.C., (2018) Chapter 1 - Microbiology of the Built Environment in Spacecraft Used for Human Flight. In: *Methods in Microbiology*. V. Gurtler & J.T. Trevors (eds). Academic Press, pp. 3-26.
- Yi, X., Liu, J., Faeder, J.R., and Setlow, P. (2011) Synergism between different germinant receptors in the germination of *Bacillus subtilis* spores. *Journal of Bacteriology* **193**: 4664-4671.
- Yi, X., and Setlow, P. (2010) Studies of the commitment step in the germination of spores of *Bacillus* species. *Journal of Bacteriology* **192**: 3424-3433.
- Zammuto, V., Fuchs, F.M., Fiebrandt, M., Stapelmann, K., Ulrich, N.J., Maugeri, T.L., Pukall, R., Gugliandolo, C., and Moeller, R. (2018) Comparing spore resistance of *Bacillus* strains isolated from hydrothermal vents and spacecraft assembly facilities to environmental stressors and decontamination treatments. *Astrobiology* **18**: 1425-1434.
- Zea, L., Larsen, M., Estante, F., Qvortrup, K., Moeller, R., Dias de Oliveira, S., Stodieck, L., and Klaus, D. (2017) Phenotypic changes exhibited by *E. coli* cultured in space. *Frontiers in microbiology* **8**: 1598.
- Zeigler, D.R., Pragai, Z., Rodriguez, S., Chevreux, B., Muffler, A., Albert, T., Bai, R., Wyss, M., and Perkins, J.B. (2008) The origins of 168, W23, and other *Bacillus subtilis* legacy strains. *Journal of Bacteriology* **190**: 6983-6995.
- Zhang, P., Setlow, P., and Li, Y. (2009) Characterization of single heat-activated *Bacillus* spores using laser tweezers Raman spectroscopy. *Optics express* **17**: 16480-16491.
- Zhang, Y., Lau, P., Pansky, A., Kassack, M., Hemmersbach, R., and Tobiasch, E. (2014) The influence of simulated microgravity on purinergic signaling is different between individual culture and endothelial and smooth muscle cell coculture. *BioMed Research International*. **2014**: 11.
- Zhu, B., and Stülke, J. (2018) SubtiWiki in 2018: from genes and proteins to functional network annotation of the model organism *Bacillus subtilis*. *Nucleic acids research* **46**: 743-748.
- Zweers, J.C., Barak, I., Becher, D., Driessen, A.J., Hecker, M., Kontinen, V.P., Saller, M.J., Vavrova, L., and van Dijk, J.M. (2008) Towards the development of *Bacillus subtilis* as a cell factory for membrane proteins and protein complexes. *Microbial cell factories* **7**: 10.

## 7. Appendix

### 7.1 Short history of microbial space research

#### Space exploration

Humankind has always observed stars and planets at night skies and wondered what lies beyond. Star constellations gave rise to signs of the zodiac, belief in gods and served for orientation at sea. All great cultures looked up and used the night sky panorama for inspiration in art, philosophy and science. The scientific approach was accelerated enormously by progressive knowledge of optics and the associated invention of the telescope. As a result, it was possible to study our solar system and the Milky Way, which is still an important task in modern astronomy. The great breakthrough of astronomy and space travel started with space race between the Soviet Union and the USA during the cold war. The two rival sides massively increased their military budgets and invested in research into satellites, rockets, communication systems and computer technology. The first satellite, which orbited our planet, was Sputnik 1, launched by the Soviet Union in October 1957. In the sixties and seventies, however, satellites served less for research than for enlightenment and espionage, as well as for the establishment of communication networks. It was hardly of interest at that time, but with Sputnik 1 mankind probably unintentionally brought the first microorganisms into a stable orbit around Earth. While Sputnik 1 had no scientific function and only served as technical demonstration (West, 2001), one month later in 1957, the first dog, Laika was sent to space. What was originally intended to be a feasibility study could also be understood as first biological space experiment, monitoring heart and respiration rate as well as blood pressure. Many other biological and technical experiments were carried out by the UDSSR and the USA for example the first US satellite, Explorer 1, which already included a Geiger counter to measure cosmic rays (Gerzer *et al.*, 2006). In April 1961, the Soviet astronaut Yuri Gagarin became the first human in space orbiting Earth, followed almost one year later by the U.S. astronaut John Glenn in February 1962.

Apart from sending satellites, animals and astronauts into space, the Moon awakened covetousness in the space race. Luna-2 was the first successful mission by the USSR, bringing instruments to the Moon in 1959 and therewith bringing the first microorganisms to our closest celestial body. Ten years later on July 20<sup>th</sup> 1969, the “*Eagle* landed” on the Moon (Eagle: name for Apollo lunar module). In frame of the U.S. mission Apollo 11, Neil Armstrong and Edwin “Buzz” Aldrin were the first humans walking on Moon’s surface and defining a new milestone in space research. The successful Apollo program (1961-1972) directed by NASA was groundbreaking for the subsequent Space Shuttle missions (1981-2011), which enabled reusable platforms to perform scientific experiments in space and supplied the Soviet and later Russian *Mir*-station (Russian: Мир = peace/world, 1986-1996) and helped to construct the International Space Station (ISS). The *Mir* offered long-term space missions for the first time in human history and harbored more than 100 astronauts, performing hundreds of scientific experiments (Feuerbacher & Stoewer, 2006). Based on the acquired knowledge from the *Mir*, the ISS was started to be constructed in 1998 and still serves as experimental platform in space.

Activities in space raised a scientific concern about microbial contamination to space (forward) and from space to Earth (backward). Analyzed environments, such as the Moon’s or Mars surface were intended to be left as pristine as possible, so that life, if it exists on celestial bodies, can be recognized correctly and is not interpreted false-positively by microorganisms brought along (Council, 2006). In order not to influence future experiments and space missions, as well as for self-preservation, the national Academy of Sciences (NAS) publicly discussed the preliminary plans of today’s planetary protection guidelines in 1958 (Horneck & Rettberg, 2007). The cold war and the

space race complicated an amicable agreement between the UDSSR and the USA, which were the only space-faring nations in the sixties. In parallel, the Committee of Space Research (COSPAR) was founded in 1958 and the first planetary protection guidelines were defined in 1959 – ten years before the first manned Moon-mission (COSPAR, 2012). In 1967, the “Outer Space Treaty” of the United Nations has been ratified including Article IX, which comprised the objectives proposed by COSPAR for compliance with the planetary protection guidelines.

As result of these guidelines, which are frequently updated by an active panel of the COSPAR, new sterilization and prevention methods were developed and applied to decontaminate space crafts (Rummel, 2000). Depending on the mission type, length and aim, the COSPAR defined different levels of necessary decontamination techniques (e.g.  $<1 \times 10^{-4}$  viable microorganisms per spacecraft, 1964) (Baglioni *et al.*, 2008). To verify the compliance of the space craft assembly with the guidelines, numerous methods have been developed to detect microorganisms and minimize them on surfaces (Rettberg *et al.*, 2006, Venkateswaran *et al.*, 2003, Pillinger *et al.*, 2006).

According to NASA, in the near future of space exploration more missions to Mars (i.e. MARS 2020 rover mission) with the long-term goal to safely send humans to the red planet in the 2030s will be conducted. Currently more and more nations are interested in travelling to space and in parallel a commercial launch market constantly develops.

### **Astrobiology**

The multidisciplinary field of astrobiology investigates the origin of biological evolution by theoretical and experimental-driven scientific approaches. In addition, astrobiology investigates the possibility of life on other celestial bodies, such as planets, moons or even asteroids. The scientific fields of mineralogy, geology, physics, chemistry, biology, astrophysicists and other scientific disciplines collaborate to generate evidence-based data and theoretical models to answer the question of the origin of life. Humankind always wanted to know more about their origin and how life is formed. Early experiments of van Helmont in the 17<sup>th</sup> century demonstrated spontaneous generation of life, which in turn were refuted by subsequent studies. The invention of the first microscope by van Leeuwenhoek changed the macroscopic perspective of life to the microscale, which was used by Pasteur to state, that life can only originate from preexisting life (Brack, 2008). Unfortunately, the question of the origin of life still remained unanswered, but that was an important insight which demonstrated how life propagated. The transfer of life between celestial bodies is still under constant investigation.

A hypothesis in astrobiology is the Panspermia theory, which states that (microbial) life on Earth might be brought from outer space by meteorites or other extra-terrestrial vehicles (Kawaguchi *et al.*, 2016). Interestingly, many microorganisms inhabit extreme resistances towards desiccation, nutrient depletion, radiation (X-ray and UV), high temperature fluxes, toxic chemicals and low pressure conditions (Horneck *et al.*, 2010). These resistances appear to be disproportionate to the conditions under which these microorganisms are exposed on Earth. Some of these multi-resistant organisms are able to survive harsh space conditions and even the re-entry in Earth atmosphere (Stöffler *et al.*, 2007, Mileikowsky *et al.*, 2000, Nicholson *et al.*, 2000). One theory behind these extraordinary resistances might be that they were adapted and developed by evolution in the past - when Earth was younger and other climatic and atmospheric conditions prevailed. Svante Arrhenius proposed the hypothesis in the early 1900s (Horneck, 2015) and found followers such as Stephen Hawking and other prominent scientists (Di Giulio, 2010). Astrobiology also investigates the survival of microorganisms in space, trying to simulate and analyze a possible transmission between celestial bodies, which would be in accordance with the Panspermia theory. Space conditions offer unique

experimental conditions, which are used to study the most fundamental aspects of life. Gravity for example is the only constant parameter during evolution, which barely changed for billions of years (Morita, 2010). All life on Earth is adapted to gravity and exposing organisms to microgravity conditions in space might help to understand how far life is affected by gravity. Furthermore, other space conditions, such as vacuum, extreme temperatures or enhanced radiation levels are a challenging environment to develop and conduct studies in life sciences starting with single (bacterial) cells, over complex tissues and higher organisms such as the first dog in space, Laika. Many other animals followed Laikas destiny: Monkeys, mice, rats, fruit flies, fish, chicken and other animals (Burgess & Dubbs, 2007). In terms of microgravity, astronauts have probably been better studied than any other organism. They are under constant monitoring and therefore helped to understand the loss of bone mass (Grimm *et al.*, 2016), behavior of the cardio-vascular system (Hughson *et al.*, 2018, Klein *et al.*, 2019) and further physiological changes.

In order to analyze the resistance properties of microbial strains, many different ground and space experiments such as BION-M, BIOPAN, ERA, EXOSTACK and the EXPOSE-R/2 or EXPOSE-E missions among other studies were conducted to determine the limits of microbial life under space conditions (Horneck *et al.*, 2010, Gerzer *et al.*, 2006, Yang *et al.*, 2018, Rabbow *et al.*, 2017). Studying archaeal and bacterial extremophiles such as *Deinococcus radiodurans*, which demonstrates an extraordinary radiation resistance (Ott *et al.*, 2017, Krisko & Radman, 2013), are used in astrobiology to support the panspermia theory and to gain more insight into the origin of life. Apart from the experimental approaches, astrobiology is maintaining the planetary protection guidelines defined by the COSPAR committee. The aim of planetary protection is to preserve Earth as well as other planets and celestial bodies for unwanted microbial contamination. Only by preserving the pristine nature of the environments allows generating conclusive data. Nevertheless, life-detection missions can still produce false-positive results, which can be largely ruled out by prior sterilization of space hardware.

### **Excursion: Sporulation of *B. subtilis***

Under certain environmental conditions such as nutrient deprivation or water deficiency and other stresses, *B. subtilis* is able to form highly resistant endospores (further mentioned as spores) (Higgins & Dworkin, 2012, Checinska *et al.*, 2015a, Nicholson *et al.*, 2000). Unlike other spore-forming bacteria, only two genera, *Bacillus* and *Clostridium* (both Gram-positive), are capable of forming metabolically-inactive endospores. These do not serve for sexual reproduction, but protect and maintain the dormant cell-like apparatus, which can develop into a vegetative cell in better environmental conditions (Paredes-Sabja *et al.*, 2011, van Vliet, 2015). Similar to biofilm formation, the process of sporulation is energetically expensive and is therefore not initiated when there is little stress (Fujita & Losick, 2005). If better environmental conditions arise, the germination of dormant spores is triggered and the shapeshifting to a vegetative phenotype of *B. subtilis* is initiated. Sporulation serves several purposes: The most important is the survival of individual descendants from a population, which underwent extreme and harmful conditions. In biofilms, sporulation allows to downregulate the overall nutrient and water consumption of the population since spores no longer participate in the active metabolism of resources (Lindsay *et al.*, 2005). Spores function as DNA-carrying vectors which support the dispersion and spreading of the species. Spore-containing dust, for example, can be transported over long distances by air or on animal skin and fur (Heyndrickx, 2011, Calfee *et al.*, 2014, Alekhova *et al.*, 2015, Tena *et al.*, 2007). In addition, spores are able to survive the gastrointestinal passage of animals and can therefore be distributed via feces (Hoa *et al.*, 2001). *B. subtilis* spores have been found in the air (Calfee *et al.*, 2014), soil, in water as well as on surfaces within cleanrooms or the ISS (Alekhova *et al.*, 2015, Mahnert *et al.*, 2015).

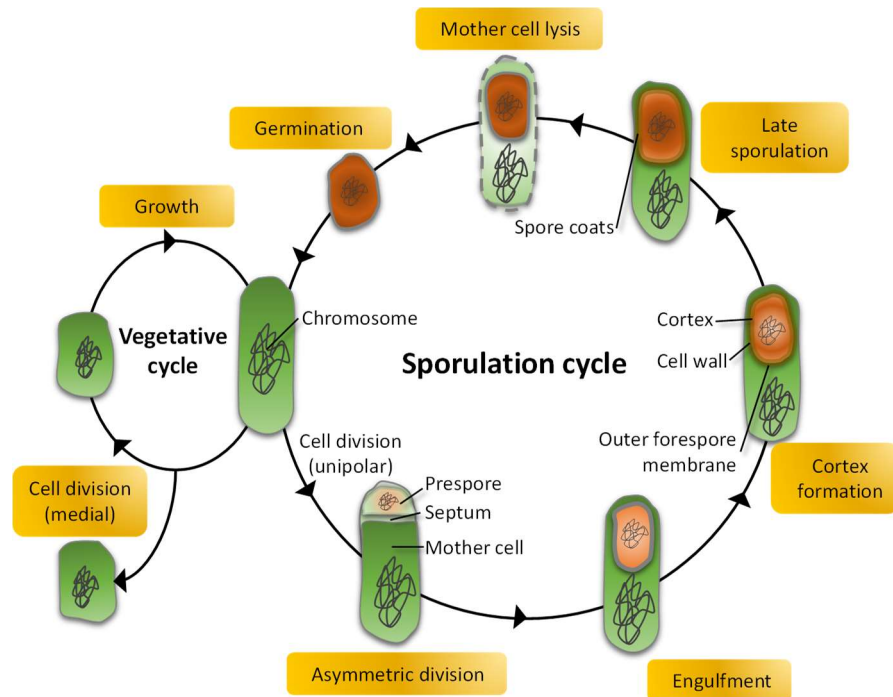


**Figure 58: Sporulation cycle of *B. subtilis***

*B. subtilis* cells are able to undergo two lifestyle cycles: A vegetative cycle in which the cell is medial divided into two cells and the sporulation cycle. If environmental conditions change and the vegetative cell senses high stress levels that can be harmful, the master regulator Spo0A is phosphorylated and if present in high doses can initiate the sporulation, starting with an asymmetric (unipolar) cell division. This process separates the mother cell via a septum from the prespore. The prespore harbors a full copy of the maternal chromosome and potential plasmids and will be completely engulfed by the mother cell. In several steps, first the inner membrane (outer forespore membrane), then the cortex and the spore coat protein layers are formed (late sporulation phase). During these processes  $\text{Ca}^{2+}$ -DPA and  $\alpha$ -,  $\beta$ - and  $\gamma$ -SASP are synthesized and integrated into the spore.  $\text{Ca}^{2+}$ -DPA protects the spore from heat stress and SASP bind to the DNA and protect it from UV-irradiation. After the formation of the spore is completed, the mother cell is lysed and the spore is released. In this stadium spores can survive for decades until they germinate and enter the vegetative cell status. Figure is adapted after (Stragier & Losick, 1996, Errington, 2003).

The process of sporulation is well understood, because *B. subtilis* has been used as a model for cross-species research (Tan & Ramamurthi, 2014). Especially *B. cereus* and several *Clostridia sp.* are a serious concern in the food industry (Soni *et al.*, 2016, Andersson *et al.*, 1995). Therefore, identifying the process of sporulation and germination was intensively investigated in the last decades (Stragier & Losick, 1996, Setlow, 2003, Setlow, 2016). In brief, a spore is formed within its mother cell, which decays and releases the spore. Sporulation can be initiated by several environmental and interspecies influences, which ultimately result in the phosphorylation of the master regulator Spo0A (to Spo0A~P) (Fujita & Losick, 2005). Very high levels of Spo0A~P and DegU~P promote regulatory pathways of several hundred genes to enter the sporulation cycle (Marlow *et al.*, 2014b, Molle *et al.*, 2003). The first step of sporulation is the entry into an asymmetric cell division, which separates the mother cell and the Prespore by a septum. This process is under the control of several sigma factors ( $\sigma$ ) that govern the function of RNA polymerase-binding to change the promoter specificity of spore-specific genes. The sigma factors  $\sigma^A$  and  $\sigma^H$  are essential for the initiation of sporulation by regulating the production of filaments, which define the polar end of the rod, which will form the forespore (Riley *et al.*, 2018). In the following, sigma factors which are specific for the forespore ( $\sigma^F$  and  $\sigma^G$ ) and mother cell ( $\sigma^E$  and  $\sigma^K$ ) are activated and stimulate the separation of the forespore and the maternal



cell envelope (Hilbert & Piggot, 2004). The bacterial chromosome is translocated from the mother cell into the forespore under the regulation of  $\sigma^F$  (Wang *et al.*, 2006). The septum is then degraded and exchanged by a membrane (later: inner membrane), which closes the compartmentalization cycle and engulfs the forespore (driven by  $\sigma^E$ ) as a protoplast-like structure into the mother cell (Feucht *et al.*, 2003). Attached to the inner membrane, the germ cell wall is being synthesized, which functions as chemical barrier in the final spore form. Under expression of  $\sigma^E$  (mother cell) the outer coating with the cortex is initiated, whereas  $\sigma^G$  starts the activation of several spore-specific genes within the forespore (Wang *et al.*, 2006). Small acid soluble proteins ( $\alpha$ -,  $\beta$ - and  $\gamma$ - SASP and other) are generated, that strongly interact with the spore DNA to protect it during dormancy against desiccation, disruption and UV-light (Moeller *et al.*, 2009, Dittmann *et al.*, 2015). Rising levels of SpoVFA (dipicolinate synthase) enable the synthesis of  $\text{Ca}^{2+}$ -DPA (dipicolinic acid) within the mother cell which is transferred and incorporated into the spore core (Tovar-Rojo *et al.*, 2002, Steil *et al.*, 2005). The main function of  $\text{Ca}^{2+}$ -DPA is the reduction of water from more than 80 % to 25-45 %, which leads to an inactivation of the core metabolism by immobilizing water, proteins and membrane lipids (Kaieda *et al.*, 2013, Loison *et al.*, 2013, Huang *et al.*, 2007). Furthermore,  $\text{Ca}^{2+}$ -DPA protects the spore against heat and can take up to 5-15 % of the dry weight and significantly reduces the water content within the spore core (Slieman & Nicholson, 2001). The inner and outer spore coats are finalized by the mother cell under transcriptional regulation of  $\sigma^K$ , which also initiates the degradation of the mother cell (McKenney *et al.*, 2013). Spores developed under planktonic conditions have higher chances of being released into the environment, whereas spores within biofilms are stuck until the biofilm dissolves or is mechanically disrupted.

## 7.2 Abbreviations and units

Table 11: Abbreviation list

<b>Abbreviation</b>	<b>Connotation</b>
<b><math>\mu\text{g}</math></b>	microgravity
<b>ad.</b>	<i>lat.</i> adjust [to]
<b>AGFK</b>	germinant mix of L-asparagine, D-glucose, D-fructose and KCl
<b><i>B. subtilis</i></b>	<i>Bacillus subtilis</i>
<b><i>C. metallidurans</i></b>	<i>Cupriavidus metallidurans</i>
<b><math>\text{Ca}^{2+}</math>-DPA</b>	$\text{Ca}^{2+}$ - pyridine-2,6-dicarboxylic acid
<b>cDNA</b>	copy DNA
<b>COSPAR</b>	Committee on Space Research
<b>CPD</b>	critical point drying
<b>DIC</b>	differential interference contrast microscopy
<b>DNA</b>	deoxyribonucleic acid
<b>dNTPs</b>	nucleoside triphosphate
<b>EDTA</b>	ethylenediaminetetraacetic acid
<b>EPS</b>	extracellular polymeric substances
<b>ESA</b>	European Space Agency
<b>Fig.</b>	figure
<b>fwd</b>	forward
<b>g /1g</b>	g-force (9.81 m/s <sup>2</sup> ), terrestrial

<b>Abbreviation</b>	<b>Connotation</b>
<b>GA</b>	glutaraldehyde
<b>GCR</b>	galactic cosmic radiation
<b>gDNA</b>	genomic DNA
<b>GFP</b>	green fluorescent protein
<b>HARV</b>	High aspect rotating vessel
<b>HEPA</b>	High efficiency particulate air filter
<b>HPLC</b>	high-performance liquid chromatography
<b>HTTP</b>	mixed cellulose ester
<b>ISS</b>	International Space Station
<b>JAXA</b>	Japan Aerospace Exploration Agency
<b>Lab.</b>	laboratory
<b>LB</b>	lysogeny broth medium
<b>LET</b>	linear energy transfer
<b>LFH</b>	long-flanking homology
<b>LSM</b>	laser scanning microscopy
<b>MALDI-TOF</b>	matrix-assisted laser desorption/ionization -time of flight (mass spectroscopy)
<b>mRNA</b>	messenger RNA
<b>NASA</b>	National Aeronautics and Space Administration
<b>NYU</b>	New York University
<b>OD</b>	optical density (nm)
<b>PBS</b>	phosphate buffered saline
<b>PCR</b>	polymerase chain reaction
<b>PFA</b>	paraformaldehyde
<b>pH</b>	potential of hydrogen: measure of acidity or alkalinity
<b>PSU</b>	power supply unit
<b>PTFE</b>	polytetrafluoroethylene, also known as Teflon™
<b>R2A</b>	Reasoner's 2A [agar]
<b>rev</b>	reverse
<b>RNA</b>	ribonucleic acid
<b>rRNA</b>	ribosomal RNA
<b><i>S. desiccabilis</i></b>	<i>Sphingomonas desiccabilis</i>
<b>SASP</b>	small acid soluble protein
<b>sec</b>	seconds
<b>SEM</b>	scanning electron microscopy
<b>sim-μg</b>	simulated microgravity
<b>TAE</b>	Tris, acetic acid and EDTA (buffer)
<b>TE</b>	Tris-EDTA (buffer)
<b>TEM</b>	transmission electron microscopy
<b>Tris</b>	tris(hydroxymethyl)aminomethane
<b>UHV</b>	ultra high vacuum
<b>UV</b>	ultra violet [light]
<b>veg.</b>	vegetative [cells]
<b>wt</b>	wild type

Table 12: Units and their description

<b>Unit</b>	<b>Description</b>
(x) g	times g-force
°C	degrees Celsius
µl	microliter
µm	micrometer
A	ampere
a.u.	arbitrary unit
bp	base pairs
CFU	colony forming unit
g	gram
h	hour
keV	kilo electronvolt
kp	kilo base pairs
l	liter
m	meter
M	Mol
min	minutes
ml	milliliter
mM	millimolar
mm	millimeter
N	number of single experiments
ng	nano gram
nm	nanometer
Pa	Pascal
rel.	relative [%]
rpm	rounds/revelations per minute
sec	second(s)
u	unit
V	volt

### 7.3 Material, Devices & Software

Table 13: Materials

<b>Material</b>	<b>Manufacturer</b>
<b>Agilent 6000 Nano Kit</b>	Agilent Technologies, Santa Clara, USA
<b>Cover slips for microscopy</b>	VWR, Langenfeld, Germany
<b>Eppendorf tubes</b>	Eppendorf Research, Hamburg, Germany
<b>Filter syringes</b>	Greiner Bio-One GmbH, Kremsmünster, Austria

<b>Material</b>	<b>Manufacturer</b>
<b>Germ count dishes</b>	Greiner Bio-One GmbH, Kremsmünster, Austria
<b>Glass beads, acid-washed</b>	Sigma-Aldrich, Steinheim, Germany
<b>Glass slides for microscopy</b>	VWR, Langenfeld, Germany
<b>ibidi® dishes</b>	ibidi GmbH, Gräfeling, Germany
<b>LEIT C PLAST</b>	Plano, Wetzlar, Germany
<b>LR White</b>	London Resin Company, Reading, UK
<b>MF-Millipore™ Membrane Filter, 0.45 µm pore size, mixed cellulose esters (MCE)</b>	Merck KGaA, Darmstadt, Germany
<b>Microporous Specimen Pots</b>	Leica, Wetzlar, Germany
<b>Millicell Cell Culture Insert, 30 mm, hydrophilic PTFE, 0.4 µm</b>	Merck KGaA, Darmstadt, Germany
<b>NEBNext® Multiplex Oligos for Illumina®</b>	New England Biolabs, Ipswich, USA
<b>Nitrile Gloves</b>	Kimberly-Clark Professional, Koblenz, Germany
<b>Parafilm®</b>	Bemis Company, Neenah, USA
<b>peqGOLD Bacterial DNA Kit</b>	VWR, Langenfeld, Germany
<b>PFE Gloves</b>	Kimberly-Clark Professional, Koblenz, Germany
<b>Pipettes, 10µl, 20 µl, 100 µl, 200 µl, 1000 µl, 5000 µl</b>	Eppendorf Research, Hamburg, Germany
<b>QIAquick PCR Purification Kit</b>	Qiagen, Hilden, Germany
<b>Ribo-Zero® rRNA Removal Kit</b>	Illumina, San Diego, USA
<b>RNaseZap™</b>	Invitrogen/ Thermo Fisher, Carlsbad, USA
<b>RNeasy Kit</b>	Qiagen, Hilden, Germany
<b>Scalpell</b>	B. Braun, Melsungen, Germany
<b>Sterile filter</b>	Greiner Bio-One GmbH, Kremsmünster, Austria
<b>Taq- Polymerase</b>	New England Biolabs, Ipswich, USA

Table 14: Devices

<b>Device</b>	<b>Manufacturer</b>	<b>Utilization</b>
<b>µsurf custom</b>	Nanofocus, Oberhausen, Germany	Profilometry
<b>2D-Clinostat</b>	Advanced Engineering Services Co., Ltd., Japan	µg-simulation
<b>Bandelin Sonorex Super BioAnalyser</b>	Berlin, Germany	Sonication
<b>CPD 300</b>	Agilent Technologies, Santa Clara, USA	RNA quality control
<b>E5100 Polaron</b>	Leica, Wetzlar, Germany	Critical point drying
<b>Eppendorf Centrifuge 5417 R</b>	Quorum Technologies, Laughton, UK	Gold/ Palladium sputtercoating
<b>FastPrep-24 5G</b>	Eppendorf Research, Hamburg, Germany	Centrifugation
	MP Biomedical, Santa Ana, USA	Spore disruption

<b>Device</b>	<b>Manufacturer</b>	<b>Utilization</b>
<b>FEI Tecnai12 Biotwin</b>	FEI, Hillsboro, USA	Transmission electron microscopy
<b>Gulmay X-Ray RS225</b>	Gulmay Medical Limited, Camberley, UK	X-ray-treatments
<b>Hermle Z36HK</b>	HERMLE Labortechnik GmbH, Wehningen, Germany	Centrifugation
<b>HMC Biosafety Cabinet BSC-700II-I</b>	HMC Europe	Sterile working
<b>Ionizing chamber TM30013</b>	PTW GmbH, Freiburg, Germany	X-ray-treatments
<b>Leo 1530 FEG SEM</b>	Zeiss, Oberkochen, Germany	Scanning electron microscopy
<b>NanoDrop</b>	Thermo Fisher Scientific, Waltham, USA	RNA and DNA measurements
<b>Nikon Eclipse TE2000-E</b>	Nikon, Tokyo, Japan	Inverted microscope for growth experiments
<b>Qubit</b>	Thermo Fisher Scientific, Waltham, USA	RNA and DNA measurements
<b>RPM</b>	ETH, Zurich, Swiss	µg-simulation
<b>Sartorius E19278</b>	Sartorius, Göttingen, Germany	fine scale
<b>Sony α5100</b>	Sony, Tokyo, Japan	Camera
<b>TB1 Thermoblock</b>	Biometra	Ultra-sonic bath
<b>Thermocycler PEQstar 96 UN</b>	VWR, Langenfeld, Germany	Heating of samples
<b>Tischwaage</b>	Kern & Sohn, Balingen-Frommern, Germany	Scale
<b>UNIDOS<sup>webline</sup></b>	PTW GmbH, Freiburg, Germany	Dosimeter
<b>Uzusio Mixer</b>	Laboratory & Medical Supplies	Vortex
<b>X-ray tube, THX 225/G</b>	Thales electron devices, Vélizy Cedex, France	X-ray-treatments
<b>Zeiss Axio Imager M2</b>	Zeiss, Oberkochen, Germany	Microscope
<b>Zeiss LSM 780</b>	Zeiss, Oberkochen, Germany	Confocal laser scanning microscopy

Table 15: Software

<b>Software/ Version</b>	<b>Developer</b>	<b>Utilization</b>
<b>µsoft</b>	Nanofocus	Profilometry
<b>Adobe Acrobat Pro</b>	Adobe Inc	Document management
<b>cellSens Entry</b>	Olympus	Phase-constrast microscopy
<b>EndNote X7.3 /X9</b>	Thopson Reuters	Reference manager
<b>Gen5 2.00</b>	BIOREADER	Wellplate-Reader
<b>i-control™</b>	TECAN	Wellplate-Reader
<b>ImageJ 1.46r/FIJI</b>	Wayne Rasband, National Institutes of Health	Statistics
<b>Microsoft Office 2010</b>	Microsoft, Inc.	Word, Excel, Outlook, PowerPoint
<b>Mozilla Firefox</b>	Mozilla Foundation	Diverse applications
<b>Nanodrop 1000</b>	Thermo Scientific™	Determining DNA/RNA/protein

<b>Software/ Version</b>	<b>Developer</b>	<b>Utilization</b>
Nikon Imaging NIS-Elements AR	Nikon	concentration DIC-Imaging
OSIS ITEM	Olympus	TEM-imaging
OSIS Scandium software	Olympus	SEM-imaging
R	The R Foundation	Statistics
SigmaPlot V13.0	Systat Software, Inc.	Statistics
SubtiWiki	Prof. Jörg Stülke et al.	Database for <i>B. subtilis</i> genes
VLC Media Player	VLC	Video editing
ZEN (blue & black)	Carl Zeiss Microscopy GmbH	Image acquisition and editing

#### 7.4 Chemicals, antibiotics, marker and primer

Table 16: Chemicals

<b>Chemical</b>	<b>Manufacturer /Distributor</b>
Acid-phenol	Sigma-Aldrich, Steinheim, Germany
Agarose SERVA	Serva, Heidelberg, Germany
Bacto Agar	Sigma-Aldrich, Steinheim, Germany
Beef/ meat extract	Merck KGaA, Darmstadt, Germany
Bromophenol blue	Merck KGaA, Darmstadt, Germany
Ca(NO <sub>3</sub> ) <sub>4</sub>	Sigma-Aldrich, Steinheim, Germany
CaCl <sub>2</sub>	Roth, Karlsruhe, Germany
Cacodylate acid	Sigma-Aldrich, Steinheim, Germany
Casamino acids (hydrolysate)	Sigma-Aldrich, Steinheim, Germany
Chloramphenicol	Serva, Heidelberg, Germany
Chloroform	Sigma-Aldrich, Steinheim, Germany
Crystal violett	Merck KGaA, Darmstadt, Germany
D(+)-Glucose Monohydrate	Sigma-Aldrich, Steinheim, Germany
EDTA, disodium salt	AppliChem, Darmstadt, Darmstadt
Erythromycin	Sigma-Aldrich, Steinheim, Germany
Ethanol	PanReacAppliChem, Darmstadt, Germany
Ethidiumbromide (1 %)	Merck KGaA, Darmstadt, Germany
Fe(II)SO <sub>4</sub> · 7H <sub>2</sub> O	Sigma-Aldrich, Steinheim, Germany
FeCl <sub>3</sub>	Sigma-Aldrich, Steinheim, Germany
Ferric ammonium citrate	Sigma-Aldrich, Steinheim, Germany
Glacial acetic acid	Merck KGaA, Darmstadt, Germany
Glutaraldehyde, 25 %	Sigma-Aldrich, Steinheim, Germany
Glycerol	Sigma-Aldrich, Steinheim, Germany
HCl (37 %)	Sigma-Aldrich, Steinheim, Germany
HEPES (acid free)	Sigma-Aldrich, Steinheim, Germany
Isopropanol	Sigma-Aldrich, Steinheim, Germany
K <sub>2</sub> HPO <sub>4</sub>	Sigma-Aldrich, Steinheim, Germany

<b><i>Chemical</i></b>	<b><i>Manufacturer /Distributor</i></b>
<b>Kanamycin</b>	Sigma-Aldrich, Steinheim, Germany
<b>KCl</b>	Sigma-Aldrich, Steinheim, Germany
<b>KH<sub>2</sub>PO<sub>4</sub></b>	Sigma-Aldrich, Steinheim, Germany
<b>L-Alanine</b>	Roth, Karlsruhe, Germany
<b>LB-Agar</b>	Sigma-Aldrich, Steinheim, Germany
<b>LB-broth (Luria Bertani Broth)</b>	Sigma-Aldrich, Steinheim, Germany
<b>LiCl</b>	Sigma-Aldrich, Steinheim, Germany
<b>LMP-Agarose</b>	Promega, Mannheim, Germany
<b>L-Phenylalanine</b>	Merck KGaA, Darmstadt, Germany
<b>L-Tryptophan</b>	Sigma-Aldrich, Steinheim, Germany
<b>Methanol</b>	Sigma-Aldrich, Steinheim, Germany
<b>MgCl<sub>2</sub> · 6 H<sub>2</sub>O</b>	Merck KGaA, Darmstadt, Germany
<b>MgSO<sub>4</sub> x 7 H<sub>2</sub>O</b>	Merck KGaA, Darmstadt, Germany
<b>MnCl<sub>2</sub></b>	Merck KGaA, Hohenbrunn, Germany
<b>MOPS</b>	Sigma-Aldrich, Steinheim, Germany
<b>NaCl</b>	Sigma-Aldrich, Steinheim, Germany
<b>NaCl</b>	Sigma-Aldrich, Steinheim, Germany
<b>NaOH</b>	Sigma-Aldrich, Steinheim, Germany
<b>Na-pyruvate</b>	AppliChem, Darmstadt, Darmstadt
<b>NOTOXhisto<sup>®</sup></b>	Scientific Device Laboratory, Des Plaines, USA
<b>Nutrient broth</b>	MP Biomedicals, Illkirch Cedex, France
<b>Osmium tetroxide</b>	Sigma-Aldrich, Steinheim, Germany
<b>Paraformaldehyde</b>	Sigma-Aldrich, Steinheim, Germany
<b>Peptone</b>	Sigma-Aldrich, Steinheim, Germany
<b>Phenol-chloroform (5:1)</b>	Sigma-Aldrich, Steinheim, Germany
<b>Poly-L-Lysine</b>	Sigma-Aldrich, Steinheim, Germany
<b>Sodium-L-Glutamate Monohydrate</b>	Merck KGaA, Darmstadt, Germany
<b>Spectinomycin</b>	Sigma-Aldrich, Steinheim, Germany
<b>Starch (soluble)</b>	Merck KGaA, Darmstadt, Germany
<b>Tannic acid</b>	Sigma-Aldrich, Steinheim, Germany
<b>Tetracycline</b>	Sigma-Aldrich, Steinheim, Germany
<b>Tris-base</b>	AppliChem, Darmstadt, Darmstadt
<b>Uranyl acetate</b>	Sigma-Aldrich, Steinheim, Germany
<b>Xylene cyanol FF</b>	Sigma-Aldrich, Steinheim, Germany
<b>ZnCl<sub>2</sub></b>	Sigma-Aldrich, Steinheim, Germany

Table 17: Antibiotics and their preparation and application

<b>Antibiotic</b>	<b>Selective concentration [<math>\mu\text{g/ml}</math>]</b>	<b>Solvent</b>	<b>Stock [<math>\text{mg/ml}</math>]</b>
Chloramphenicol	5	70 % Ethanol	1
Erythromycin	2	70 % Ethanol	1
Kanamycin	10	ddH <sub>2</sub> O	1
Lincomycin	10	ddH <sub>2</sub> O	1
Spectinomycin	150	ddH <sub>2</sub> O	5
Tetracycline	12.5	70 % Ethanol	1

Table 18: DNA Markers and ladders

<b>Name</b>	<b>Range [kb]</b>	<b>Agarose [%]</b>	<b>Main targets</b>	<b>Manufacturer/ Distributor</b>
50 bp	0.05 - 1	2.5	PCR	New England Biolabs, Ipswich, USA
100 bp	0.1 - 1	1.5	PCR, RNA	New England Biolabs, Ipswich, USA
100 bp Plus	0.1 - 3	1.5	PCR, RNA	New England Biolabs, Ipswich, USA
1 kb	0.25 - 10	1	gDNA	New England Biolabs, Ipswich, USA
1 kb Plus	0.075 - 20	1	gDNA	New England Biolabs, Ipswich, USA
2-log	0.1 - 10	1 - 1.5	irradiation	New England Biolabs, Ipswich, USA

Table 19: Primer, their sequence, melting temperature and purpose

<b>Primer name</b>	<b>Sequence (5'...3')</b>	<b>T<sub>m</sub> [°C]</b>	<b>Purpose</b>
Cat-fwd	CGGCAATAGTTACCTTATT ATCAAG	63.4	LFH: Amplification of the chloramphenicol resistance gene
Cat-rev	CCAGCGTGGACCGGCGAGG CTAGTTACCC	82.3	LFH: Amplification of the chloramphenicol resistance gene
JR220 (LFH)	CCTATCACCTCAAATGGTTC GCTGCAAATGGAAGTCGCC GAGGA	87.5	LFH: Amplification of the upstream sequence
JR221 (LFH)	CGGCCGATCCTGATTCCATA A	69.8	LFH: Amplification of the upstream sequence
JR222 (LFH check)	TCAGGTCAAAGGGTTGAG ACAA	66.7	LFH: Control and sequencing of transformants
JR223 (LFH)	CGAGCGCCTACGAGGAATT TGTATCGTATCCACCCCGCA GATTTCCG	87.4	LFH: Amplification of the downstream sequence
JR224 (LFH)	GGCAAGGCTGTCAAACACG	66.9	LFH: Amplification of the downstream sequence
JR225 (LFH check)	GGGAGTTGGTCAGCAAAT CAATT	67.8	LFH: Control and sequencing of transformants

**Dual Index Primers Set 1 for RNAseq**

<b>Name</b>	<b>Sequence (5'...3')</b>
1g_0	i505 AGGCGAAG / i705 ATTCAGAA
1g_4	i505 AGGCGAAG / i706 GAATTCGT
1g_8	i505 AGGCGAAG / i707 CTGAAGCT



<b>Primer name</b>	<b>Sequence (5'...3')</b>	<b>Tm [°C]</b>	<b>Purpose</b>
<b>1g_16</b>	i505 AGGCGAAG / i708 TAATGCGC		
<b>sim_4</b>	i506 TAATCTTA / i705 ATTCAGAA		
<b>sim_8</b>	i506 TAATCTTA / i706 GAATTCGT		
<b>sim_16</b>	i506 TAATCTTA / i707 CTGAAGCT		

## 7.5 Additional results

**Table 20: LD90 values of *B. subtilis* spores exposed to Helium and Argon ions and X-ray**

*B. subtilis* NCIB 3610 spores (wt,  $\Delta epsA-O$ ,  $\Delta tasA$  and  $\Delta bsIA$ ) and B1 spores were grown on SSM-media for 5 days at 30 °C under regular gravity conditions (1g) and simulated microgravity by using a fast rotating 2-D clinostat (sim- $\mu g$ ). Harvested spores have been irradiated with 100, 250, 500 and 1000 Gy of the respective radiation source (Helium and Argon ions as well as X-ray). The data given in the table represent calculated LD90 values (lethal dose) which indicate at which applied dose 90 % inactivation would occur. Argon irradiation proved to be most effective in comparison to Helium ions and X-ray treatments which is represented by comparably lower LD90 values. In order to inactivate *B. subtilis* spores, relatively high doses of Helium would have to be used compared to X-ray and Argon irradiation. Differences among LD90 values between 1g and sim- $\mu g$  vary widely and a pattern between the two growth conditions is not discernible. Some LD90 values were not determinable (n.d.) due to scattered data. All data is given in Gy.

<b>wt</b>	<b>Helium</b>	<b>Argon</b>	<b>X-ray</b>	<b><math>\Delta epsA-O</math></b>	<b>Helium</b>	<b>Argon</b>	<b>X-ray</b>
1g	2687±161	1921±215	2156±91	1g	n.d.	2950±269	2015±249
sim- $\mu g$	2574±157	2298±173	2187±143	sim- $\mu g$	2784±170	2383±185	2371±100
<b><math>\Delta tasA</math></b>	<b>Helium</b>	<b>Argon</b>	<b>X-ray</b>	<b><math>\Delta bsIA</math></b>	<b>Helium</b>	<b>Argon</b>	<b>X-ray</b>
1g	3630±298	n.d.	2715±176	1g	3464±617	2060±149	2553±416
sim- $\mu g$	n.d.	2309±135	2162±147	sim- $\mu g$	n.d.	2274±144	n.d.
<b>B1</b>	<b>Helium</b>	<b>Argon</b>	<b>X-ray</b>				
1g	n.d.	1698±165	1675±252				
sim- $\mu g$	3248±682	n.d.	1719±141				

## 7.6 Curriculum vitae

### Personal Data:

**Name:** Felix Matthias Fuchs

**E-Mail:** [fuchs@aept.rub.de](mailto:fuchs@aept.rub.de)



### Scientific Education:

**03/2015 – 08/2019**

**Ph.D, Georg-August-University Göttingen, German  
Aerospace Center**

**04/2011 – 10/2014**

**Master (M. Sc.) Biology, RWTH-Aachen University**

**10/2008 – 03/2011**

**Bachelor (B. Sc.) Biology, RWTH-Aachen University**

## 7.7 Publication list

### Submitted & accepted:

Friederike Kogelheide, Farina Voigt, Bastian Hillebrand, Ralf Moeller, **Felix M. Fuchs**, Andrew Gibson, Peter Awakowicz, Katharina Stapelmann and Marcel Fiebrandt, 2020. The role of humidity and UV-C emission in the inactivation of *B. subtilis* spores during atmospheric-pressure DBD treatment, J Phys D, Ref. No. 123160.R1.

### Published:

Emanuel Ott, **Felix M. Fuchs**, Ralf Moeller, Ruth Hemmersbach, Yuko Kawaguchi, Akihiko Yamagishi, Wolfram Weckwerth and Tetyana Milojevic, 2019. Molecular response of *Deinococcus radiodurans* to simulated microgravity explored by proteometabolomic approach, Sci Rep. **9**, 18462 (2019).

Marta Cortesão, **Felix M. Fuchs**, Fabian M. Commichau, Patrick Eichenberger, Andrew C. Schuerger, Wayne L. Nicholson, Peter Setlow and Ralf Moeller, 2019. *Bacillus subtilis* spore resistance to simulated Mars surface conditions, Front Microbiol, **10**, (133).

**Felix M. Fuchs\***, Gudrun Holland, Ralf Moeller and Michael Laue, 2018. Directed freeze-fracturing of *Bacillus subtilis* biofilms for conventional scanning electron microscopy, J Microbiol Methods. **152**, 165-172.

**Felix M. Fuchs\***, Marina Raguse, Marcel Fiebrandt, Kazimierz Madela, Peter Awakowicz, Michael Laue, Katharina Stapelmann and Ralf Moeller, 2017. Monitoring of spore vitality parameters and DNA repair in response to plasma sterilization, J Vis Exp. (129), e56666 (2017).

Vincenzo Zammuto, **Felix M. Fuchs**, Marcel Fiebrandt, Katharina Stapelmann, Teresa L. Maugeri, Rüdiger Pukall, Concetta Gugliandolo and Ralf Moeller, 2018. Comparing spore resistance of *Bacillus* strains isolated from hydrothermal vents and spacecraft assembly facilities to environmental stressors and decontamination treatments. Astrobiol. **18**, 1425-1434.

Claire-Marie Loudon, Natasha Nicholson, Kai Finster, Natalie Leys, Bo Byloos, Rob Van Houdt, Petra Rettberg, Ralf Moeller, **Felix M. Fuchs**, René Demets, Jutta Krause, Marco Vukich, Alessandro Mariani, Charles Cockell, 2018. BioRock: New Experiments and Hardware to Investigate Microbe-Mineral Interactions in Space. Int. J. Astrobiol. **17**, 303-313.

**Felix M. Fuchs\***, Adam Driks, Peter Setlow, Ralf Moeller, 2017. An improved protocol for harvesting *Bacillus subtilis* colony biofilms. J Microbiol Methods. **134**, 7-13.

Karsten Henne, **Felix M. Fuchs**, Sebastian Kruth, Hans-Peter Horz, Georg Conrads, 2014. Shifts in *Campylobacter* species abundance may reflect general microbial community shifts in periodontitis progression. J Oral Microbiol. **6**, 25874.

*“There is grandeur in this view of life, with its several powers, [...] and that, whilst this planet has gone cycling on according to the fixed law of gravity, from so simple a beginning endless forms most beautiful and most wonderful have been and are being evolved.”*

– Charles Darwin, *The Origin of Species*



